Wireless Communication Systems Based on Spatial Modulation MIMO

Xiping Wu

A thesis submitted for the degree of Doctor of Philosophy.
The University of Edinburgh.
May 2015

Abstract

Spatial modulation (SM) is a unique single-stream, multiple-input multiple-output (MIMO) transmission technique. Unlike traditional MIMO schemes, SM sends out signals through a single active antenna, and achieves multiplexing gains by encoding information bits into the index of the currently active antenna. In contrast to multi-stream MIMO systems, this particular characteristic offers great superiority in two main aspects. Firstly, SM completely avoids inter-channel interference. Secondly, SM requires a single radio-frequency chain, regardless of the number of antennas used, and therefore exhibits a significant energy saving. However, the property of a single active antenna challenges the channel estimation process for SM: the transmit antennas have to be activated sequentially for sending pilot signals. As a result, the time consumed in pilot transmission is proportional to the number of transmit antennas. However, this fact has so far been neglected in related research. Also, published research on SM has focused on point-to-point communications, and few have covered a network perspective. In this thesis, a comprehensive study is undertaken on SM systems in single-user, multi-user and multi-cell scenarios.

As a unique three-dimensional modulation scheme, SM enables a trade-off between the size of the signal constellation diagram and the size of the spatial constellation diagram. In this thesis, an optimum transmit structure is proposed for SM to employ an adaptive scale of antennas against channel correlations. Unlike traditional antenna selection methods, this new approach is not sensitive to fast fading, due to the exploitation of statistical channel state information (CSI) instead of instant CSI. The proposed transmit structure is demonstrated to have a near-optimal performance against exhaustive search, while achieving very low computational complexity.

In addition, three novel methods are developed to improve the channel estimation process for SM. A first method estimates the entire MIMO channel by sending pilot signals through only one of the transmit antennas, among which the channel correlation is exploited. In a similar way but focusing on the receiver, a second method can improve the estimation accuracy without increasing the pilot sequence length. A third method balances the transmission power between pilot and data to minimise the bit error rate. A framework of combined channel estimation is also proposed, in which the three methods are jointly applied.

Furthermore, the antenna allocation in multi-user SM is studied, in order to explore multi-user diversity gains. A method that jointly manages transmit antennas and receive antennas for all co-channel users is proposed. The aim of this new method is to maximise the channel capacity for each user, and the fairness among users is taken into account. It is demonstrated that the proposed method significantly improves the performance of multi-user SM, especially when serving a large number of users.

Finally, a novel cooperative scheme is proposed for SM in a multi-cell scenario. Based on the concept of coordinated multi-point transmission (CoMP), this scheme enables the coordinated users to swap the base station antennas pertaining to them. A three-tier cellular architecture is further developed to switch between CoMP and the cooperative scheme.

Declaration of originality

I hereby declare that the research recorded in this thesis and the thesis itself was composed and originated entirely by myself in the Department of Electronics and Electrical Engineering at The University of Edinburgh.

Xiping Wu
Edinburgh, UK
May 2015

Acknowledgements

I would like to express the deepest gratitude to my supervisor, Professor Harald Haas of the Institute for Digital Communications (IDCOM) at the University of Edinburgh, UK. Professor Haas' academic excellence, enthusiasm for research and unappeasable desire to pursue novel ideas have greatly inspired me. Without his pragmatic advice and continuous support, this dissertation would not have been possible.

I would like to thank my second supervisor, Dr James Hopgood, who has supported me with his patience and knowledge. He was also the supervisor of my master study, and introduced me to the magic of scientific research.

In addition, I say thank you to my colleagues in both IDCOM and GREENET project. Their support and companionship gave me wonderful experiences and joyful memories these particular three years. A special word of appreciation goes to Dr Marco Di Renzo and Dr Sinan Sinanovic for their consistent help and fruitful discussions.

I gratefully acknowledge the European Union's Seventh Framework Programme (FP7) under Grant 264759 (GREENET Project) for the support of this work. Also, many thanks to Mrs Nicola Ferguson and Mrs Adean Lutton for their support.

This thesis is dedicated to my family and friends, the people who have always been with me and shared happiness and sadness. An unparalleled thank to my father, Zhijian, who taught me everything during my growth. Finally, I would like to deliver my faithful love to two special women in my life: my mother, Min, and my wife, Shufen. With their selfless love and continuous encouragement, I was able to pull through some stressed and challenging times.

Contents

List of figures

List of tables

Acronyms and abbreviations

3GPP	3rd Generation Partnership Project
ABEP	Average Bit Error Probability
APEP	Average Pair-wise Error Probability
AWGN	Additive White Gaussian Noise
BER	Bit Error Rate
BS	Base Station
CCE	Conventional Channel Estimation
CDI	Channel Difference Information
CE	Channel Estimation
CoMP	Coordinated Multi-Point transmission
CoSM	Cooperative Spatial Modulation
CSI	Channel State Information
CSIR	Channel Side Information at the Receiver
CSIT	Channel Side Information at the Transmitter
DAS	Distributed Antennas Systems
DTX	Discontinuous Transmission
EPA	Equal Power Allocation
FFR	Fractional Frequency Reuse
GSM	Generalised Spatial Modulation
ICI	Inter-Channel Interference
ICP	Ideal Circle Packing
IGI	Inter-Group Interference
IUI	Inter-User Interference
LS	Least Square
LTE	Long-Term Evolution
MGF	Moment Generate Function
MIMO	Multiple-Input Multiple-Output
ML	Maximum Likelihood
MMSE	Minimum Mean Square Error

MRT	Maximum Ratio Transmission
MUD	Multi-User Detection
MU-SM	Multi-User Spatial Modulation
OFDM	Orthogonal Frequency Division Multiplexing
OFDMA	Orthogonal Frequency Division Multiplexing Access
OPA	Optimal Power Allocation
PA	Power Amplifier
PCSI	Perfect Channel State Information
PSK	Phase Shift Keying
QAM	Quadrature Amplitude Modulation
QPSK	Quadrature Phase Shift Keying
RCP	Realistic Circle Packing
RF	Radio-Frequency
RLS	Recursive Least Square
RV	Random Variable
Rx-SD	Receiver-centric Sphere Decoding
SD	Sphere Decoding
SER	Symbol Error Rate
SFR	Soft Frequency Reuse
SIMO	Single-Input Multiple-Output
SINR	Signal-to-Interference-plus-Noise Ratio
SISO	Single-Input Single-Output
SM	Spatial Modulation
SMMA	Spatial Modulation Multiple Access
SNR	Signal-to-Noise Ratio
SSK	Space Shift Keying
STBC	Space-Time Block Coding
TAS	Transmit Antenna Selection
TCCE	Transmit Cross Channel Estimation
TOSM	Transmission Optimised Spatial Modulation
Tx-SD	Transmitter-centric Sphere Decoding
V-BLAST	Vertical Bell Laboratories Layered Space-Time
WLAN	Wireless Local Area Network

Nomenclature

$\{\cdot\}^H$	Hermitian transpose
c	Speed of light
$d_{m,k}$	Distance between BS m and user k
d_{ref}	Reference distance
d_{t_i,t_j}	Absolute distance between antennas t_i and t_j
$\text{diag}(\cdot)$	The operator that extracts the diagonal of a matrix
$\mathbf{H}$	Channel matrix
$\tilde{h}$	Estimated channel
$\mathbf{H}_{\text{eff}}$	Effective channel-modulation matrix
$\mathbf{H}_{\text{req}}$	Desired signal vector
$h_{m,k}^{t,r}$	Fading coefficient of the link from antenna t of BS m to antenna r of user k
$h_{r,t}$	Fading coefficient of the link from transmit antenna t to receive antenna r
$\mathbf{h}_t$	The t-th column of channel matrix
$\exp\{\cdot\}$	Exponential function
$\mathbf{E}\{\cdot\}$	Expectation operator
E_a	Average energy consumption per symbol transmission
E_b	Energy consumption per bit transmission
E_{BS}	BS energy consumption per bit transmission
E_m	Energy consumption per symbol transmission
E_p	Energy consumption per pilot symbol transmission
E_s	Energy consumption per information-carrying symbol transmission
f_c	Centre carrier frequency
$J_0(\cdot)$	The zeroth-order Bessel function of the first kind
l	Symbol index
L	Path loss
$\hat{l}$	Detection result of symbol index
m	Shape parameter of Nakagami-m distribution
M	Size of signal constellation diagram
M_{opt}	The optimal size of signal constellation diagram

n	Discrete time index
N	Number of selected transmit antennas
N_0	Noise power density
N_{act}	Number of activated transmit antennas
$N_H(\cdot)$	Hamming distance
N_{opt}	The optimal number of transmit antennas
N_p	Pilot sequence length
N_r	Number of receive antennas
N_t	Number of transmit antennas
N_{tot}	Total number of transmit antennas in multi-user spatial modulation
N_u	Number of users
p	Pilot signal
P	Precoding mask
P_0	Constant power consumption of base station in the active mode
P_{BS}	Average power consumption of base station
P_{CE}	Estimation period
P_{in}	Instantaneous power consumption of base station
P_{max}	Maximum radio-frequency output power
P_{out}	Radio-frequency output power
$\bar{P}_{\text{out}}$	Average radio-frequency output power
P_{req}	Required radio-frequency output power
P_s	Constant power consumption of base station in the sleep mode
$Q(x)$	Q-function
r	Receive antenna
R_b	Average data rate
$R_{b\text{max}}$	Maximum data rate
R_e	Target bit error rate
R_r	Transmit correlation matrix
R_t	Receive correlation matrix
s_k	The original signal for user k before precoding
$\dot{s}_k$	The transmitted signal for user k after precoding
$\text{sgn}(\cdot)$	Sign function
t	Transmit antenna

t_{act}	Currently active antenna
$\hat{t}_{\text{act}}$	Detection result of currently active antenna
T_s	Sampling period
v	The speed of mobile user
$\mathbf{w}$	Noise vector
$\mathbf{x}$	Transmitted signal vector
$\mathbf{y}$	Received signal vector
α	Fast fading coefficient
$A_{(\theta_{m,k})}$	Gain patten of directional antennas
A_m	The maximum attenuation for the side-lobe
β	Amplitude of fast fading
B	Shadow fading coefficient
γ	Signal-to-noise ratio
Γ	Signal-to-interference-plus-noise ratio
$\bar{\gamma}$	Average signal-to-noise ratio
γ_e	Effective signal-to-noise ratio in the presence of channel estimation errors
γ_p	SNR for pilot symbols
γ_{ref}	SNR at the reference distance
γ_s	SNR for information-carrying symbols
γ_{t,r_k}	SNR of the link from the t-th transmit antenna to the r-th receive antenna at user k
$\Gamma(x)$	Gamma function
Δ_{t_1,t_2}	Channel difference information between antennas t_1 and t_2
ζ	The slope that quantifies the load dependence
η	Pilot ratio
η_s	Number of bits per symbol
θ	Angle between the user and the origin point
θ_{3dB}	Angle at which the signal power is half of that at the main-beam direction
$\theta_{m,k}$	Angle between BS m and user k with respect to the main-beam direction
κ	Speed controlling parameter in the Gauss-innovations channel model
λ	Lagrange multiplier
μ	Path loss exponent
ν	Distance between the user and the origin point
π	Circumference ratio

Π	Multiplication calculator
ρ	Correlation degree
ρ_{av}	Average correlation degree
ρ_{rx}	Correlation degree between two receive antennas at the reference distance
ρ_s	Correlation degree between two antennas separated at a unit distance
ρ_{tx}	Correlation degree between two transmit antennas at the reference distance
ϱ	Activation ratio of BS in the discontinuous transmission mode
Σ	Summation calculator
σ_ϵ	Standard deviation of channel estimation errors
φ	Phase of fast fading
χ_l	The l-th symbol of signal constellation diagram
Ω	Spread controlling parameter of Nakagami-m distribution

Chapter 1
Introduction

1.1 Motivation

At the present time, the whole information and communication technology industry contributes 2% to the global carbon emission [1]. With the aim of reducing the carbon footprint and the operating cost of wireless networks, an overall energy reduction is required in the region of two to three orders of magnitude. Meanwhile, a significant increase of the network spectrum efficiency from currently around 1.5 bit/s/Hz to at least 10 bit/s/Hz is needed to cope with the exponentially increasing traffic loads [2]. Due to those factors, a mass of attention has been drawn to spatial modulation (SM), a unique single-stream multiple-input multiple-output (MIMO) transmission technique [3–5]. In SM, in addition to signal modulation, the antenna positions are used to carry information bits. Unlike conventional MIMO schemes, SM activates a single transmit antenna and conveys a single data stream at any time instance. Therefore SM requires one radio-frequency (RF) chain only, regardless of the number of transmit antennas used. This characteristic makes SM a truly energy efficient MIMO technique, since each RF chain contains one power amplifier that consumes about 60% of the entire energy of an RF chain [6]. Another significant advantage due to a single active antenna is that SM completely avoids inter-channel interference (ICI). Conversely, ICI is inevitable in the conventional MIMO schemes, leading to a drawback in their decoding processes.

The concept of SM has emerged and been developed in the recent decade. The original idea of exploiting antenna positions to carry information bits was introduced by Chau *et al.* in 2001, where the signal can be sent by different numbers of transmit antennas [7]. In 2004, Haas *et al.* first considered conveying information bits via activating one transmit antenna out of the antenna array [8], which forms the foundation of SM. Later in 2006, this unique single-stream MIMO scheme was termed as SM by Mesleh *et al.*, and a two-stage detection method was proposed to estimate the transmit antenna index and the transmitted signal [3]. Since then, research related to SM has been conducted extensively. A joint maximum likelihood (ML) detection method was proposed in [9], where the transmit antenna index and the transmitted symbol are

estimated together, providing an optimal detector for SM. In [10], endeavours were made to combine SM with space-time block coding (STBC). In addition, MIMO-orthogonal frequency-division multiplexing (OFDM) is one of the most sought-after research directions. When SM confronts an OFDM system, the main challenge lies on the conflict between the constraint of a single RF chain in SM and the requirement of different streams for OFDM subcarriers [11]. Furthermore, theoretical work has been done to analyse the performance for SM in terms of bit error probability [12–14]. Results show that SM offers a better performance than many state-of-the-art MIMO techniques, while achieving a low-complexity implementation [12].

Some variants of SM concepts have also been studied. Removing the signal modulation part from SM, space shift keying (SSK) transfers the information bits solely by antenna indices [15]. Instead of activating a single transmit antenna, generalised spatial modulation (GSM) activates a certain number of antennas at any time instance, and exploits the combinations of the active antennas to construct the spatial constellation diagram [16]. Compared with the original SM, GSM can effectively increase the spectrum efficiency when using the same number of transmit antennas. Receive-spatial modulation (R-SM) uses the beamforming technique in order to carry information bits through the index of the antenna receiving signals [17]. This thesis is focused on the SM structure, and the proposed methods are also applicable to the above variants. So far, most studies on SM have been conducted in the single-user scenario under the assumption of known channel state information (CSI). In order to study the SM system in a practical and comprehensive environment, three cases will be considered in this thesis: i) a single user with perfect channel state information (PCSI); ii) a single user with practical channel estimation; and iii) multi-user and/or multi-cell scenarios.

When PCSI is assumed in a single-user scenario, one of the upmost issues raised in MIMO systems is the performance degradation caused by channel correlations. Table 1.1 summarises the technologies that have been reported to improve the bit error rate (BER) performance of MIMO schemes against multipath imperfection. Like all other MIMO schemes, SM experiences performance degradation over correlated channels [18]. With the aim of increasing the antenna diversity, the transmit antenna selection (TAS) techniques are widely applied in the MIMO systems, where a subset is selected from an antenna array to form the group of transmit antennas [19]. However, few studies have been done with respect to developing TAS methods for SM, and in those few, the subset contains a fixed number of antennas [20–22]. In [23], an adaptive spatial modulation method was proposed, which selects one candidate from several optional

SM structures of different transmit-antenna numbers. Although the performance of SM can be improved to some extent, this method has the following weaknesses: i) it offers a limited range of options; ii) it requires instant CSI and therefore is not suitable for fast fading; and iii) in despite of using a simplified modulation order selection criterion, it still requests significant processing power. To date, the optimal transmit structure for SM has not been addressed in literature.

Perfect channel knowledge is however impractical, and channel estimation (CE) is of vital importance. A massive body of literature, e.g. [44] and [45], has been done on the topic of CE for multi-stream MIMO systems, where all transmit antennas can send their respective pilot signals simultaneously. While the property of a single active antenna benefits SM in saving energy and avoiding ICI, this challenges the channel estimation process: the transmit antennas have to be activated sequentially when sending the pilot signal. As a result, the CE time for SM is proportional to the number of transmit antennas. Unfortunately, this fact has so far been neglected in literature. In [46] and [47], the BER performance of SM with imperfect CSI is studied for uncorrelated channels and correlated channels, respectively. A similar work on SSK was reported in [48], where the effects of pilot sequence lengths were considered. Although the above papers fill some gaps in the knowledge, they have two major limitations: i) the CSI errors are artificial instead of being obtained from practical CE methods; and ii) the relation between the CE time and the number of transmit antennas is not addressed. Until now, only a few studies have been conducted to develop the CE methods for SM. In [49], the authors attempted to apply recursive least square (RLS) to SM. Another CE method for SM was introduced in [50], using joint channel estimation with data detection. However, those methods are based on existing CE techniques, and the issue of the costly CE time in SM remains to be unsolved.

When the scenario changes from single-user to multi-user/multi-cell, the interference between co-channel users becomes the bottleneck in wireless communications. Multi-user detection (MUD) methods for SM offer multiple accessing at the cost of an increase in the complexity of receivers [51, 52]. Alternatively, precoding techniques proposed in [53, 54] aim to cancel inter-user interference at the transmitter, while maintaining the same receiver structure as that for a single user. The above studies, however, failed to exploit the multi-user diversity, and their performance degrades as the number of users increases. So far, it appears that no user selection method has been investigated for multi-user SM systems. In the multi-cell scenario, with the aim of improving the overall system capacity in the multi-cell scenario, coordinated multi-point

(CoMP) transmission techniques and distributed antennas systems (DAS) are two research directions that draw considerable attention. The former enables the dynamic coordination of transmission and reception over a variety of different base stations, turning inter-cell interference into useful signals. The latter focuses on enhancing the quality of desired signals, where the antennas are distributed within a geographic area instead of being centralised. Research has been conducted to apply SM to CoMP or DAS systems [55, 56]. However, both methods have their respective shortcomings: CoMP is ineffective against multipath fading, while DAS is costly in deployment of antennas and backhauls. Effectively applying SM in a multi-cell scenario is still an open issue.

1.2 Contributions

In this thesis, the optimal transmit structure balancing the number of transmit antennas with the order of signal modulation is studied for SM in a single-user scenario. In addition, the difficulty in estimating CSI caused by a single active antenna is analysed, and three channel estimation methods specially tailored for SM are proposed. Finally, the application of SM in multi-user/multi-cell scenarios is investigated, and novel methods are proposed to exploit the multi-user diversity for SM systems. The results of the studies have been published in two journal papers in the *IEEE Transactions on Communications* and the *IEEE Transactions on Wireless Communications* [57, 58]. In addition, the results have been presented in eight conference papers at *IEEE GLOBECOM*, *IEEE ICC*, *IEEE VTC*, *IEEE PIMRC* and *IEEE CAMAD* [59–66].

1.2.1 Antenna selection

As a unique three-dimensional modulation scheme, SM enables a trade-off between the size of the spatial constellation diagram and the size of the signal constellation diagram for a certain spectrum efficiency. As a first contribution of this thesis, a novel two-stage TAS method is proposed to obtain the optimal transmit structure for SM that minimises the average bit error probability (ABEP). In the first step, the optimal number of transmit antennas is determined to balance the diversity gain against the degradation caused by channel correlation. The second step is to select the required number of transmit antennas from an antenna array. The BER performance of the proposed method is analysed for generalised fading channels as well as a

special case of Rayleigh fading channel, and in the latter a deployment table of the transmit structure is developed. In addition, the BER performance of the proposed method is compared with exhaustive search. The detailed work is presented in Chapter 3, and it has been published in [58–61].

1.2.2 Channel estimation

Because of the fact that SM has to activate transmit antennas sequentially for sending pilots, the CE process becomes challenging and using the traditional CE techniques for SM would severely compromise its throughput. As a second contribution of this thesis, novel CE methods are developed for SM in two aspects. On the one hand, the correlation information between antennas at the transmitter/receiver is exploited to improve the CE performance for SM. Based on the transmit-side antenna correlation, a novel CE method is proposed which enables SM to estimate the entire MIMO channel by sending the pilot signal through one antenna only. Another CE method, focusing on using the antenna correlation at the receiver, can increase the estimation accuracy without adding the pilot sequence length. On the other hand, the power allocation between pilot symbols and information-carrying symbols is significant to the BER performance. Allocating more energy to pilot symbols can increase the estimation accuracy, and thus reduce the probability of misdetections caused by imperfect CSIs. Meanwhile, the level of signal-to-noise ratio (SNR) is impaired since less energy is available for information-carrying symbols. Based on this fact, the optimal power allocation (OPA) between those two types of symbols is studied for SM systems. In addition, OPA is able to combine with the above two methods to further improve the performance of SM. The studies with respect to the channel estimation for SM are presented in Chapter 4, and they have been published in [57, 62–64].

1.2.3 Exploitation of multi-user diversity

As a third contribution of this thesis, the exploitation of multi-user diversity is studied for SM systems in the multi-user/multi-cell scenario. When serving multiple users in the same time-frequency slot, the transmit antennas of a SM system are divided into groups and each group is dedicated to one user. In order to intelligently allocate the antennas to users, a novel method is proposed to deal with the management and selection of antennas. The performance of the proposed method is compared with multi-user SM when no antenna management is applied. This study is presented in Chapter 5, and it has been published in [66]. When considering

the multi-cell scenario, a novel cooperative scheme is proposed to combine the advantages of CoMP and DAS techniques. The proposed scheme enables the mobile users to be served by multiple BSs dynamically. Similar to the multi-user scenario, antenna management is needed here for the co-channel users in different cells. The cooperative scheme can improve the quality of service for cell-edge users significantly, but barely for cell-centre users. A three-tier cellular architecture is therefore proposed to demarcate the effective region for the cooperative scheme. The cooperative SM framework and the results of the studies are presented in Chapter 6.

1.3 Thesis outline

The remainder of the thesis is organised as follows. **Chapter 2** introduces the fundamentals of SM, including the transmission principle, the detection methods and the analysis with respect to its advantages and disadvantages.

Chapter 3 presents the work on optimising the transmit structure of SM for a single user. Section 3.2 introduces the system model, including the signal model, the channel model and the detector. In Section 3.3, the optimal transmit structure of SM is derived. Section 3.4 discusses the optimal transmit structure in a special case of Rayleigh fading. The optimality of the proposed method is verified through a Monte Carlo simulation in Section 3.5.

Chapter 4 elaborates the CE process for SM systems. Section 4.2 introduces the channel model and the model of pilot-assisted estimator. Two novel CE methods, focusing on exploiting the correlation between antennas at the transmitter/receiver, are presented in Section 4.3 and Section 4.4, respectively. Section 4.5 presents the optimal solution to allocate the transmission power between pilot symbols and information-carrying symbols. The framework of combined CE is studied in Section 4.6.

In **Chapter 5**, the general model of multi-user SM is presented in Section 5.2. It includes the bitstream mapping for multiple users and the channel model. Section 5.3 depicts the precoding method for multi-user SM and the decoding process. In Section 5.4, a novel method is proposed to manage the antennas in multi-user SM. The performance of the proposed method is analysed in Section 5.5.

Chapter 6 discusses the application of SM in a multi-cell scenario. Section 6.2 introduces the model of cellular networks. The work of applying SM to the CoMP system is presented in

Section 6.3. Section 6.4 presents a novel cooperative scheme for SM which enables the users to be served by multiple BSs. In Section 6.5, the effective region of the proposed scheme is discussed. Simulation results of the studies are shown in Section 6.6.

Finally, **Chapter 7** concludes the thesis with the key findings of this study. The limitations of the work are discussed, and an outlook for future work is presented.

1.4 Chapter summary

Acknowledging the costly energy consumption of multi-stream MIMO schemes, some of the notable advances in the current SM systems have been presented in this Chapter. The main challenges in improving the capacity of SM systems considering the limitations of a single active antenna have been introduced. In this context, methods to maximise the system capacity of SM in single-user, multi-user and multi-cell scenarios have been summarised as the contributions of this thesis. The Chapter concluded with the thesis outline.

Category	Description
Antenna selection	A subset of antennas is selected from a large antenna array in order to increase the antenna diversity.
Precoding	A precoding mask is added before sending out the signal so that the channel characteristics can be altered as designed.
Equalisation	An equaliser is a filter at the receiver that tackles inter-symbol interference. Those filters are normally based on the knowledge of the channel statistics or the transmitted signal's statistics.
Space-time coding (STC)	STCs are aimed to improve decoding reliability by transmitting multiple, redundant copies of a data stream.
Channel coding	Channel coding introduces redundant bits, i.e. parity bits, into each symbol to reduce decoding errors.

Advantages	Limitations	Relevant references
Antenna selection does not increase the complexity of receivers.	A large number of antennas and additional processing power for selection are required.	[19, 24–28]
Precoding does not require additional antennas.	Feedback is needed to inform the transmitter of the channel knowledge.	[29–32]
Equalisation does not require any change of the transmitters.	The equalisation process increases the complexity of receivers and causes delay.	[33–36]
STCs are readily implemented as they simply duplicate the signals to be transmitted.	Both STCs and channel coding schemes cost additional bandwidth and increase decoding complexity.	[37–40]
Channel coding does not require any channel knowledge at the transmitter.		[41–43]

Table 1.1: *Major categories of technologies on improving the BER performance for MIMO schemes in a single-user scenario.*

Chapter 2
Background

2.1 Introduction

Multiple-input multiple-output (MIMO) refers to the methods that use multiple transmit and receive antennas to multiply the capacity of a radio link. Compared with the traditional wireless communication system of a single antenna, MIMO techniques are able to increase the data rate significantly without additional bandwidth or transmission power. Due to the dense deployment of wireless networks and the enormous increase of mobile devices, the spectrum resource of radio-frequency (RF) band has become exhausted. This has drawn much attention to the development of MIMO systems to satisfy the exponentially increasing demand for data rates. In this chapter, a new perception of categorising the MIMO techniques is introduced, where spatial modulation (SM) is presented as a unique single-stream MIMO scheme. Next, the transmission principle of SM and different detection methods are discussed.

2.2 Multiple-input multiple-output

2.2.1 The development of MIMO

The concept of MIMO has emerged over the past two decades. In April 1996, Gregory Raleigh and John Cioffi were first to propose that natural multipath propagation can be exploited to transmit multiple, independent information streams using co-located antennas and multi-dimensional signals [67]. Up to that time, radio engineers had treated natural multipath propagation as an impairment to be mitigated. Later that year, Gerard Foschini also suggested it is possible to multiply the channel capacity of a wireless link through layered space-time signalling [68]. Two years later, Bell Labs demonstrated the first laboratory prototype of spatial multiplexing, which is well known as vertical Bell Laboratories layered space-time (V-BLAST) [69]. At the same time, Siavash Alamouti proposed the famous Alamouti coding [70], which was then extended to space-time block coding (STBC) by Tarokh *et al.* [71]. MIMO techniques are often combined with orthogonal frequency division multiplexing (OFDM) to achieve higher

data rates [67, 72]. In the recent decade, MIMO-OFDM has become the foundation of most advanced wireless local area network (WLAN) standards and the dominant air interface for broadband wireless communications. In 2003, Airgo Networks designed and shipped the first MIMO-OFDM chipsets for what became the IEEE 802.11n standard (commercialised as WiFi), supporting up to four spatial streams and a maximum net data rate of 600 Mbit/s. Meanwhile, MIMO-orthogonal frequency division multiplexing access (MIMO-OFDMA) based solutions were developed for IEEE 802.16e standard (commercialised as WiMAX). Multi-user MIMO was included in IEEE 802.11ac standard, allowing up to four simultaneous downlink clients with up to eight spatial streams for each client. MIMO technology is also planned to be used in mobile radio telephone standards, such as high-speed packet access plus (HSPA+) and long-term evolution (LTE) in 3rd Generation Partnership Project (3GPP).

When compared with single-input single-output (SISO) systems, MIMO techniques offer a number of advantages that are usually described by the terms array gain, diversity gain and multiplexing gain [73]. The array gain denotes the improvement of signal-to-noise ratio (SNR) at the receiver, which can be obtained through a coherent combining effect of the information signals, such as equal-gain combining, selection combining and maximum-ratio combining. Alternatively, those combining schemes can request less transmission power than SISO to achieve the equivalent level of SNR, leading to interference mitigation between co-channel users. Based on this point of view, the diversity gain is defined as the increase in signal-to-interference ratio, while there is not a loss of SNR against SISO. The array gain and the diversity gain are both metrics with respect to the capability of decoding transmitted signals. In contrast, multiplexing gain measures the growth in data rates offered by spatial multiplexing schemes, e.g. V-BLAST and STBC. Those methods convey different data streams simultaneously, and thus can increase the channel capacity without additional bandwidth or transmission power. It is worth noting that the three types of gains are exchangeable [74]. Spatial multiplexing schemes can also achieve array gain or diversity gain by lowering the modulation order of each data stream.

Another widely used classification of the MIMO techniques is based on exploiting antenna diversity at the receiver side or at the transmitter side. The receive-diversity MIMO, such as the combining schemes, benefits from the propagation difference between the receive antennas. Those methods however normally work with one transmit antenna only, due to the fact that two signals received at the same antenna could diminish each other. The remedies, such as maximum ratio transmission (MRT) [75], request channel side information at the transmitter (CSIT)

for modifying the signals to be transmitted. The propagation difference between transmit antennas, on the other hand, is exploited in the transmit-diversity MIMO, e.g. STBC. Note that STBC does not need CSIT, and multiple receive antennas are applicable. In addition, V-BLAST is a transmit-receive diversity scheme which relies on the multiplicity of both transmit antennas and receive antennas.

Recent research on MIMO includes antenna selection, multi-user MIMO, massive MIMO and cooperative MIMO. Antenna selection methods, including transmit antenna selection and receive antenna selection, aim to increase the diversity between operative antennas by selecting a subset of an antenna array that minimises the bit error rate (BER) [24]. Multi-user MIMO allows multiple transmitters to send separate signals and multiple user terminals to receive separate signals simultaneously in the same band [76]. Multi-user detection (MUD) [77] or the precoding technique [78], making use of channel side information at the receiver (CSIR) and CSIT respectively, is normally employed to eliminate the interference between co-channel users. In order to boost the spectrum efficiency by supporting a large number of user terminals in the same time-frequency slot, massive MIMO considers a very large number of base station antennas (e.g. hundreds or thousands) operating in a multi-user MIMO environment [79]. Cooperative MIMO enables single-antenna terminals in a multi-user system to share their antennas and thus creates a virtual multiple-antenna transmitter for uplink services [80].

2.2.2 A new perception of MIMO classification

While MIMO techniques offer a variety of gains over SISO, more RF chains are needed to fit the increase in the number of data streams. Each RF chain requires a power amplifier (PA), which consumes about 60% of the entire energy of an RF chain [6]. As a result, the system requires more quiescent power to increase the number of RF chains. When delivering the same amount of total transmission power, using more RF chains in a MIMO system leads to a lower energy efficiency. This raises a concern over the number of RF chains needed, and MIMO schemes are thus classified into two categories: multi-stream MIMO and single-stream MIMO.

The traditional MIMO schemes, e.g. V-BLAST and STBC, are multi-stream MIMO as they convey different data streams simultaneously. In V-BLAST, the data stream is split into several slices, and each slice is emitted through one antenna. STBC, different from V-BLAST, sends multiple copies of the slices and exploits channel orthogonality based on the various received versions of the data. Nevertheless both V-BLAST and STBC require one RF chain for each

transmit antenna, i.e. the number of required RF chains is equal to the number of transmit antennas. Another type of multi-stream MIMO is that the number of required RF chains is smaller than the number of transmit antennas but larger than one, e.g. generalised spatial modulation (GSM).

Conversely, single-stream MIMO refers to the MIMO schemes employing a single RF chain, regardless of the number of antennas used. There are two types of single-stream MIMO. One is when the same signal is sent through multiple transmit antennas simultaneously, e.g. MRT. The other one is that a single transmit antenna is activated at any time instance, such as space shift keying (SSK) [15] and SM [3]. In SSK, the entity of transmit antennas comprises the constellation diagram of modulation, and the information bits are solely carried by the index of the active antenna. With the same mechanism of antenna activation as that in SSK, SM conveys extra information bits by combining with the conventional signal modulation. Due to the need for a single RF chain, single-stream MIMO schemes exhibit a great saving in quiescent power in comparison with multi-stream MIMO.

2.3 Spatial modulation

2.3.1 Transmission principle

The basic concept of SM is to map the information bits of each block into two information carrying units:

- One transmit antenna is activated from the antenna array.
- One symbol is determined out of a certain signal constellation diagram.

Taking four transmit antennas as an example, Fig. 2.1 illustrates the bitstream mapping of SM systems. For instance, quadrature phase shift keying (QPSK) is considered. The bits used for selecting the active antenna are in given red colour, whereas the bits for picking one symbol from the signal constellation diagram are shown in blue colour. The chosen symbol is then sent from the currently active antenna. At the receiver, the index of the active antenna and the transmitted symbol are both decoded to retrieve the information bits. The detection methods for SM are discussed in Section 2.4.

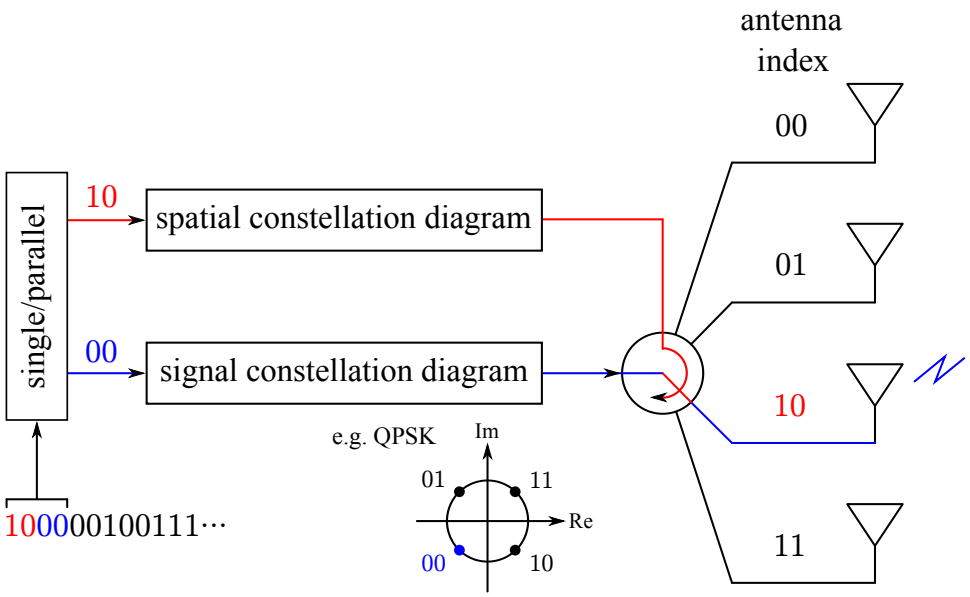

Figure 2.1: *Bitstream mapping in SM.*

A $N_t \times N_r$ SM system is considered in a general way, where N_t and N_r are the number of transmit antennas and the number of receive antennas, respectively. The size of the spatial constellation diagram is exactly the number of transmit antennas, and the size of the signal constellation diagram is denoted by M. The bitstream is divided into blocks with the length of η_s bits, where $\eta_s = \log_2(N_t) + \log_2(M)$ is the number of bits per symbol. Each block is then split into two units of $\log_2(N_t)$ and $\log_2(M)$ bits. The first part activates a single transmit antenna from the spatial constellation diagram, and the currently active antenna is denoted by t_{act}. The second part selects one symbol χ_l $(1 \leq l \leq M)$ from the signal constellation diagram, and sends it out through the activated antenna. The transmitted signal of SM is represented by a vector $\mathbf{x} = [0, \ldots, x_{t_{\text{act}}}, \ldots, 0]^T$ of N_t elements, where the t_{act}-th element is χ_l and all other elements are zero. The received signal is denoted by a vector $\mathbf{y}$ of N_r elements, and it is expressed as:

$$\mathbf{y} = \mathbf{H}\mathbf{x} + \mathbf{w}, \tag{2.1}$$

where $\mathbf{H}$ denotes the MIMO channel matrix; $\mathbf{w} = [w_1, \ldots, w_r, \ldots, w_{N_r}]^T$ and w_r is the noise at the r-th receive antenna. The t-th column of $\mathbf{H}$ is denoted by $\mathbf{h}_t$. Since all elements in $\mathbf{x}$ but $x_{t_{\text{act}}}$ are zero, (2.1) can be reduced to:

$$\mathbf{y} = \mathbf{h}_{t_{\text{act}}} x_{t_{\text{act}}} + \mathbf{w}. \tag{2.2}$$

2.3.2 Constellation diagram

In addition to the two dimensions of signal constellation diagrams, i.e. amplitude and phase, SM adds in an extra dimension of antenna index. For this reason, SM is entitled as a tri-dimensional modulation scheme. The received signal is however still of two dimensions, and this raises a question: what is the constellation diagram of SM like in the domain of two dimensions?

Fig. 2.2 shows the equivalent constellation diagram of SM in two dimensions. The two charts on the left side are the signal constellation diagram and the diagram of channel coefficients. Each dot in the latter diagram denotes the link attenuation from one of the transmit antennas to a certain receive antenna, and the dot related to the active antenna is marked in red colour. On the right side is the constellation diagram of received symbols at a certain receive antenna. The dot in pink colour represents the desired symbol, which is the production of the transmitted symbol and the channel coefficient of the active antenna. The remaining dots are the symbols that can possibly be decoded.

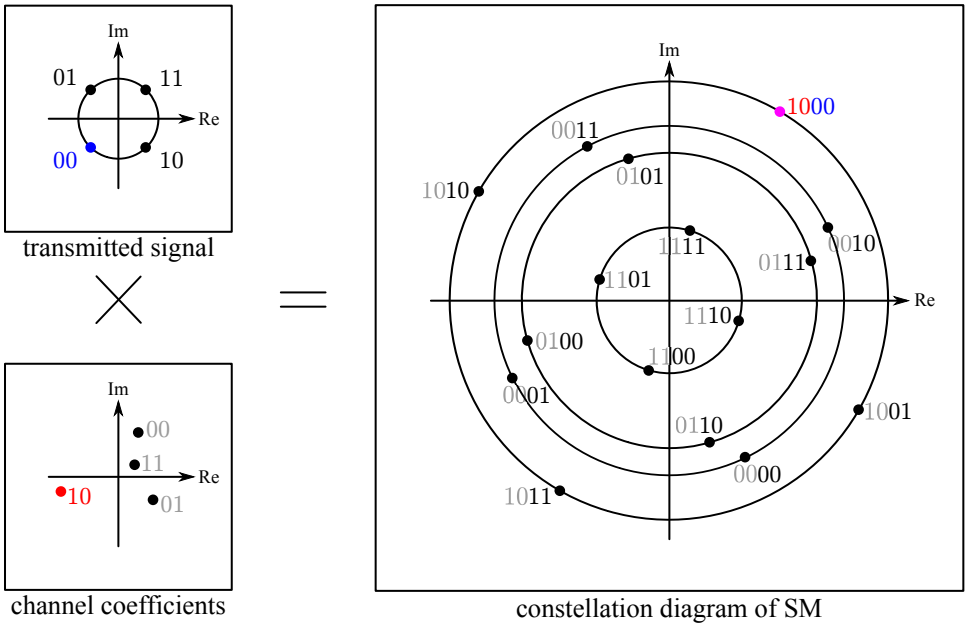

Figure 2.2: *The equivalent constellation diagram of SM in two dimensions.*

When compared with phase shift keying (PSK), SM offers multiple levels of amplitude in the constellation diagram. This property is similar to quadrature amplitude modulation (QAM), but SM does not need to grade the transmit power, leading to a more efficient usage of transmit energy than QAM. However unlike fixed symbol positions in QAM, the symbol positions in

SM are variable as they depend on channel coefficients. This introduces an uncertainty in the Hamming distance between symbols. In this case, the pair of symbols “0010” and “0111” and other three pairs have a much smaller Hamming distance than the other pairs of symbols. This is because the corresponding two channel coefficients are close to each other in amplitude. As the channel correlation increases, the channel coefficients of different transmit antennas would become statistically closer to each other. Consequently, the Hamming distances in the constellation diagram of SM decrease, making it difficult to detect the desired symbols.

2.3.3 Advantages and disadvantages of spatial modulation

2.3.3.1 Advantages of spatial modulation

The four main advantages of SM can be summarised as follows:

- SM offers a higher spectrum efficiency than SISO systems. In addition to the traditional signal modulation, SM conveys extra information bits through activating one of the transmit antennas. The multiplexing gain offered by SM is a logarithm to base 2 with respect to the number of transmit antennas. This also results in SM having a larger capacity than the traditional low-complexity coding methods for MIMO systems such as STBC.

- In contrast to the conventional MIMO schemes, e.g. V-BLAST and STBC, SM completely avoids inter-channel interference (ICI) due to using a single active antenna.

- Another important benefit from a single active antenna is that SM requires only one RF chain, regardless of the number of transmit antennas used. Compared with the multi-stream MIMO schemes of multiple RF chains, SM exhibits a significant energy saving in terms of quiescent power at the power amplifier stage.

- SM is able to operate under the condition $N_r < N_t$. In contrast, V-BLAST requires a number of receive antennas larger than or equal to the number of transmit antennas. In addition, V-BLAST needs a high-complexity receiver to perform successive interference cancellation, whereas SM inherently has a simple receiving structure, due to the complete avoidance of ICI.

2.3.3.2 Disadvantages of spatial modulation

The four main disadvantages of SM can be summarised as follows:

- SM requires at least two transmit antennas.
- When compared with V-BLAST, SM can offer only a logarithmic (instead of linear) increase of the data rate with the number of transmit antenna. This could impede SM to achieve a high spectrum efficiency when the number of transmit antennas is limited due to some practical reasons, e.g. the compact size of mobile devices.
- The BER performance of SM is impaired by channel correlations, like all other MIMO schemes. As previously analysed, when the links of different transmit antennas are not diverse sufficiently, SM might encounter difficulties in identifying the active antenna from the idle antennas.
- SM needs channel state information (CSI) to decode the transmitted signal. In order to acquire CSI of the entire MIMO channel, SM has to activate all transmit antennas sequentially for the sending of training signals. Therefore the time consumed by the channel estimation process for SM is proportional to the number of transmit antennas. This leads to a significant compromise of throughput, especially when a large number of transmit antennas are used.

2.4 Detection methods for spatial modulation

2.4.1 Two-stage detection

A two-stage detection method was proposed for SM in [3]. The first step is to estimate the index of the currently active antenna, and this is formulated as follows:

$$\hat{t}_{\text{act}} = \underset{t_{\text{act}}}{\text{argmin}} \parallel \mathbf{g} \parallel, \tag{2.3}$$

where $\mathbf{g} = [g_1, \ldots, g_t, \ldots, g_{N_t}]^T$ and $g_t = \mathbf{h}_t^H \mathbf{y}$. The second step is to detect the transmitted symbol based on the decoding result of t_{act}:

$$\hat{l} = \underset{l}{\text{argmin}} \parallel \chi_l - g_{\hat{t}_{\text{act}}} \parallel . \tag{2.4}$$

The computational complexity of this two-stage detection is $O(N_t + M)$, where $O(\cdot)$ is used to classify algorithms by how they respond to changes in input size. The two-stage detection method is however not optimal, as it causes error propagations when an incorrect decision is made on detecting the active antenna.

2.4.2 Joint maximum likelihood detection

With the aim of implementing an optimal detection for SM, the joint maximum likelihood (ML) detection was introduced in [9]. The active antenna and the transmitted symbol are decoded together as follows:

$$\left[\hat{t}_{\text{act}}, \hat{l}\right] = \arg\min_{t,l} \parallel \mathbf{h}_t \chi_l - \mathbf{y} \parallel^2 . \tag{2.5}$$

Although offering much better decoding performance than the two-stage detection method, the joint ML detection requires much higher computational complexity ($O(N_t M)$) than the two-stage detection. Despite this, the joint ML detection is in common use due to the need for analysing the BER bound.

2.4.3 Sphere decoding

With the aim of reducing the computational complexity of the joint ML detection, the sphere decoding (SD) techniques for SM were proposed, including receiver-centric SD (Rx-SD) [81] and transmitter-centric SD (Tx-SD) [82]. Rx-SD aims to reduce the search space of receive antennas. The decoding process can be written as follows:

$$\left[\hat{t}_{\text{act}}, \hat{l}\right]_{\text{Rx-SD}} = \arg\min_{t,l} \sum_{r=1}^{\tilde{N}_r(t,l)} \parallel y_r - h_{r,t}\chi_l \parallel^2, \tag{2.6}$$

where $1 \leq \tilde{N}_r(t,l) \leq N_r$ is the number of Euclidean distance evaluations $\left(\parallel y_r - h_{r,t}\chi_l \parallel^2\right)$ that have to be calculated by the Rx-SD detector. Given a sphere with radius R, $\tilde{N}_r(t,l)$ is computed by:

$$\tilde{N}_r(t,l) = \max_{n \in \{1,2,\ldots,N_r\}} \left\{ n \left| \sum_{r=1}^{n} \parallel y_r - h_{r,t}\chi_l \parallel^2 \leq R^2 \right. \right\}. \tag{2.7}$$

Rx-SD is most effective when the number of receive antennas is large. Otherwise Rx-SD fails

to lower the computational complexity of the ML-optimum detector. Alternatively, Tx-SD reduces the range of symbols to be searched as follows:

$$\left[\hat{t}_{\text{act}}, \hat{l}\right]_{\text{Tx-SD}} = \underset{(t,l)\in\Theta_{\text{R}}}{\arg\min} \parallel \mathbf{h}_t \chi_l - \mathbf{y} \parallel^2, \tag{2.8}$$

where Θ_{R} is the subset of points (t, l) that lie inside a sphere centred around the received signal and with radius R. Due to a reduction of the full search space, the computational complexity of sphere decoding methods is lower than the joint ML detection, but higher than the two-stage detection.

2.5 Chapter summary

In this chapter, a brief summary of the history of MIMO has been presented. According to the number of required RF chains, a new perception of MIMO classification has been introduced. It was pointed out that SM is a unique single-stream MIMO transmission technique. The transmission principle of SM has been detailed, and the equivalent constellation diagram of SM in two dimensions has been analysed. In addition, the advantages and disadvantages of SM have been presented. Finally, the detection methods for SM have been summarised.

Chapter 3
Optimum transmitter design for spatial modulation

3.1 Introduction

One key property of spatial modulation (SM) is that there are two constellation diagrams: the spatial constellation diagram and the signal constellation diagram. Using the antenna index to carry information bits can offload the density of signal constellation points, especially when a high spectrum efficiency is required. However, this fact does not mean the SM system should use as many transmit antennas as possible. As the channel correlation increases, the channel coefficients of different antennas are closer to each other. This impedes the ability of distinguishing the active antenna from the others, leading to a trend of using less transmit antennas. Given a spectrum efficiency, SM enables a trade-off between the size of spatial constellation diagram and the size of signal constellation diagram. Consequently, there exists the optimal combination of those two constellation diagrams that minimises the bit error rate (BER). In this chapter, an optimum transmit structure is proposed for SM by developing the above concept. In addition, the total energy consumption of base stations (BSs) is studied.

3.2 System model

3.2.1 Dynamic modulation

A $N_t \times N_r$ SM-MIMO system is considered for a single user, where N_t and N_r denote the number of transmit antennas and the number of receive antennas, respectively. Unlike in the original SM system, only a subset of the transmit-antenna array is in use. The number of used transmit antennas, i.e. the size of the spatial constellation diagram, is denoted by N. The size of the signal constellation diagram is denoted by M. The bit stream is divided into blocks with the length of η_s bits, where $\eta_s = \log_2(N) + \log_2(M)$ is the number of bits per symbol. Each block is then split into two units of $\log_2(N)$ and $\log_2(M)$ bits. The first part activates a

single transmit antenna from the spatial constellation diagram, and the currently active antenna is denoted by t_{act}. The second part selects a symbol χ_l $(1 \leq l \leq M)$ from a specific signal constellation diagram, such as phase shift keying (PSK) or quadrature amplitude modulation (QAM), and sends it out through the activated antenna. The transmitted signal is represented by a vector $\mathbf{x} = [0, \ldots, x_{t_{\text{act}}}, \ldots, 0]^T$ of N elements, where the t_{act}-th element is χ_l and all other elements are zero. The received signal is expressed as:

$$\mathbf{y} = \mathbf{H}\mathbf{x} + \mathbf{w}, \tag{3.1}$$

where **H** stands for the channel matrix, of which the details are presented in Section 3.2.2; $\mathbf{w} = [w_1, w_2, ..., w_{N_r}]^T$ is the noise vector, and each noise component is a sample of complex additive white Gaussian noise with distribution $\mathcal{CN}(0, N_0)$. Across the receive antennas, the noise components are statistically independent. The signal-to-noise ratio (SNR) is defined as $\gamma = E_m L/N_0$, where E_m denotes the average energy per symbol transmission and L is the path loss without shadowing. In addition, the radio-frequency (RF) output energy consumed for conveying one bit is denoted by $E_b = E_m/\eta_s$. At the receiver, the transmitted signal is decoded by the joint maximum likelihood (ML) detection in (2.5).

3.2.2 Channel model

3.2.2.1 Channel distribution

The fading coefficient of the link from the t-th transmit antenna to the r-th receive antenna is denoted by $\alpha_{r,t} = \beta_{r,t}\text{exp}(j\varphi_{r,t})$, where $\beta_{r,t}$ and $\varphi_{r,t}$ are the amplitude and the phase, respectively. The channel fading distribution as well as channel state information (CSI) is assumed to be known at the receiver. Nakagami-m fading is widely used to model attenuation of wireless signals traversing multiple paths. Thus $\beta_{r,t} \sim \text{Nakagami}(m_{r,t}, \Omega_{r,t})$, where $m_{r,t}$ is the shape parameter (when $m_{r,t} = 1$, the channel is Rayleigh fading) and $\Omega_{r,t}$ is the spread controlling parameter. The phase $\varphi_{r,t}$ is uniformly distributed between $(-\pi, \pi]$.

3.2.2.2 Channel correlation

Since we focus on selecting the transmit antennas, the receive antennas are assumed to be independent without loss of the generality. The correlation coefficient between the amplitudes

of the two propagation paths from the transmit antennas t_i and t_j to the r-th receive antenna is denoted by $\rho_{t_i,t_j,r}$. Note that the correlation model here is for the purpose of understanding the relationship between the proposed method and the channel correlation. For the sake of simplicity, the exponential correlation matrix model in [83] is considered, which is based on the fact that the channel correlation decreases with increasing the distance between antennas. As shown in Fig. 3.1, the transmit antennas are located in a normalised square area, i.e. the distance between t_1 and t_A is unity. The correlation coefficient between between t_1 and t_A with respect to the r-th receive antenna is denoted by $\rho_{s(r)}$. The number of antennas on each side of the antenna array is formulated as follows:

$$A = \begin{cases} \sqrt{N_t} & \text{if } \log_2(N_t) \text{ is even} \\ 3 \times \sqrt{\frac{N_t}{8}} & \text{if } \log_2(N_t) \text{ is odd} \end{cases}. \tag{3.2}$$

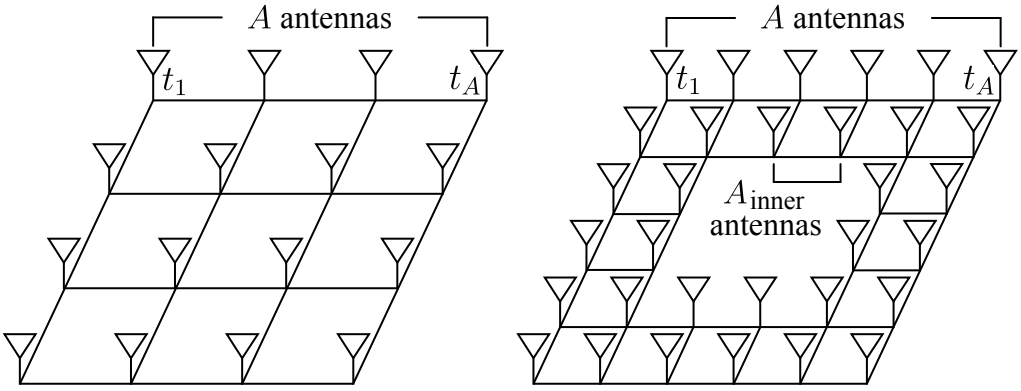

(a) $N_t = 16$ (b) $N_t = 32$

Figure 3.1: *Placement of transmit antenna arrays.*

When $\log_2(N_t)$ is even, the antennas form a square array with the dimension of $A \times A$. If $\log_2(N_t)$ is odd, the antennas are placed in the shape shown in Fig. 3.1(b), where $A_{\text{inner}} = \sqrt{\frac{N_t}{8}}$. Denoting the absolute distance between t_i and t_j by d_{t_i,t_j}, the correlation between those two antennas is given by [83, Eq. (10)]:

$$\rho_{t_i,t_j,r} = \rho_{s(r)}^{d_{t_i,t_j}}, \qquad 0 \leq \rho_{s(r)} \leq 1, \tag{3.3}$$

and the average channel correlation, denoted by ρ_{av}, is calculated by:

$$\rho_{\text{av}} = \frac{1}{N_r} \sum_{r=1}^{N_r} \left(\frac{1}{N_t(N_t-1)} \sum_{t_i=1}^{N_t} \sum_{t_j \neq t_i=1}^{N_t} \rho_{t_i,t_j,r} \right). \tag{3.4}$$

3.2.3 Base station power model

In [6], a linear relationship between the RF output power and the overall consumed power of a multi-sector BS was established. The overall BS power consumption is divided into two parts: the load-dependent portion and the constant portion. The former is dependent on the RF output power, while the latter is invariant. In addition, when no data is transmitted, a sleep mode is enabled to reduce the consumption by switching off unneeded components. The details of the BS power model are presented as follows.

3.2.3.1 Power model

Based on the above literature, a power model named SOTA 2010 was proposed for BSs with one sector and one RF chain [84]. This power model is chosen here due to two facts: i) it is based on empirical results; ii) it suits the the property of a single RF chain in SM. Table 3.1 specifies the parameters: P_{max} is the maximum RF output power; P_0 and P_s denote the constant power consumption in the active mode and the sleep mode, respectively; ζ stands for the slope that quantifies the load dependence. The instantaneous BS power consumption, denoted by P_{in}, is formulated as a function of the RF output power P_{out} [84, Eq. (1)]:

$$P_{\text{in}} = \begin{cases} P_0 + \zeta P_{\text{out}} & \text{if} \quad 0 < P_{\text{out}} \leq P_{\text{max}} \\ P_s & \text{if} \quad P_{\text{out}} = 0 \end{cases}. \tag{3.5}$$

Power model	P_{max} (W)	P_0 (W)	P_s (W)	ζ
SOTA 2010	40	119	63	2.4

Table 3.1: *BS power model parameters.*

Also, the ratio of the time consumed in the active mode and the total period is referred to as the activation ratio ϱ. The average power consumption of a single-RF-chain BS is thus computed by:

$$P_{\text{BS}} = \varrho(P_0 + \zeta P_{\text{out}}) + (1-\varrho)P_s. \tag{3.6}$$

Unlike SM using a single RF chain, multi-stream MIMO schemes require multiple RF chains to activate the transmit antennas simultaneously. For N_{act} *activated* antennas, the RF output power of each antenna is $1/N_{\text{act}}$ of P_{out}. As a result, the overall power consumption of a BS with multiple RF chains is calculated by:

$$P_{\text{BS}} = N_{\text{act}} \left[\varrho \left(P_0 + \zeta \frac{P_{\text{out}}}{N_{\text{act}}} \right) + (1 - \varrho) P_s \right]. \tag{3.7}$$

3.2.3.2 Continuous mode and DTX mode

There are two modes for operating the RF chains: the continuous mode and the discontinuous transmission (DTX) mode [85]. In the continuous mode, the RF chains are always delivering output power of the same level. As a result, P_{out} is equal to the average RF output power, denoted by $\bar{P}_{\text{out}}$, and $\varrho = 1$. Substituting those conditions into (3.7), the overall BS power consumption in the continuous mode is obtained by:

$$P_{\text{BS(cont.)}} = N_{\text{act}} P_0 + \zeta \bar{P}_{\text{out}}. \tag{3.8}$$

The data rate of the continuous mode is equal to the average data rate, which is denoted by $\bar{R}_b = \bar{P}_{\text{out}}/E_b$. Conversely, the DTX mode conveys data with full load, and the instantaneous data rate is $R_{b\text{max}} = P_{\text{max}}/E_b$ that is higher than $\bar{R}_b$. Then the system is enabled into sleep mode during the saved time to maintain the same average data rate. The parameter ϱ of the DTX mode is computed by:

$$\varrho = \frac{\bar{R}_b}{R_{b\text{max}}} = \frac{\bar{P}_{\text{out}}}{P_{\text{max}}}. \tag{3.9}$$

Substituting (3.9) and $P_{\text{out}} = P_{\text{max}}$ into (3.7), the overall BS power consumption in the DTX mode is expressed as:

$$P_{\text{BS(DTX)}} = N_{\text{act}} P_s + \left(\zeta + \frac{N_{\text{act}}(P_0 - P_s)}{P_{\text{max}}} \right) \bar{P}_{\text{out}}. \tag{3.10}$$

3.3 Optimum transmit structure over generalised channels

As mentioned, SM enables to trade off the size of signal constellation diagrams with the size of spatial constellation diagrams. To achieve a certain spectrum efficiency η_s, there are $\eta_s + 1$ possible combinations of (M, N), based on the requirement of a power of two to provide a full

usage in the constellation diagrams. In order to supply a complete selection range of N, N_t is set to be equal to 2^{η_s}. In this section, an optimisation algorithm is presented to select the best (M, N) as well as the specific antennas. The context is arranged in four portions: i) an average bit error probability (ABEP) upper bound is introduced for SM over generalised fading channels; ii) the ABEP upper bound is simplified to suit the minimisation on the subject of either M or N; iii) the optimum (M, N) is obtained by solving the minimisation problem; and iv) the required number of transmit antennas are selected from the antenna array.

3.3.1 ABEP upper bound

Union bound is widely used to evaluate event probability, which says that the probability that at least one of the events happens is no greater than the sum of the probabilities of the individual events [86]. Based on the joint ML detection, the ABEP upper bound of SM is given by [12, Eq. (6)]:

$$\text{ABEP} \leq \text{ABEP}_{\text{spatial}} + \text{ABEP}_{\text{signal}} + \text{ABEP}_{\text{joint}}, \tag{3.11}$$

where:

$$\begin{cases} \text{ABEP}_{\text{spatial}} = \dfrac{\log_2(N)}{\eta_s M} \displaystyle\sum_{l=1}^{M} \text{ABEP}_{\text{SSK}}(l) & \text{(3.12a)} \\ \text{ABEP}_{\text{signal}} = \dfrac{\log_2(M)}{\eta_s N} \displaystyle\sum_{t=1}^{N} \text{ABEP}_{\text{MOD}}(t) & \text{(3.12b)} \\ \text{ABEP}_{\text{joint}} = \dfrac{1}{\eta_s M N} \displaystyle\sum_{t_i=1}^{N} \sum_{l_i=1}^{M} \sum_{t_j \neq t_i=1}^{N} \sum_{l_j \neq l_i=1}^{M} \text{ABEP}_{\text{MIX}} & \text{(3.12c)} \end{cases}$$

with the terms in summations expressed as:

$$\begin{cases} \text{ABEP}_{\text{SSK}}(l) = \dfrac{1}{N \log_2(N)} \displaystyle\sum_{t_i=1}^{N} \sum_{t_j \neq t_i=1}^{N} N_H(t_j \to t_i) \text{APEP}((t_j, \chi_l) \to (t_i, \chi_l)) & \text{(3.13a)} \\ \text{ABEP}_{\text{MOD}}(t) = \dfrac{1}{M \log_2(M)} \displaystyle\sum_{l=1}^{M} P_s(l, t) & \text{(3.13b)} \\ \text{ABEP}_{\text{MIX}} = N_H((t_j, \chi_{l_j}) \to (t_i, \chi_{l_i})) \text{APEP}((t_j, \chi_{l_j}) \to (t_i, \chi_{l_i})) & \text{(3.13c)} \end{cases}$$

where $P_s(l, t)$ is the average symbol error rate of the symbol χ_l emitted from transmit antenna t; $N_H(\cdot)$ denotes the Hamming distance; the probability of pair-wise error event is defined as

the average pair-wise error probability (APEP), which is computed by [12, Eq. (5)]:

$$\text{APEP}((t_j, \chi_{l_j}) \to (t_i, \chi_{l_i})) = \mathbf{E}\left\{ Q\left(\sqrt{\frac{\gamma |\alpha_{t_j}\chi_{l_j} - \alpha_{t_i}\chi_{l_i}|^2}{4}} \right) \right\}, \tag{3.14}$$

where $\mathbf{E}\{\cdot\}$ is the expectation operator and $Q(x)$ stands for the Q-function.

3.3.2 Optimisation problem

Due to the relaxation of linearity requirements, unlike QAM, PSK can work in power amplifier (PA) saturation [87]. This makes PSK a more energy efficient modulation scheme. In addition, results in [12] have shown that for SM, PSK is not worse than QAM in many cases and in some cases it is even better. For those reasons, PSK modulation is assumed where each symbol has an equal amplitude. As a result, the average over different signal symbols in (3.12) can be neglected and $P_s(t, l)$ reduces to $P_s(t)$.

3.3.2.1 ABEP of spatial part

First, we focus on the term $\text{ABEP}_{\text{spatial}}$ in the union bound. Assuming a sufficiently high SNR, the APEP of SSK over correlated Nakagami fading can be obtained by the moment generate function (MGF) as follows [88, Eq. (15)]:

$$\text{APEP}(t_j \to t_i) = \frac{2^{3N_r-1}\Gamma(N_r + 0.5)}{\gamma^{N_r}\sqrt{\pi}\Gamma(N_r + 1)} \prod_{r=1}^{N_r} f(r), \tag{3.15}$$

where:

$$f(r) = \frac{m_r(\Omega_{r,t_i}\Omega_{r,t_j})^{m_r-1}(1 - \rho_{t_i,t_j,r})^{m_r-1}}{(\Omega_{r,t_i} + \Omega_{r,t_j})^{2m_r-1}\Gamma(m_r)} \times \sum_{k_r=0}^{+\infty} \frac{\rho_{t_i,t_j,r}^{k_r}\Gamma(2m_r + 2k_r - 1)}{(k_r!)\Gamma(m_r + k_r)} \left(\frac{\sqrt{\Omega_{r,t_i}\Omega_{r,t_j}}}{\Omega_{r,t_i} + \Omega_{r,t_j}} \right)^{2k_r}. \tag{3.16}$$

We define:

$$C_{t_i,t_j} = \frac{1}{2} \times \frac{2^{3N_r-1}\Gamma(N_r + 0.5)}{\sqrt{\pi}\Gamma(N_r + 1)} \prod_{r=1}^{N_r} f(r). \tag{3.17}$$

Note that C_{t_i,t_j} is constant when m_r, $\Omega_{r,t}$, and $\rho_{t_i,t_j,r}$ are fixed. Consequently, (3.15) can be

rewritten as:

$$\text{APEP}(t_j \to t_i) = 2C_{t_i,t_j}\gamma^{-N_r}. \tag{3.18}$$

Gray codes are assumed for encoding. When a certain antenna is activated, there are $N/2$ other antennas that can cause an error for any particular bit. Therefore the total Hamming distance of any symbol to the others is calculated by:

$$\sum_{t_j \neq t_i = 1}^{N} N_H(t_j \to t_i) = \frac{N}{2}\log_2(N). \tag{3.19}$$

Combining (3.19) and (3.13a), this gives:

$$\text{ABEP}_{\text{SSK}}(l) = \frac{1}{2(N-1)} \sum_{t_i=1}^{N} \sum_{t_j \neq t_i = 1}^{N} \text{APEP}(t_j \to t_i). \tag{3.20}$$

Substituting (3.18) and (3.20) into (3.12a), $\text{ABEP}_{\text{spatial}}$ can be expressed as a function of N:

$$\text{ABEP}_{\text{spatial}} = \frac{N\log_2(N)}{\eta_s} \left(\frac{1}{N(N-1)} \sum_{t_i=1}^{N} \sum_{t_j \neq t_i = 1}^{N} C_{t_i,t_j} \right) \gamma^{-N_r}. \tag{3.21}$$

3.3.2.2 ABEP of signal part

The average symbol error rate (SER) of PSK modulation over Nakagami fading is given by [89, Eq. (9.16)]:

$$P_s(t) = \frac{1}{\pi} \int_0^{\frac{M-1}{M}\pi} \prod_{r=1}^{N_r} \left(1 + \frac{\bar{\gamma}_{r,t}\sin^2(\frac{\pi}{M})}{2m_r \sin^2(\theta)} \right)^{-m_r} d\theta, \tag{3.22}$$

where $\bar{\gamma}_{r,t} = \Omega_{r,t}\gamma$ is the average SNR of the symbol sent from the t-th transmit antenna at the input of the r-th receive antenna. The assumption of a high SNR results in $\frac{\gamma \sin^2(\frac{\pi}{M})}{2m_r \sin^2(\theta)} \gg 1$. Hence (3.22) can be rewritten as:

$$P_s(t) = \frac{1}{\pi} \left[\prod_{r=1}^{N_r} \left(\frac{2m_r}{\Omega_{r,t}\gamma \sin^2(\frac{\pi}{M})} \right)^{m_r} \right] \int_0^{\frac{M-1}{M}\pi} (\sin\theta)^{\sum_{r=1}^{N_r} 2m_r} d\theta. \tag{3.23}$$

When $M \geq 4$, we have: i) $\int_0^{\frac{M-1}{M}\pi} (\sin\theta)^{\sum_{r=1}^{N_r} 2m_r} d\theta \approx \int_0^{\pi} (\sin\theta)^{\sum_{r=1}^{N_r} 2m_r} d\theta$, which is independent of M; and ii) $\sin(\pi/M) \approx \pi/M$. The average shape parameter of the fading distributions across all receive antennas is denoted by $\bar{m}_r = \frac{1}{N_r} \sum_{r=1}^{N_r} m_r$. Then the average SER of PSK can be formulated by:

$$P_s(t) = \left\{ \frac{1}{\pi^{2\bar{m}_r N_r + 1}} \left[\prod_{r=1}^{N_r} \left(\frac{2m_r}{\Omega_{r,t}} \right)^{m_r} \right] \int_0^{\pi} (\sin\theta)^{2\bar{m}_r N_r} d\theta \right\} \left(\frac{M^2}{\gamma} \right)^{\bar{m}_r N_r}. \tag{3.24}$$

A simplified $\text{ABEP}_{\text{signal}}$ is obtained by substituting (3.24) into (3.12b):

$$\text{ABEP}_{\text{signal}} = \frac{\bar{B}_N}{\eta_s} M^{2\bar{m}_r N_r} \gamma^{-\bar{m}_r N_r}, \tag{3.25}$$

with

$$\bar{B}_N = \left(\frac{1}{\pi^{2\bar{m}_r N_r + 1}} \int_0^{\pi} (\sin\theta)^{2\bar{m}_r N_r} d\theta \right) \frac{1}{N} \sum_{t=1}^{N} \prod_{r=1}^{N_r} \left(\frac{2m_r}{\Omega_{r,t}} \right)^{m_r}. \tag{3.26}$$

It is worth noting that similar to $\text{ABEP}_{\text{spatial}}$ in (3.21), $\text{ABEP}_{\text{signal}}$ is also a function of N after replacing M by $2^{\eta_s}/N$.

3.3.2.3 ABEP of joint part

Using PSK modulation, the symbol χ_l of the signal constellation diagram is given by $\chi_l = \exp(j\varphi_l)$ where $\varphi_l = 2\pi(l-1)/M$. Thus (3.14) can be rewritten as follows:

$$\text{APEP}((t_j, \chi_{l_j}) \to (t_i, \chi_{l_i})) = E\left\{ Q\left(\sqrt{\frac{\gamma |\beta_{t_j} \exp(j\varphi_{t_j} + j\varphi_{l_j}) - \beta_{t_i} \exp(j\varphi_{t_i} + j\varphi_{l_i})|^2}{4}} \right) \right\}, \tag{3.27}$$

where φ_l is a constant, while φ_t is uniformly distributed between $(-\pi, \pi]$ as mentioned before. The sum of φ_t and φ_l also complies with a uniform distribution over the same region as φ_t. As a result, $\text{APEP}((t_j, \chi_{l_j}) \to (t_i, \chi_{l_i})) = \text{APEP}(t_j \to t_i)$. Similar to (3.19), the Hamming

distance in (3.13c) can be obtained by:

$$\sum_{t_j \neq t_i=1}^{N} \sum_{l_j \neq l_i=1}^{M} N_H((t_j, \chi_{l_j}) \rightarrow (t_i, \chi_{l_i})) = \frac{(M-1)N}{2} \log_2(N) + \frac{(N-1)M}{2} \log_2(M). \quad (3.28)$$

Substituting (3.18) and (3.28) into (3.12c), this gives:

$$\text{ABEP}_{\text{joint}} = \frac{\eta_s 2^{\eta_s} - M \log_2 M - N \log_2(N)}{\eta_s \gamma^{N_r}} \left(\frac{1}{N(N-1)} \sum_{t_i=1}^{N} \sum_{t_j \neq t_i=1}^{N} C_{t_i,t_j} \right). \quad (3.29)$$

3.3.2.4 Simplified ABEP expression

Combining (3.21), (3.25) and (3.29), the ABEP expression of SM is simplified as follows:

$$\text{ABEP}(M, N) = \frac{M^{2\bar{m}_r N_r}}{\eta_s} \bar{B}_N \gamma^{-\bar{m}_r N_r} + \frac{\eta_s 2^{\eta_s} - M \log_2(M)}{\eta_s} \bar{C}_N \gamma^{-N_r}, \quad (3.30)$$

with

$$\bar{C}_N = \frac{1}{N(N-1)} \sum_{t_i=1}^{N} \sum_{t_j \neq t_i=1}^{N} C_{t_i,t_j}. \quad (3.31)$$

The term $\bar{C}_N$ quantifies the effects of the fading distribution and the channel correlation on selecting the antenna array. Since the production of M and N is fixed for a certain spectrum efficiency, the optimisation problem of (3.30) is subjected to one variable, either M or N. The aim is thus to determine the optimal transmitter structure, including the number of antennas and their locations. However, a joint optimisation of both of them requires an exhaustive search of prohibitive computational complexity. Alternatively, a two-stage approach is proposed where the optimisation problem is split into two steps: i) obtain the best combination of (M, N) that minimises the ABEP of SM; ii) select the specific transmit antennas from the antenna array.

3.3.3 Optimisation on the number of transmit antennas

In the first step, the minimisation of the simplified ABEP expression with respect to M is carried out for a given scenario, which is comprised of the spectrum efficiency, the number of receive antennas, the SNR, the fading distribution, and the correlation coefficients. The term

$1/\eta_s$ in (3.30) is a positive constant, hence it can be removed without affecting the optimisation result. In addition, the difference between antennas is considered in the second step. As a result, $\bar{B}_N$ and $\bar{C}_N$ are replaced by $\bar{B}_{N_t}$ and $\bar{C}_{N_t}$ to avoid the dependence on the antenna dissimilarity. The optimisation problem is thus formulated as follows:

$$\begin{aligned} M_{\text{opt}} = \underset{M}{\text{argmin}} \quad & \frac{\bar{B}_{N_t}}{\gamma^{\bar{m}_r N_r}} M^{2\bar{m}_r N_r} + \frac{\bar{C}_{N_t}}{\gamma^{N_r}} \left(2^{\eta_s}\eta_s - M\log_2(M)\right) \\ \text{s.t.} \quad & 1 \leq M \leq 2^{\eta_s} \end{aligned}, \tag{3.32}$$

where both $\bar{C}_{N_t}\gamma^{-N_r}$ and $\bar{B}_{N_t}\gamma^{-\bar{m}_r N_r}$ are constant for a certain scenario. In other words, they are independent of the variable M. The above optimisation problem can be solved numerically by non-linear programming [90]. Note that the optimisation result of $\log_2(M)$ could be, and most likely is, a non-integer. However, without considering special encoding methods such as fractional bit encoding [91], both M and N must be a power of two to supply a full usage of the constellation diagram. This can readily be achieved by comparing the ABEP values of the two nearest integers around the optimal M. Afterwards, the best combination of (M, N) is obtained and denoted by $(M_{\text{opt}}, N_{\text{opt}})$.

3.3.4 Selection on antenna locations

The second step is to select a subarray of N_{opt} antennas from the size-N_t antenna array. The chosen subset should minimise the BER among all subarrays with the same size. Since $\bar{B}_N$ in (3.30) is irrelevant to the channel correlation, the problem is equivalent to finding the subarray that minimises $\bar{C}_N$.

Like the traditional transmit antenna selection (TAS) methods, this issue can be solved through exhaustive search. However, this results in unaffordable computational-complexity for a large η_s. Taking $\eta_s = 6$ and $N_{\text{opt}} = 16$ as an example, the full search space is about 5×10^{14} possible subsets. Alternatively, a novel selection method is proposed on the basis of circle packing, in which the subset can be selected directly.

Since the channel correlation is inversely proportional to the distance between two antennas, a rational solution is maximising the minimum geometric distance between any pair of the chosen antennas. This forms the circle packing problem in mathematics that can be worked out numerically [92]. Fig. 3.2 shows the circle packing solutions for various numbers of antennas, where the antennas are located at the circle centres. In the original problem, each circle must fit

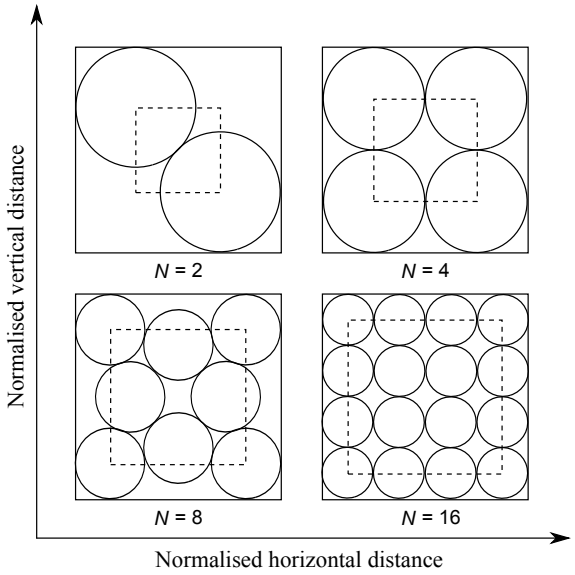

Figure 3.2: *Examples of the circle packing solution.*

inside the square boundary. The problem at hand is slightly different where the circle centres are restricted to be inside the boundary, and in Fig. 3.2 this is shown by dashed lines. This solution requires fully flexible positions, and thus is referred to as ideal circle packing (ICP). However, the antenna positions are normally fixed in practice, and those antennas closest to the ideal positions are selected instead. This method is thus named realistic circle packing (RCP). Fig. 3.3 shows the RCP solution for selecting 8 out of 32 antennas. As can be observed, the selection presents a similarity to the solution for $N = 8$ in Fig. 3.2. As N_t increases, the RCP solution becomes closer to ICP because the antenna array offers a larger flexibility in positions.

3.4 Optimum transmit structure over Rayleigh channels

In this section, the optimum transmit structure for SM is studied in a special case of Rayleigh fading channels. It is presented that the optimum transmit structure is independent of SNR in this specific scenario. In addition, a look-up table is built for quickly determining the best choice of (M, N). The SM system using the optimum transmit structure is named transmission optimised spatial modulation (TOSM). Furthermore, a closed-form expression of the BS energy consumption is derived for TOSM, allowing us to evaluate the proposed scheme analytically.

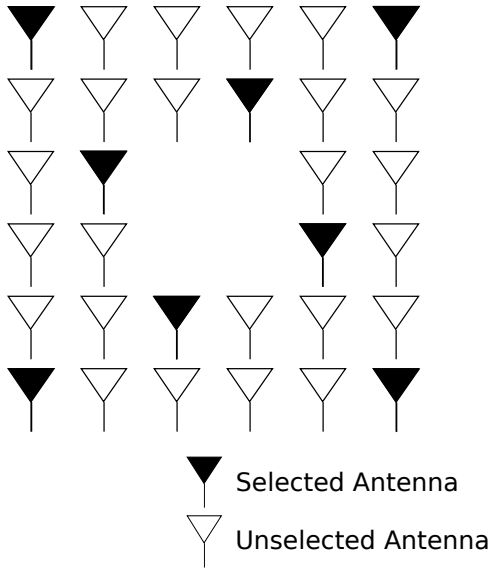

Figure 3.3: *An example of the RCP solution.*

3.4.1 Analytical modelling

For correlated and identically distributed (c.i.d.) Rayleigh fading channels, we have $m_r = 1$ and $\Omega_{r,t} = \Omega$ for all t and r. As a result, $\bar{B}_N$ in (3.26) and $\bar{C}_N$ in (3.31) can be reduced to:

$$B = \left(\frac{2}{\Omega}\right)^{N_r} \pi^{-2N_r-1} \int_0^{\pi} (\sin\theta)^{2N_r} d\theta, \tag{3.33}$$

and:

$$C = \frac{2^{2N_r-2}\Gamma(N_r+0.5)}{\Omega^{N_r}\sqrt{\pi}\Gamma(N_r+1)} \left[\sum_{k=0}^{+\infty} \left(\frac{\rho_{\text{av}}}{4}\right)^k \frac{\Gamma(2k+1)}{(k!)\Gamma(k+1)}\right]^{N_r}. \tag{3.34}$$

Correspondingly, the ABEP expression in (3.30) reduces to:

$$\text{ABEP} = \frac{\gamma^{-N_r}}{\eta_s} \left(B(M)^{2N_r} + C(2^{\eta_s}\eta_s - M\log_2(M))\right). \tag{3.35}$$

The term γ^{-N_r}/η_s is a positive constant, and therefore can be removed without influencing the optimisation result. After further removing the constant item $C2^{\eta_s}\eta_s$, the optimisation problem over Rayleigh fading can be formally expressed as follows:

$$\begin{aligned} M_{\text{opt}} = \underset{M}{\text{argmin}} \quad & B(M)^{2N_r} - CM\log_2(M) \\ \text{s.t.} \quad & 1 \le M \le 2^{\eta_s} \end{aligned}. \tag{3.36}$$

3.4.2 Look-up table

From the objective function derived in (3.36), it is not hard to find that M_{opt} is irrelevant to SNR in the case of c.i.d. Rayleigh fading. Also, M_{opt} is independent of η_s when η_s is large enough. In other words, for a certain N_r and a sufficiently large η_s, the optimum transmit structure is determined by ρ_{av} only. As shown in Table 3.2, this allows us to build a look-up table to quickly decide the best SM deployment for various channel correlation degrees. The look-up table is analysed in detail in Section 3.5.2.

3.4.3 Base station energy consumption

Substituting $\gamma = E_m L/N_0$ into (3.35), the required E_m using TOSM is computed by :

$$E_m = \frac{N_0}{L}\left(\frac{F(M_{\text{opt}})}{\eta_s R_e}\right)^{\frac{1}{N_r}}, \tag{3.37}$$

where $F(M) = B(M)^{2N_r} + C(2^{\eta_s}\eta_s - M\log_2(M))$ and R_e denotes the value of the target BER. The required RF output power, denoted by P_{req}, is then given by:

$$P_{\text{req}} = \frac{R_b N_0}{\eta_s L}\left(\frac{F(M_{\text{opt}})}{\eta_s R_e}\right)^{\frac{1}{N_r}}. \tag{3.38}$$

3.4.3.1 Continuous mode

The BS energy consumption per bit, denoted by E_{BS}, is obtained by:

$$E_{\text{BS}} = \frac{P_{\text{BS}}}{R_b}. \tag{3.39}$$

Substituting (3.8), (3.38) and $N_{\text{act}} = 1$ into (3.39), the energy consumption per bit for a BS using TOSM in the continuous mode can be formulated as:

$$E_{\text{BS}} = \frac{P_0}{R_b} + \frac{\zeta N_0}{\eta_s L}\left(\frac{F(M_{\text{opt}})}{\eta_s R_e}\right)^{\frac{1}{N_r}}. \tag{3.40}$$

	$N_r = 1$				$N_r = 2$			
ρ_{av}	$\eta_s = 4$	$\eta_s = 5$	$\eta_s = 6$	$\eta_s = 7$	$\eta_s = 4$	$\eta_s = 5$	$\eta_s = 6$	$\eta_s = 7$
0.0	(**16,1**)	(16,2)	(16,4)	(16,8)	(4,4)	(4,8)	(4,16)	(4,32)
0.1	(**16,1**)	(16,2)	(16,4)	(16,8)	(4,4)	(4,8)	(4,16)	(4,32)
0.2	(**16,1**)	(16,2)	(16,4)	(16,8)	(4,4)	(4,8)	(4,16)	(4,32)
0.3	(**16,1**)	(16,2)	(16,4)	(16,8)	(4,4)	(4,8)	(4,16)	(4,32)
0.4	(**16,1**)	(16,2)	(16,4)	(16,8)	(4,4)	(4,8)	(4,16)	(4,32)
0.5	(**16,1**)	(16,2)	(16,4)	(16,8)	(4,4)	(4,8)	(4,16)	(4,32)
0.6	(**16,1**)	(16,2)	(16,4)	(16,8)	(8,2)	(8,4)	(8,8)	(8,16)
0.7	(**16,1**)	(**32,1**)	(32,2)	(32,4)	(8,2)	(8,4)	(8,8)	(8,16)
0.8	(**16,1**)	(**32,1**)	(32,2)	(32,4)	(8,2)	(8,4)	(8,8)	(8,16)
0.9	(**16,1**)	(**32,1**)	(**64,1**)	(64,2)	(8,2)	(8,4)	(8,8)	(8,16)
1.0	(**16,1**)	(**32,1**)	(**64,1**)	(**128,1**)	(**16,1**)	(**32,1**)	(32,2)	(32,4)
	$N_r = 3$				$N_r = 4$			
ρ_{av}	$\eta_s = 4$	$\eta_s = 5$	$\eta_s = 6$	$\eta_s = 7$	$\eta_s = 4$	$\eta_s = 5$	$\eta_s = 6$	$\eta_s = 7$
0.0	(4,4)	(4,8)	(4,16)	(4,32)	(4,4)	(4,8)	(4,16)	(4,32)
0.1	(4,4)	(4,8)	(4,16)	(4,32)	(4,4)	(4,8)	(4,16)	(4,32)
0.2	(4,4)	(4,8)	(4,16)	(4,32)	(4,4)	(4,8)	(4,16)	(4,32)
0.3	(4,4)	(4,8)	(4,16)	(4,32)	(4,4)	(4,8)	(4,16)	(4,32)
0.4	(4,4)	(4,8)	(4,16)	(4,32)	(4,4)	(4,8)	(4,16)	(4,32)
0.5	(4,4)	(4,8)	(4,16)	(4,32)	(4,4)	(4,8)	(4,16)	(4,32)
0.6	(4,4)	(4,8)	(4,16)	(4,32)	(4,4)	(4,8)	(4,16)	(4,32)
0.7	(4,4)	(4,8)	(4,16)	(4,32)	(4,4)	(4,8)	(4,16)	(4,32)
0.8	(8,2)	(8,4)	(8,8)	(8,16)	(4,4)	(4,8)	(4,16)	(4,32)
0.9	(8,2)	(8,4)	(8,8)	(8,16)	(8,2)	(8,4)	(8,8)	(8,16)
1.0	(**16,1**)	(16,2)	(16,4)	(16,8)	(**16,1**)	(16,2)	(16,4)	(16,8)

Table 3.2: *TOSM deployment* (M, N) *in the case of Rayleigh fading.*

3.4.3.2 DTX mode

Similarly, based on (3.10), E_{BS} in the DTX mode can be computed as follows:

$$E_{\text{BS}} = \frac{P_s}{R_b} + \frac{N_0}{\eta_s L}\left(\zeta + \frac{P_0 - P_s}{P_{\max}}\right) \times \left(\frac{F(M_{\text{opt}})}{\eta_s R_e}\right)^{\frac{1}{N_r}}. \tag{3.41}$$

3.5 Results

In this section, Monte Carlo simulations are implemented to validate the performance of the proposed scheme. Two scenarios are studied: i) c.i.d. Nakagami-m fading and ii) c.i.d. Rayleigh fading. In the first case, we focus on verifying the accuracy of the simplified ABEP expression. The reason for choosing the second case is threefold: i) multipath fading is typically modelled by a Rayleigh distribution; ii) by fixing the parameter m, the main trends of TOSM in relation to the channel correlation can be studied; and iii) a look-up table is formed within this scenario to exhibit the optimum transmit structure. The complexity and feedback cost introduced by TOSM is negligible, as TOSM is based on channel statistics and does not require frequent updates. Therefore this section is focused on the BER performance of TOSM, which is evaluated against some other schemes including fixed-SM, vertical Bell Laboratories layered space-time (V-BLAST) and space-time block coding (STBC). Also, the BS energy consumption and the maximum transmission rate are analysed for the proposed scheme. In order to guarantee the fairness of different values of η_s, the transmission energy per bit against noise, i.e. E_b/N_0, is used instead of SNR.

3.5.1 Accuracy of the simplified ABEP expression

In Fig. 3.4, the simplified ABEP expression of SM in (3.32) is verified against simulation results. In order to present an extensive comparison, several different scenarios are illustrated in terms of shape factor m, the number of receive antennas N_r, spectrum efficiency η_s and E_b/N_0. A unit spread controlling factor is considered. For each scenario, the BER performance of TOSM is shown as a function of the average correlation degree ρ_{av}. As can be seen, in general, the theoretical curves match the simulation results well. Because the simplified ABEP expression is an approximation based on the upper bound, we expect some deviations especially at high channel correlations. Despite this, the simplified ABEP expression is still very close to the simulation results.

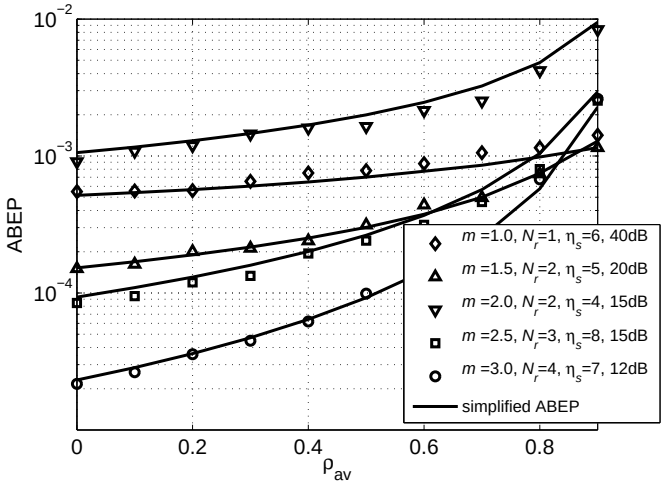

Figure 3.4: *Simplified ABEP expression versus simulations.*

3.5.2 Optimality of the look-up table

Table 3.2 quantises the relationship between the optimal number of transmit antennas for SM and the channel correlation. Bold font is used to highlight the situations where the optimal number of transmit antennas is one. In other words, SM is not applied in those situations. The following outcomes are observed: i) given η_s and N_r, N_{opt} decreases when ρ_{av} increases, as expected; ii) if $N_r = 1$, the optimum transmit structure regresses to a single transmit-antenna scheme when ρ_{av} is high; iii) when increasing N_r, SM is suitable for more cases of $(\eta_s, \rho_{\text{av}})$, and N_{opt} becomes larger; and iv) given N_r and ρ_{av}, the best selection of M maintains a constant when η_s is large enough.

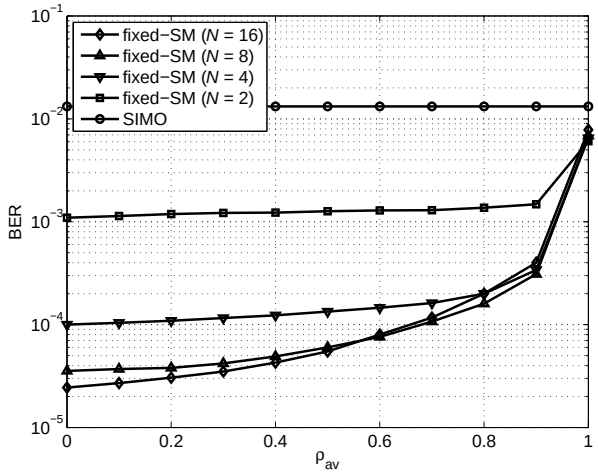

Figure 3.5: *BER performance of fixed-SM schemes ($E_b/N_0 = 25$ dB, $\eta_s = 6$ and $N_r = 2$).*

The look-up table can be extended to any needed situation and easily used to configure the deployment of the TOSM system. The parameters N_r and η_s are usually fixed in practice. Therefore the only parameter which needs to be determined is the correlation coefficient, and this can be obtained by the structured correlation estimator [93]. Taking $\eta_s = 6$ and $N_r = 2$ as an example, Fig. 3.5 shows the BER performance of various fixed-SM schemes at 25 dB. As shown, SM using $N = 16$ outperforms $N = 8$ when ρ_{av} is below 0.5. However, the opposite result happens for $0.6 \leq \rho_{\text{av}} \leq 0.9$. At an extremely high correlation of $\rho_{\text{av}} = 1$, two transmit-antenna SM achieves the lowest BER. It can be observed that Table 3.2 fits the simulation results.

3.5.3 Optimality of direct antenna selection

The performance of the proposed RCP is evaluated against two baselines: i) the exhaustive search (ES); and ii) the worst situation (WS) where neighbouring antennas are selected. Fig. 3.6 and Fig. 3.7 show the BER performance of RCP for $\eta_s = 4$ and 5, respectively. Due to the intractable complexity of ES, the results when $\eta_s > 5$ are not presented.

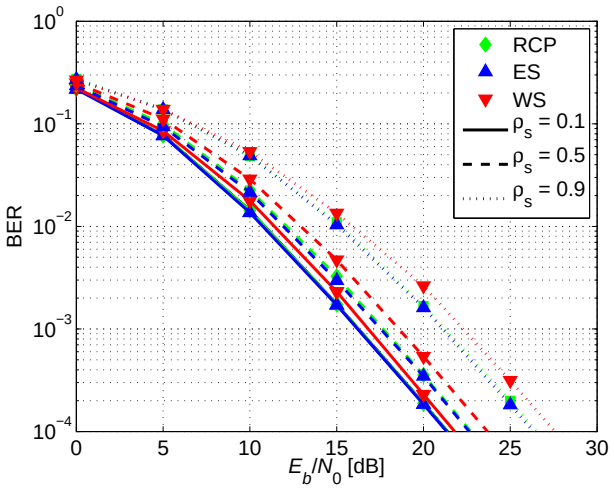

Figure 3.6: *BER performance of RCP ($N_t = 16$ and $N = 8$).*

The antenna arrays are assumed to be located in the same area in order to ensure the fairness of different η_s. For this reason, ρ_s is used instead of ρ_{av}. As can be seen, RCP achieves almost the same performance as ES, with a gap of less than 0.3 dB. Also, the negligible difference between RCP and ES is hardly affected by channel correlations. Conversely, the performance of WS becomes much worse as ρ_s increases.

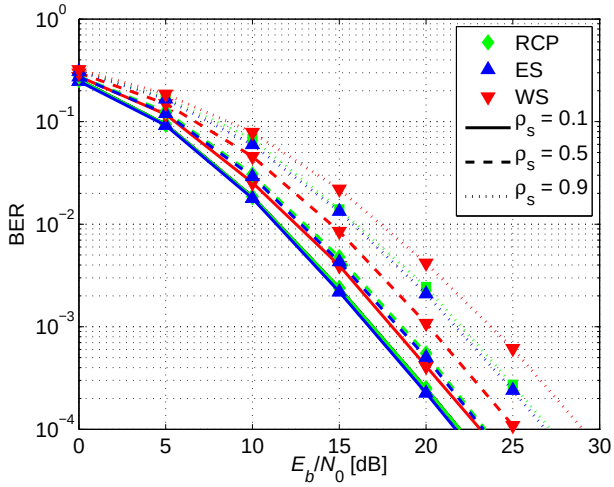

Figure 3.7: *BER performance of RCP ($N_t = 32$ and $N = 8$).*

3.5.4 BER performance of TOSM

The complexity of a MIMO system depends on the number of RF chains rather than the total number of transmit antennas. TOSM requires only one RF chain, regardless of the number of antennas used. Thus it is reasonable to compare TOSM with fixed-SM schemes using the same η_s. Fig. 3.8 and Fig. 3.9 show the BER performance of TOSM as a function of the channel correlation for $\eta_s = 4$ and 5, respectively.

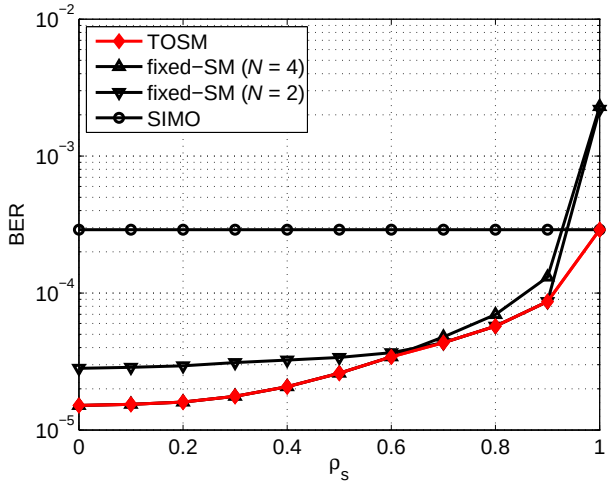

Figure 3.8: *BER performance of TOSM against channel correlations ($E_b/N_0 = 25$ dB, $\eta_s = 4$ and $N_r = 2$).*

The following trends are observed: i) fixed-SM with more antennas is not always better than those using fewer antennas, as expected; ii) TOSM always performs better than or equal to the

fixed-SM schemes, and this validates the optimality of TOSM; and iii) as η_s increases, TOSM tends to employ more transmit antennas, and performs much better than fixed-SM with a small number of transmit antennas. For $\eta_s = 4$, TOSM slightly outperforms fixed-SM with $N = 2$ at low correlations. However, for $\eta_s = 5$, TOSM can always achieve a significant gain against fixed-SM with $N = 2$, except when the channel correlation is extremely high. Similar, but less pronounced trends are noticed at lower SNRs.

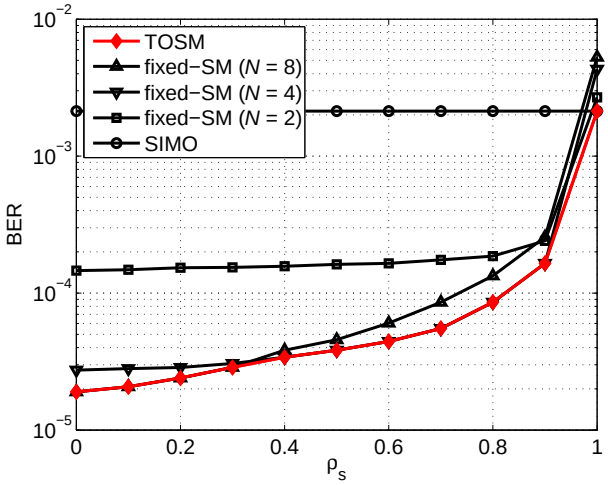

Figure 3.9: *BER performance of TOSM against channel correlations ($E_b/N_0 = 25$ dB, $\eta_s = 5$ and $N_r = 2$).*

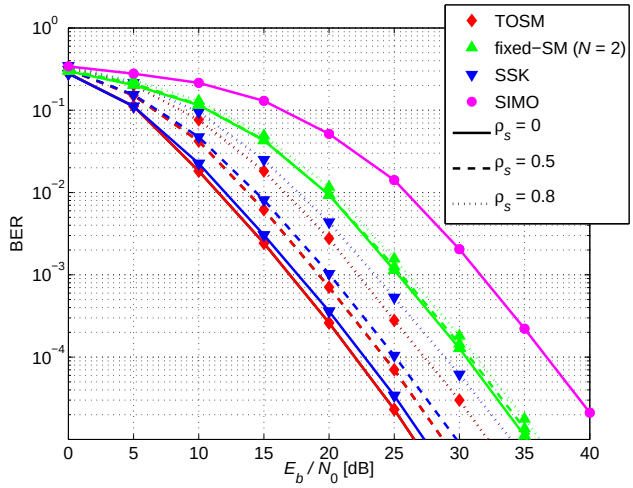

Figure 3.10: *BER performance of TOSM against SNR ($\eta_s = 6$ and $N_r = 2$).*

Assuming $\eta_s = 6$, the BER performance of TOSM is shown as a function of E_b/N_0 in Fig. 3.10, in comparison with fixed-SM with $N = 2$ as well as space shift keying (SSK) and single-input multiple-output (SIMO). As shown, TOSM outperforms the other schemes signif-

icantly for all presented SNRs and channel correlation degrees. When the channel links are independent ($\rho_s = 0$), TOSM achieves SNR gains of 0.8 dB, 8.7 dB and 15.1 dB against SSK, fixed-SM with $N = 2$ and SIMO, respectively. As the channel correlation increases, TOSM outmatches SSK more significantly. Fixed-SM with $N = 2$ is slightly affected by the channel correlation, and the gain of TOSM is diminishing with an increase of ρ_s. However, this gain still exceeds 4 dB at $\rho_s = 0.8$.

3.5.5 BS energy consumption

The BS energy consumption of TOSM is studied in comparison with V-BLAST and STBC. The simulations are restricted in two aspects. On the one hand, the number of transmit antennas for V-BLAST is limited due to the constraint $N_t \leq N_r$. On the other hand, SM can save more energy in RF chains for a larger N_t. The purpose here is to present the energy efficiency of TOSM. In order to carry out a relatively fair comparison, the case of $\eta_s = 4$ and $N_r = 4$ is chosen, where TOSM employs four transmit antennas when ρ_s varies from 0 to 0.8. The same 4×4 MIMO structure is arranged for both V-BLAST in [69] and rate 3/4 STBC in [71]. In addition, the path loss is assumed to be 100 dB without shadowing [94].

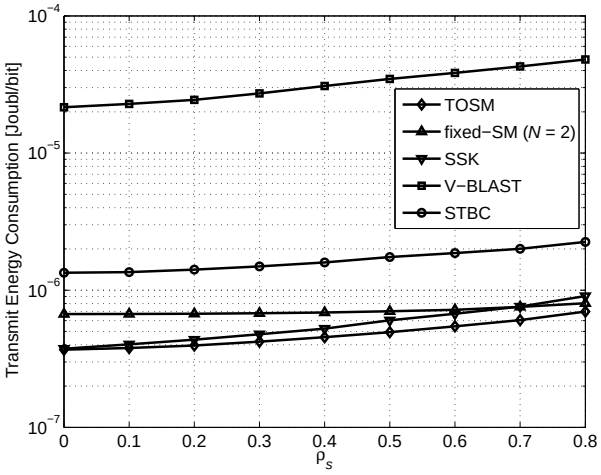

Figure 3.11: *Transmit energy consumption ($\eta_s = 4, N_r = 4$ and a target BER value of 1×10^{-4}).*

For a target BER value of 1×10^{-4}, Fig. 3.11 shows the required transmit energy consumption for various schemes. It is noticed that, TOSM provides a remarkable and stable gain of around 5 dB against STBC and much more against V-BLAST. The overall BS energy consumptions in both the continuous mode and the DTX mode are shown in Fig. 3.12. To maintain a certain E_b,

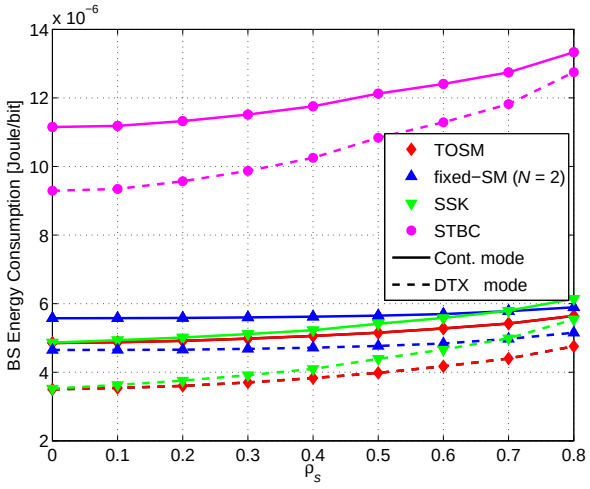

Figure 3.12: *BS energy consumption ($\eta_s = 4, N_r = 4$ and a target BER value of 1×10^{-4}).*

the restriction on $P_{\max}$ leads to a ceiling of the transmission rate. For this reason, a transmission rate of 30 Mbit/s is chosen to ensure the BS works physically, and TOSM is compared with STBC to show the trends. The following outcomes are observed: i) using the DTX mode for TOSM offers an energy gain of 1.4 dB over the continuous mode; ii) compared with STBC, TOSM requests much less energy because of the single RF chain requirement. In the continuous mode and the DTX mode, TOSM saves at least 6.3 μJoule/bit (56%) and 5.8 μJoule/bit (62%) against STBC, respectively; iii) in both modes, TOSM outperforms STBC more significantly as ρ_s increases; and iv) compared with STBC, TOSM saves more energy in the DTX mode than in the continuous mode, especially at high channel correlations. For a higher spectrum efficiency, the power efficiency decreases for all involved methods, but TOSM still achieves noticeable gains over other schemes.

3.5.6 Maximum transmission rate

The above simulations are conducted when the same RF output power is considered for all involved techniques. In contrast to the multi-stream MIMO schemes, SM requires only one RF chain, and therefore less energy is requested to drive it. However, the maximum RF output power for SM is $1/N_{\text{act}}$ of that for a MIMO system with N_{act} simultaneously-active antennas. This fact restricts the maximum transmission rate in the SM systems. Fig. 3.13 presents the maximum transmission rate as a function of the channel correlation. Note that maximum RF output signifies a very high SNR, and in this case the BER performance of V-BLAST is

bottlenecked due to the inevitability of ICI.

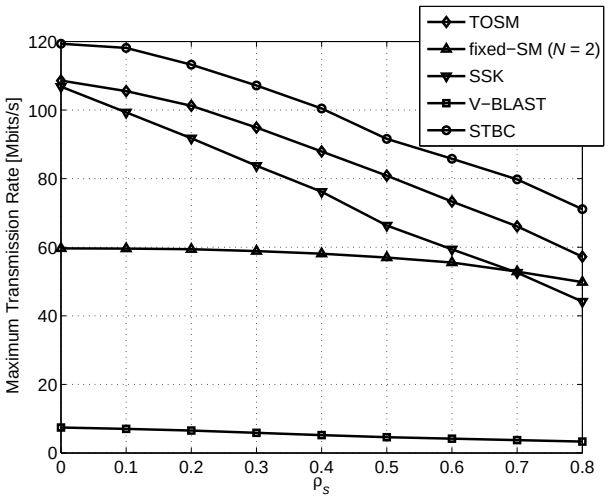

Figure 3.13: *Maximum transmission rate ($\eta_s = 4, N_r = 4$ and $P_{out} = P_{max}$).*

As shown, the maximum transmission rate of fixed-SM outperforms V-BLAST, but is much smaller than STBC. Meanwhile, TOSM yields a great improvement over fixed-SM (up to 1.8 times) and diminishes the gap between SM and STBC significantly. In addition, the BS energy consumption gains between TOSM and STBC with respect to the transmission rate is presented in Fig. 3.14. The gain obtained by TOSM in the DTX mode is larger than that in the continuous mode. Also, the DTX mode performs much better than the continuous mode when R_b increases to the full load. This signifies that TOSM is more energy efficient when combined with DTX.

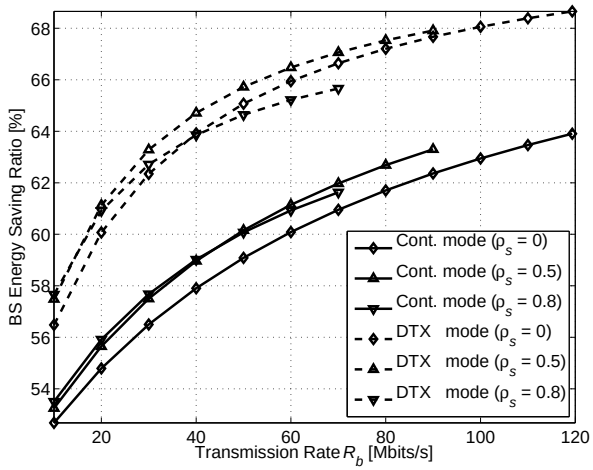

Figure 3.14: *BS energy saving ratio between TOSM and STBC ($\eta_s = 4, N_r = 4$).*

3.6 Chapter summary

In this chapter, an optimum transmit structure for SM has been presented, which balances the size of the spatial constellation diagram and the size of the signal constellation diagram. Instead of using exhaustive search, a novel two-stage TAS method has been proposed for reducing the computational complexity, where the optimal number of transmit antennas and the specific antenna positions are determined separately. The first step is to calculate the optimal number of transmit antennas by minimising a simplified ABEP expression. In the second step, based on circle packing, a direct antenna selection method named RCP has been developed to pick the required number of transmit antennas from an antenna array. Due to the exploitation of channel statistics, the complexity, latency and feedback cost of TOSM are negligible in comparison with the conventional TAS methods. The optimality of the proposed scheme as well as its BER performance has been presented. TOSM shows a lower SNR requirement for the same spectral efficiency as compared with fixed-SM.

In addition, a look-up table has been built in the case of c.i.d. Rayleigh fading, which can readily be used to obtain the optimum transmit structure. Furthermore, the overall BS energy consumption of TOSM has been compared with both V-BLAST and STBC. Thanks to the requirement of a single RF chain, TOSM exhibited a much higher energy efficiency than the other two schemes for achieving the same BER and transmission rate targets. A further study has shown that TOSM is more energy efficient when combined with the DTX mode than the continuous mode. Moreover, the issue with respect to the maximum transmission rate in the SM systems has been addressed, which is caused by the limited output power of a single RF chain. It was shown that TOSM uplifts the maximum transmission rate of fixed-SM greatly and diminishes the gap between fixed-SM and STBC.

Chapter 4

Channel estimation for spatial modulation

4.1 Introduction

In spatial modulation (SM) systems, a single transmit antenna is activated at any time instance, and the remaining antennas are idle. While this property offers a high energy efficiency as well as a complete avoidance of inter-channel interference, it challenges the channel estimation (CE) process. In current literature, the CE methods for SM separately estimate the channel links that pertain to different antennas. In order to estimate the entire MIMO channel, SM has to activate the transmit antennas sequentially for sending the training signal. Therefore the time spent on the CE process is proportional to the number of transmit antennas, leading to a substantial reduction in throughput especially when using a large number of transmit antennas. Also, the pilot sequence length is restricted for each transmit antenna, which impedes SM to improve the CE performance by increasing the pilot sequence length. New CE methods are needed to strengthen the performance of SM in practical systems.

In this chapter, the CE process for SM is studied in two aspects. On the one hand, the research focuses on improving the CE accuracy by exploiting the channel correlation between antennas. Two novel CE methods are proposed for SM, making a use of the antenna correlation at the transmitter and at the receiver, respectively. On the other hand, the power allocation between training symbols and information-carrying symbols imposes on the bit error rate (BER) performance. With more power allocated to training symbols, the CE results are more accurate. However, this reduces the signal-to-noise ratio (SNR), since less power is available for information-carrying symbols. A trade-off is therefore enabled between the power of those two types of symbols. Based on this fact, an optimal power allocation is proposed by minimising the BER. In addition, a framework that combines different CE methods is proposed.

4.2 System model

A $N_t \times N_r$ SM-MIMO system is considered for a single user, where N_t and N_r denote the number of transmit antennas and the number of receive antennas, respectively. The signal modulation and the decoding method are referred to Section 2.3. The channel model and the estimator used for CE are introduced in the following context.

4.2.1 Channel model

A space-correlated and time-variant MIMO channel is considered. The channel coefficient between the t-th transmit antenna and the r-th receive antenna is denoted by $h_{r,t(n)}$, where n is the discrete time index. The corresponding $N_r \times N_t$ channel matrix, denoted by $\mathbf{H}_{(n)}$, is generated in two steps: i) create the channel matrix at the initial point, i.e. $\mathbf{H}_{(0)}$, of which the entries are correlated; and ii) produce a consecutive channel based on the temporal correlation, while maintaining the same spatial correlation. It is worth noting that the proposed CE method is not restricted to a specific channel model. The channel model here is for the purpose of evaluating the performance of the proposed method in simulations.

4.2.1.1 Spatial correlation

The Kronecker model is commonly used for spatially-correlated channels [95]. According to this model, the channel matrix is initialised as follows:

$$\mathbf{H}_{(0)} = \mathbf{R}_{\mathrm{r}}^{1/2} \mathbf{G}_{(0)} \left(\mathbf{R}_{\mathrm{t}}^{1/2} \right)^{H}, \tag{4.1}$$

where matrix $\mathbf{G}$ has the same dimension as $\mathbf{H}_{(0)}$, and its entries are independent and identically distributed (i.i.d.) complex Gaussian distribution $\mathcal{CN}(0,1)$; $\mathbf{R}_{\mathrm{t}}$ and $\mathbf{R}_{\mathrm{r}}$ denote the transmit correlation matrix and the receive correlation matrix, respectively. The correlation coefficient between the transmit antennas t_1 and t_2 is denoted by ρ_{t_1,t_2}. The transmit correlation matrix is

then expressed as:

$$\mathbf{R}_{\mathrm{t}} = \begin{bmatrix} 1 & \rho_{1,2} & \cdots & \rho_{1,N_t} \\ \rho_{2,1} & 1 & \cdots & \rho_{2,N_t} \\ \vdots & \vdots & \ddots & \vdots \\ \rho_{N_t,1} & \rho_{N_t,2} & \cdots & 1 \end{bmatrix}. \tag{4.2}$$

Similarly, the element ρ_{r_1,r_2} in $\mathbf{R}_{\mathrm{r}}$ represents the correlation coefficient between the receive antennas r_1 and r_2. The correlation between antennas is modelled in the same way as that in Section 3.2.2.2, and the Euclidean distance between the two diagonal ends of the antenna array is normalised to be unity. The correlation coefficient between any pair of transmit antennas is then formulated as:

$$\rho_{t_1,t_2} = \rho_{\mathrm{tx}}^{d_{t_1,t_2}}, \tag{4.3}$$

where d_{t_1,t_2} is the Euclidean distance between transmit antennas t_1 and t_2; ρ_{tx} denotes the correlation degree when two transmit antennas are separated at the reference distance. Similar to ρ_{t_1,t_2}, the correlation coefficient between any pair of receive antennas is given by:

$$\rho_{r_1,r_2} = \rho_{\mathrm{rx}}^{d_{r_1,r_2}}. \tag{4.4}$$

4.2.1.2 Temporal correlation

The Gauss-innovations channel model formulates the channel variation as a function of the speed of users [96]. Using the Gauss-innovations channel model, the channel matrix at the n-th time index can be expressed as:

$$\mathbf{H}_{(n)} = \sqrt{\kappa}\mathbf{H}_{(n-1)} + \sqrt{1-\kappa}\mathbf{H}'_{(n)}, \tag{4.5}$$

where κ is a parameter related to the user speed, and it is given by [96, Eq. (10)]:

$$\kappa = J_0\left(\frac{2\pi v f_c T_s}{c}\right)^2, \tag{4.6}$$

where $J_0(\cdot)$ is the zeroth-order Bessel function of the first kind; T_s is the sampling period; f_c is the centre carrier frequency; v and c denote the speed of mobile user and the speed of light, respectively. The term $\mathbf{H}'_{(n)}$ in (4.5) is also generated from (4.1), but it is independent of

$\mathbf{H}_{(n-1)}$. In addition, $\mathbf{H}'_{(n)}$ is independent from time to time. Substituting (4.1) and $n = 1$ into (4.5), this gives:

$$\mathbf{H}_{(1)} = \mathbf{R}_r^{1/2} \left(\sqrt{\kappa}\mathbf{G}_{(0)} + \sqrt{1-\kappa}\mathbf{G}'_{(1)} \right) \left(\mathbf{R}_t^{1/2} \right)^H . \tag{4.7}$$

Note that $\mathbf{H}_{(1)}$ is a Rayleigh fading channel of the same correlation matrices as $\mathbf{H}_{(0)}$. Similarly, the expression for $\mathbf{H}_{(n)}$ in (4.5) is rewritten as:

$$\mathbf{H}_{(n)} = \mathbf{R}_r^{1/2} \bar{\mathbf{G}}_{(n)} \left(\mathbf{R}_t^{1/2} \right)^H , \tag{4.8}$$

and

$$\bar{\mathbf{G}}_{(n)} = \sum_{m=0}^{n} \left(\sqrt{1-\kappa} \right)^{\text{sgn}(m)} \left(\sqrt{\kappa} \right)^{n-m} \mathbf{G}_{(m)}, \tag{4.9}$$

where $\text{sgn}(\cdot)$ is the sign function. It is straightforward to infer that, $\mathbf{H}_{(n)}$ is also a correlated Rayleigh fading channel of the same correlation matrices as $\mathbf{H}_{(0)}$. Note that the above model also suits spatially-uncorrelated and/or time-invariant channels, by setting the correlation coefficients and/or the speed of mobile user to be zeros.

4.2.2 Pilot-assisted channel estimation

So far, the channel estimation methods for SM has been based on existing CE techniques, such as least square (LS), minimum mean square error (MMSE) and recursive least square (RLS). All those estimators are also available for the proposed CE methods. In order to keep simplicity and ensure a fair comparison, LS is adopted for both the conventional methods and the proposed methods in this chapter. The pilot signal and the LS estimator are described as follows.

4.2.2.1 Pilot signal

A large quantity of studies have been performed on the optimal design of the training signal for estimating correlated MIMO channels [97–99]. Those optimal patterns are also applicable to the channel estimation for SM. However, the study here focuses on developing CE methods that are specially tailored for SM. For this reason, a simple pilot signal of N_p repeated symbols is considered, where N_p is the pilot sequence length. The optimal pilot design is kept for future research.

The estimation period, denoted by P_{CE}, is defined as the interval between two adjacent CE

processes of any transmit antenna. In addition, the pilot ratio is defined as the ratio of the number of pilot symbols to the number of total symbols during one estimation period, and it is denoted by denoted by η. Furthermore, we use $p_{t(n)}$ to represent the pilot symbol transmitted through transmit antenna t at the n-th time index. To be distinguished from the information-carrying symbols, the transmission energy per pilot symbol is denoted by E_p. The signal-to-noise ratio (SNR) for pilot signals is denoted by $\gamma_p = E_p/N_0$.

4.2.2.2 Least square estimator

When sending out a pilot symbol through the t-th transmit antenna at the n-th time index, the received signal at the r-th receive antenna can be obtained by replacing χ_l in (2.1) with $p_{t(n)}$:

$$y_{r(n)} = h_{r,t(n)} p_{t(n)} + w_{r(n)}. \tag{4.10}$$

We focus on a single CE period, and the LS estimate during the considered period is denoted by $\tilde{h}_{r,t}$, where the time index is neglected for simplicity. According to [100, p. 224, Eq. (8.9)], $\tilde{h}_{r,t}$ is calculated by:

$$\tilde{h}_{r,t} = \arg\min_{h} \sum_{m=1}^{N_p} \parallel y_{r(m)} - h p_{t(m)} \parallel^2, \tag{4.11}$$

where m is the symbol index of the pilot sequence. Since both $y_{r(m)}$ and $p_{t(m)}$ are scalar, we have:

$$\tilde{h}_{r,t} = \frac{1}{N_p} \sum_{m=1}^{N_p} \frac{y_{r(m)}}{p_{t(m)}}. \tag{4.12}$$

4.3 Channel estimation across transmit antennas

In the conventional channel estimation (CCE) for SM, all transmit antennas are activated in sequence to send the pilot signal. In the following context, the pilot structure of CCE is introduced, followed by a novel CE method, named transmit cross channel estimation (TCCE). By exploiting the channel correlation between transmit antennas, the new approach is able to estimate the entire MIMO channel by sending the pilot signal through only one transmit antenna. In order to clearly demonstrate the concept of the proposed method and keep a moderate complexity of analysis, the pilot sequence length is assumed to be one in this section, i.e. $N_p = 1$. The case of a generalised N_p is studied in Section 4.6.

4.3.1 Conventional method

In Fig. 4.1, the pilot structure of CCE is presented for an example of four transmit antennas. During each blue coloured slot, a pilot symbol is sent out through the corresponding transmit antenna. Those slots are referred to as pilot slots. The remaining time slots are used to convey information-carrying symbols. The estimated channel state information (CSI) is used instead of the perfect CSI in (2.5). Based on the estimation results in (4.12), the detected symbols using CCE are obtained by:

$$\left[\hat{t}_{\text{act}}, \hat{l}\right] = \arg\min_{t,l} \sum_{r=1}^{N_r} \parallel y_r - \tilde{h}_{r,t}\chi_l \parallel^2 . \tag{4.13}$$

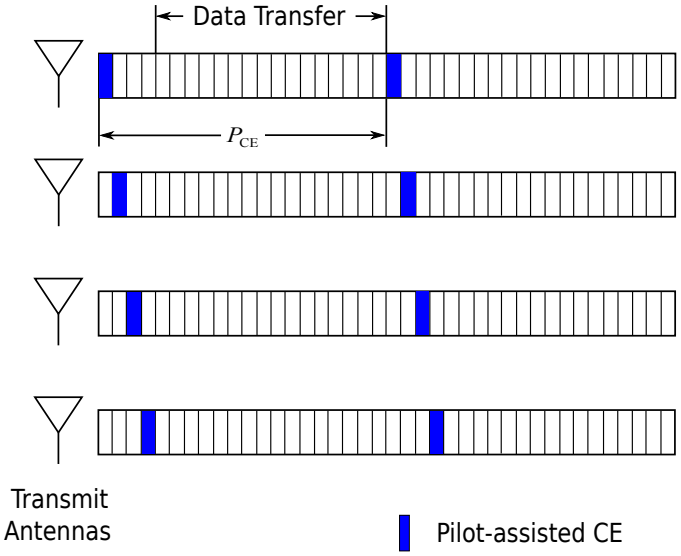

Figure 4.1: *The pilot structure of CCE.*

The estimation period of CCE is calculated by:

$$P_{\text{CE}} = \frac{N_t T_s}{\eta}. \tag{4.14}$$

Note that the estimation period of CCE is proportional to the number of transmit antennas, as mentioned previously. Each LS process requires one division, which costs ξ^2 operations for ξ-digit numbers. Thus the computational complexity of CCE during one estimation period is given by:

$$O_{\text{CCE}}(N_t N_r \xi^2). \tag{4.15}$$

4.3.2 Proposed method

The channel difference information (CDI) is defined as the difference between the channel coefficients of a pair of transmit antennas. If CDI is known, then it is possible to obtain the CSI of the entire MIMO channel by estimating the channel information of any single transmit antenna. In the other words, only one transmit antenna is required to send the pilot signal. The CE time is therefore significantly shortened in comparison with CCE. A constant channel difference is however unrealistic. In order to make it available for time-varying channels, the channel difference information needs to keep updated. Taking four transmit antennas as an example, Fig. 4.2 depicts the schematic diagram of the proposed method.

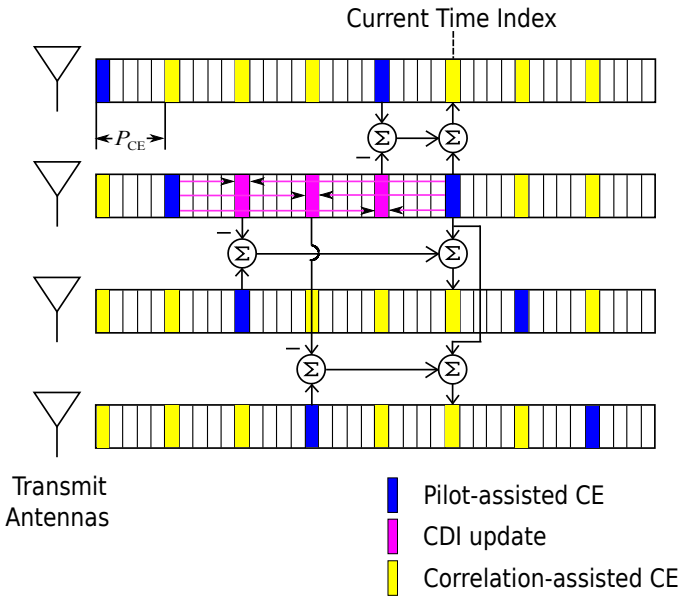

Figure 4.2: *The pilot structure of TCCE.*

The pilot transmissions are represented by blue coloured slots, similar to Fig. 4.1. Note that, unlike CCE, the pilot slots pertaining to different transmit antennas are equally allocated along the time. At any pilot slot, the CSI of the currently active antenna is obtained in the same way as that of CCE. For those idle antennas, CSI is measured based on the estimated CSI of the active antenna and the CDI between the active antenna and the corresponding idle antenna. We refer to this type of CE as correlation-based CE, which is shown by yellow coloured slots. The CDI for a certain idle antenna is calculated at the latest pilot slot of that antenna. The CSI of the currently active antenna at that slot, which is highlighted in pink colour, is corrected by using interpolation based on the estimated CSIs at the current pilot slot and some previous pilot slots. At any pilot slot, the algorithm is comprised of four steps as follows:

Step 1: Pilot-assisted CE

In the first step, the pilot-assisted CE in Section 4.2.2 is implemented for the currently active antenna, i.e. t_{act}. The corresponding estimation result is denoted by $\tilde{h}_{t_{\text{act}}(n)}$, where the index for receive antennas is neglected for simplicity.

Step 2: CDI update

For each transmit antenna, the pilot is conveyed once for every N_t pilot slots. At the previous $N_t - 1$ pilot slots, the CSI of t_{act} is estimated by the correlation-assisted CE which will be detailed in step 3. In this step, those CSIs are corrected by a low-pass interpolation based on $\tilde{h}_{t_{\text{act}}(n)}$ and $L-1$ previous estimates $\tilde{h}_{t_{\text{act}}(n-lN_t/\eta)}$, $l = 1, 2, \ldots, L-1$. The number of totally used estimates, i.e. L, is defined as the interpolation sequence length. The corrected CSI is denoted by $\dot{h}_{t_{\text{act}}(n-k/\eta)}$, $k = 1, 2, \ldots, N_t - 1$. For clarity, the simplest case of $L = 2$ is chosen, and the corrected CSI is computed by:

$$\dot{h}_{t_{\text{act}}(n-k/\eta)} = \left(1 - \frac{k}{N_t}\right) \tilde{h}_{t_{\text{act}}(n)} + \left(\frac{k}{N_t}\right) \tilde{h}_{t_{\text{act}}(n-N_t/\eta)}, \quad k = 1, 2, \ldots, N_t - 1. \tag{4.16}$$

For $L > 2$, interested readers are referred to [101]. Regarding transmit antenna t, the last pilot slot is at the time index of $n - k_{t,t_{\text{act}}}/\eta$, and:

$$k_{t,t_{\text{act}}} = \begin{cases} t_{\text{act}} - t & \text{if} \quad t \leq t_{\text{act}} \\ t_{\text{act}} - t + N_t & \text{if} \quad t > t_{\text{act}} \end{cases}. \tag{4.17}$$

The channel difference information between t and t_{act}, denoted by $\Delta_{t,t_{\text{act}}}$, is updated as follows:

$$\Delta_{t,t_{\text{act}}(n-k_{t,t_{\text{act}}}/\eta)} = \tilde{h}_{t(n-k_{t,t_{\text{act}}}/\eta)} - \dot{h}_{t_{\text{act}}(n-k_{t,t_{\text{act}}}/\eta)}. \tag{4.18}$$

Step 3: Correlation-assisted CE

After collecting the CDI, it is possible to measure the CSI of the idle antennas. The estimation result of correlation-based CE is denoted by $\acute{h}_{t(n)}$ and it is obtained by:

$$\acute{h}_{t(n)} = \tilde{h}_{t_{\text{act}}(n)} + \Delta_{t,t_{\text{act}}(n-k_{t,t_{\text{act}}}/\eta)}, \quad t \neq t_{\text{act}}. \tag{4.19}$$

Substituting (4.16) and (4.18) into (4.19), this gives:

$$\acute{h}_{t(n)} = \tilde{h}_{t(n-k_{t,t_{\text{act}}}/\eta)} + \frac{k_{t,t_{\text{act}}}}{N_t}\left(\tilde{h}_{t_{\text{act}}(n)} - \tilde{h}_{t_{\text{act}}(n-N_t/\eta)}\right), \quad t \neq t_{\text{act}}. \tag{4.20}$$

Note that when $t = t_{\text{act}}$ in (4.17), the value of $k_{t,t_{\text{act}}}$ equals zero. Correspondingly, the right side of the above equation reduces to $\tilde{h}_{t_{\text{act}}(n)}$. Therefore, the estimated CSI obtained by both pilot-based CE and correlation-based CE can be written as the same expression in (4.20). The estimated CSI of any transmit antennas is denoted by $\hat{h}_{t(n)}$, and (4.20) can be rewritten as:

$$\hat{h}_{t(n)} = \tilde{h}_{t(n-k_{t,t_{\text{act}}}/\eta)} + \frac{k_{t,t_{\text{act}}}}{N_t}\left(\tilde{h}_{t_{\text{act}}(n)} - \tilde{h}_{t_{\text{act}}(n-N_t/\eta)}\right), \quad t = 1, \ldots, N_t. \tag{4.21}$$

Step 4: Antenna index update

The index of the transmit antenna to convey the pilot next time is then updated to:

$$t_{\text{act}} = \begin{cases} t_{\text{act}} + 1 & \text{if} \quad t_{\text{act}} < N_t \\ 1 & \text{if} \quad t_{\text{act}} = N_t \end{cases}. \tag{4.22}$$

The CE period of TCCE is computed by:

$$P_{\text{CE}} = \frac{T_s}{\eta}. \tag{4.23}$$

The CE period of TCCE is independent of the number of transmit antennas. In addition to one LS process for the currently active antenna, TCCE requires one interpolation and two additions for each idle antenna. According to (4.16), the interpolation needs two multiplications and one addition. As a result, TCCE consumes $2\xi^2 + 3\xi$ operations for each idle antenna. The computational complexity of TCCE during one estimation period is given by:

$$O_{\text{TCCE}}(N_r(\xi^2 + (N_t - 1)(2\xi^2 + 3\xi))). \tag{4.24}$$

Compared with CCE, TCCE approximately doubles the computational complexity.

4.3.3 Results

In this section, Monte Carlo simulation results are presented to validate the performance of the proposed method. Various numbers of transmit antennas are considered. In order to conduct a fair comparison, the antennas are located in a square area with a normalised diagonal distance. The BER performance of SM using TCCE is compared with CCE. Also, the effects of channel correlations on both CCE and TCCE are studied. In all simulations, a user speed of 5 m/s is assumed, and the pilot ratio is fixed to be 5% [102].

4.3.3.1 Effects of channel correlation

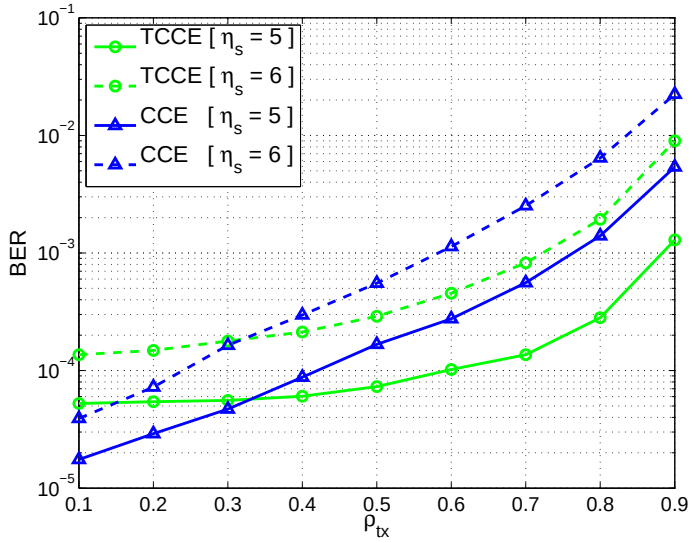

Figure 4.3: *BER performance of TCCE against channel correlations (SNR = 20 dB and* $N_t = 16$*).*

In Fig. 4.3, the BER performance of TCCE is shown as a function of ρ_{tx}. The SNR is assumed to be 20 dB, and 16 transmit antennas are considered. Two η_s values of 5 and 6 are considered. As shown, the proposed method falls behind CCE when ρ_{tx} is smaller than 0.3. The reason for this fact is as the channel correlation decreases, the CDI between antennas becomes larger and more random. Therefore the CDI updating process in TCCE is less accurate in this situation. However, when ρ_{tx} is greater than 0.4, TCCE offers a much better BER performance than CCE. Similar, but less pronounced trends are noticed at lower SNRs.

4.3.3.2 Effects of the number of transmit antennas

Fixing ρ_{tx} to be 0.8, Fig. 4.4 presents the BER performance of TCCE for two N_t values of 8 and 16. The number of bits per symbol is fixed to ensure a fair comparison. Also, the case of perfect channel state information (PCSI) is considered as a baseline.

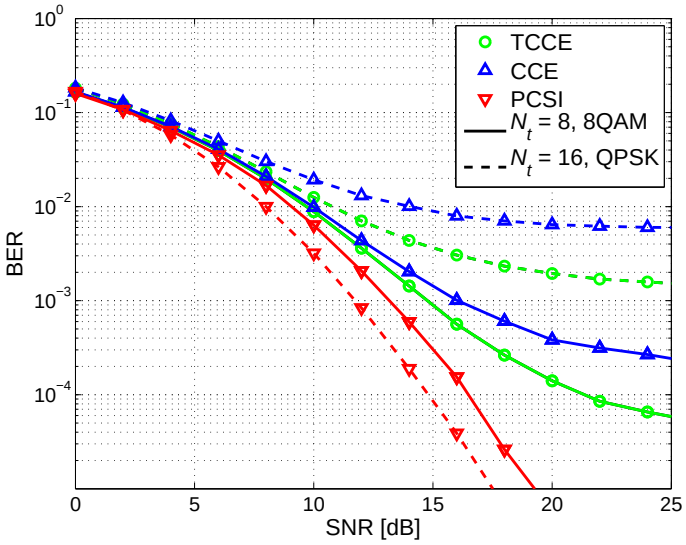

Figure 4.4: *BER performance of TCCE against the numbers of transmit antennas ($\rho_{\text{tx}} = 0.8$).*

The following outcomes are observed: i) unlike PCSI, the achievable BERs of both TCCE and CCE tend towards saturation with an increase of SNR, due to the inevitability of estimation errors; ii) compared with CCE, the BER performance of TCCE is much closer to that of PCSI; and iii) TCCE outperforms CCE more significantly as N_t increases. For $N_t = 8$ and 16, to achieve the same BER value of CCE at 20 dB, TCCE requires 2.8 dB and 7.5 dB less, respectively. This is because the CE period of CCE is proportional to N_t, while that of TCCE is regardless of N_t. At a lower channel correlation, the gain gap between TCCE and CCE diminishes. Despite this, TCCE can still effectively improve the achievable BER over CCE when $\rho_{\text{tx}} = 0.5$, as shown in Fig. 4.5.

4.4 Channel estimation across receive antennas

In order to improve the CE accuracy, a longer pilot sequence length or a larger transmission power is usually required. However, as mentioned, the estimation time in the CCE methods for SM is proportional to the number of transmit antennas. Therefore the pilot sequence length

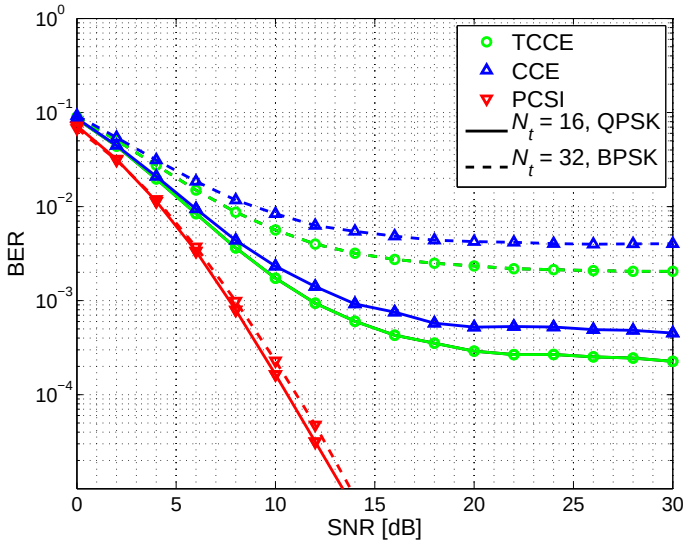

Figure 4.5: *BER performance of TCCE against the numbers of transmit antennas ($\rho_{tx} = 0.5$).*

for each transmit antenna is constrained to avoid compromising the throughput significantly. In addition, the transmission power is limited due to the dynamic range of power amplifiers. This raises the question, how to improve the CE performance without increasing the pilot sequence length or the transmission power. Based on exploiting the channel correlation between receive antennas, another CE method for SM is proposed in this section. For the sake of simplicity, here we consider the pilot structure of Section 4.3.1, and keep the relevant study on the pilot structure of TCCE in Section 4.6.

4.4.1 Conventional method

In the CCE methods for SM, the CSI related to each receive antenna is estimated separately. Since the focus is on the receiver side, the indices of transmit antennas are neglected without loss of generality. For a certain transmit antenna, the CCE result of the r-th receive antenna at the n-th estimation slot is written as:

$$\tilde{h}_{r(n)} = \frac{y_{r(n)}}{p_{(n)}}. \tag{4.25}$$

4.4.2 Proposed method

The proposed method is named spatially-averaging channel estimation (SACE), of which the schematic diagram for $N_r = 2$ is shown in Fig. 4.6. Unlike CCE, SACE jointly estimates the channel of different receive antennas, which resembles the way of exploiting the correlation between transmit antennas in TCCE. A similar definition of CDI is used in receive antennas, and it is used to estimate the channel of one receive antenna from the estimation result of another one. The estimated CSI of SACE for each receive antenna is a combination of the CCE results of all receive antennas. For a arbitrary number of receive antennas, the detailed algorithm of the proposed method is comprised of two steps.

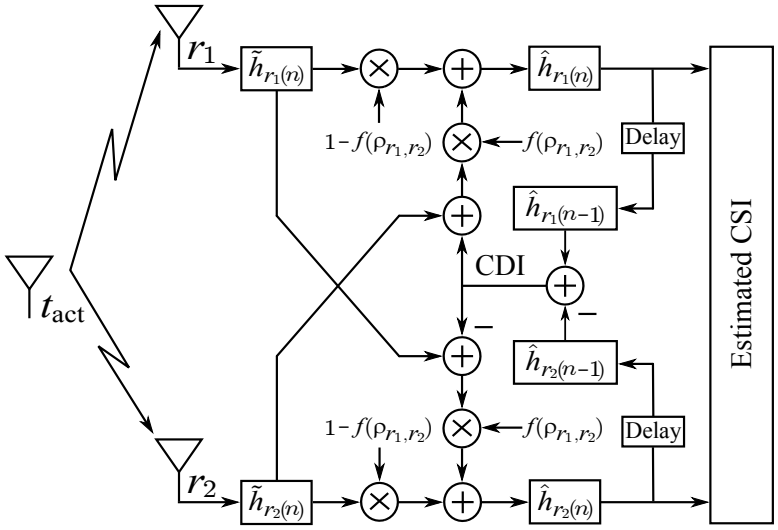

Figure 4.6: *Schematic diagram of SACE for two receive antennas.*

Step 1: channel difference update

Regarding the proposed method, we use $\hat{h}_{r(n)}$ to denote the estimated CSI of the r-th receive antenna at the n-th estimation slot. The CDI between the r_1-th and r_2-th receive antennas, denoted by Δ_{r_1,r_2}, is obtained by differentiating the previous estimation results of those antennas:

$$\Delta_{r_1,r_2(n-1)} = \hat{h}_{r_1(n-1)} - \hat{h}_{r_2(n-1)}. \tag{4.26}$$

Step 2: weighted average

Based on the CDI obtained in (4.26), the channel of r_1 can be estimated via the CCE result of r_2, i.e. $\tilde{h}_{r_2(n)}$. In order to reduce the affect of noise, the estimate for any receive antenna is

formed by a weighted average of the samples from all receive antennas. The estimation result of SACE is then formulated as:

$$\hat{h}_{r_1(n)} = \left(1 - \sum_{r_2=1\neq r_1}^{N_r} f(\rho_{r_1,r_2})\right) \tilde{h}_{r_1(n)} + \sum_{r_2=1\neq r_1}^{N_r} f(\rho_{r_1,r_2}) \left(\tilde{h}_{r_2(n)} + \Delta_{r_1,r_2(n-1)}\right), \quad (4.27)$$

where $f(\rho_{r_1,r_2})$ is the weight for the pair of r_1 and r_2, and it is subject to:

$$\begin{cases} 0 \leq f(\rho_{r_1,r_2}) \leq 1 & \text{(4.28a)} \\ 0 \leq \sum_{r_2=1\neq r_1}^{N_r} f(\rho_{r_1,r_2}) \leq 1 & \text{(4.28b)} \end{cases}$$

Besides the above conditions, two extreme situations of $\rho_{r_1,r_2} = 1$ and $\rho_{r_1,r_2} = 0$ are analysed to further restrict the weights. When the antennas are completely correlated, the weights for all components in (4.27) should be equal. On the contrary, if the antennas are independent of each other, the estimation based on other antennas becomes difficult. Therefore, it is better to just use $\tilde{h}_{r_1(n)}$ in this situation. Then the weight $f(\rho_{r_1,r_2})$ is required to satisfy:

$$f(\rho_{r_1,r_2}) = \begin{cases} 0 & \text{if } \rho_{r_1,r_2} = 0 \\ \dfrac{1}{N_r} & \text{if } \rho_{r_1,r_2} = 1 \end{cases} . \quad (4.29)$$

Combining (4.28) and (4.29), one solution for the weight function is simply given by:

$$f(\rho_{r_1,r_2}) = \frac{\rho_{r_1,r_2}}{N_r}. \quad (4.30)$$

Besides the estimation process of CCE, the weighted average process for each receive antenna mainly requires N_r multiplications. Therefore, the computational complexity of SACE is estimated as:

$$O_{\text{SACE}}(N_t(N_r + N_r^2)\xi^2). \quad (4.31)$$

Compared with (4.15), it can be found that the complexity of SACE is $N_r + 1$ times as much as CCE. In practice, N_r is restricted due to the compact size of mobile devices. Therefore SACE requires limited processing power in addition to CCE.

4.4.3 Results

In this section, Monte Carlo simulation results are shown to validate the performance of the proposed method. In all simulations, quadrature phase shift keying (QPSK) symbols are sent from a transmitter of four antennas. The pilot ratio and the user speed are set to be the same values as in Section 4.3.3. The BER performance of SACE is compared with CCE in two aspects: the receiver correlation and the number of receive antennas.

4.4.3.1 Effects of channel correlation

Assuming two antennas at the receiver, Fig. 4.7 presents the BER performance of SACE for different channel correlations. Due to the facts that N_r is smaller than N_t and the system uses practical CSIs, both SACE and CCE require a relatively large SNR to achieve a certain BER target. Two outcomes are observed: i) SACE always offers a better performance than CCE; and ii) when the channel correlation increases, SACE outperforms CCE more significantly. For $\rho_{\text{rx}} = 0.2$ and 0.8, SACE achieves SNR gains of 0.2 dB and 0.6 dB against CCE, respectively. As ρ_{rx} decreases, the CDI between receive antennas becomes larger and more random, which is similar to the situation in TCCE. However, unlike TCCE, SACE still performs better than CCE when the channel correlation between receive antennas is low. Because there are only two receive antennas involved in this case, the advantage of SACE is not well pronounced. The following context discusses the performance of SACE with a larger number of receive antennas.

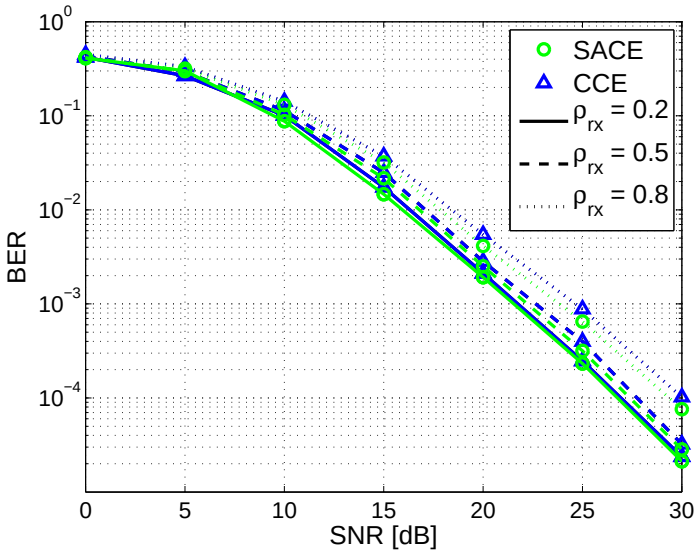

Figure 4.7: *BER performance of SACE ($N_t = 4$ and $N_r = 2$).*

4.4.3.2 Effects of the number of receive antennas

Fig. 4.8 shows the BER performance of both SACE and CCE when 4 receive antennas are employed. As can be seen, the SNR gaps between SACE and CCE are larger than those in the case of 2 antennas. When $\rho_{\text{rx}} = 0.8$, for example, an SNR gain of 1.8 dB is obtained by SACE over CCE, which is greater than the gain of 0.6 dB when $N_r = 2$. The reason is simple and direct. When more receive antennas are involved, more samples are available for the averaging process in SACE, and this is equivalent to increase the pilot sequence length. Correspondingly, SACE requires higher computational complexity (4 times larger than CCE) in this case.

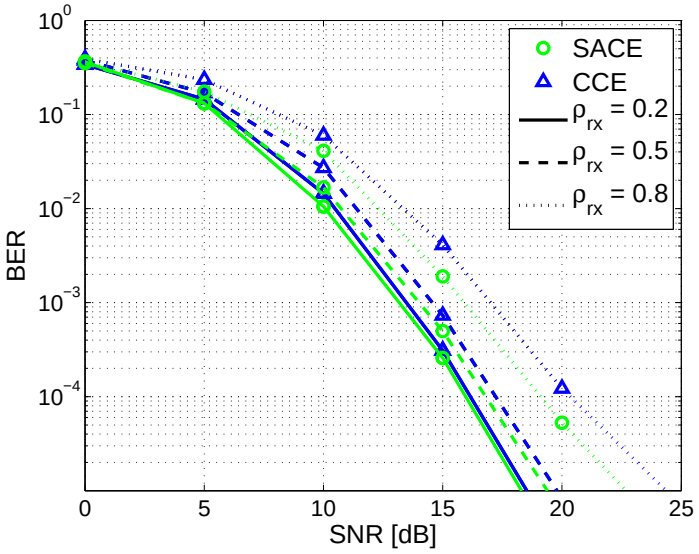

Figure 4.8: *BER performance of SACE ($N_t = 4$ and $N_r = 4$).*

4.5 Optimal power allocation in channel estimation

Since the CE process for SM occupies a substantial portion of time period, the power consumed for transmitting pilot symbols cannot be neglected. In current literature about the channel estimation for SM, equal power allocation (EPA) is considered between the pilot symbols and the information-carrying symbols. However, the power allocation needs to be treated carefully because it affects the BER performance in two aspects. On the one hand, an increased power for pilot symbols can improve the estimation accuracy, especially when the pilot sequence length is constrained. On the other hand, allocating less power to information-carrying symbols leads to an increase in the impairment caused by noise. This in fact enables a trade-off between

the transmission power of pilot symbols and the transmission power of information-carrying symbols. In this section, an optimal power allocation (OPA) method in CE for SM is proposed.

4.5.1 Optimisation problem

In [47], an average bit error probability (ABEP) upper bound is derived for SM in the presence of channel estimation errors. However, the ABEP bound is not a closed-form, and hence, it is difficult to be minimised. Alternatively, we focus on minimising the pair-wise error probability (PEP), which is given by [47, Eq. (12)]:

$$\text{PEP}_{\hat{\mathbf{H}}}(\mathbf{x}_{t,l} \to \mathbf{x}_{t',l'}) = \frac{1}{\pi}\int_0^{\pi/2}\left(1+\frac{\text{g}_{\text{SM}}}{4\text{sin}^2\theta}\times\frac{E_s}{N_0(1+\sigma_\epsilon^2)+E_s\sigma_\epsilon^2}\right)^{-N_r}d\theta, \tag{4.32}$$

where $\mathbf{x}_{t,l}$ means the symbol χ_l is sent from the t-th transmit antenna; σ_ϵ^2 denotes the variance of CE errors; and:

$$\text{g}_{\text{SM}} = \begin{cases} 2, & \text{if} \quad t \neq t' \\ |\chi_l - \chi_{l'}|^2, & \text{if} \quad t = t' \end{cases}. \tag{4.33}$$

The PEP of SM under the assumption of PCSI is computed by [103, Eq. (5)]:

$$\text{PEP}_{\mathbf{H}}(\mathbf{x}_{t,l} \to \mathbf{x}_{t',l'}) = \frac{1}{\pi}\int_0^{\pi/2}\left(1+\frac{\text{g}_{\text{SM}}\gamma_s}{4\text{sin}^2\theta}\right)^{-N_r}d\theta. \tag{4.34}$$

It can be found that γ_s in (4.34) is replaced by γ_e when CE errors are involved, where:

$$\gamma_e = \frac{E_s}{N_0(1+\sigma_\epsilon^2)+E_s\sigma_\epsilon^2}, \tag{4.35}$$

and γ_e is thus referred to as effective SNR. The variance of CE errors is calculated by:

$$\sigma_\epsilon^2 = \frac{N_0}{E_p N_p N}, \tag{4.36}$$

where N is a parameter depending on the chosen estimation approach [104]. When the LS estimator is considered, this results in $N = 1$, and (4.35) is thus rewritten as:

$$\gamma_e = \frac{E_p E_s}{(E_p + E_s + N_0)N_0}. \tag{4.37}$$

Similar to the situation of PCSI, minimising the PEP in (4.32) is equivalent to maximising the effective SNR. The power allocation is normally restricted to a certain power budget. In other words, the average energy consumption per symbol is predefined, and it is denoted by E_a. Correspondingly, the average SNR is defined as $\gamma_a = E_a/N_0$. During a unit interval, the time consumed in conveying pilot symbols is $\frac{1}{\eta}$, while the time for sending information-carrying symbols is $1 - \frac{1}{\eta}$. The optimisation problem is then formulated by:

$$\begin{aligned} (E_p^\dagger, E_s^\dagger) = & \underset{(E_p, E_s)}{\arg\max} \quad \gamma_e(E_p, E_s), \\ \text{s.t.} \quad & \eta E_p + (1-\eta) E_s = E_a \\ & E_p \geq 0, E_s \geq 0 \end{aligned} \tag{4.38}$$

where $(E_p^\dagger, E_s^\dagger)$ denotes the optimal solution of (E_p, E_s).

4.5.2 Analytical Modelling

The Lagrange multiplier maximisation method [105] is applicable to solve the problem in (4.38), for which the Lagrangian function is formed by:

$$\Lambda(E_p, E_s, \lambda) = \gamma_e(E_p, E_s) + \lambda(\eta E_p + (1-\eta) E_s - E_a), \tag{4.39}$$

where λ is the Lagrange multiplier. In order to achieve the maximum of the above Lagrangian function, stationary points are obtained by solving the following system of equations:

$$\begin{cases} \partial \Lambda(E_p^s, E_s^s, \lambda^s)/\partial E_p^s &= 0 \\ \partial \Lambda(E_p^s, E_s^s, \lambda^s)/\partial E_s^s &= 0 \\ \partial \Lambda(E_p^s, E_s^s, \lambda^s)/\partial \lambda^s &= 0 \end{cases}, \tag{4.40}$$

where λ^s is the Lagrange multiplier associated to the stationary point (E_p^s, E_s^s). The stationary points of E_p are thus computed by:

$$E_p^{s_1,s_2} = E_a \frac{-f(\gamma_a) \pm \sqrt{f^2(\gamma_a) + \frac{g}{\eta} f(\gamma_a)}}{g}, \tag{4.41}$$

where:

$$\begin{cases} f(\gamma_a) = 1 + \dfrac{1-\eta}{\gamma_a} & \text{(4.42a)} \\ g = (1-\eta)N_p - \eta & \text{(4.42b)} \end{cases}$$

Note that $f(\gamma_a)$ is always positive, and $g \geq 1 - 2\eta$ because of $N_p \geq 1$. In practice, the pilot ratio is usually less than 10% [102]. Therefore the parameter g is also positive. Consequently, $E_p^{s_1}$ is positive whereas $E_p^{s_2}$ is negative. However, energy is non-negative, and thus $E_p^{s_1}$ is the only possible stationary point.

Proposition 4.5.1. *$E_p^{s_1}$ is the maximum point for the effective SNR in (4.37).*

Proof. The second derivative of Λ with respect to E_p is calculated by:

$$\frac{\partial \Lambda(E_p)}{\partial^2 E_p} = -\frac{2N_p E_a^2}{N_0} \times \frac{\eta f^2(\gamma_a) + g f(\gamma_a)}{(gE_p + f(\gamma_a)E_a)^3}. \tag{4.43}$$

Substituting (4.41) into (4.43), this gives:

$$\left.\frac{\partial \Lambda(E_p)}{\partial^2 E_p}\right|_{E_p = E_p^{s_1}} = -\frac{2\eta N_p}{E_a N_0}\left(f^2(\gamma_a) + \frac{g}{\eta} f(\gamma_a)\right)^{-\frac{1}{2}}. \tag{4.44}$$

It is obvious that the right side of (4.44) is always negative. Based on the second derivative rule, it is proved that the effective SNR in (4.37) achieves its maximum value at $E_p = E_p^{s_1}$.

□

Therefore the optimal solution of E_p is obtained by:

$$E_p^{\dagger} = E_a \frac{\sqrt{f^2(\gamma_a) + \left(\dfrac{1-\eta}{\eta} N_p - 1\right) f(\gamma_a)} - f(\gamma_a)}{(1-\eta)N_p - \eta}. \tag{4.45}$$

4.5.3 Simplified solution for high SNRs

Assuming the SNR is sufficiently high, i.e. $\gamma_a \gg 1$, (4.42a) can be approximated to:

$$f(\gamma_a) \cong 1. \tag{4.46}$$

Substituting (4.46) into (4.45), this gives:

$$E_p^{\dagger} = E_a \frac{\sqrt{\frac{1-\eta}{\eta} N_p} - 1}{(1-\eta)N_p - \eta}. \tag{4.47}$$

It can be found that, in this case, the ratio of $E_p^{\dagger}$ to E_a depends on the pilot sequence length N_p and the pilot ratio η. Fig. 4.9 plots the OPA solutions against N_p and η, in comparison with EPA. As shown, when the product of N_p and η is larger than one, the optimal power of pilot symbols is slightly below the average power. However, as the product of N_p and η decreases in the region of $\eta N_p < 1$, the optimal power of pilot symbols increases dramatically.

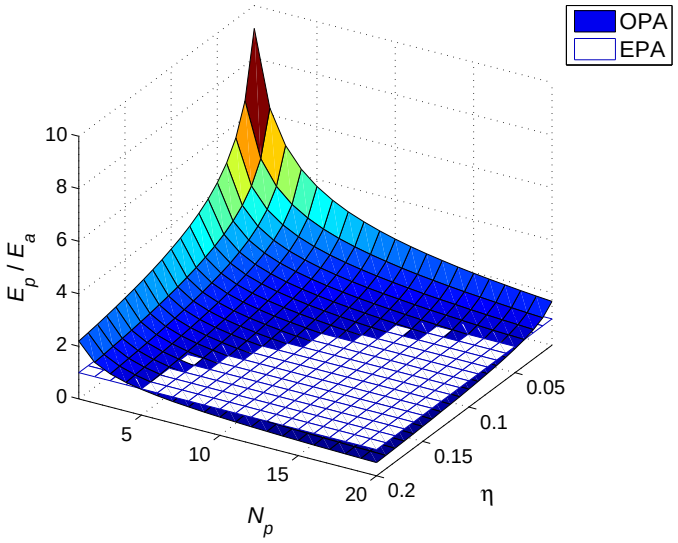

Figure 4.9: *Power allocation in channel estimation for SM.*

4.5.4 Results

The performance of the proposed OPA method is validated in this section. Simulations are implemented for two purposes: i) to verify the accuracy of the optimisation solutions; and ii) to compare the BER performance of OPA with EPA for different values of N_p and η. In all simulations, 4 antennas are assumed at both the transmitter and the receiver, without considering the correlation between antennas. QPSK is used for the signal modulation. Since the temporal correlation is not involved here, the users are assumed to be static for the sake of convenient analysis.

4.5.4.1 Optimisation accuracy

First, assuming $\gamma_a = 20$ dB, the BER performance of OPA is shown as a function of E_p/E_a in Fig. 4.10. Different choices for N_p and η are considered to validate the optimisation accuracy for a broad range of scenarios, and the OPA results of the simplified solution are highlighted by red dots.

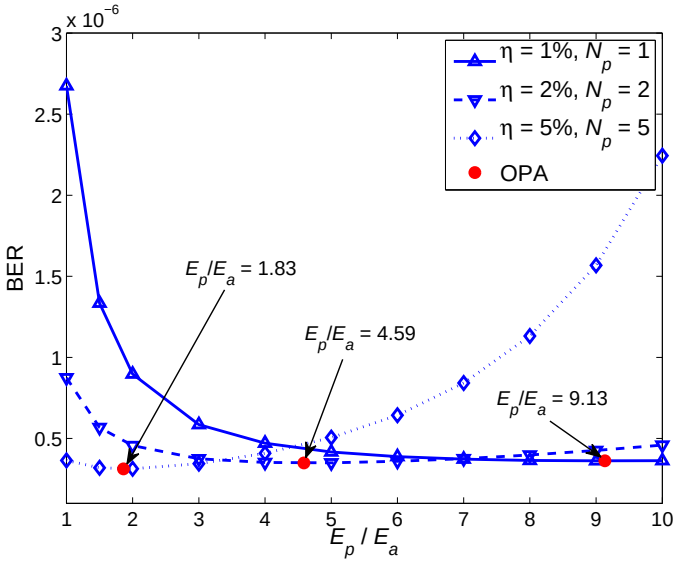

Figure 4.10: *Optimality of the proposed OPA method ($\gamma_a = 20$ dB, $N_t = 4$ and $N_r = 4$).*

As shown, the proposed OPA method always achieves the minimum BER. For different η and N_p, the optimal value of E_p/E_a varies. In general and as expected, it is better to allocate more transmission power to the pilot signal when the pilot ratio decreases. At $\eta = 5\%$, the optimal E_p/E_a approaches one, i.e. the EPA method. When the pilot ratio reduces to 2%, the optimal power of pilot symbols is 4.59 times of the average power. As the pilot ratio is further decreased to 1%, the optimum ratio of the pilot power to the average power increases to 9.13. The reason for this trend is that a low pilot ratio results in a poor CE accuracy, which impairs the BER performance more significantly than reducing the transmission power of information-carrying symbols. Therefore, it is beneficial to trade off the power of information-carrying symbols for the power of pilot symbols, so that the CE errors can be reduced. On the contrary, more power should be allocated to information-carrying symbols when a CE of sufficient accuracy is achieved.

4.5.4.2 BER performance of OPA

In Fig. 4.11, the BER performance of OPA is presented as a function of the average SNR. To ensure a fair comparison, the CE period $\frac{N_p N_t}{\eta}$ is fixed for different values of (η, N_p). Besides EPA, the case of PCSI is considered as a benchmark.

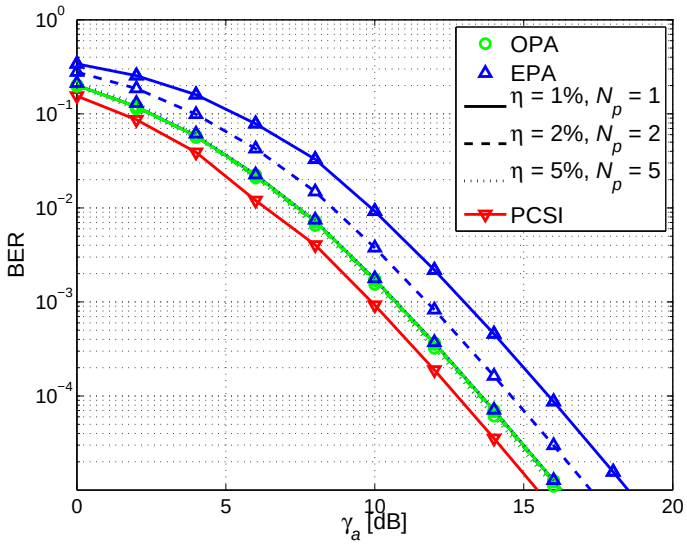

Figure 4.11: *BER performance of OPA ($N_t = 4$ and $N_r = 4$).*

The following outcomes are observed: i) the performance of OPA is closer than EPA to the results of PCSI; and ii) the performance of EPA degrades rapidly when reducing the pilot ratio. In contrast, OPA provides a fairly stable performance against the change of pilot ratio. To achieve the same performance as PCSI, OPA requires an extra SNR of less than 1 dB. This makes OPA superior to EPA in a more significant way when the pilot ratio becomes smaller.

4.6 Combined channel estimation

In the previous context, three novel CE methods have been proposed to improve the BER performance of SM in the presence of CE errors. Among those methods, TCCE and SACE focus on exploiting the channel correlation between antennas at the transmitter and at the receiver, respectively. In addition, OPA balances the transmission power of pilot symbols with the transmission power of information-carrying symbols to achieve the minimum BER. In this section, a combined CE technique for SM is presented, where the above CE methods are integrated.

4.6.1 Concept

The block diagram of the combined CE for SM is shown in Fig. 4.12, which consists of four main modules: i) the pilot structure; ii) the power allocation; iii) the CE for individual receive antenna; and iv) the CE across receive antennas. At the transmitter, an adaptive switch between CCE and TCCE is used in accordance with the channel correlation between transmit antennas. After the pilot structure is determined, the OPA algorithm is applied for allocating the optimal transmission power to pilot symbols.

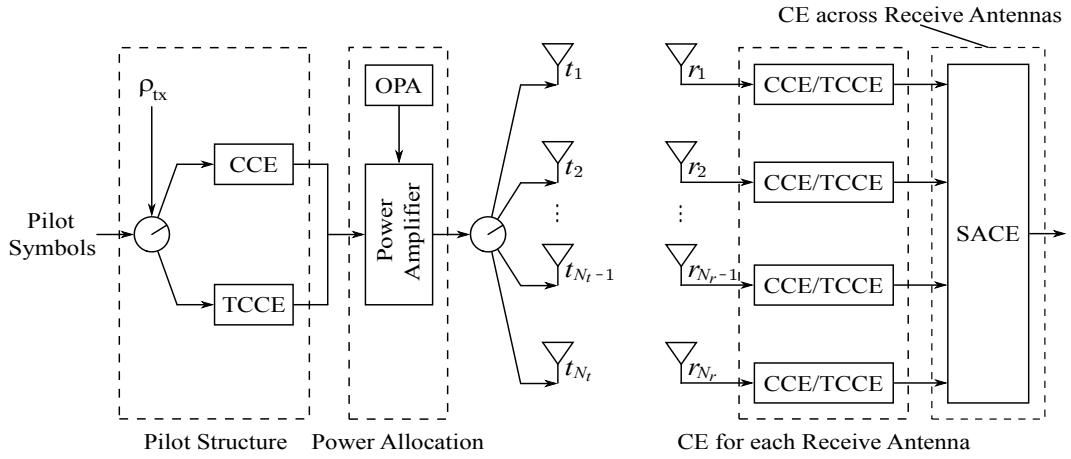

Figure 4.12: *Block diagram of the combined channel estimation for SM.*

A dedicated channel is required to inform the receiver of the selection result regarding the pilot structure. According to the selection of pilot structure, either CCE or TCCE is used to estimate the CSI between the active transmit antenna and each receive antenna. Afterwards, the SACE method is enabled, and the estimation results are then output to decode the following information-carrying symbols.

4.6.2 Results

Fig. 4.13 presents the BER performance of combined CE, where an SM system of 8 transmit antennas and 4 receive antennas is considered. In addition, both ρ_{tx} and ρ_{rx} are assumed to be 0.5. In order to ensure a fair comparison, the CE period is fixed, i.e. the ratio of N_p to η is constant. Besides CCE, two cases of PCSI are considered for comparison: i) time-invariant channel; and ii) time-variant channel, and PCSI is only at the estimation slots.

As shown, the error floor occurs in all cases with time-variant channels, due to the inevitable errors between the CE results and the varying channel. When compared with CCE, the BER

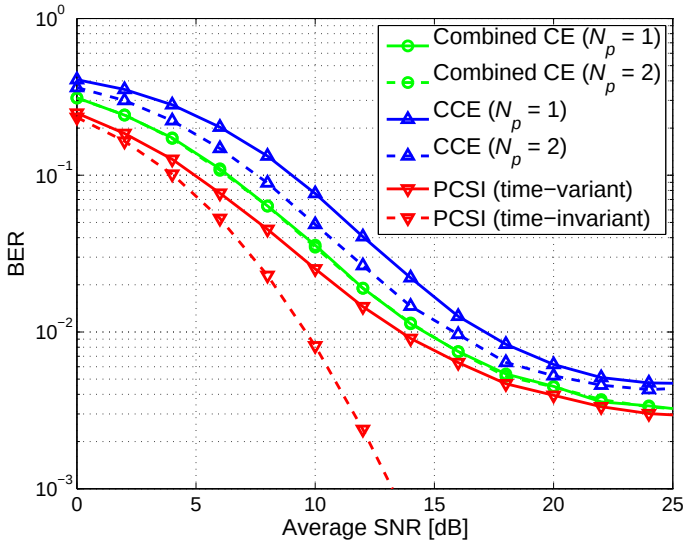

Figure 4.13: *BER performance of combined channel estimation ($N_t = 8$ and $N_r = 4$).*

performance of combined CE is much closer to that of PCSI. Taking $N_p = 2$ as an example, combined CE obtains an SNR gain of 1.2 dB against CCE, which is more pronounced than any CE method being used individually. Also, the performance of CCE degrades significantly as the pilot sequence length decreases. When N_p is reduced from 2 to 1, CCE requires an extra SNR of 1.3 dB to maintain the BER performance. In contrast, combined CE presents a stable performance against the reduction of the pilot sequence length. As a result, the SNR gain achieved by combined CE over CCE at $N_p = 1$ is larger than that at $N_p = 2$.

4.7 Summary

In this chapter, three novel CE methods have been presented to improve the performance of SM in the presence of CE errors. In order to shorten the time consumed in the CE process, TCCE enabled to estimate the entire MIMO channel by sending pilots through one transmit antenna only. By exploring the channel correlation between transmit antennas, this particular method offers a better estimation accuracy than the conventional methods for medium and high correlation degrees. Considering SM as well as other MIMO schemes encounters performance degradation over correlated channels, an accurate CE is of importance in particular. Results have shown that TCCE can effectively improve the performance of SM against the channel correlations.

In addition, SACE has been presented, aimed to increase the CE performance for SM under the constraint of a limited pilot sequence length. SACE exploits the channel correlation in a similar way to TCCE but at the receiver, and jointly estimates the channel of receive antennas. Simulation results have been presented to compare the performance of SACE with CCE. It has been shown that SACE improves the CE performance for SM without increasing the pilot sequence length. For various channel correlations, unlike TCCE, SACE always offers a better CE accuracy than CCE.

Furthermore, the power allocation between pilot symbols and information-carrying symbols has been studied. An optimal power allocation has been presented to balance the impairment caused by the CE errors and the noise, in order to minimise the BER. It has been shown that for a high SNR, the optimal transmission power is only determined by the pilot ratio and the pilot sequence length. Results have been presented to verify the optimality of the proposed method and to evaluate its performance against EPA and PCSI. Moreover, a framework on the combined CE for SM has been presented, where the above CE methods are combined in order to further improve the performance of SM systems. According to the practical environment, combined CE can adaptively switch between CCE and TCCE, and adjust the weights of SACE at the cost of limited feedback and complexity.

Chapter 5
Spatial modulation in a multi-user scenario

5.1 Introduction

In current literature, the research on spatial modulation (SM) in the multi-user scenario focuses on coordinating the interference among users [53, 54], while the user selection is neglected. Like other MIMO schemes, the precoding technique is applicable to SM in order to cancel inter-user interference (IUI). However, multi-stream MIMO can be decomposed into parallel non-interfering spatial layers, and each layer is available for one user. In contrast, the SM system requires at least two transmit antennas for each user in order to keep its function. This fact challenges the process of allocating the transmit antennas of the SM system to the users. In this chapter, an novel method that adaptively groups and allocates the antennas of the SM system is presented.

5.2 System model

5.2.1 SM system for multiple users

Consider the signal is transmitted from one base station (BS) to multiple users at the same time-frequency slot. The number of users is denoted by N_u, and each user is equipped with N_r antennas. The total number of antennas at the BS is denoted by N_{tot}. Those antennas are divided into N_u groups, and each group contains $N_t = N_{\text{tot}}/N_u$ antennas.

Fig. 5.1 draws the block diagram of the SM system in the multi-user scenario. For each user, a $N_t \times N_r$ SM-MIMO is operated in the same way as in Section 2.3. At the BS side, one antenna out of each group is activated at any time instance. Therefore there are N_u antennas being active simultaneously, and each user receives the signals sent from all groups. For a certain user, the signal from the corresponding group is the desired signal, while the signals from the

remaining groups are interference. The desired signals and the interfering signals are shown by solid lines and dashed lines, respectively.

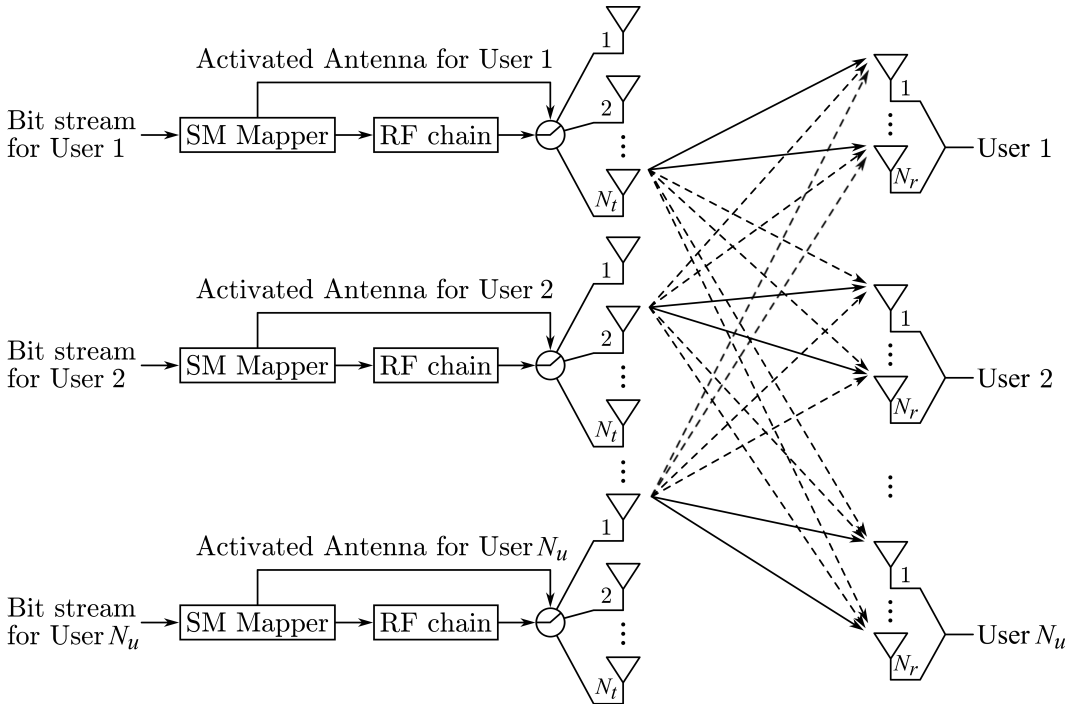

Figure 5.1: *SM system in a multi-user scenario.*

The symbol chosen from the signal constellation diagram for user k is denoted by s_k, and the channel from the transmit antenna t of group j to the receive antenna r of user k is denoted by h_{t_j,r_k}. Assuming t_j is the currently active antenna of group j, the received signal at the r-th receive antenna of user k is expressed as:

$$y_{r_k} = h_{t_k,r_k} s_k + \sum_{j=1 \neq k}^{N_u} h_{t_j,r_k} s_j + w_{r_k}, \tag{5.1}$$

where w_{r_k} is the noise at r-th receive antenna of user k.

5.2.2 Channel model

Consider a Rayleigh fading channel without shadowing. The constant correlation model in Section 3.2.2 is applied to the channel links from the BS to each user. Across the users, the channel links are statistically independent. For the sake of simplicity, the same channel correlation degree is assumed for all users. The correlation coefficients of the transmit antennas and

the receive antennas are denoted by ρ_{tx} and ρ_{rx}, respectively.

5.3 Multi-user SM

Unlike the traditional MIMO schemes, SM encodes part of the information bits into channel impulse responses. As a result, the conventional precoding techniques, such as zero forcing (ZF) and minimum mean square error (MMSE), are not applicable to MU-SM. In this section, the precoding method in [55] is introduced.

5.3.1 Design of precoding mask

Fig. 5.2 shows the application of the precoding technique in MU-SM, where perfect channel state information (PCSI) are assumed to be known at both the transmitter and the receiver. Note that the precoding method proposed in [55] is only available for a single antenna at each user terminal. The precoding mask is defined as the vector that is used to shape the signal before transmission. The precoding mask is denoted by $\mathbf{P} = [p_1, p_2, \ldots, p_{N_u}]^T$, where p_k is the element pertaining to user k. The transmitted signal for user k is the product of the chosen symbol and the precoding mask, i.e. $\dot{s}_k = s_k p_k$. Replacing s_k in (5.1) by $\dot{s}_k$, the signal received by user k is expressed as:

$$y_{r_k} = \underbrace{h_{t_k,r_k}\dot{s}_k}_{A} + \sum_{j=1\neq k}^{N_u} h_{t_j,r_k}\dot{s}_j + w_{r_k}. \tag{5.2}$$

Substituting $\dot{s}_k = s_k p_k$ into (5.2), this gives:

$$y_{r_k} = \underbrace{[h_{t_1,r_k}s_1, h_{t_2,r_k}s_2, \cdots, h_{t_{N_u},r_k}s_{N_u}]\mathbf{P}}_{B} + w_{r_k}. \tag{5.3}$$

In order to cancel the interference among users, term B is required to be equal to term A for all

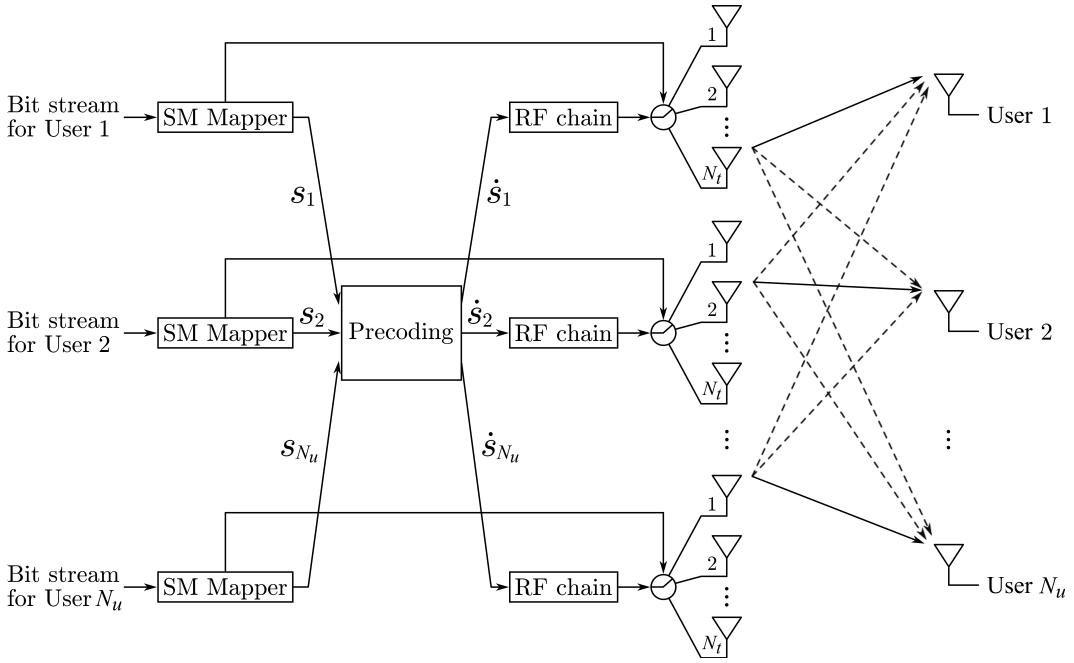

Figure 5.2: *The application of the precoding technique in MU-SM.*

users. The effective channel-modulation matrix is defined as:

$$\mathbf{H}_{\text{eff}} = \begin{bmatrix} h_{t_1,r_1}s_1 & h_{t_2,r_1}s_2 & \cdots & h_{t_{N_u},r_1}s_{N_u} \\ h_{t_1,r_2}s_1 & h_{t_2,r_2}s_2 & \cdots & h_{t_{N_u},r_2}s_{N_u} \\ \vdots & \vdots & \ddots & \vdots \\ h_{t_1,r_{N_u}}s_1 & h_{t_2,r_{N_u}}s_2 & \cdots & h_{t_{N_u},r_{N_u}}s_{N_u} \end{bmatrix}, \tag{5.4}$$

and the desired signals of all users formulates a vector as follows:

$$\mathbf{H}_{\text{req}} = \begin{bmatrix} h_{t_1,r_1}s_1 \\ h_{t_2,r_2}s_2 \\ \vdots \\ h_{t_{N_u},r_{N_u}}s_{N_u} \end{bmatrix}. \tag{5.5}$$

Equalising A and B for all users is thus equivalent to solve the following equation:

$$\mathbf{H}_{\text{eff}}\mathbf{P} = \mathbf{H}_{\text{req}}. \tag{5.6}$$

Note that $\mathbf{H}_{\text{req}}$ is the diagonal of the matrix $\mathbf{H}_{\text{eff}}$, and receive constellation optimisation is not

considered here in order to keep moderate complexity of analysis. Therefore the precoding mask is obtained by:

$$\mathbf{P} = (\mathbf{H}_{\text{eff}})^{-1}\text{diag}(\mathbf{H}_{\text{eff}}), \tag{5.7}$$

where $\text{diag}(\cdot)$ extracts the diagonal of a matrix.

5.3.2 Normalisation of precoding mask

In order not to affect the average transmission power, the norm of the vector **P** must be restricted to one. The normalised precoding mask is denoted by $\mathbf{P}_{\text{norm}}$, and it is calculated by:

$$\text{P}_{\text{norm}} = \beta\mathbf{P}, \tag{5.8}$$

and:

$$\beta = \mathbf{E}\left\{\sqrt{\frac{1}{\text{tr}\left(\mathbf{P}\mathbf{P}^{H}\right)}}\right\}, \tag{5.9}$$

where $\mathbf{E}\{\cdot\}$ is the expectation operator, and $\text{tr}(\cdot)$ denotes the trace of a matrix. Substituting (5.7) and (5.9) into (5.8), the normalised precoding mask for MU-SM is computed by:

$$\text{P}_{\text{norm}} = \mathbf{E}\left\{\sqrt{\frac{1}{\text{tr}\left((\mathbf{H}_{\text{eff}})^{-1}\text{diag}(\mathbf{H}_{\text{eff}})\left((\mathbf{H}_{\text{eff}})^{-1}\text{diag}(\mathbf{H}_{\text{eff}})\right)^{H}\right)}}\right\}(\mathbf{H}_{\text{eff}})^{-1}\text{diag}(\mathbf{H}_{\text{eff}}). \tag{5.10}$$

The decoding process for each user is the same as that in the single-user scenario.

5.4 Spatial modulation multiple access

Although MU-SM eliminates IUI and realises space division for multiple users, it is based on a fixed grouping of the transmit antennas. Like the frequency carriers can be allocated to different users, the antennas are also a manageable resource, and they are significant for improving the performance of MU-SM. A novel method that adaptively allocates the antennas to the users in MU-SM is presented in this section. The new method is named spatial modulation multiple access (SMMA).

5.4.1 Concept

In Section 3.3.4, the transmit antenna selection (TAS) issue for SM in the single-user scenario has been addressed, which selects a portion of the antenna array in order to minimise the bit error rate (BER). Similarly, there exists an antenna selection when multiple users are involved. In MU-SM, each user requires N_t transmit antennas from the total number of N_{tot}. The basic concept of SMMA is to adaptively allocate the transmit antennas to multiple users. Fig. 5.3 depicts the block diagram of SMMA in the case of two users. Based on the knowledge of CSI, the transmit antennas and the receive antennas are jointly scheduled for all users. Since MU-SM also requires CSI at the transmitter, SMMA in fact does not cost additional feedback. At the BS, the antennas are divided into N_u groups, and each group is corresponding to one user. At the same time, one of the receive antennas is determined for each user. After the process of antenna allocation is done, MU-SM is applied to the SMMA system.

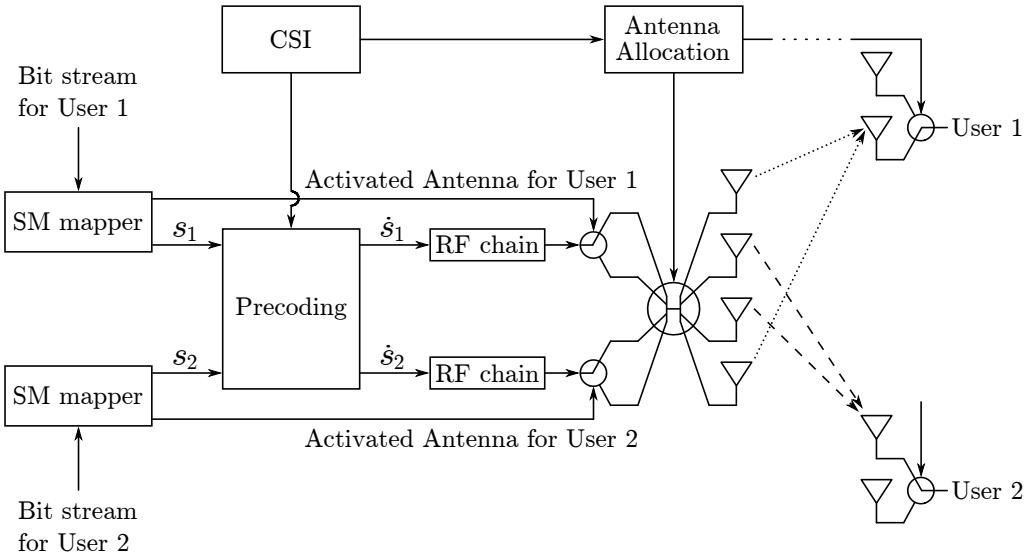

Figure 5.3: *Block digram of spatial modulation multiple access.*

Exhaustive search is commonly used in solving TAS issues. However, from single-user to multi-user, the TAS problem becomes more complicated and more challenging. In Table 5.1, the exhaustive search methods for TAS in single-user and multi-user scenarios are compared in terms of the computational complexity and the feedback cost. Note that in MU-SM, the number of transmit antennas per user depends on the total number of transmit antennas and the number of users. Therefore the computational complexity in that case is formulated as a function of the number of users. Using exhaustive search in the multi-user scenario costs a much higher complexity than that in the single-user scenario. Take $N_{\text{tot}} = 16$ and $N_t = 2$ as an example.

The TAS for single-user SM has 120 possible solutions, while TAS for MU-SM needs to deal with over 8×10^{10} candidates even if a single receive antenna is considered. In addition, TAS for MU-SM has an exponentially increasing complexity when the number of receive antennas increases. As a result, exhaustive search is not feasible for the antenna allocation in SMMA, due to the prohibitive complexity. Regarding the feedback cost per user, TAS for MU-SM requires the same amount of CSI as TAS for single-user SM. In the following context, a low-complexity method on the antenna allocation in SMMA is presented.

Scenarios	Search space	Feedback required for CSI
Single-user	$\frac{N_{\text{tot}}!}{N_t!(N_{\text{tot}}-N_t)!}$	$N_{\text{tot}}N_r$
Multi-user	$\frac{N_{\text{tot}}!N_r^{N_u}}{\left(\left(\frac{N_{\text{tot}}}{N_u}\right)!\right)^{N_u}}$	$N_{\text{tot}}N_rN_u$

Table 5.1: *Search space and feedback cost of TAS in single-user and multi-user scenarios.*

5.4.2 Antenna allocation

The antenna allocation here is focused on maximising the received SNR, which is defined as the ratio of the received signal power to the noise power. The influence of channel correlations is reserved for future research. First, consider a single receive antenna at each user end. In order to maximise the channel capacity for a certain user, the transmit antennas of strong SNR values should be chosen, and they are referred to as strong candidate antennas. However, one antenna could be a strong candidate to several users. In order to avoid one user from occupying all strong candidates of other users, the users are arranged to select the transmit antennas sequentially, and each user selects one antenna at a time.

When N_r receive antennas are used at each user end, there are $(N_r)^{N_u}$ possible combinations for choosing one receive antenna from each user. Each combination corresponds to a receiver structure of MU-SM, where the above antenna scheduling method is applicable. Regarding the channel link from the t-th transmit antenna to the r-th receive antenna of user k, the received SNR is denoted by Γ_{t,r_k}. The average received SNR is defined as the average value of all Γ_{t,r_k} in a certain combination, and the combination of the largest value is chosen for SMMA. The set of all possible combinations is denoted by $\mathcal{I}$. For the n-th combination, the average received

SNR is denoted by $\bar{\Gamma}_n$. In addition, $\mathcal{G}_n$ is used to to denote the set of Γ_{t,r_k} for all t and r_k in the n-th combination. The antenna-scheduling algorithm is implemented as follows:

1. Select the n-th combination of $[r_1, \ldots, r_k, \ldots, r_{N_u}]$ from $\mathcal{I}$, where n is initialised to be one;
2. The index of the antenna-selection round is denoted by $\mathcal{F}$, which is initialised to be one. Set $f = 0$, where $f = [f_1, \ldots, f_k, \ldots, f_{N_u}]$ and f_k indicates whether user k has been allocated one transmit antenna in the current round;
3. Select the strongest Γ_{t,r_k} in $\mathcal{G}_n$, and the corresponding antenna and user are denoted by $\tilde{t}$ and $\tilde{k}$;
4. If $f_{\tilde{k}} = 0$, then allocate $\tilde{t}$ to user $\tilde{k}$, and set $f_{\tilde{k}} = 1$. Otherwise, ignore the chosen result and repeat 3);
5. Remove all Γ_{t,r_k} related to $\tilde{t}$ from $\mathcal{G}_n$. If $f_k = 0$ for any k, repeat 3);
6. If $\mathcal{F} < \dfrac{N_{\text{tot}}}{N_u}$, let $\mathcal{F} = \mathcal{F} + 1$ and repeat 2);
7. Compute $\bar{\Gamma}_n$ for the n-th combination;
8. Let $n = n + 1$ and repeat 1). After all combinations have been gone through, select the one of the largest $\bar{\Gamma}_n$;

The flowchart of the antenna-scheduling method is drawn in Fig. 5.4. It is worth noting that for each combination of receive antennas, the transmit antennas are directly allocated to the users, without the need of exhaustive search. Therefore the search space of the above method is $(N_r)^{N_u}$. Compared with the complexity of exhaustive search in Table 5.1, the proposed method requests much less processing power, and thus is more feasible in practice.

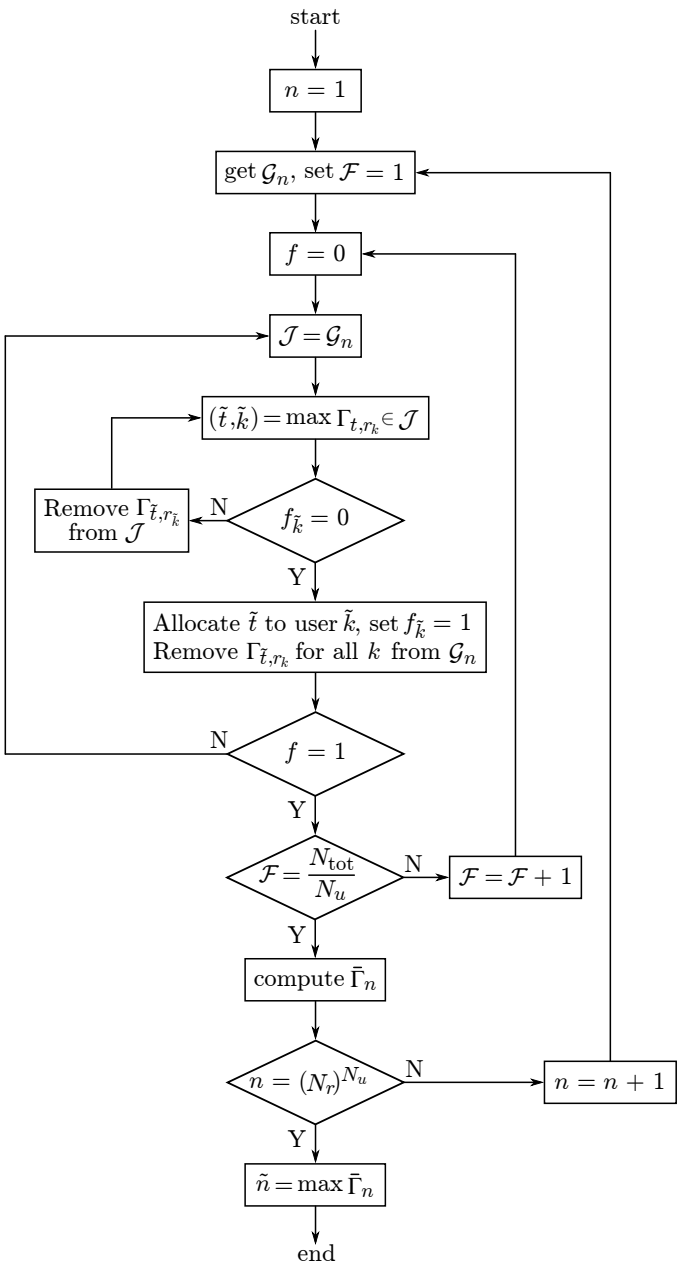

Figure 5.4: *Flowchart of the antenna-scheduling method in SMMA.*

5.5 Results

In this section, Monte Carlo simulation results are presented to validate the performance of SMMA. The analysis is conducted in two cases: i) independent channels; and ii) correlated channels. In each case, the cumulative density function (CDF) of received SNR is compared between SMMA and MU-SM. Also, the BER performance of SMMA is compared with the

exhaustive search, in order to verify the optimality of the antenna-scheduling scheme. Due to the extensive computational complexity, exhaustive search is implemented for some simple cases only. In all simulations, $\eta_s = 4$ is assumed for all users, and quadrature amplitude modulation (QAM) is adopted for signal modulation.

5.5.1 Independent channels

First, the case of independent channels is studied. Different transceiver structures and user numbers are considered in order to perform a comprehensive analyse of SMMA.

5.5.1.1 CDF of received SNR

The transmitted SNR is defined as the ratio between the transmit power of a signal and the noise power. Assuming a fixed transmitted SNR of 20 dB and Rayleigh fading channels, Fig. 5.5 presents the CDF of the received SNR for both SMMA and MU-SM. The total number of transmit antennas is 16, while 4 and 8 users are considered.

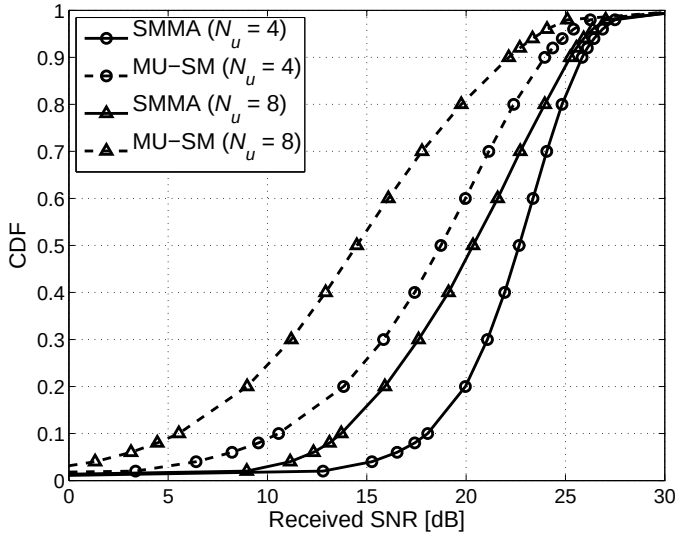

Figure 5.5: *CDF of received SNR for SMMA over independent channels ($N_{tot} = 16$ and transmitted SNR = 20 dB).*

The outage probability is defined as the probability that the received SNR is below a certain target. A smaller outage probability signifies that the communication system is more reliable. As can be seen, SMMA achieves a much smaller outage probability than MU-SM. Take the

SNR target of 10 dB for example. The outage probabilities of MU-SM are 9% and 24% for the cases of 4 users and 8 users, respectively. Meanwhile, the outage probabilities of SMMA achieving the same SNR target are merely 2.1% and 3.3%. Another finding is that when the target SNR increases (e.g. to 15 dB), the outage probability of MU-SM increases significantly. In contrast, SMMA remains at a relatively small outage probability of the received SNR.

5.5.1.2 BER performance

In the following, the BER performance of SMMA is studied for different transceiver structures and different numbers of users. As mentioned, MU-SM is suitable for only one receive antenna at the user end. To ensure a fair comparison, a single receive antenna is taken into account for both methods, except when analysing the effects of N_r on the performance of SMMA.

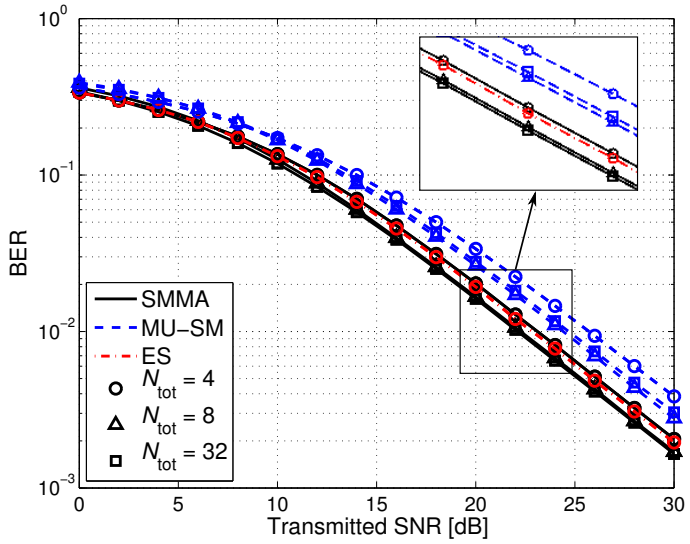

Figure 5.6: *BER performance of SMMA for different values of* N_{tot} *(*$N_u = 2$ *and* $N_r = 1$*).*

Fig. 5.6 shows the performance of SMMA with different numbers of transmit antennas, while the number of users is fixed to be two. The exhaustive search is referred to as ES in the figure. The following outcomes are observed: i) the performance of SMMA is tightly close to ES, with a SNR gap of less than 0.3 dB; ii) SMMA performs better than MU-SM for various numbers of transmit antennas (up to 3 dB). As N_{tot} increases, the performance of MU-SM increases at first and then drops, of which the trend is the same as that in SM for a single user [103]. On the contrary, the performance of SMMA keeps increasing when N_{tot} increases. The reason for this trend is that when more transmit antennas are used, the number of candidate antennas

is correspondingly increased in SMMA. Therefore the users are more likely to be allocated strong candidate antennas. Note that the BER curves of SMMA for $N_{\text{tot}} = 8$ and 32 are almost overlapping in this case. In order to clearly show the trends, a 3/4 (code rate) convolutional coding [106] is applied in the rest of this chapter.

The effect of the user number on the performance of SMMA is shown in Fig. 5.7, where the total number of transmit antennas is fixed to be 16. As can be seen, the BER performance of MU-SM decreases as the number of users increases. The reason is that an increased number of users causes a decrease in the number of transmit antennas per user, leading to a reduced diversity gain. This performance degradation becomes more significant when the number of users increases from 4 to 8, where MU-SM requires an extra SNR of 2.6 dB to maintain the same BER. In contrast to MU-SM, the performance of SMMA is slightly affected by the number of users, with an SNR gap of less than 0.5 dB. The reason is straightforward. When more users are involved, the antenna allocation in SMMA becomes more flexible, and thus each user has a larger chance to obtain strong candidate antennas. As a result, SMMA is more robust than MU-SM against the performance degradation caused by the reduction of N_t. In other words, SMMA outperforms MU-SM more significantly for a larger number of users. Compared with MU-SM, SMMA obtains an SNR gains of 3.2 dB in the case of $N_u = 4$. This gain increases to 6 dB in the case of $N_u = 8$.

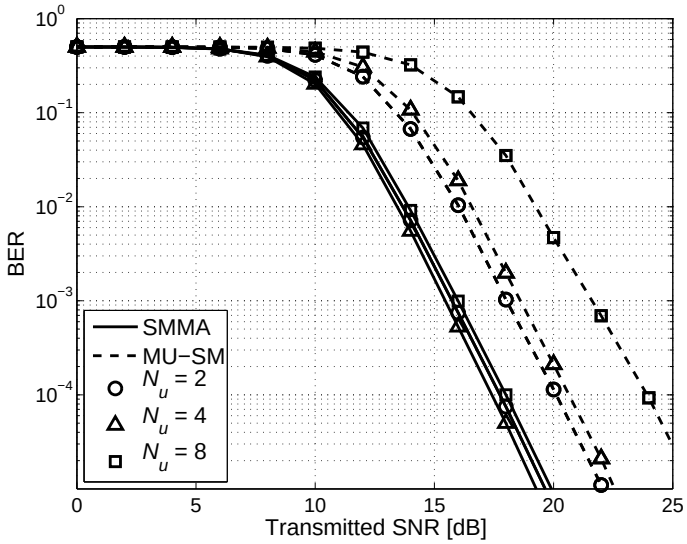

Figure 5.7: *BER performance of SMMA for different values of* N_u *(*$N_{tot} = 16$ *and* $N_r = 1$*).*

In Fig. 5.8, different numbers of receive antennas are applied in the SMMA system. The total

number of transmit antennas is still fixed to be 16, while 8 users are assumed. As shown, the performance of SMMA increases along with the number of receive antennas. At the same time, the performance of MU-SM is limited due to the restriction of a single receive antenna. When compared with MU-SM, SMMA achieves an SNR gain of 5.5 dB when a single receive antenna is used in both methods. When 4 receive antennas are employed in SMMA, this gain is increased to 8 dB.

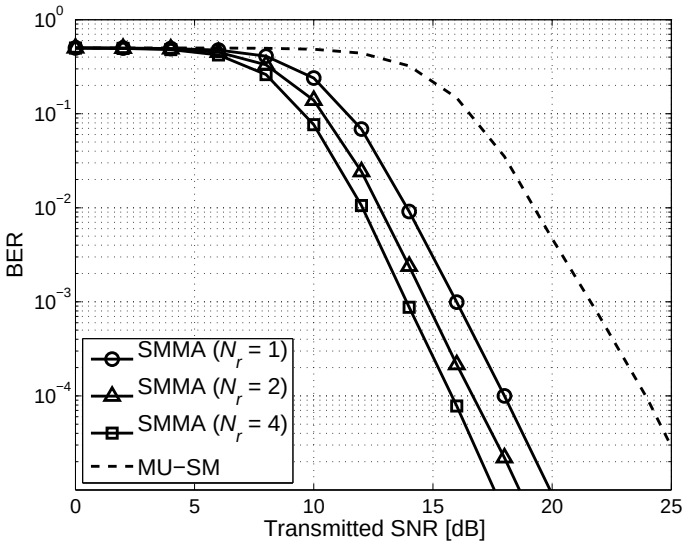

Figure 5.8: *BER performance of SMMA with different numbers of receive antennas ($N_{tot} = 16$ and $N_u = 8$).*

5.5.2 Correlated channels

Second, channel correlations are considered among the channel links of each user. The main purpose is to analyse the effects of channel correlations on the performance of SMMA. For the sake of simplicity, the total number of transmit antennas and the number of users are fixed to be 16 and 8, respectively.

5.5.2.1 CDF of received SNR

Fig. 5.9 presents the CDF of received SNR for SMMA over correlated channels. Since a single receive antenna is assumed, only the correlation between transmit antennas is considered. As expected, the received SNR of MU-SM is independent of the channel correlation. However, the outage probability of SMMA becomes larger when the channel correlation increases. This

is because the similarity between antennas impairs the benefit of antenna allocation. If the channel links are completely correlated, the antenna-scheduling method would lose its function. Although the channel correlation causes a performance degradation in SMMA, the performance of SMMA is still much better than MU-SM. Take $\rho_{\text{tx}} = 0.7$ and a target SNR of 10 dB for example. The outage probability of MU-SM is 25%, while it is only 5% for SMMA.

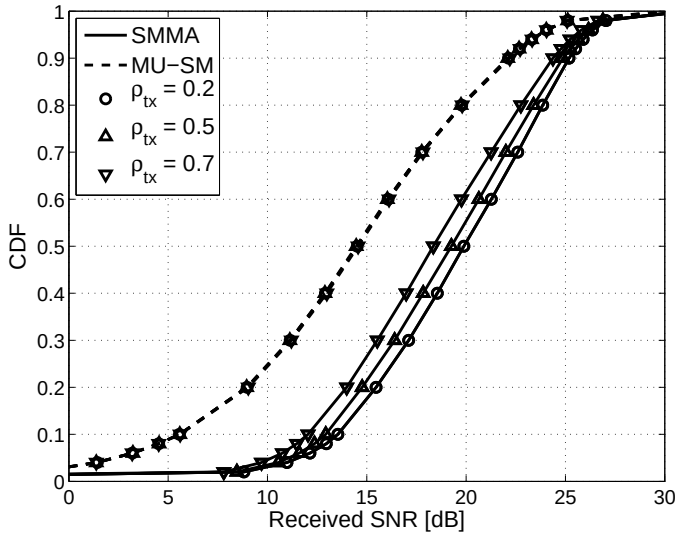

Figure 5.9: *CDF of received SNR for SMMA over correlated channels ($N_{tot} = 16$, $N_u = 8$ and transmitted SNR = 20 dB).*

5.5.2.2 BER performance

Considering different channel correlations between transmit antennas, the BER performance of SMMA is shown in Fig. 5.10. As can be seen, for various values of ρ_{tx}, SMMA always performs better than MU-SM. In addition, an increased ρ_{tx} causes a performance degradation to SMMA and MU-SM both. However, the reasons for those two methods are different. With respect to MU-SM, the performance degradation is caused by the difficulties in distinguishing the active antenna from the idle ones, since the channel coefficients of different links becomes statistically closer to each other. As for SMMA, in addition to the decrease in decoding capacity, the channel correlation impairs the effectiveness of the antenna-scheduling method. Therefore, as the channel correlation increases, the performance of SMMA decreases faster than MU-SM. Despite this, SMMA still outperforms MU-SM significantly at a high correlation degree. For $\rho_{\text{tx}} = 0.7$, SMMA achieves an SNR gain of 5 dB in comparison with MU-SM.

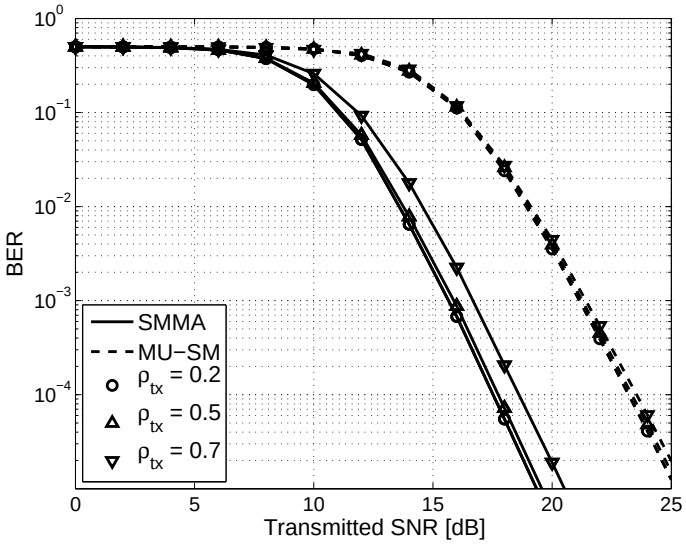

Figure 5.10: *BER performance of SMMA with correlated transmit antennas ($N_{tot} = 16$ and $N_u = 8$).*

In Fig. 5.11, the BER performance for SMMA is shown when the channel correlation between receive antennas is considered. The number of receive antennas used in SMMA is assumed to be 4. In order to study the trends of SMMA in relation to the channel correlation between receive antennas, the transmit antennas are assumed to be independent of each other. Two outcomes are observed: i) the performance of SMMA slightly reduces as ρ_{rx} increases. When ρ_{rx} is increased from 0.2 to 0.7, SMMA needs an extra SNR of 0.5 dB to maintain the same BER; and ii) SMMA achieves a much better BER performance than MU-SM, with an SNR gap of at least 7.3 dB.

5.6 Summary

In this chapter, the concept of SMMA that adaptively allocates the antennas in MU-SM has been presented. Unlike MU-SM using a fixed group of antennas for each user, SMMA exploits multi-user diversity by enabling the users to swap the transmit antennas pertaining to them. Aimed to maximise the channel capacity for each user, SMMA jointly manages the selection on the transmit antennas and the receive antennas, without additional feedback requirement as compared with MU-SM.

In addition, a novel antenna-scheduling method has been presented, which implements the

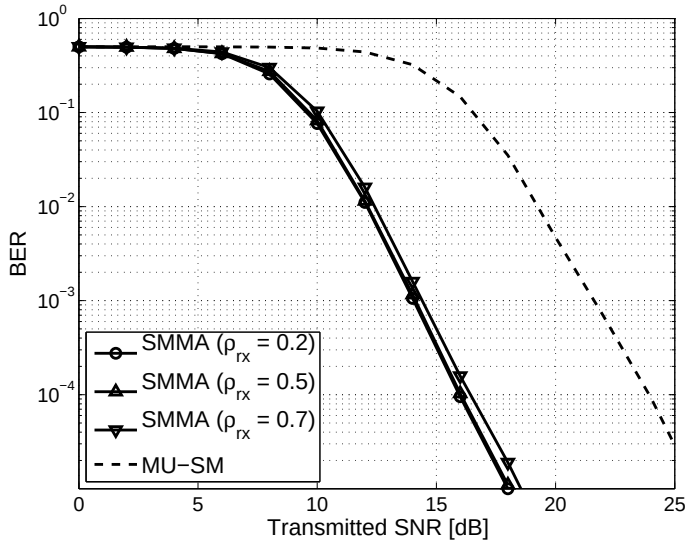

Figure 5.11: *BER performance of SMMA with correlated receive antennas ($N_{tot} = 16$ and $N_u = 8$).*

antenna allocation for SMMA instead of exhaustive search. It has been shown that the proposed method has a near-optimal performance in comparison with exhaustive search, while achieving very low computational complexity. Simulation results have been presented to validate the performance of SMMA against MU-SM. Furthermore, the effects of the transceiver structures on the performance of SMMA have been studied. Moreover, the performance of SMMA in relation to the channel correlations has been analysed.

Chapter 6
Spatial modulation in a multi-cell scenario

6.1 Introduction

In this chapter, the application scenario of SM is extended to multiple cells, with the focus on mitigating inter-cell interference (ICI). Network MIMO [107] is a relative new technique in the field of ICI coordination, which is also known as coordinated multi-point (CoMP) transmission in the long-term evolution-advanced (LTE-A) standard. The concept of network MIMO is similar to multi-user MIMO, but the users are located in different cells. Therefore network MIMO can effectively eliminate the interference inside a group of cells.

The application of network MIMO to the SM system is studied in this context, which is named network SM-MIMO. In addition, the limitation of network MIMO that the user can only be served by its closest base station (BS) is addressed. Like in the multi-user scenario, the antenna allocation among users is of great potential to improve the system capacity of network SM-MIMO. Motivated by this fact, a novel scheme named cooperative spatial modulation (CoSM) is proposed, which enables the user to be served by multiple BSs at the same time. More importantly, a novel three-tier cellular architecture is proposed that can effectively improve the performance of cell-edge users.

6.2 System model

6.2.1 Fractional frequency reuse

Fractional frequency reuse (FFR) is a widely-used technique for avoiding the interference caused by frequency repetition among cells. By partitioning the bandwidth of each cell, FFR can: i) avoid cell-edge users in adjacent cells from interfering with each other; and ii) increase the frequency reusability of cell-centre areas. FFR schemes are commonly classified in two categories: strict FFR and soft frequency reuse (SFR). In strict FFR, the same bandwidth is

allocated to the centre areas of all cells [108]. In contrast to strict FFR, the bandwidth of cell-centre areas in SFR is a superposition of the cell-edge bandwidths of neighbouring cells [109], and this offers a higher frequency reusability but with more interference among users. For the sake of simplicity, only strict FFR is considered in this context, and two different types are introduced: regular FFR and rearranged FFR.

6.2.1.1 Regular FFR

Fig. 6.1(a) depicts the schematic diagram of strict FFR in a tri-sector cellular network. As shown, each cell is divided into two tiers: the interior tier is a circular area in the cell centre, and the exterior tier is the remainder of the cellular coverage. The exterior tier is equally partitioned into three sectors. Each cell is thus split into four regions in total. The bandwidth is also divided into four equal portions, with each portion comprised of a number of subcarriers and using the same power level. Each region is allocated one portion of the entire bandwidth. Since the interior tiers of all cells are separated from each other in geography, they can share the same bandwidth without severe interference. On the other hand, the adjacent sectors in the exterior tiers use different bandwidths in order to avoid interference. Note that the partitioning patterns of all cells are identical, and this type is thus known as regular FFR.

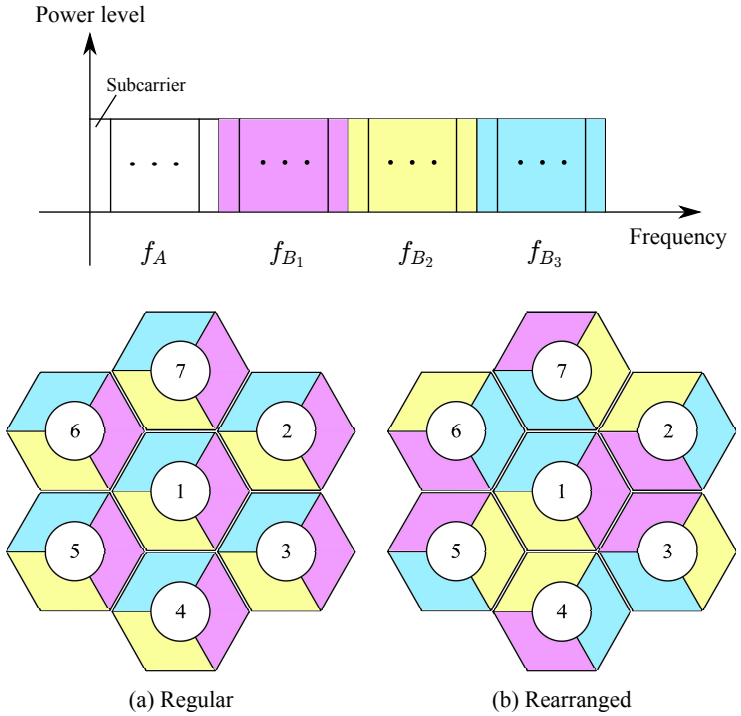

Figure 6.1: *Fraction frequency reuse in a tri-sector cellular network.*

6.2.1.2 Rearranged FFR

Another type is called rearranged FFR [107], which was originally proposed in [110]. Rearranged FFR is a variety of regular FFR, and its schematic diagram is drawn in Fig. 6.1(b). As shown, in rearranged FFR, the adjacent sectors of two neighbouring cells employ the same bandwidth. As a result, the adjacent sectors of three neighbouring cells reunite a near-hexagonal cell of a single bandwidth. Unlike the traditional cell using one BS in the cell centre, the reunited cell has three BSs in corners, and the precoding technique is applicable to eliminate interference inside the reunited cell. In contrast to regular FFR, this arrangement can achieve interference avoidance inside a group of cells, and therefore is more robust against the frequency reusing requirement.

6.2.2 Cellular network model

Consider a cellular network of 31 cells based on rearranged FFR, as shown in Fig. 6.2. At each BS, N_t omni-directional antennas are used to serve the mobile users in the cell-centre area, while N_t directional antennas are equipped for each sector. An equal number of receive antennas is assumed for all mobile user, and it is denoted by N_r. In order to keep a moderate complexity of analysis, the wrap-around technique is not considered. In this case, the affect of interference from those sectors in grey colour is negligible to the users in BS 1.

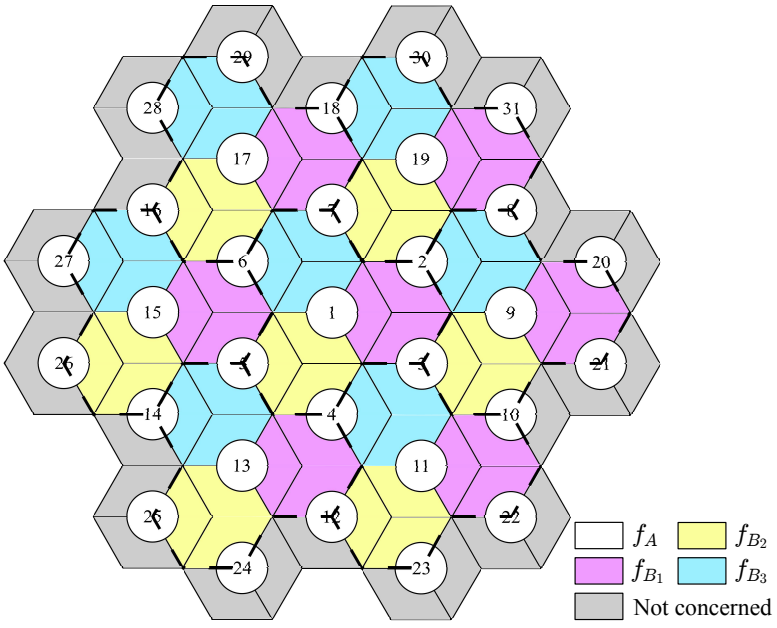

Figure 6.2: *Cellular network model.*

6.2.3 Channel model

With respect to the channel links from BS m to user k, the fading coefficient between the t-th transmit antenna and the r-th receive antenna is denoted by $h_{m,k}^{t,r}$. Consider a flat Rayleigh channel, of which the coefficient is denoted by $\alpha_{m,k}^{t,r}$. In addition, $A_{(\theta_{m,k})}$ is used to represent the gain patten of directional antennas [111], and it is expressed as:

$$A_{(\theta_{m,k})\text{dB}} = -\min\left[12\left(\frac{\theta_{m,k}}{\theta_{3\text{dB}}}\right)^2, A_m\right], \tag{6.1}$$

where $\theta_{m,k}$ is the angle between BS m and user k with respect to the main-beam direction of the transmit antenna; $\theta_{3\text{dB}}$ is the angle at which the signal power is half of the signal power at the main-beam direction; A_m is the maximum attenuation for the side-lobe. According to [111], it is assumed that $\theta_{3\text{dB}} = 70°$ and $A_m = 20$ dB. The fading channel is then formulated as follows:

$$h_{m,k}^{t,r} = \alpha_{m,k}^{t,r}\sqrt{A_{(\theta_{m,k})}L_{m,k}B_{m,k}}, \tag{6.2}$$

where $L_{m,k}$ and $B_{m,k}$ are the path loss and the shadow fading in relation to BS m and user k. Using the log-distance path loss model [112], $L_{m,k}$ is calculated by:

$$L_{m,k} = \left(\frac{d_{m,k}}{d_{\text{ref}}}\right)^{-\mu}, \tag{6.3}$$

where $d_{m,k}$ denotes the distance between BS m and user k, while d_{ref} is the reference distance; μ denotes the path loss exponent. In the SM systems, only one transmit antenna is activated at any time instance, and the currently active antennas is denoted by l. Also, the interference-free signal-to-noise ratio (SNR), denoted by $\gamma_{m,k}^{l,r}$, is defined as the received SNR of a certain user when interference is not taken into account. Based on the channel expression in (6.2), the interference-free SNR is calculated by:

$$\gamma_{m,k}^{l,r} = |\alpha_{m,k}^{l,r}|^2 A_{(\theta_{m,k})}L_{m,k}B_{m,k}\gamma_{\text{ref}}, \tag{6.4}$$

where γ_{ref} denotes the received SNR at the reference distance.

6.3 Network SM-MIMO

6.3.1 Cellular grouping

Network MIMO coordinates a number of geographically-adjacent BSs in order to mitigate the interference caused by the frequency reuse among those BSs. As mentioned, the precoding technique is used to cancel the interference inside each group of coordinated BSs. Therefore the performance in terms of interference mitigation depends on the number of coordinated BSs. When more BSs are coordinated, the users receive less interference since the interfering source is further away. The number of coordinated BSs, however, is restricted in a realistic system, due to the prohibitive computational-complexity and the extensive feedback requirement. In this chapter, the size of coordinated BSs is considered to be three [107].

Correspondingly, the cellular network in Fig. 6.2 is divided into seven groups, and each group is comprised of three reunited cells. The users are uniformly distributed in the cells. Consider downlink communications, i.e. the signal is transmitted from BS to user. The information bits are modulated by SM to serve each user, and see Section 2.3 for the system model of SM. For the sake of simplicity, multi-user SM is not considered inside cells. In each sector, one subcarrier serves one user at a time. As a result, there are three users sharing the same bandwidth in each group. The precoding method in [53] is used to cancel the interference among those co-channel users.

6.3.2 Inter-group interference

Since network MIMO eliminates the interference among co-channel users inside each group, the users are mainly affected by the interference coming from other groups, which is referred to as inter-group interference (IGI). With respect to user k, the set of BSs outside the group is denoted by $\mathcal{I}_k$. The signal-to-interference-plus-noise ratio (SINR) is defined as the ratio of the signal power to the total power of interference and noise, and it is calculated by:

$$\Gamma_{m,k}^{l,r} = \frac{\gamma_{m,k}^{l,r}}{1 + \sum\limits_{m' \in \mathcal{I}_k} \gamma_{m',k}^{l',r}}, \tag{6.5}$$

where $\Gamma_{m,k}^{l,r}$ denotes the SINR at the r-th receive antenna of user k, while $\gamma_{m',k}^{l',r}$ represents the SNR of the interfering signal sent from BS m' to user k.

6.4 Cooperative spatial modulation

6.4.1 Concept

In the multi-cell scenario, the users in cell centres usually have a quality link because the signal source is much closer than the interfering source. Unfortunately, the quality of service for cell-edges users is compromised for two reasons: i) the desired signal experiences a relatively severe attenuation; and ii) the users receive stronger interference as they are moving towards interfering BSs. Although network MIMO manages to mitigate interference, it cannot improve the quality of the desired signal against channel fading.

In order to strengthen the desired signal, CoSM enables the co-channel users inside groups to swap the transmit antennas that are allocated to them. Note that this antenna-rescheduling process is not necessary but available. As a result, the users can be served by one or multiple BSs at a time. Compared with network SM-MIMO that serves the user with its closest BS only, this novel cooperative scheme offers each user a higher antenna diversity, and therefore is more powerful against selective fading. The antenna-rescheduling process is similar to the antenna allocation for multi-user SM in Chapter 5, but allows one user to select antennas from different BSs. The problem at hand is to allocate the antennas of BSs in the same group to their co-channel users. Therefore this process also faces the challenge that each user requires a certain number of transmit antennas, and each transmit antenna is dedicated to one user. Two antenna-rescheduling algorithms are presented in the following context.

6.4.2 Antenna rescheduling

6.4.2.1 Strongest prior

Similar to the antenna allocation method in Section 5.4.2, a straightforward strategy is to select the antennas of the largest SNR for each user. Again, one antenna might be the best candidate for several users at the same time. Therefore the same sequencing model is used in order to avoid a certain user from occupying all strong candidate antennas of another one. Note that the precoding method in [53] is suitable for multiple receive antennas, and the decoding capability is in fact dominated by the receive antenna of the strongest SNR. Regarding the channel links from the t-th antenna of BS m to different receive antennas of user k, among them the strongest SNR is denoted by $\tilde{\gamma}_{m,k}^{t}$. In addition, $\mathcal{S}$ is used to denote the set of $\tilde{\gamma}_{m,k}^{t}$ for all m, k, and t in

a certain group. Since aimed to allocate the strongest links to the users, this method is named *strongest prior* (SP). The detailed algorithm is illuminated as follows:

1. select the transmit antenna of the largest SNR value in $\mathcal{S}$ for a certain user. The chosen antenna is denoted by $\dot{t}$;
2. remove all $\tilde{\gamma}_{m,k}^{\dot{t}}$ from $\mathcal{S}$;
3. move to the next user and repeat 1), until all users have been allocated the required number of antennas.

6.4.2.2 Weakest-avoiding prior

Despite the SP method is aimed to allocate the antennas of the strongest SNR to the users, it may result in the situation that the worst candidate antenna is assigned to a certain user. Table 6.1 illustrates an example of using SP when there are two transmit antennas in each BS sector. The chosen antennas for each user are highlighted in bold font. As shown, user 1 obtains two antennas of the largest SNR values. User 2 does not get both the two strongest links, but still has a better quality than being served by its closest BS only. However, user 3 has no choice but to use the antenna of the smallest SNR value, which is merely 4.9 dB.

	BS 1		BS 2		BS 3	
	Tx 1	Tx 2	Tx 1	Tx 2	Tx 1	Tx 2
User 1	11.5	16.1	14.6	**19.3**	15.8	**18.7**
User 2	13.2	**10.1**	**15.1**	8.2	7.2	10.3
User 3	**10.6**	8.0	13.2	15.2	**4.9**	8.3

Table 6.1: *An example of antenna rescheduling based on SP.*

In order to conduct a relatively fair allocation for all users, another method focuses on avoiding the worst candidate antenna alternatively. This method is thus referred to as *weakest-avoiding prior* (WAP). The corresponding algorithm is comprised of five steps as follows:

1. select the antenna of the smallest SNR in $\mathcal{S}$, and denote the chosen antenna by $\tilde{t}$;
2. select the user of the largest SNR with respect to antenna $\tilde{t}$, and denote the chosen user by $\tilde{k}$;

3. if $\tilde{k}$ has been allocated a full number of antennas, remove $\tilde{k}$ from the candidate users and repeat 2);

4. allocate antenna $\tilde{t}$ to user $\tilde{k}$;

5. remove all $\tilde{\gamma}_{m,k}^{\tilde{t}}$ from $\mathcal{S}$ and repeat 1); until all user have been allocated the required number of antennas.

Unlike the SP method, WAP tries to allocate the best candidate user to each antenna. Under the same conditions as Table 6.1, the antenna rescheduling result of WAP is shown in Table 6.2. As can be seen, by using WAP instead of SP, the link quality for user 3 is increased from [4.9 dB, 10.6 dB] to [13.2 dB, 15.2 dB]. Meanwhile, the link quality for user 1 and user 2 slightly drops (with a gap of less than 3 dB).

	BS 1		BS 2		BS 3	
	Tx 1	Tx 2	Tx 1	Tx 2	Tx 1	Tx 2
User 1	11.5	**16.1**	14.6	19.3	**15.8**	18.7
User 2	**13.2**	10.1	15.1	8.2	7.2	**10.3**
User 3	10.6	8.0	**13.2**	**15.2**	4.9	8.3

Table 6.2: *An example of antenna rescheduling based on WAP.*

In both SP and WAP methods, the only needed information at the transmitter side is the largest SNR value for each pair of the BS antenna and the user, regardless of the number of receive antennas used at each user. Note that the precoding technique in network SM-MIMO requires each user to feedback the full channel state information (CSI) in relation to the operating BS as well as other BSs in the same group. Therefore, CoSM requires no extra feedback in addition to network SM-MIMO.

6.4.3 Theoretical analysis

As mentioned, in CoSM, the antennas of one BS can be allocated to different users. As a result, the currently active antennas pertaining to different users may come from the same BS, while some BS has no active antennas. This leads to difficulties in analysing the SINR of users, as the activation status of the interfering BSs is indeterminate. In this context, the probability of a BS being activated is derived, and an expression for the SINR of users in CoSM is presented.

6.4.3.1 The probability of a BS being activated

The locations of the three BSs in a certain group are denoted by P_1, P_2 and P_3, respectively. Without loss of generality, P_1 is assumed to be the origin point. User k is located in one sector of the reunited cell, and that sector is denoted by Area k. The user position is denoted by $P_{\text{MS}} = \nu e^{j\theta}$, where ν and θ are the distance and the angle between the user and the origin, respectively. The interference-free SNR for this user with respect to BS m is denoted by γ_m, and it is expressed as:

$$\gamma_m = |\alpha_m|^2 C_m, \tag{6.6}$$

where:

$$C_m = A_{(\theta_m)} \left(\frac{|P_{\text{MS}} - P_m|}{d_{\text{ref}}} \right)^{-\mu} B_m \gamma_{\text{ref}}. \tag{6.7}$$

Note that C_m is constant for given P_{MS} and P_m. For a Rayleigh fading, the random variable $|\alpha_m|^2$ has a Gamma distribution. Therefore, γ_m is also Gamma distributed with the shape parameter equal to 1 and the rate parameter equal to C_m. The probability of a certain user choosing antennas from BS m other than BS m' can be formulated as:

$$P(\gamma_m > \gamma_{m'}) = P(\gamma_m - \gamma_{m'} > 0). \tag{6.8}$$

The probability density function (PDF) of differentiating two Gamma-distributed variables was derived in [113]. Define $\delta = \gamma_m - \gamma_{m'}$, and then the PDF of δ can be determined by the MaKay's distribution as follows:

$$f(\delta) = \frac{\left(1 - c^2\right)^{a+\frac{1}{2}} |\delta|^a}{\sqrt{\pi} 2^a b^{a+1} \Gamma(a + \frac{1}{2})} e^{-\frac{\delta c}{b}} K_a \left(\frac{|\delta|}{b} \right), \tag{6.9}$$

where $K_a(\cdot)$ is the modified Bessel function of the second kind and of the order of a, and:

$$\begin{cases} a = \frac{1}{2} \\ b = \frac{2\phi_m \phi_{m'}}{\phi_m - \phi_{m'}} \\ c = \frac{\phi_{m'} - \phi_m}{\phi_m + \phi_{m'}} \end{cases} . \tag{6.10}$$

Thus, (6.8) is calculated by:

$$P(\gamma_m > \gamma_{m'}) = \int_0^{+\infty} f(\delta) d\delta. \tag{6.11}$$

The antenna that is chosen for activation is denoted by l. The event of selecting the active antenna from BS m is denoted by $l \in$ BS m, and the corresponding probability is given by:

$$P(l \in \text{BS } m) = \prod_{m'=1 \neq m}^{3} P(\gamma_m > \gamma_{m'}). \tag{6.12}$$

Note that the above derivation is for a fixed user position. When the user moves in the available area, the probability of BS m being activated for user k is computed by:

$$P(m,k) = \iint_{\text{Area } k} \prod_{m'=1 \neq m}^{3} P(\gamma_m > \gamma_{m'}) d\nu d\theta. \tag{6.13}$$

Now consider the situation of multiple users. The probability of the event that BS m activates n_{act} antennas is denoted by $P(m|n_{\text{act}})$, and it can be obtained as follows:

$$\begin{cases} P(m|n_{\text{act}}=1) = \sum_{k=1}^{3} P(m,k) \prod_{k'=1 \neq k}^{3} (1 - P(m,k')) \\ P(m|n_{\text{act}}=2) = \sum_{k=1}^{3} (1 - P(m,k)) \prod_{k'=1 \neq k}^{3} P(m,k') \\ P(m|n_{\text{act}}=3) = \prod_{k=1}^{3} P(m,k) \end{cases}. \tag{6.14}$$

6.4.3.2 Analytical bound for inter-group interference

With respect to a certain user, the directional antennas of BSs impose an influence on the strength of interfering sources. If the use does not drop in the beamforming coverage of an interfering BS, then the interfering signal from that BS can deliver a very slight influence on the user. Otherwise, the user would receive a relatively strong interference. Fig. 6.3 depicts the schematic diagram of IGI situations with respect to the users located in the central cell. The group of coordinated BSs is denoted by G_j. In this case, $G_0 = \{1,2,3\}$ is the group providing service to the users, while $G_1 = \{8,19,31\}$, $G_2 = \{9,20,21\}$, $G_3 = \{10,11,22\}$, $G_4 = \{4,12,13\}$, $G_5 = \{5,6,15\}$ and $G_6 = \{7,17,18\}$ are the groups concerned as the

interfering sources. The set of interfering groups is denoted by $\mathcal{I}_{\mathcal{G}}$. According to the strength of influence, the interfering BSs can be classified into two categories: strongly-interfering BS and weakly-interfering BS. As shown, the strongly-interfering BSs are further away from the coverage of G_0 than those weakly-interfering BSs are. This signifies that the IGI in network MIMO can be effectively reduced by using directional antennas.

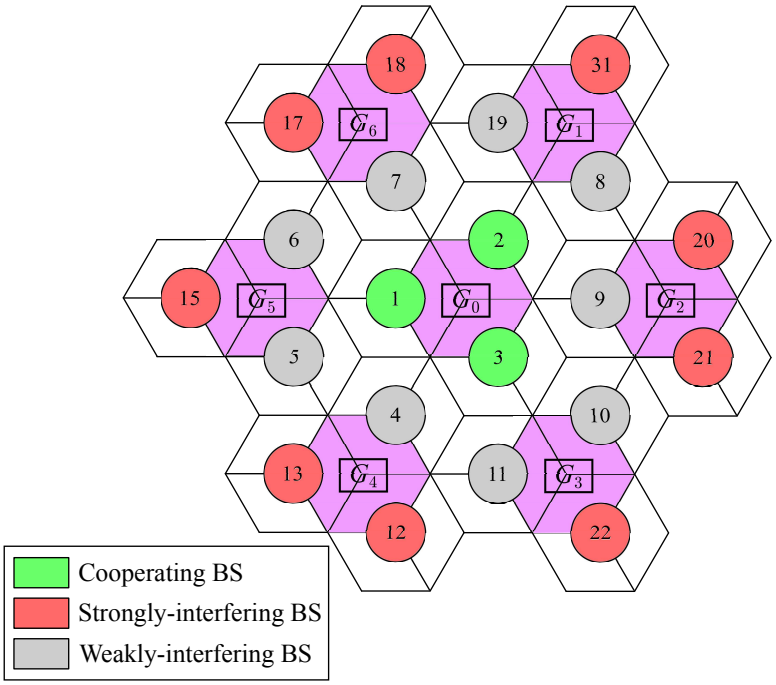

Figure 6.3: *IGI situations in network MIMO.*

As mentioned, the BSs in the same group of CoSM are not necessarily active at the same time. This offers an opportunity that a strongly-interfering BS could be not sending signals temporarily. The SNR with respect to the total interference received by user k is denoted by $\gamma_{\text{IGI}(k)}$, and it can be obtained by:

$$\gamma_{\text{IGI }(k)} = \sum_{G_j \in \mathcal{I}_{\mathcal{G}}} \sum_{m' \in G_j} \sum_{n_{\text{act}}} P(m'|n_{\text{act}}) n_{\text{act}} \gamma_{m',k}. \tag{6.15}$$

Substituting (6.15) into (6.5), the SINR of users in CoSM can be evaluated by:

$$\Gamma_{m,k} = \frac{\gamma_{m,k}}{1 + \sum_{G_j \in \mathcal{I}_{\mathcal{G}}} \sum_{m' \in G_j} \sum_{n_{\text{act}}} P(m'|n_{\text{act}}) n_{\text{act}} \gamma_{m',k}}. \tag{6.16}$$

6.5 Three-tier cellular architecture

6.5.1 Concept

In CoSM, the users are enabled to select transmit antennas from the coordinated BSs instead of using the antennas of the closest BS only. Since the coordinated BSs are located in different corners of the reunited cell, CoSM in fact constructs a distributed antenna system for the users. As a result, the users benefit from an increased diversity between antennas. However, when a user is much closer to one of the BSs than the others, it is more likely to select the antennas from the closest BS, of which the channel experiences a much smaller path loss. In this case, CoSM would lose the advantage against network SM-MIMO. For this reason, it is beneficial to operate network SM-MIMO and CoSM for users in different regions. A three-tier cellular architecture is thus proposed, as shown in Fig. 6.4.

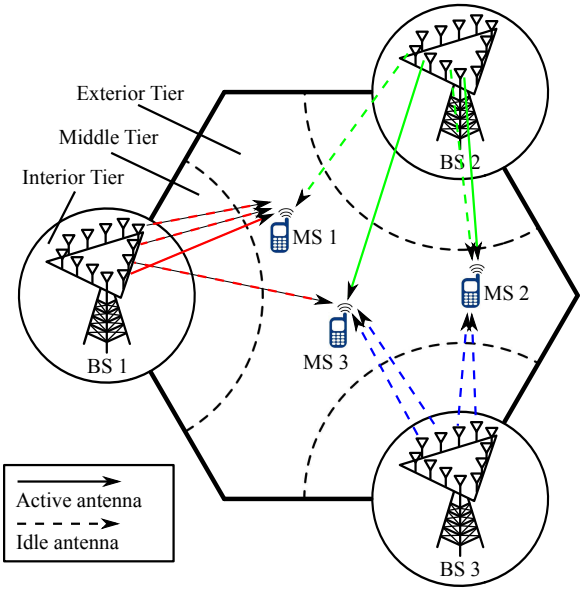

Figure 6.4: *A three-tier cellular architecture for CoSM.*

Based on the two-tier structure of FFR, the exterior tier is further split into two parts, and each cell has three tiers in total: the interior tier, the middle tier and the exterior tier. The interior tier remains the same as that in FFR, and the other two tiers are working with coordinated BSs. For those users in the middle tier, network SM-MIMO is used to eliminate the interference among them, but the antenna-rescheduling scheme is not applicable. CoSM is only applied to the users that are located in the exterior tier. The area ratio of a certain region is defined as the ratio of the area of that region to the entire cell coverage. Assuming users are uniformly distributed, the area

ratio signifies the percentage of users that drop in the corresponding region, as compared with the user population in a cell. Therefore, the regions for different tiers are expressed in terms of area ratios rather than radius. The three-tier cell is demarcated by two circles with the same centre. The circular area of the smaller one defines the interior-tier region. The region between those two circles is the middle tier, while the remaining area pertains to the exterior tier. The area ratios of the smaller circle and the larger circle are denoted by a_1 and a_2. Consequently, the area ratios of the middle-tier region and the exterior-tier region are $a_2 - a_1$ and $1 - a_2$, respectively.

6.5.2 Effective region

In order to analyse the superiority of CoSM against network SM-MIMO, the cellular coverage is divided into a series of rings, and the performance comparison between CoSM and network SM-MIMO is conducted for the users that are uniformly distributed in each ring. The inner radius of the ring is denoted by r. The user population in each ring is assumed to be equal in order to facilitate the analysis. In other words, the difference of the squares between the outer radius and the inner radius is the same for all rings, and this parameter is referred to as the ring step. A smaller ring step provides a more accurate evaluation, but leads to a larger number of rings. Assuming a ring step of 0.05, Fig. 6.5 presents the relation between the SINR gain achieved by CoSM over network SM-MIMO and the user-to-BS distance.

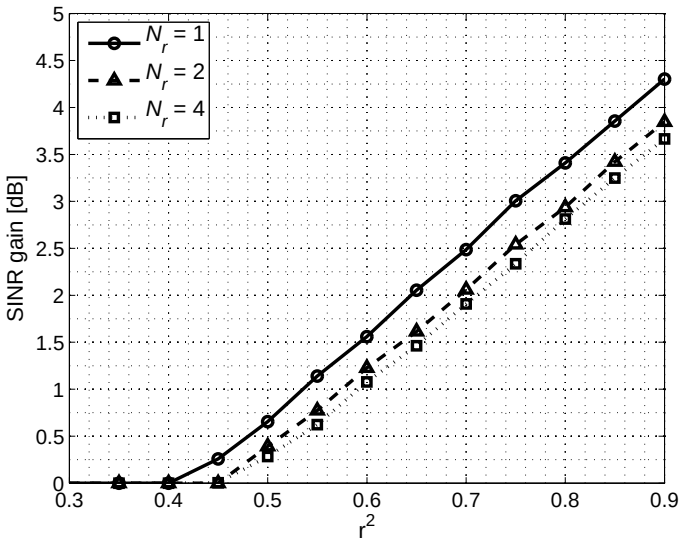

Figure 6.5: *SINR gains achieved by CoSM against network SM-MIMO.*

Different numbers of receive antennas are taken into account. Note that the number of transmit antennas does not affect the SINR, as SM activates a single transmit antenna at any time instance. In order to determine the effective region for CoSM, i.e. the value of $1 - a_2$ in the three-tier cellular architecture, the minimum SINR gain is required. Consider the minimum SINR gain of 2 dB to balance the additional processing power requested by CoSM. For each case of N_r in Fig. 6.5, the minimum SINR gain corresponds to a certain value of r^2, and this value is in fact the choice for a_2. Table 6.3 lists the deployment of the effective region for CoSM with different numbers of receive antennas in use.

Cases	$N_r = 1$	$N_r = 2$	$N_r = 4$
$1 - a_2$	35.6%	30.7%	29%

Table 6.3: *Deployment of the effective region for CoSM.*

As mentioned, the area ratio of effective region represents the percentage of users that are served by CoSM. It is noticed that the user percentage for CoSM drops as more receive antennas are employed at the user ends. The reason for this trend is that CoSM takes advantage of transmit antenna selection. Therefore when increasing the number of receive antennas, the SINR performance of CoSM increases slower than network SM-MIMO. Despite this, CoSM can still benefit 29% of the users in the case of 4 receive antennas.

6.6 Results

In this section, the performance of CoSM is validated by Monte Carlo simulations. The BS-to-BS distance is assumed to be 2 km, while the path loss exponent is 4 and the standard deviation of shadowing is 8 dB [111]. In each cell, the users are uniformly distributed. Perfect CSI is assumed to be known at both the BS and the user end, and synchronised feedback links are considered between the coordinated BSs. The interference-free SNR at the cell edge is fixed to be 18 dB [111], i.e. the transmission power is fixed, in order to analyse the received SINR at different locations. Also, the average bit error rate (BER) performance of CoSM is compared with spatial multiplexing (SMX) using the same antenna-rescheduling method, where the interference-free SNR at the cell-edge varies from 0 dB to 25 dB.

6.6.1 Effects of the effective region

First, the SINR performance of CoSM is studied against the different choices for its effective region. Four antennas are assumed at each BS sector as well as at each user end. In addition to network SM-MIMO, the cellular network that uses a single bandwidth inside each cell is considered as a benchmark, and this is referred to as the omni-cell. The cumulative distribution functions (CDFs) of the received SINR in the cases of $a_2 = 0.5$ and $a_2 = 0.9$ are shown in Fig. 6.6 and Fig. 6.7, respectively.

As shown in Fig. 6.6, CoSM significantly improves the performance of network SM-MIMO. When compared with network SM-MIMO and omni-cell, WAP achieves SINR gains of 2 dB and 5.5 dB at the 50-th percentile, respectively. Using SP instead of WAP, CoSM can further increase this SINR gain by 0.8 dB. However, SP is overcome by WAP when the SINR is below the 30-th percentile. At the 10-th percentile, for example, the SINR achieved by SP is 1.5 dB less than WAP. This trend validates that WAP is relatively fair for vulnerable users against SP.

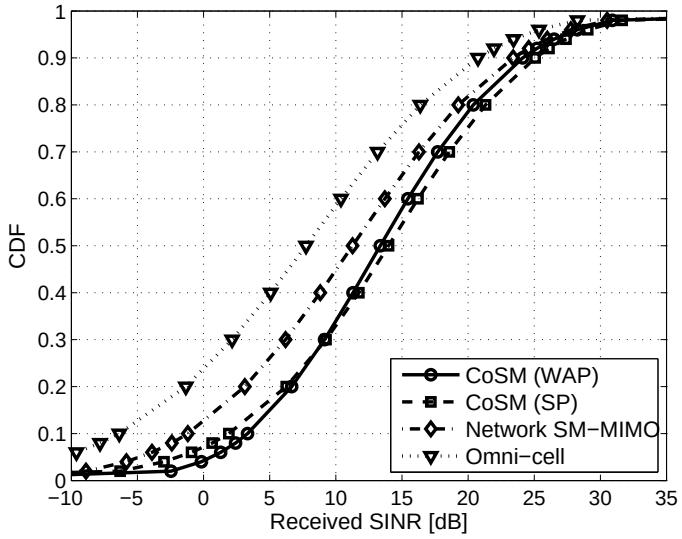

Figure 6.6: *SINR Performance of CoSM for* $a_2 = 0.5$ *(*$N_t = 4$ *and* $N_r = 4$*).*

When the value of a_2 is increased from 0.5 to 0.9, the users served by CoSM reduce from 50% to 10% accordingly, and they are concentrated in the area of cell edge. By comparing those two cases of a_2, it can be found that with respect to network SM-MIMO, the SINR performance degrades rapidly as a_2 increases, i.e. the users are moving towards the cell edge. At the 50-th percentile, network SM-MIMO experiences an SINR loss of 2.3 dB when a_2 is increased from 50% to 90%. In contrast to network SM-MIMO, CoSM has a very slight SINR reduction of up

to 0.3 dB, leading to an SINR gain of more than 4 dB against network SM-MIMO. This trend matches the fact that CoSM is more effective for cell-edge users than cell-centre users. Similar to the case of $a_2 = 0.5$, SP outperforms WAP when the SINR is above the 30-th percentile, but the opposite result happens otherwise.

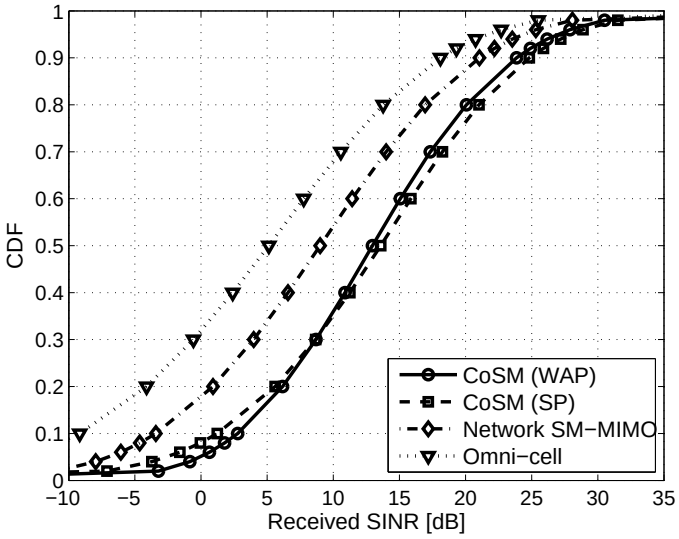

Figure 6.7: *SINR Performance of CoSM for* $a_2 = 0.9$ *(*$N_t = 4$ *and* $N_r = 4$*).*

6.6.2 Effects of the antenna number

Second, the SINR performance of CoSM in relation to the number of antennas is analysed. The case of $a_2 = 0.9$ is assumed. The coverage probability is defined as the probability that the received SINR is above a certain requirement. Considering various MIMO transceiver structures in terms of $N_t \times N_r$, Fig. 6.8 presents the coverage probability of CoSM with an SINR requirement of 10 dB.

The left-side three cases compare the results for different numbers of receive antennas, while fixing the number of transmit antennas. Three outcomes are observed: i) when the number of receive antennas increases, the coverage probabilities of all candidate schemes increase; ii) compared with network SM-MIMO, CoSM improves the coverage probability more significantly when fewer receive antennas are used; and iii) the gap between SP and WAP reduces as the number of receive antennas increases. When using four receive antennas, WAP achieves almost the same coverage probability as SP.

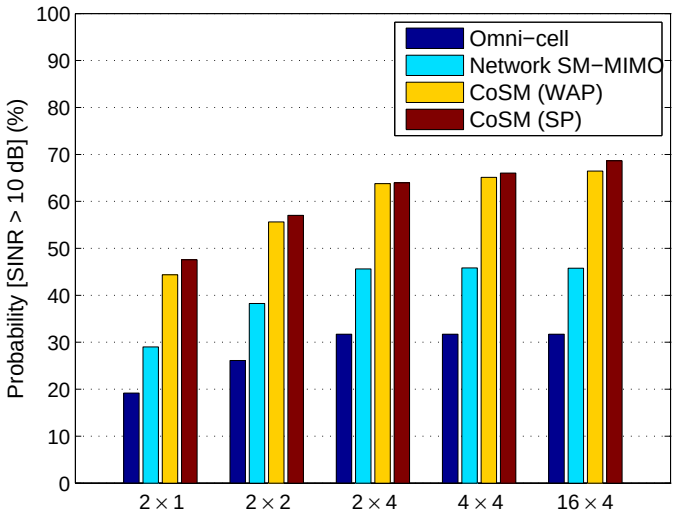

Figure 6.8: *The probability for an SINR above the requirement of 10 dB ($a_2 = 0.9$).*

Fixing the number of receive antennas at four, the right-side three cases present the results for different numbers of transmit antennas. As expected, the coverage probability of network SM-MIMO as well as omni-cell is constant against the variation of N_t. Unlike network SM-MIMO, the coverage probability of CoSM increases as N_t increases. This reason is that when more transmit antennas are involved in the antenna-rescheduling process of CoSM, each user is more likely to be allocated the strong candidate antennas.

6.6.3 Comparison with spatial multiplexing

At last, the BER performance of CoSM is compared with spatial multiplexing (SMX) using the same SP method. The later is referred to as CoSMX. Two cases of a_2 are studied: i) $a_2 = 0$, i.e. the users are distributed over the entire cell; and ii) $a_2 = 0.9$, i.e. the cell-edge users only. In addition, a 3/4 (code rate) convolutional coding [106] is applied in order to present the BER range of interest. Fig. 6.9 shows the BER performance for both CoSM and CoSMX as a function of the interference-free SNR at the cell edge. As can be seen, the error floor occurs due to the inevitable interference among groups. Compared with CoSMX, CoSM offers a better performance of BER for both cases of a_2. To achieve the BER target of 1×10^{-4} at $a_2 = 0$, for example, the cell-edge SNR required by CoSM is 1.2 dB less than CoSMX. When achieving the same BER target at $a_2 = 0.9$, CoSM obtains an increased SNR gain of 1.7 dB in comparison with CoSMX.

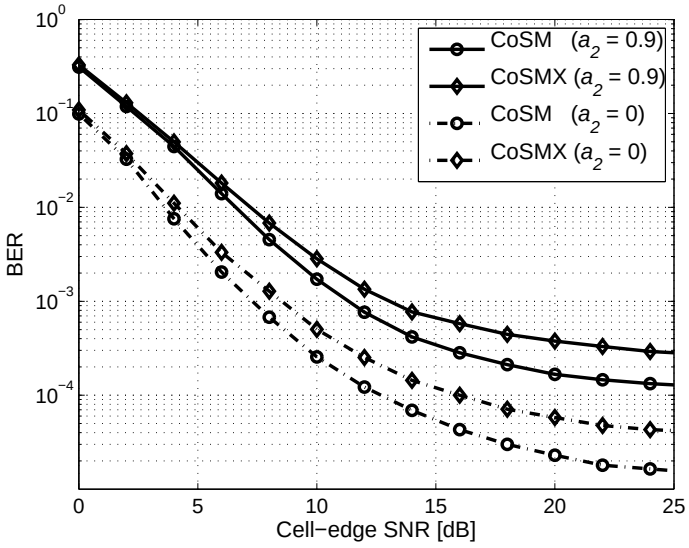

Figure 6.9: *BER performance comparison between CoSM and CoSMX ($N_t = 4$ and $N_r = 4$).*

6.7 Summary

In this chapter, the implementation of SM systems has been studied in the multi-cell scenario. Combining SM with the concept of CoMP, the framework of network SM-MIMO has been presented. A further research has been conducted on CoSM that enables the co-channel users in network SM-MIMO to swap their transmit antennas. Two antenna-rescheduling methods, SP and WAP, have been proposed. SP is aimed to allocate the strongest candidate antennas to each user, while WAP focuses on avoiding the weakest candidate antennas from being used. It has been shown that between those two methods, SP has an advantage in achievable SINR, but WAP offers a better fairness among the users.

Furthermore, an expression for the received SINR in CoSM has been derived. More importantly, a three-tier cellular architecture has been proposed, which adaptively switches between CoSM and network SM-MIMO in accordance with the distance between user and BS. Results have shown that CoSM outperforms network SM-MIMO by up to 4 dB. Also, CoSM has a superior performance as compared with SMX using the same cooperative scheme.

Chapter 7
Conclusions

7.1 Key findings

This thesis presented a novel and comprehensive study of spatial modulation (SM) in three different scenarios, i.e. single-user, multi-user and multi-cell. In the single-user scenario, an optimum transmit structure balancing the number of transmit antennas with the order of signal modulation has been proposed for SM. Considering practical channel state information (CSI), three novel channel estimation (CE) methods specially tailored for SM have been developed in order to deal with the challenge in the CE process raised by a single active antenna. When the scenario moves to multiple users, the management of transmit antennas has been studied to exploit the multi-user diversity for SM systems. In addition, a novel cooperative scheme has been proposed for SM systems in the multi-cell scenario. The new scheme enables mobile users to be served by multiple base stations (BSs) simultaneously.

In the first part of the thesis, a simplified analytical bound of the bit error rate (BER) performance of SM has been presented. Based on the minimisation of the derived BER bound, an optimum transmit structure has been developed in two stages. The first stage is to determine the optimal number of transmit antennas by balancing it with the order of signal modulation. In the second stage, based on the mathematical solutions of circle packing, a direct antenna selection method has been proposed to select the specific antennas from an antenna array. Unlike the conventional adaptive SM methods relying on instant CSIs, the proposed structure exploits statistical information, and thus does not require frequent updates. Simulation results have shown that in comparison with exhaustive search, the proposed method achieves a near-optimum BER performance, and requires very low complexity of computation.

The research on the CE process for SM, presented in the second part of the thesis, addressed the issue that SM has to activate the transmit antennas sequentially for sending pilot signals. By exploiting the correlation information between antennas, two novel CE methods have been proposed to improve the estimation accuracy for SM. One method enables SM to estimate the entire MIMO channel by sending pilot signals through one transmit antenna only. Results have

shown that when the correlation between the transmit antennas is medium or high, this method can improve the BER performance of SM by up to 7.5 dB over the convetional CE method. The other method treats the reception at different antennas as a multiplicity of sending the same pilot signal, and implements a joint CE across the receive antennas. This method results in an increase in the estimation accuracy without increasing the length of pilot sequences or the transmission power. In addition, considering the effects of both CE errors and noises on the BER, the optimisation of allocating power between the pilot signal and the information-carrying signal has been studied under the constraint of the average transmission power. Results have shown that using optimal power allocation, SM achieves a BER performance close to that in the presence of perfect CSI, with an SNR gap of less than 1 dB. Moreover, the above three methods can be combined to further improve the CE performance, and a framework of combined CE for SM has been presented.

The study on improving the system capacity in a multi-user scenario has been presented in the third part of the thesis. Instead of the fixed or random antenna scheduling given in published research, a novel method has been proposed for adaptively allocating the transmit antennas to different users. The basic concept is to allocate the antennas of the best channel quality to their corresponding users. In order to ensure fairness between users, the proposed method restricts each user to selecting only one antenna at a time. This procedure can prevent a certain user from occupying all strong candidate antennas. It has been shown that when managing the antennas in a fixed way, the BER performance of multi-user SM degrades severely as the number of users increases. Fortunately, the adaptive antenna scheduling can effectively improve the BER performance (up to 8 dB), and counteract the impairment caused by dense users.

In the last part of the thesis, a novel scheme CoSM has been proposed for the SM systems in the multi-cell scenario. This new scheme takes the advantages of both coordinated multi-point (CoMP) transmission and distributed antenna system (DAS) by allowing multiple BSs to share their antennas in the downlink service. In other words, the BS antennas dedicated to a certain user are selected from multiple BSs instead of from its closest BS. This offers an opportunity to reschedule the antennas of multiple BSs to their co-channel users. Results have shown that the cooperative scheme improves the system capacity especially for cell-edge users. As expected, those cell-centre users can benefit little from sharing the antennas of multiple BSs. Based on this fact, a three-tier cellular architecture has been presented, which enables a switch among full-bandwidth service, network SM-MIMO and CoSM.

7.2 Limitations of work, outlook and future work

The proposed methods have been shown to be powerful in improving the performance of SM in various scenarios. However, several essential assumptions have been made for the purpose of keeping moderate complexity of analysis. The violation of these assumptions in some system implementations is not envisioned as a fundamental limiting factor for the performance of the SM system, although it can lead to a sub-optimum system performance. The following suggestions can be considered to validate the performance of the proposed methods in practical implementation setups.

First, the optimum transmit structure for SM is derived on the basis of channel modelling. Although a generalised channel model is considered, the model cannot fully represent the channels in practice. Therefore the performance of the optimum structure is still to be studied for practical channels, in order to understand the benefit of balancing the number of transmit antennas with the order of signal modulation comprehensively. Furthermore, the proposed structure relies on the assumption that the correlation between a pair of antennas decreases as the distance between them increases. The exponential channel correlation model is assumed in the simulation setup. Moreover, the correlation of the receive antenna array is not considered. A study of the influence of these system building blocks on the the performance of the proposed structure can be considered in future work.

Second, the spatially-averaging channel estimation (SACE) method relies on the knowledge of the correlation degree of the receive antenna array. However, the process of estimating the correlation degree is not considered. Future work can include analysing the performance of SACE in the presence of errors in the correlation information. Also, the complexity of SACE is linear to the number of receive antennas, and the trade-off between the benefit and the complexity remains to be studied. Furthermore, the round-robin manner is used in the transmission cross channel estimation (TCCE) method for the activation sequence. A further study of an adaptive activation sequence can be considered to address the issue caused by the dissimilarity of antennas.

Third, the knowledge of channel side information at the transmitter (CSIT) is assumed for the antenna management in the multi-user SM system, and the CSIT error is not considered in the study. In addition, the proposed antenna scheduling is still heuristic where the users are ranked in an arbitrary way. Optimising the user queue and analysing the performance in the presence

of CSIT errors can be included in future work. Further to the above considerations, user priority can be involved in the antenna management to meet the demands of premium users.

Finally, in the study of SM systems in the multi-cell scenario, hexagonal cells are used to perform the simulations. The positions and ranges of practical BSs are however complicated and variant. In addition, an analytical capacity bound for the cooperative scheme is absent due to the complexity of celluar networks. Therefore, a closed-form expression of the system capacity should be studied for the proposed scheme through stochastic geometry. Furthermore, perfect synchronisation is assumed between BSs in order to exchange the information for sharing their antennas. Future work can include validating the performance of the proposed method under a more practical implementation setup.

Appendix A
List of Publications

This section contains a list of published papers.

A.1 Journal papers

X. Wu, H. Claussen, M. Di Renzo, and H. Haas, "Channel estimation for spatial modulation," *IEEE Trans. Commun.*, vol. 62, pp. 4362-4372, Dec. 2014.

X. Wu, M. Di Renzo, and H. Haas, "Adaptive selection of antennas for optimum transmission in spatial modulation," *IEEE Trans. Wireless Commun.*, 2015.

A.2 Conference papers

X. Wu, S. Sinanovic, M. Di Renzo, and H. Haas, "Base station energy consumption for transmission optimised spatial modulation (TOSM) in correlated channels," *in 17th IEEE International Workshop on Computer Aided Modeling and Design of Communication Links and Networks (CAMAD)*, pp. 261-265, Sept. 2012.

X. Wu, S. Sinanovic, M. Di Renzo, and H. Haas, "Structure optimisation of spatial modulation over correlated fading channels," *in 2012 IEEE Global Communications Conference (GLOBECOM)*, pp. 4049-4053, Dec. 2012.

X. Wu, M. Di Renzo, and H. Haas, "Direct transmit antenna selection for transmit optimized spatial modulation," *in 78th IEEE Vehicular Technology Conference (VTC Fall)*, pp. 1-5, Sept. 2013.

X. Wu, M. Di Renzo, and H. Haas, "Channel estimation for spatial modulation," *in 24th IEEE International Symposium on Personal Indoor and Mobile Radio Communications (PIMRC)*, pp. 306-310, Sept. 2013.

X. Wu, M. Di Renzo, and H. Haas, “Effect of pilot ratio on channel estimation for spatial modulation,” *in 18th IEEE International Workshop on Computer Aided Modeling and Design of Communication Links and Networks (CAMAD)*, pp. 144-148, Sept. 2013.

X. Wu, M. Di Renzo, and H. Haas, “Optimal power allocation for channel estimation in spatial modulation,” *in 2014 IEEE International Conf. on Commun. (ICC)*, pp. 5481-5485, June 2014.

X. Wu, M. Di Renzo, and H. Haas, “Spatially-averaging channel estimation for spatial modulation,” *in 80th IEEE Vehicular Technology Conference (VTC Fall)*, pp. 1-5, Sept. 2014.

X. Wu, M. Di Renzo, and H. Haas, “A novel multiple access scheme based on spatial modulation MIMO,” *in 19th IEEE International Workshop on Computer Aided Modeling and Design of Communication Links and Networks (CAMAD)*, pp. 285-289, Dec. 2014.

Appendix B
Selected Publications

This section contains all published work.

This article has been accepted for publication in a future issue of this journal, but has not been fully edited. Content may change prior to final publication. Citation information: DOI 10.1109/TWC.2015.2409067, IEEE Transactions on Wireless Communications

Adaptive Selection of Antennas for Optimum Transmission in Spatial Modulation

Xiping Wu*, *Student Member, IEEE*, Marco Di Renzo†, *Member, IEEE*, and Harald Haas*, *Member, IEEE*
*Institute for Digital Communications, Joint Research Institute for Signal and Image Processing
School of Engineering, The University of Edinburgh, EH9 3JL, Edinburgh, UK
†French National Centre for Scientific Research, Laboratory for Signals and Systems, École Supérieure d'Électricité
(SUPELEC), 3 rue Joliot-Curie, 91192 Gif-sur-Yvette (Paris), France
{xiping.wu, h.haas}@ed.ac.uk, marco.direnzo@lss.supelec.fr

***Abstract*—In this paper, we propose an optimum transmit structure for spatial modulation (SM), a unique single-stream multiple-input multiple-output (MIMO) transmission technique. As a three-dimensional modulation scheme, SM enables a trade-off between the size of the spatial constellation diagram and the size of the signal constellation diagram. Based on this fact, the novel method, named transmission optimized spatial modulation (TOSM), selects the best transmit structure that minimizes the average bit error probability (ABEP). Unlike the traditional antenna selection methods, the proposed method relies on statistical channel state information (CSI) instead of instant CSI, and feedback is only needed for the optimal number of transmit antennas. The overhead for this, however, is negligible. In addition, TOSM has low computational complexity as the optimization problem is solved through a simple closed-form objective function with a single variable. Simulation results show that TOSM significantly improves the performance of SM at various channel correlations. Assuming Rayleigh fading channels, TOSM outperforms the original SM by up to 9 dB. Moreover, we propose a single radio-frequency (RF) chain base station (BS) based on TOSM, which achieves low hardware complexity and high energy efficiency. In comparison with multi-stream MIMO schemes, TOSM offers an energy saving of at least 56% in the continuous transmission mode, and 62% in the discontinuous transmission mode.**

***Index Terms*—Spatial modulation (SM), channel correlation, transmit antenna selection, MIMO**

I. Introduction

THE need to curtail the carbon footprint and the operation cost of wireless networks requires an overall energy reduction of base stations (BSs) in the region of two to three orders of magnitude [3]. At the same time, a significant increase in spectrum efficiency from currently about 1.5 bit/s/Hz to at least 10 bit/s/Hz is required to cope with the exponentially increasing traffic loads [4]. This challenges the design of multiple-input multiple-output (MIMO) systems associated with the BS. A typical long-term evolution (LTE) BS consists of radio-frequency (RF) chains, baseband interfaces, direct current to direct current (DC-DC) converters, cooling fans, etc. Each RF chain contains a power amplifier (PA), and PAs contribute around 65% of the entire energy consumption [5]. The efficiency of state-of-the-art (SOTA) PAs is about 30% only [6], i.e. more than two thirds of the energy is consumed in quiescent power. This drives research on minimizing the overall BS energy consumption instead of the energy required for the RF output stage only. As a result, power optimization of PAs has been studied. In [7], cell discontinuous transmission (DTX) was proposed to enable the BSs to fall into a sleep mode when there is no data to convey, so that the overall energy consumption can be reduced. Based on that concept, another optimization method using on/off PAs was reported in [8], and a similar work was conducted for MIMO orthogonal frequency division multiple access (OFDMA) systems [9]. However, those studies have the following limitations: i) they focus on the operation of RF chains, while modulation schemes are not considered; ii) the optimization is implemented within each individual RF chain; and iii) the benefit is inversely proportional to the traffic load. When the BS has to be operated in the active mode continuously, the above methods would fail to achieve any energy-saving gain. Therefore it is necessary to study energy reduction on a more comprehensive level, including not only hardware operations, but also modulation schemes.

While multi-stream MIMO schemes, such as vertical Bell Labs layered space-time (V-BLAST) and space-time block coding (STBC), offer high spectrum efficiency, unfortunately, they need multiple RF chains that heavily compromise the energy efficiency. Meanwhile, spatial modulation (SM) is a unique single-stream MIMO technique [10]–[12], where the bit stream is divided into blocks and each block is split into two parts: i) the first part activates one antenna from the antenna array while the remaining antennas do not emit a signal; ii) the bits in the second part are modulated by a signal constellation diagram, and sent out through the activated antenna. The use of a single active antenna makes SM a truly energy-efficient MIMO transmission technique, because only one RF chain is required, regardless of the number of transmit antennas used. At the same time, SM ensures spatial multiplexing gains as information is encoded in the antenna index. However, like all other MIMO schemes, SM suffers performance degradation caused by channel correlations [13]. Trying to improve the performance of SM against channel variations, an adaptive method was proposed in [14], where one candidate is selected from several optional SM structures. Although the performance of SM can be improved to some extent, this method has the following weaknesses: i) it requires instant channel state information (CSI), and therefore it is not suitable for fast fading channels; ii) the relation between the adaptive selection and the channel correlation has not been exploited; and iii) despite using a simplified modulation order

[1]This paper was presented in part at the IEEE GLOBECOM 2012 [1] and IEEE CAMAD 2012 [2].

This article has been accepted for publication in a future issue of this journal, but has not been fully edited. Content may change prior to final publication. Citation information: DOI 10.1109/TWC.2015.2409067, IEEE Transactions on Wireless Communications

selection criterion, it still requires significant processing power.

In this context, we propose a novel adaptive antenna selection method for optimum transmission in SM. As a three-dimensional modulation scheme, SM enables a trade-off between the size of the spatial constellation diagram and the size of the signal constellation diagram, while achieving the same spectrum efficiency. Based on this unique characteristic, transmission optimized spatial modulation (TOSM) aims to select the best combination of these two constellation sizes, which minimizes the average bit error probability (ABEP). In order to avoid the prohibitive complexity caused by exhaustive search, a two-stage optimization strategy is proposed. The first step is to determine the optimal number of transmit antennas, and this is performed at the receiver. In the second step, the required number of antennas are selected at the transmitter. In addition to low computational complexity, TOSM needs very limited feedback because of two aspects: i) since it is based on statistical CSI, the frequency of updating is relatively low; and ii) feedback is required only to inform the transmitter of the number of selected antennas, instead of the index of each selected antenna. Therefore, the feedback overhead is negligibly low and not considered in this paper. In addition, assuming the SOTA 2010 power model [15], the overall BS energy consumption is studied for TOSM. The DTX technique is combined with TOSM to further improve the energy efficiency. Compared with our preceding studies in [1] and [2], the contributions in this paper are four-fold: i) a two-stage optimization method is proposed to balance the spatial modulation order with the signal modulation order in SM systems; ii) a complete derivation of a simplified ABEP bound for SM over generalized fading channels is presented; iii) a direct antenna selection method based on circle packing is proposed; and iv) the energy efficiency of TOSM in terms of the BS energy consumption is evaluated for both the continuous mode and the DTX mode.

The remainder of this paper is organized as follows. Section II describes the system model, including the SM transceiver, the channel model, and the BS power model. In Section III, a two-stage antenna selection method is proposed for optimum transmission in SM. Section IV studies the proposed method in the case of Rayleigh fading channels. Simulation results are presented in Section V to validate the optimization accuracy and the bit error rate (BER) performance of the proposed method. Finally, the paper is concluded in Section VI.

II. System Model

A. MIMO System and Signal Model

A $N_t \times N_r$ SM-MIMO system is considered, where N_t and N_r are the number of transmit antennas and the number of receive antennas, respectively. Unlike the original SM, only a subset of the transmit antennas is used. The size of the spatial constellation diagram, i.e. the number of utilized transmit antennas, is denoted by N, while the size of the signal constellation diagram is denoted by M. The bit stream is divided into blocks with the length of η_s bits, where $\eta_s = \log_2(N) + \log_2(M)$ is the number of bits per symbol. Each block is then split into two units of $\log_2(N)$ and $\log_2(M)$ bits. The first part activates a single transmit antenna from the spatial constellation diagram, and the currently active antenna is denoted by t_{act}. The second part chooses the corresponding symbol χ_l $(1 \le l \le M)$ from a specific signal constellation diagram, such as phase shift keying (PSK) or quadrature amplitude modulation (QAM), and sends it out through the activated antenna. The transmitted signal of SM is represented by a vector $\mathbf{x} = [0, \ldots, x_{t_{\text{act}}}, \ldots, 0]^T$ of N elements, where the t_{act}-th element is χ_l and all other elements are zero.

The received signal is given by $\mathbf{y} = \mathbf{H}\mathbf{x} + \mathbf{w}$, where $\mathbf{H}$ stands for the channel matrix and it is described in Section II. B; the vector $\mathbf{w} = [w_1, w_2, ..., w_{N_r}]^T$ and w_r, the noise at the r-th receive antenna, is a sample of complex additive white Gaussian noise with distribution $\mathcal{CN}(0, N_0)$. Across receive antennas, the noise components are statistically independent. The signal-to-noise ratio (SNR) is defined as $\gamma = E_m L/N_0$, where E_m is the average energy per symbol transmission and L denotes the path loss without shadowing. In addition, the required RF output energy per bit is denoted by $E_b = E_m/\eta_s$. The transmitted information bits are decoded by the joint maximum likelihood (ML) detection in [12] as follows:

$$\left[\hat{t}_{\text{act}}, \hat{l}\right] = \arg\min_{t,l} \parallel \mathbf{h}_t \chi_l \parallel^2 - 2\Re\{\mathbf{y}^H \mathbf{h}_t \chi_l\}, \qquad (1)$$

where $\mathbf{h}_t$ is the t-th column of $\mathbf{H}$; $\Re\{\cdot\}$ is the real part of a complex number; $\hat{t}_{\text{act}}$ and $\hat{l}$ are the detection results of t_{act} and l, respectively.

B. Channel Model

1) Channel Distribution: The fading coefficient of the link from the t-th transmit antenna to the r-th receive antenna is denoted by $h_{t,r} = \beta_{t,r}\exp(j\varphi_{t,r})$, where $\beta_{t,r}$ and $\varphi_{t,r}$ are the amplitude and the phase, respectively. The channel fading distribution as well as the CSI is assumed to be known at the receiver. Nakagami-m fading is considered in this paper, i.e. $\beta_{t,r} \sim$ Nakagami$(m_{t,r}, \Omega_{t,r})$, where $m_{t,r}$ is the shape parameter (when $m_{t,r} = 1$, the channel is Rayleigh fading) and $\Omega_{t,r}$ is the spread controlling parameter. The phase $\varphi_{t,r}$ is uniformly distributed between $(-\pi, \pi]$.

2) Channel Correlation: Since we focus on selecting the transmit antennas, the receive antennas are assumed to be independent without loss of the generality. The correlation coefficient between the amplitudes of the two propagation paths from the transmit antennas t_i and t_j to the r-th receive antenna is denoted by $\rho_{t_i,t_j,r}$. The exponential correlation matrix model in [16] is considered, which is based on the fact that the channel correlation decreases with increasing the distance between antennas. As shown in Fig. 1, the transmit antennas are located in a normalized square area, i.e. the distance between t_1 and t_A is unity. The correlation coefficient between t_1 and t_A with respect to the r-th receive antenna is denoted by $\rho_{s(r)}$. The number of antennas on each side of the antenna array is formulated as follows:

$$A = \begin{cases} \sqrt{N_t} & \text{if } \log_2 N_t \text{ is even} \\ 3 \times \sqrt{\frac{N_t}{8}} & \text{if } \log_2 N_t \text{ is odd} \end{cases}. \qquad (2)$$

This article has been accepted for publication in a future issue of this journal, but has not been fully edited. Content may change prior to final publication. Citation information: DOI 10.1109/TWC.2015.2409067, IEEE Transactions on Wireless Communications

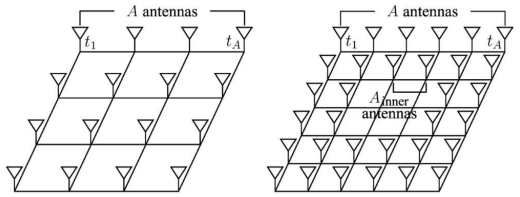

(a) $N_t = 16$ (b) $N_t = 32$

Fig. 1. Examples of the transmit antenna array

When $\log_2 N_t$ is even, the antennas form a square array with the dimension of $A \times A$. If $\log_2 N_t$ is odd, the antennas are placed in the shape shown in Fig. 1(b), where $A_{\text{inner}} = \sqrt{\frac{N_t}{8}}$. The absolute distance between t_i and t_j is denoted by d_{t_i,t_j}, and the correlation between those two antennas is given by [16, Eq. (10)]:

$$\rho_{t_i,t_j,r} = \rho_{s(r)}^{d_{t_i,t_j}}, \qquad 0 \le \rho_{s(r)} \le 1. \tag{3}$$

The average degree of the channel correlations, denoted by ρ_{av}, is calculated by:

$$\rho_{\text{av}} = \frac{1}{N_r}\sum_{r=1}^{N_r}\left(\frac{1}{N_t(N_t-1)}\sum_{t_i=1}^{N_t}\sum_{t_j\neq t_i=1}^{N_t}\rho_{t_i,t_j,r}\right). \tag{4}$$

C. Base Station Power Model

In [17], a linear relationship between the RF output power and the overall consumed power of a multi-sector BS was established. The overall BS power consumption is divided into two parts: the load-dependent portion and the constant portion. The former is dependent on the RF output power, while the latter is invariant. In addition, when no data is transmitted, a sleep mode is enabled to reduce the consumption by switching off unneeded components. In this section, a practical BS power model is introduced for the purpose of evaluating the energy efficiency of the proposed method.

1) Power Model: In [15], based on the above literature, a power model named SOTA 2010 was proposed for a one-sector, single-RF-chain BS. Table I specifies the parameters: P_{max} is the maximum RF output power; P_0 and P_s denote the constant power consumption for the active mode and the sleep mode, respectively; ζ stands for the slope that quantifies the load dependence. The instantaneous BS power consumption, denoted by P_{in}, is formulated as a function of the RF output power P_{out} [15, Eq. (1)]:

$$P_{\text{in}} = \begin{cases} P_0 + \zeta P_{\text{out}} & \text{if} \quad 0 < P_{\text{out}} \le P_{\text{max}} \\ P_s & \text{if} \quad P_{\text{out}} = 0 \end{cases}. \tag{5}$$

Also, the ratio of the time consumed in the active mode and the total period is referred to as the activation ratio μ. The average power consumption of a single-RF-chain BS is then computed by:

$$P_{\text{BS}} = \mu(P_0 + \zeta P_{\text{out}}) + (1-\mu)P_s. \tag{6}$$

TABLE I
BS POWER MODEL PARAMETERS [15].

Power model	P_{max} (W)	P_0 (W)	P_s (W)	ζ
SOTA 2010	40	119	63	2.4

Unlike SM using a single RF chain, multi-stream MIMO schemes require multiple RF chains to activate the transmit antennas simultaneously. For N_{act} *activated* antennas, the RF output power of each antenna is $1/N_{\text{act}}$ of P_{out}. As a result, the overall power consumption of a BS with multiple RF chains is calculated by:

$$P_{\text{BS}} = N_{\text{act}}\left[\mu\left(P_0 + \zeta\frac{P_{\text{out}}}{N_{\text{act}}}\right) + (1-\mu)P_s\right]. \tag{7}$$

2) Continuous Mode and DTX Mode: Two modes are considered to operate the RF chains: the continuous mode and the DTX mode [7]. In the continuous mode, the RF chains are always delivering output power of the same level. As a result, P_{out} is equal to the average RF output power $\bar{P}_{\text{out}}$, and $\mu = 1$. Substituting those conditions into (7), the overall BS power consumption in the continuous mode is obtained by:

$$P_{\text{BS-cont.}} = N_{\text{act}}P_0 + \zeta\bar{P}_{\text{out}}. \tag{8}$$

The data rate of the continuous mode is equal to the average data rate, which is denoted by $\bar{R}_b = \bar{P}_{\text{out}}/E_b$. Conversely, the DTX mode conveys data with full load, and the instantaneous data rate is $R_{b\text{max}} = P_{\text{max}}/E_b$ that is higher than $\bar{R}_b$. Then the system is enabled into sleep mode during the saved time to maintain the same average data rate. The parameter μ of the DTX mode is computed by:

$$\mu = \frac{\bar{R}_b}{R_{b\text{max}}} = \frac{\bar{P}_{\text{out}}}{P_{\text{max}}}. \tag{9}$$

Substituting (9) and $P_{\text{out}} = P_{\text{max}}$ into (7), the overall BS power consumption in the DTX mode is expressed as:

$$P_{\text{BS-DTX}} = N_{\text{act}}P_s + \left(\zeta + \frac{N_{\text{act}}(P_0 - P_s)}{P_{\text{max}}}\right)\bar{P}_{\text{out}}. \tag{10}$$

III. TOSM over Generalized Fading Channels

As mentioned, SM enables to balance the size of the signal constellation diagram with the size of the spatial constellation diagram. To achieve a certain spectrum efficiency η_s, there are $\eta_s + 1$ possible combinations of (M, N), based on the requirement of a power of two to provide a full usage in the constellation diagrams. In order to supply a complete selection range of N, N_t is set to be equal to 2^{η_s}. In this section, an optimization algorithm is proposed to select the best (M, N) as well as the specific antennas. The context is arranged in four portions: i) an ABEP upper bound is introduced for SM over generalized fading channels; ii) the ABEP upper bound is simplified to suit the minimization on the subject of either M or N; iii) the optimum (M, N) is obtained by solving the minimization problem; and iv) the required number of transmit antennas are selected from the antenna array.

This article has been accepted for publication in a future issue of this journal, but has not been fully edited. Content may change prior to final publication. Citation information: DOI 10.1109/TWC.2015.2409067, IEEE Transactions on Wireless Communications

A. ABEP Upper Bound

The ABEP upper bound of SM with the joint ML detector is given by [18, Eq. (6)]:

$$\text{ABEP} \leq \text{ABEP}_{\text{spatial}} + \text{ABEP}_{\text{signal}} + \text{ABEP}_{\text{joint}}, \quad (11)$$

and:

$$\begin{cases} \text{ABEP}_{\text{spatial}} = \dfrac{\log_2(N)}{\eta_s M} \displaystyle\sum_{l=1}^{M} \text{ABEP}_{\text{SSK}}(l) & (12a) \\ \text{ABEP}_{\text{signal}} = \dfrac{\log_2(M)}{\eta_s N} \displaystyle\sum_{t=1}^{N} \text{ABEP}_{\text{MOD}}(t) & (12b) \\ \text{ABEP}_{\text{joint}} = \dfrac{1}{\eta_s MN} \displaystyle\sum_{t_i=1}^{N}\sum_{l_i=1}^{M}\sum_{t_j=1}^{N}\sum_{l_j=1}^{M} \text{ABEP}_{\text{MIX}} & (12c) \end{cases}$$

with the terms in summations expressed in (13) where: i) $P_s(l,t)$ is the average symbol error rate (SER) of the l-th signal symbol χ_l emitted from the t-th transmit antenna; ii) $N_H(\cdot)$ denotes the Hamming distance between two symbols; iii) the average pair-wise error probability (APEP) is defined as the probability of pair-wise error event which is calculated by (14). The denotation $E[\cdot]$ is the expectation operator, and $Q(\cdot)$ is the Q-function.

B. Simplification

Due to the relaxation of linearity requirements, unlike QAM, PSK can work in PA saturation [19]. This makes PSK a more energy efficient modulation scheme. Moreover, results in [18] have shown that, for SM, PSK is not worse than QAM in many cases and in some cases it is even better. Therefore, PSK modulation is applied in the rest of this paper to keep a moderate level of analytical complexity. Every symbol has an equal weight and the average of different signal symbols in (12) can be neglected. In addition, $P_s(t,l)$ reduces to $P_s(t)$.

1) ABEP of Spatial Part: At first, we focus on $\text{ABEP}_{\text{spatial}}$ in the union bound. Assuming a high SNR, the APEP of space shift keying (SSK) modulation over correlated Nakagami-m fading channels (with the assumption of $m_{t,r} = m_r$ for $t = 1, 2, \ldots, N_t$) can be obtained based on the moment generate function (MGF) as follows [20, Eq. (15)]:

$$\text{APEP}(t_j \to t_i) = \gamma^{-N_r} \frac{2^{3N_r-1}\Gamma(N_r+0.5)}{\sqrt{\pi}\Gamma(N_r+1)} \prod_{r=1}^{N_r} f(r), \quad (15)$$

where $f(r)$ is computed in (16). We define:

$$C_{t_i,t_j} = \frac{1}{2} \times \frac{2^{3N_r-1}\Gamma(N_r+0.5)}{\sqrt{\pi}\Gamma(N_r+1)} \prod_{r=1}^{N_r} f(r). \quad (17)$$

Note that C_{t_i,t_j} is constant when m_r, $\Omega_{t,r}$ and $\rho_{t_i,t_j,r}$ are given. Consequently, (15) can be rewritten as:

$$\text{APEP}(t_j \to t_i) = 2C_{t_i,t_j}\gamma^{-N_r}. \quad (18)$$

The $\log_2(N)$ bits provided to the spatial constellation is assumed to be encoded by Gray codes. When a certain antenna is activated, there are $N/2$ other antennas that may cause an error for any particular bit. Therefore the total Hamming distance from one symbol to the other symbols is calculated by:

$$\sum_{t_j \neq t_i = 1}^{N} N_H(t_j \to t_i) = \frac{N}{2}\log_2(N). \quad (19)$$

Combining (19) and (13a), we have:

$$\text{ABEP}_{\text{SSK}}(l) = \frac{1}{2(N-1)} \sum_{t_i=1}^{N} \sum_{t_j \neq t_i = 1}^{N} \text{APEP}(t_j \to t_i). \quad (20)$$

Substituting (18) and (20) into (12a), this gives $\text{ABEP}_{\text{spatial}}$ as a function of N:

$$\text{ABEP}_{\text{spatial}} = \frac{\gamma^{-N_r}\log_2(N)}{\eta_s(N-1)} \sum_{t_i=1}^{N} \sum_{t_j \neq t_i = 1}^{N} C_{t_i,t_j}. \quad (21)$$

2) ABEP of Signal Part: The average SER of the PSK modulation over Nakagami-m fading channels is given by [21, Eq. (9.16)]:

$$P_s(t) = \frac{1}{\pi}\int_0^{\frac{M-1}{M}\pi} \prod_{r=1}^{N_r} \left(1 + \frac{\overline{\gamma}_{t,r}\sin^2(\frac{\pi}{M})}{2m_r\sin^2(\theta)}\right)^{-m_r} d\theta, \quad (22)$$

where $\overline{\gamma}_{t,r} = \Omega_{t,r}\gamma$ is the average SNR of the symbol sent from the t-th transmit antenna at the input of the r-th receive antenna. The assumption of a high SNR results in $\frac{\gamma\sin^2(\frac{\pi}{M})}{2m_r\sin^2(\theta)} \gg 1$. Hence (22) can be rewritten as:

$$P_s(t) = \frac{\int_0^{\frac{M-1}{M}\pi} (\sin\theta)^{\sum_{r=1}^{N_r} 2m_r} d\theta}{\pi} \prod_{r=1}^{N_r} \left(\frac{2m_r/\Omega_{t,r}}{\gamma\sin^2(\frac{\pi}{M})}\right)^{m_r}. \quad (23)$$

When $M \geq 4$, we have: i) $\int_0^{\frac{M-1}{M}\pi} (\sin\theta)^{\sum_{r=1}^{N_r} 2m_r} d\theta \approx \int_0^{\pi} (\sin\theta)^{\sum_{r=1}^{N_r} 2m_r} d\theta$, which is independent of the signal constellation size M; ii) $\sin(\pi/M) \approx \pi/M$. The average shape parameter of the fading distributions across all receive antennas is denoted by $\overline{m}_r = \frac{1}{N_r}\sum_{r=1}^{N_r} m_r$. Then the average SER of PSK can be formulated as follows:

$$P_s(t) = \frac{M^{2\overline{m}_r N_r} \int_0^{\pi} (\sin\theta)^{2\overline{m}_r N_r} d\theta}{\gamma^{\overline{m}_r N_r} \pi^{2\overline{m}_r N_r + 1}} \prod_{r=1}^{N_r} \left(\frac{2m_r}{\Omega_{t,r}}\right)^{m_r}. \quad (24)$$

Substituting (24) into (12b), a simplified $\text{ABEP}_{\text{signal}}$ is obtained by:

$$\text{ABEP}_{\text{signal}} = \frac{\overline{B}_N}{\eta_s} M^{2\overline{m}_r N_r} \gamma^{-\overline{m}_r N_r}, \quad (25)$$

with

$$\overline{B}_N = \frac{\int_0^{\pi} (\sin\theta)^{2\overline{m}_r N_r} d\theta}{\pi^{2\overline{m}_r N_r + 1} N} \sum_{t=1}^{N} \prod_{r=1}^{N_r} \left(\frac{2m_r}{\Omega_{t,r}}\right)^{m_r}. \quad (26)$$

Note that similar to $\text{ABEP}_{\text{spatial}}$ in (21), $\text{ABEP}_{\text{signal}}$ is also a function of N after replacing M by $2^{\eta_s}/N$.

This article has been accepted for publication in a future issue of this journal, but has not been fully edited. Content may change prior to final publication. Citation information: DOI 10.1109/TWC.2015.2409067, IEEE Transactions on Wireless Communications

$$\begin{cases} \text{ABEP}_{\text{SSK}}(l) = \dfrac{1}{N\log_2(N)} \displaystyle\sum_{t_i=1}^{N} \sum_{t_j \neq t_i=1}^{N} N_H(t_j \to t_i)\text{APEP}((t_j,\chi_l) \to (t_i,\chi_l)) & \text{(13a)} \\ \text{ABEP}_{\text{MOD}}(t) = \dfrac{1}{M\log_2(M)} \displaystyle\sum_{l=1}^{M} P_s(l,t) & \text{(13b)} \\ \text{ABEP}_{\text{MIX}} \quad = N_H((t_j,\chi_{l_j}) \to (t_i,\chi_{l_i}))\text{APEP}((t_j,\chi_{l_j}) \to (t_i,\chi_{l_i})) & \text{(13c)} \end{cases}$$

$$\text{APEP}((t_j,\chi_{l_j}) \to (t_i,\chi_{l_i})) = E\left[Q\left(\sqrt{\gamma|\alpha_{t_j}\chi_{l_j} - \alpha_{t_i}\chi_{l_i}|^2/4}\right)\right] \tag{14}$$

$$f(r) = \frac{m_r(\Omega_{t_i,r}+\Omega_{t_j,r})^{1-2m_r}(1-\rho_{t_i,t_j,r})^{m_r-1}}{(\Omega_{t_i,r}\Omega_{t_j,r})^{1-m_r}\Gamma(m_r)} \sum_{k_r=0}^{+\infty} \frac{\rho_{t_i,t_j,r}^{k_r}\Gamma(2m_r+2k_r-1)}{(k_r!)\Gamma(m_r+k_r)} \left(\frac{\sqrt{\Omega_{t_i,r}\Omega_{t_j,r}}}{\Omega_{t_i,r}+\Omega_{t_j,r}}\right)^{2k_r} \tag{16}$$

3) ABEP of Joint Part: The symbols of the PSK modulation are expressed as $\chi_l = \exp(j\varphi_l)$, where $\varphi_l = 2\pi(l-1)/M$. Thus, (14) can be rewritten as (27), where φ_t is uniformly distributed between $(-\pi,\pi]$ and φ_l is a constant. The new random variable $\varphi_t+\varphi_l$ complies with a uniform distribution over the same region as φ_t. As a result, $\text{APEP}((t_j,\chi_{l_j}) \to (t_i,\chi_{l_i}))$ is reduced to $\text{APEP}(t_j \to t_i)$. Similar to (19), the Hamming distance in (13c) can be expressed as (28). Substituting (18) and (28) into (12c), $\text{ABEP}_{\text{joint}}$ is simplified in (29).

4) Simplified ABEP: Combining (21), (25) and (29), a simplified ABEP of SM is derived as follows:

$$\text{ABEP} = \frac{M^{2\overline{m}_r N_r}}{\eta_s \gamma^{\overline{m}_r N_r}} \overline{B}_N + \frac{\eta_s 2^{\eta_s} - M\log_2(M)}{\eta_s \gamma^{N_r}} \overline{C}_N, \tag{30}$$

with

$$\overline{C}_N = \frac{1}{N(N-1)} \sum_{t_i=1}^{N} \sum_{t_j \neq t_i=1}^{N} C_{t_i,t_j}. \tag{31}$$

The term $\overline{C}_N$ reflects the average degree that the selected antenna array is affected by the fading distribution, the channel correlation, and the method of transmit antenna selection. Since the production of M and N is fixed to be 2^{η_s}, the optimization problem in (30) is actually subjected to one variable, M or N. The aim of TOSM is to determine the optimal transmit structure, including the number of antennas and their locations. However, jointly optimizing both of them requires an exhaustive search of prohibitive computational complexity. Instead, we propose a two-stage approach which separates the optimization problem in two steps: i) find the best combination of (M,N) that minimizes the ABEP of SM; and ii) select the specific antennas from the antenna array.

C. Optimal Selection of the Number of Transmit Antennas

In this step, the minimization of the simplified ABEP with respect to N (or M) is implemented for a given scenario, which is comprised of the spectrum efficiency, the number of receive antennas, the SNR, the fading distribution, and the correlation coefficient. The term $1/\eta_s$ in (30) is a positive constant, hence it can be removed without affecting the optimization result. In addition, the difference between antennas is not considered in this step. As a result, $\overline{B}_N$ and $\overline{C}_N$ are replaced by $\overline{B}_{N_t}$ and $\overline{C}_{N_t}$ to avoid the dependence on the antenna dissimilarity. The optimization problem can thus be formulated as (32).

Note that both $\overline{C}_{N_t}\gamma^{-N_r}$ and $\overline{B}_{N_t}\gamma^{-\overline{m}_r N_r}$ are constant for a certain scenario. In other words, they are independent of the variable M. The optimization problem in (32) is a nonlinear programming problem and can be solved numerically [22]. The optimization result of $\log_2(M)$ could be, and most likely is, a non-integer. However, without considering special encoding methods such as fractional bit encoding [23], both M and N must be a power of two to supply a full usage in the constellation diagram. This can readily be achieved by comparing the ABEP values of the two nearest integers around the optimal M. Afterwards, the best combination of (M,N) is obtained and denoted by $(M_{\text{opt}}, N_{\text{opt}})$.

D. Direct Antenna Selection

The second step is to select a subarray of N_{opt} antennas from the size-N_t antenna array. The chosen subset should achieve the minimum ABEP of all subarrays with the same size. Since $\overline{B}_N$ in (30) is irrelevant to the channel correlations, the problem is equivalent to finding the subarray with a minimum $\overline{C}_N$. Like the traditional transmit antenna selection (TAS) methods, this issue can be solved by an exhaustive search. However, this results in an unaffordable complexity for a large η_s. Taking $\eta_s = 6$ and $N_{\text{opt}} = 16$ as an example, the full search space is about 5×10^{14}, which is prohibitive for practical implementations. Here we propose a novel TAS method based on circle packing, which can directly determine the selection.

As the correlation coefficient ρ_{t_i,t_j} is inversely proportional to the distance d_{t_i,t_j}, a rational solution is to maximize the minimum geometric distance between any pair of the chosen antennas. This is equivalent to the circle packing problem in mathematics which can be worked out numerically [24]. Fig. 2 shows the circle packing solutions for various numbers of antennas, where the antennas are located at the circle centers.

This article has been accepted for publication in a future issue of this journal, but has not been fully edited. Content may change prior to final publication. Citation information: DOI 10.1109/TWC.2015.2409067, IEEE Transactions on Wireless Communications

$$\text{APEP}((t_j,\chi_{l_j})\rightarrow(t_i,\chi_{l_i}))=E\left[Q\left(\sqrt{\gamma|\beta_{t_j}\exp(j(\varphi_{t_j}+\varphi_{l_j}))-\beta_{t_i}\exp(j(\varphi_{t_i}+\varphi_{l_i}))|^2/4}\right)\right] \tag{27}$$

$$\sum_{t_j\neq t_i=1}^{N}\sum_{l_j\neq l_i=1}^{M}N_H((t_j,\chi_{l_j})\rightarrow(t_i,\chi_{l_i}))=\frac{(M-1)N}{2}\log_2(N)+\frac{(N-1)M}{2}\log_2(M) \tag{28}$$

$$\text{ABEP}_{\text{joint}}=\frac{\eta_s 2^{\eta_s}-M\log_2 M-N\log_2(N)}{\eta_s}\left(\frac{1}{N(N-1)}\sum_{t_i=1}^{N}\sum_{t_j\neq t_i=1}^{N}C_{t_i,t_j}\right)\gamma^{-N_r} \tag{29}$$

$$M_{\text{opt}}=\underset{M}{\text{argmin}}\quad\frac{\overline{B}_{N_t}}{\gamma^{\overline{m}_r N_r}}M^{2\overline{m}_r N_r}+\frac{\overline{C}_{N_t}}{\gamma^{N_r}}\left(2^{\eta_s}\eta_s-M\log_2(M)\right),\quad\text{subject to:}\quad 1\leq M\leq 2^{\eta_s} \tag{32}$$

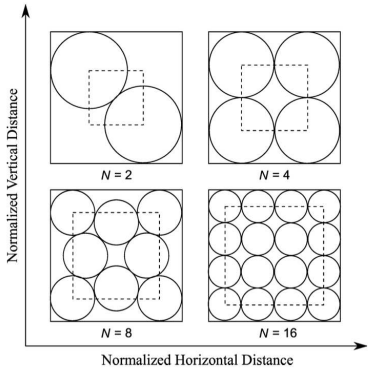

Fig. 2. Examples of circle packing problems

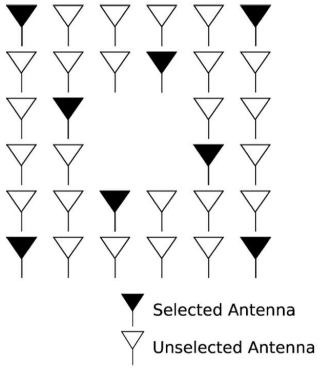

Fig. 3. RCP for selecting 8 out of 32 antennas

In the original problem, each circle must fit inside the square boundary. The problem at hand is slightly different where the circle centers are restricted to be inside the boundary, and in Fig. 2 this is shown by dashed lines. It is worth noting that this solution requires fully flexible positions. Thus, we refer to it as ideal circle packing (ICP). However, the antenna positions are fixed in practice, and the subarray cannot be perfectly allocated by ICP. Instead, a realistic circle packing (RCP) is developed by selecting those antennas closest to the ideal positions. In Fig. 3, an RCP solution is demonstrated for the case of $N_t = 32$ and $N = 8$. As can be observed, the selection presents a similarity to the solution for $N = 8$ in Fig. 2. With an increase of N_t, the RCP solution becomes closer to ICP as the antenna array supplies a larger flexibility in positions.

IV. TOSM over c.i.d. Rayleigh Fading Channels

In this section, we study TOSM in the special case of channel fading, Rayleigh fading. We present that TOSM is independent of SNR in this particular scenario, and a look-up table can be built to quickly determine the best choice of (M, N). In addition, given a target bit error rate (BER) and transmission rate, a closed-form expression of the BS energy consumption is derived for TOSM. This allows us to evaluate the proposed scheme analytically.

A. ABEP of TOSM

For correlated and identically distributed (c.i.d.) Rayleigh fading channels, we have $m_r = 1$ and $\Omega_{t,r} = \Omega$ for all t and r. As a result, $\overline{B}_N$ in (26) and $\overline{C}_N$ in (31) reduce to:

$$B=\left(\frac{2}{\Omega}\right)^{N_r}\frac{1}{\pi^{2N_r+1}}\int_0^{\pi}(\sin\theta)^{2N_r}d\theta, \tag{33}$$

and

$$C=\frac{4^{N_r-1}\Gamma(N_r+0.5)}{\Omega^{N_r}\sqrt{\pi}\Gamma(N_r+1)}\left(\sum_{k=0}^{+\infty}\frac{\Gamma(2k+1)\rho_{\text{av}}^k}{4^k(k!)\Gamma(k+1)}\right)^{N_r}. \tag{34}$$

Correspondingly, the ABEP expression in (30) reduces to:

$$\text{ABEP}=\frac{B(M)^{2N_r}+C(2^{\eta_s}\eta_s-M\log_2(M))}{\eta_s\gamma^{N_r}}. \tag{35}$$

This article has been accepted for publication in a future issue of this journal, but has not been fully edited. Content may change prior to final publication. Citation information: DOI 10.1109/TWC.2015.2409067, IEEE Transactions on Wireless Communications

The term $\eta_s \gamma^{N_r}$ is a positive constant, and therefore can be removed without influencing the optimization result. After further removing the constant item $C2^{\eta_s}\eta_s$, the optimization problem is reduced to:

$$\begin{aligned} M_{\text{opt}} = \underset{M}{\text{argmin}} \quad & B(M)^{2N_r} - CM\log_2(M) \\ \text{subject to:} \quad & 1 \le M \le 2^{\eta_s} \end{aligned}. \tag{36}$$

It is not difficult to find that the optimal solution of TOSM over c.i.d. Rayleigh fading is independent of SNR. Also, M_{opt} is independent of η_s when η_s is large enough. In other words, for a certain N_r and a large enough η_s, the optimal solution is only dependent on ρ_{av}. As shown in Table II, this allows us to build a look-up table to quickly decide the best SM deployment against different channel correlation degrees.

B. Base Station Energy Consumption based on TOSM

Substituting $\gamma = E_m L/N_0$ into (35), the required E_m using TOSM is computed by :

$$E_m = \frac{N_0}{L}\left(\frac{F(M_{\text{opt}})}{\eta_s R_e}\right)^{\frac{1}{N_r}}, \tag{37}$$

where $F(M) = B(M)^{2N_r} + C(2^{\eta_s}\eta_s - M\log_2(M))$ and R_e denotes the value of the target BER. Substituting (37) into $P_m = E_m R_b/\eta_s$, the required RF output power is obtained by:

$$P_m = \frac{R_b N_0}{\eta_s L}\left(\frac{F(M_{\text{opt}})}{\eta_s R_e}\right)^{\frac{1}{N_r}}. \tag{38}$$

The BS energy consumption per bit E_{BS} is given by:

$$E_{\text{BS}} = \frac{P_{\text{BS}}}{R_b}. \tag{39}$$

1) Continuous Mode: In the continuous mode, the energy consumption per bit of a BS based on TOSM is obtained by substituting (8) and (38) into (39) with $N_{\text{act}} = 1$:

$$E_{\text{BS}} = \frac{P_0}{R_b} + \frac{\zeta N_0}{\eta_s L}\left(\frac{F(M_{\text{opt}})}{\eta_s R_e}\right)^{\frac{1}{N_r}}. \tag{40}$$

2) DTX Mode: Similarly, based on (10), we can compute E_{BS} in the DTX mode as follows:

$$E_{\text{BS}} = \frac{P_s}{R_b} + \frac{N_0}{\eta_s L}\left(\zeta + \frac{P_0 - P_s}{P_{\max}}\right)\left(\frac{F(M_{\text{opt}})}{\eta_s R_e}\right)^{\frac{1}{N_r}}. \tag{41}$$

V. Simulation Results

In this section, Monte Carlo results are presented to validate the performance of our scheme. Two cases are studied: i) c.i.d. Nakagami-m fading; and ii) c.i.d. Rayleigh fading. In the first case, we focus on verifying the accuracy of the simplified ABEP bound. The reason for choosing the second case is threefold: i) multipath fading is typically modeled by a Rayleigh distribution; ii) by fixing the parameter m, the main trends of TOSM in relation to the channel correlation can be studied; and iii) a look-up table is formed within this scenario to exhibit the optimum transmit structure. In addition, the performance of TOSM is compared with some other schemes including fixed-SM, V-BLAST and STBC. Furthermore, the BS energy consumption and the maximum transmission rate are analyzed for the proposed scheme. In order to ensure the fairness among different values of η_s, the transmission energy per bit against noise, i.e. E_b/N_0, is used instead of SNR.

TABLE II
TOSM Deployment of (M, N) over c.i.d. Rayleigh Fading

$N_r = 1$					
$\rho_{\text{av}} \backslash \eta_s$	$\eta_s = 4$	$\eta_s = 5$	$\eta_s = 6$	$\eta_s = 7$	$\eta_s = 8$
$\rho_{\text{av}} = 0.0$	(16,1)	(16,2)	(16,4)	(16,8)	(16,16)
$\rho_{\text{av}} = 0.1$	(16,1)	(16,2)	(16,4)	(16,8)	(16,16)
$\rho_{\text{av}} = 0.2$	(16,1)	(16,2)	(16,4)	(16,8)	(16,16)
$\rho_{\text{av}} = 0.3$	(16,1)	(16,2)	(16,4)	(16,8)	(16,16)
$\rho_{\text{av}} = 0.4$	(16,1)	(16,2)	(16,4)	(16,8)	(16,16)
$\rho_{\text{av}} = 0.5$	(16,1)	(16,2)	(16,4)	(16,8)	(16,16)
$\rho_{\text{av}} = 0.6$	(16,1)	(16,2)	(16,4)	(16,8)	(16,16)
$\rho_{\text{av}} = 0.7$	(16,1)	(32,1)	(32,2)	(32,4)	(32,8)
$\rho_{\text{av}} = 0.8$	(16,1)	(32,1)	(32,2)	(32,4)	(32,8)
$\rho_{\text{av}} = 0.9$	(16,1)	(32,1)	(64,1)	(64,2)	(64,4)
$\rho_{\text{av}} = 1.0$	(16,1)	(32,1)	(64,1)	(128,1)	(256,1)
$N_r = 2$					
$\rho_{\text{av}} \backslash \eta_s$	$\eta_s = 4$	$\eta_s = 5$	$\eta_s = 6$	$\eta_s = 7$	$\eta_s = 8$
$\rho_{\text{av}} = 0.0$	(4,4)	(4,8)	(4,16)	(4,32)	(4,64)
$\rho_{\text{av}} = 0.1$	(4,4)	(4,8)	(4,16)	(4,32)	(4,64)
$\rho_{\text{av}} = 0.2$	(4,4)	(4,8)	(4,16)	(4,32)	(4,64)
$\rho_{\text{av}} = 0.3$	(4,4)	(4,8)	(4,16)	(4,32)	(4,64)
$\rho_{\text{av}} = 0.4$	(4,4)	(4,8)	(4,16)	(4,32)	(4,64)
$\rho_{\text{av}} = 0.5$	(4,4)	(4,8)	(4,16)	(4,32)	(4,64)
$\rho_{\text{av}} = 0.6$	(8,2)	(8,4)	(8,8)	(8,16)	(8,32)
$\rho_{\text{av}} = 0.7$	(8,2)	(8,4)	(8,8)	(8,16)	(8,32)
$\rho_{\text{av}} = 0.8$	(8,2)	(8,4)	(8,8)	(8,16)	(8,32)
$\rho_{\text{av}} = 0.9$	(8,2)	(8,4)	(8,8)	(8,16)	(8,32)
$\rho_{\text{av}} = 1.0$	(16,1)	(32,1)	(32,2)	(32,4)	(32,8)
$N_r = 3$					
$\rho_{\text{av}} \backslash \eta_s$	$\eta_s = 4$	$\eta_s = 5$	$\eta_s = 6$	$\eta_s = 7$	$\eta_s = 8$
$\rho_{\text{av}} = 0.0$	(4,4)	(4,8)	(4,16)	(4,32)	(4,64)
$\rho_{\text{av}} = 0.1$	(4,4)	(4,8)	(4,16)	(4,32)	(4,64)
$\rho_{\text{av}} = 0.2$	(4,4)	(4,8)	(4,16)	(4,32)	(4,64)
$\rho_{\text{av}} = 0.3$	(4,4)	(4,8)	(4,16)	(4,32)	(4,64)
$\rho_{\text{av}} = 0.4$	(4,4)	(4,8)	(4,16)	(4,32)	(4,64)
$\rho_{\text{av}} = 0.5$	(4,4)	(4,8)	(4,16)	(4,32)	(4,64)
$\rho_{\text{av}} = 0.6$	(4,4)	(4,8)	(4,16)	(4,32)	(4,64)
$\rho_{\text{av}} = 0.7$	(4,4)	(4,8)	(4,16)	(4,32)	(4,64)
$\rho_{\text{av}} = 0.8$	(8,2)	(8,4)	(8,8)	(8,16)	(8,32)
$\rho_{\text{av}} = 0.9$	(8,2)	(8,4)	(8,8)	(8,16)	(8,32)
$\rho_{\text{av}} = 1.0$	(16,1)	(16,2)	(16,4)	(16,8)	(16,16)
$N_r = 4$					
$\rho_{\text{av}} \backslash \eta_s$	$\eta_s = 4$	$\eta_s = 5$	$\eta_s = 6$	$\eta_s = 7$	$\eta_s = 8$
$\rho_{\text{av}} = 0.0$	(4,4)	(4,8)	(4,16)	(4,32)	(4,64)
$\rho_{\text{av}} = 0.1$	(4,4)	(4,8)	(4,16)	(4,32)	(4,64)
$\rho_{\text{av}} = 0.2$	(4,4)	(4,8)	(4,16)	(4,32)	(4,64)
$\rho_{\text{av}} = 0.3$	(4,4)	(4,8)	(4,16)	(4,32)	(4,64)
$\rho_{\text{av}} = 0.4$	(4,4)	(4,8)	(4,16)	(4,32)	(4,64)
$\rho_{\text{av}} = 0.5$	(4,4)	(4,8)	(4,16)	(4,32)	(4,64)
$\rho_{\text{av}} = 0.6$	(4,4)	(4,8)	(4,16)	(4,32)	(4,64)
$\rho_{\text{av}} = 0.7$	(4,4)	(4,8)	(4,16)	(4,32)	(4,64)
$\rho_{\text{av}} = 0.8$	(4,4)	(4,8)	(4,16)	(4,32)	(4,64)
$\rho_{\text{av}} = 0.9$	(8,2)	(8,4)	(8,8)	(8,16)	(8,32)
$\rho_{\text{av}} = 1.0$	(16,1)	(16,2)	(16,4)	(16,8)	(16,16)

A. Accuracy of the simplified ABEP

In Fig. 4, the simplified ABEP expression of SM in (32) is verified against simulation results. In order to present an extensive comparison, several scenarios are considered by varying the shape factor, the number of receive antennas, the spectrum efficiency and E_b/N_0. A unit spread controlling factor is assumed. For a certain scenario, the BER curve

This article has been accepted for publication in a future issue of this journal, but has not been fully edited. Content may change prior to final publication. Citation information: DOI 10.1109/TWC.2015.2409067, IEEE Transactions on Wireless Communications

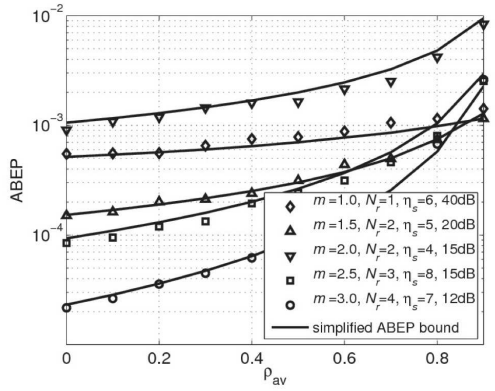

Fig. 4. The simplified ABEP bound of SM versus simulations

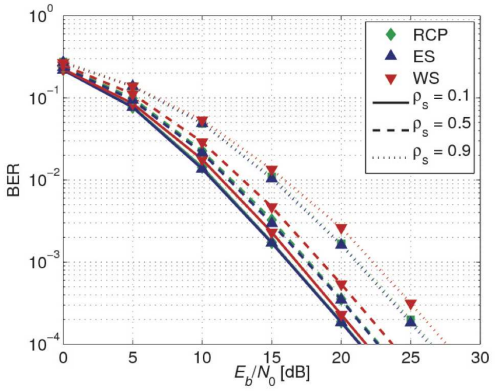

Fig. 6. BER performance of RCP for $N_t = 16$ and $N = 8$

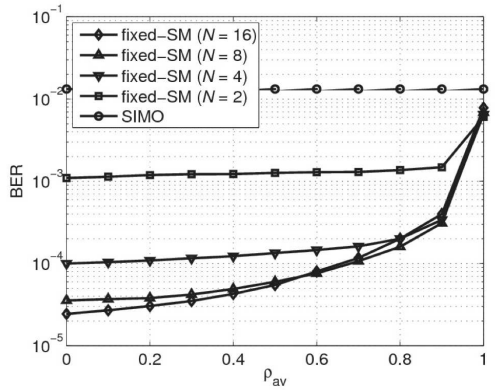

Fig. 5. BER performance of fixed-SM schemes over c.i.d. Rayleigh fading

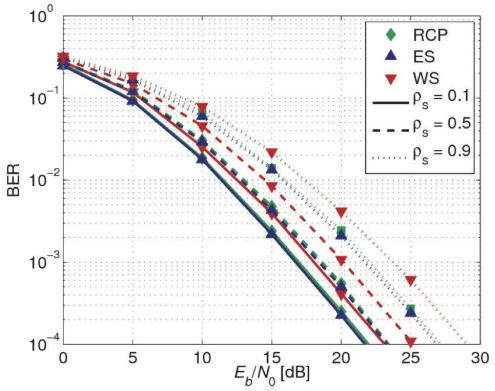

Fig. 7. BER performance of RCP for $N_t = 32$ and $N = 8$

of SM is shown as a function of the average correlation degree. As can be seen, in general, the theoretical curves match the simulation results well. Since the simplified ABEP is an approximation of the ABEP upper bound in [18], we expect some deviations especially at high channel correlations. Despite this, the simplified ABEP is still very close to the simulation results.

B. Optimality of the Look-up Table

The deployment of (M, N) for TOSM over c.i.d. Rayleigh fading channels is shown in Table II. We use gray colour to highlight the situations in which the optimal number of transmit antennas is one, i.e. SM is not applied. The following outcomes are observed: i) given a certain η_s and N_r, the optimal N decreases as ρ_{av} increases. In other words, it is better to use SM with fewer transmit antennas at high channel correlations; ii) if $N_r = 1$, the best choice regresses to a single transmit-antenna scheme for an extremely high ρ_{av}; iii) when N_r is increased, SM is suitable for more cases of $(\eta_s, \rho_{\text{av}})$, and the optimal number of transmit antennas becomes larger; and iv) for a certain N_r and ρ_{av}, the best selection of M maintains a constant when η_s is large enough.

The look-up table can be extended to any needed situation and easily used to configure the deployment of the TOSM system. In practice, N_r and η_s are usually fixed for a BS. As a result, the only parameter that needs to be determined is the correlation coefficient, which can be obtained through the structured correlation estimator [25]. Using $\eta_s = 6$ and $N_r = 2$, for example, Fig. 5 shows the simulation results of various fixed-SM schemes at $E_b/N_0 = 25$ dB. As shown, SM using $N = 16$ outperforms $N = 8$ when ρ_{av} is below 0.5. However, the opposite result happens for $0.6 \leq \rho_{\text{av}} \leq 0.9$. At an extremely high correlation of $\rho_{\text{av}} = 1$, two transmit-antenna SM achieves the lowest BER. It can be observed that Table II fits the simulation results.

C. BER Performance of Direct Antenna Selection

The BER performance of the proposed RCP approach is evaluated against two baseline schemes: i) the exhaustive search (ES); and ii) the worst case where the neighbouring

This article has been accepted for publication in a future issue of this journal, but has not been fully edited. Content may change prior to final publication. Citation information: DOI 10.1109/TWC.2015.2409067, IEEE Transactions on Wireless Communications

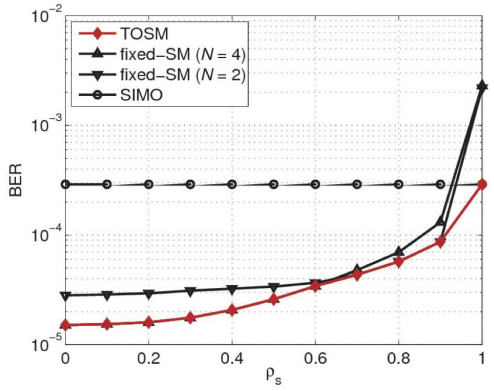

Fig. 8. BER performance of TOSM against channel correlation for $\eta_s = 4$

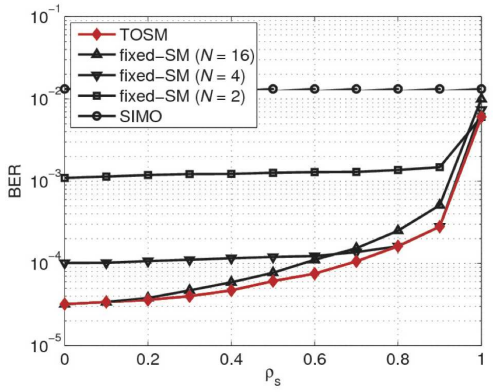

Fig. 10. BER performance of TOSM against channel correlation for $\eta_s = 6$

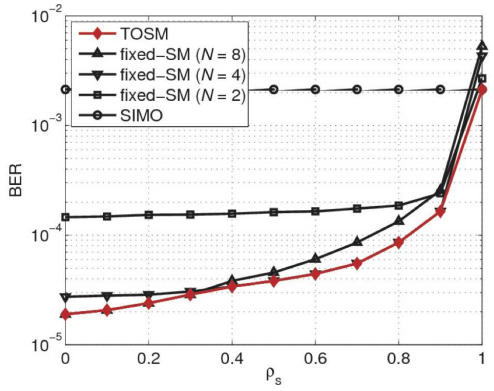

Fig. 9. BER performance of TOSM against channel correlation for $\eta_s = 5$

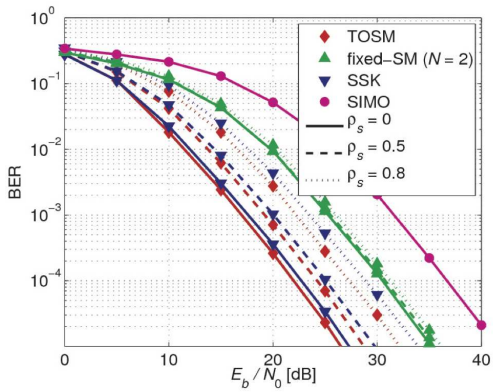

Fig. 11. BER performance of TOSM against E_b/N_0 for $\eta_s = 6$

antennas are selected. We refer to this scheme as worst selection (WS) in the sequel.

Fig. 6 and Fig. 7 present the BER performance of RCP for $\eta_s = 4$ and 5, respectively. Due to the intractable complexity of ES, the results when $\eta_s > 5$ are not presented. In addition, the antenna area is assumed to be the same to ensure a fair comparison for different η_s. Therefore, ρ_s is used instead of ρ_{av}. As shown, the RCP scheme achieves almost the same performance as ES with a gap of less than 0.3 dB. Furthermore, the negligible difference between RCP and ES is barely affected by the channel correlations, whereas the performance of WS becomes much worse as the correlation increases. To achieve the same BER value of 1×10^{-4} in the case of selecting 8 out of 32 antennas, in comparison with WS, RCP obtains an energy saving of 1.1 dB and 2.0 dB at $\rho_s = 0.1$ and 0.9, respectively.

D. BER performance of TOSM

The complexity of the MIMO system depends on the number of RF chains rather than the total number of transmit antennas. Despite the requirement of large antennas at the transmitter, TOSM needs only one RF chain. For this reason, it is reasonable to compare our approach to fixed-SM schemes with the same η_s. Based on the obtained optimal N, we evaluate the BER performance of TOSM. Assuming $N_r = 2$ and $E_b/N_0 = 25$ dB, Fig. 8 - 10 show the BER results against the channel correlation for $\eta_s = 4$, 5 and 6, respectively. The case of $N = 1$ is referred to as single-input multiple-output (SIMO).

The following trends are observed: i) fixed-SM with more antennas is not always better than those using fewer antennas. This signifies that the benefit does not simply come from employing more transmit antennas; ii) TOSM always performs better than or equal to fixed-SM schemes, which validates the optimization results; and iii) when η_s increases, TOSM employs more transmit antennas and performs much better than the fixed-SM with a small N. Specifically, TOSM slightly outperforms fixed-SM with $N = 2$ at both low and high correlations for $\eta_s = 4$. However, for $\eta_s = 5$ and 6, TOSM can always achieve a significant gain except when

This article has been accepted for publication in a future issue of this journal, but has not been fully edited. Content may change prior to final publication. Citation information: DOI 10.1109/TWC.2015.2409067, IEEE Transactions on Wireless Communications

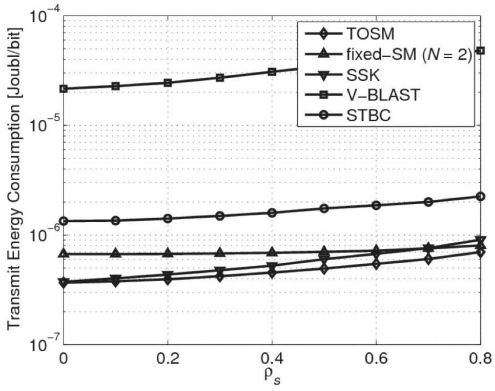

Fig. 12. Transmit energy consumption of TOSM

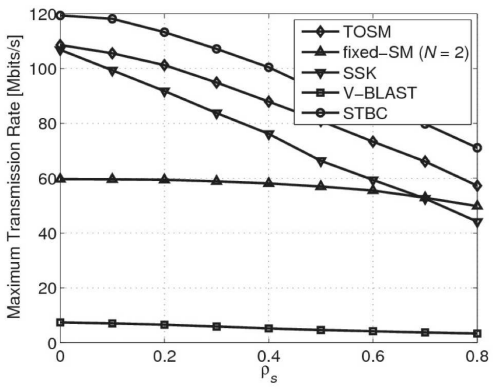

Fig. 14. Maximum transmission rate of TOSM

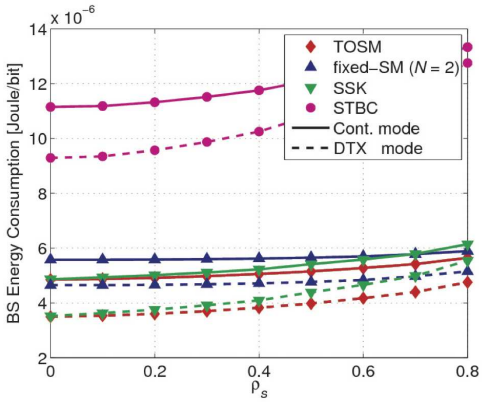

Fig. 13. BS energy consumption of TOSM for $R_b = 30$ Mbit/s

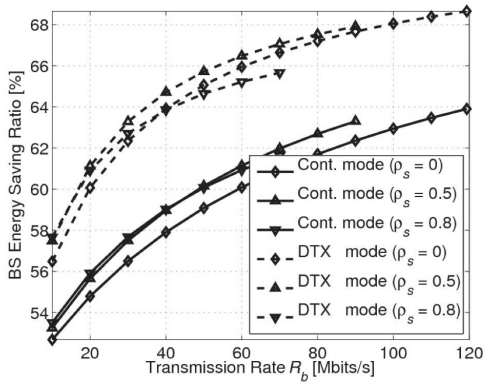

Fig. 15. BS energy saving ratio between TOSM and STBC

the channel correlation is extremely high. Similar, but less pronounced trends are noticed at lower SNRs. In Fig. 11, the BER performance of TOSM is shown as a function of E_b/N_0 for $\eta_s = 6$. As can be seen, TOSM significantly outperforms the other schemes for all presented SNRs and various channel correlation degrees. When the channels are independent, i.e. $\rho_s = 0$, TOSM saves energy in the regions of 0.8 dB, 8.7 dB, and 15.1 dB relative to SSK, fixed-SM with $N = 2$, and SIMO, respectively. As ρ_s increases, TOSM outperforms SSK more significantly. Conversely, fixed-SM with $N = 2$ is only slightly affected by the channel correlation, and the advantage of TOSM is diminishing with an increase of ρ_s. However, the gain of TOSM over fixed-SM with $N = 2$ still exceeds 4 dB at $\rho_s = 0.8$.

E. Energy Consumption

The overall BS energy consumption of TOSM is studied in contrast to V-BLAST and STBC as well as fixed-SM. The simulations are restricted in two aspects. On the one hand, the number of transmit antennas for V-BLAST is limited due to the constraint $N_r \geq N_t$. On the other hand, when using more transmit antennas, SM can save more energy in RF chains. The motivation here is to validate the energy efficiency of TOSM. To carry out a relatively fair comparison, the case of $\eta_s = 4$ and $N_r = 4$ is chosen, where TOSM employs four transmit antennas for the channel correlation varied from 0 to 0.8. The same 4×4 MIMO structure is arranged for both V-BLAST in [26] and rate 3/4 STBC in [27]. In addition, the path loss is assumed to be 100 dB without considering the shadowing.

Fig. 12 gives the transmit energy consumption results for a target BER value of 1×10^{-4}. It is noticed that, TOSM provides a remarkable and stable gain of around 5 dB in comparison with STBC and more with V-BLAST. The overall BS energy consumptions in both the continuous mode and the DTX mode are shown in Fig. 13. To maintain a certain E_b, $P_{\max}$ leads to a ceiling of the transmission rate. For this reason, a bit rate of 30 Mbit/s is chosen to ensure the BS works physically, and we compare TOSM with STBC to show the trends. The following outcomes are observed: i) using the DTX mode for TOSM provides a gain of around 1.4 dB over the

This article has been accepted for publication in a future issue of this journal, but has not been fully edited. Content may change prior to final publication. Citation information: DOI 10.1109/TWC.2015.2409067, IEEE Transactions on Wireless Communications

continuous mode; ii) TOSM significantly outperforms STBC for both the continuous mode and the DTX mode with energy-saving gains of at least 6.3 μJoule/bit (56%) and 5.8 μJoule/bit (62%), respectively; iii) compared with multi-stream MIMO schemes, TOSM requests much less energy because of the single RF chain requirement; iv) in both modes, the gain obtained by TOSM increases as ρ_s increases; and v) TOSM saves more energy in the DTX mode than the continuous mode, especially at high channel correlations. When $\rho_s = 0.8$, for example, TOSM outperforms STBC by 7.7 μJoule/bit (57%) and 8.0 μJoule/bit (63%) in the continuous mode and the DTX mode, respectively.

F. Maximum Transmission Rate

In contrast to multi-stream MIMO schemes, SM requires only one RF chain, and therefore less energy is requested to drive it. However, the maximum RF output power of SM is $1/N_{\text{act}}$ of the MIMO scheme with N_{act} active antennas, and this restricts the maximum transmission rate of SM. Fig. 14 shows $R_{b\max}$ as a function of the channel correlation in the same scenario of the previous subsection. As can be seen, the maximum transmission rate of fixed-SM outperforms V-BLAST, but is much smaller than STBC. Meanwhile, TOSM offers a great improvement of maximum transmission rate to the original SM and overcomes this disadvantage. In Fig. 15, the BS energy consumption gains between TOSM and STBC are presented in terms of the transmission rate. As shown, the gain of TOSM obtained in the DTX mode is larger than the continuous mode for various correlation degrees. Also, DTX is much better than the continuous mode when R_b increases to the full load. This signifies that TOSM is more robust and energy-efficient when combined with DTX.

VI. Conclusions

In this paper, we proposed an optimum transmit structure for SM, which balances the size of the spatial constellation diagram and the size of the signal constellation diagram. Instead of using exhaustive search, a novel two-stage TAS method has been proposed for reducing the computational complexity, where the optimal number of transmit antennas and the specific antenna positions are determined separately. The first step is to obtain the optimal number of transmit antennas by minimizing a simplified ABEP bound for SM. In the second step, a direct antenna selection method, named RCP, was developed to select the required number of transmit antennas from an antenna array. In addition, a look-up table was built in the case of c.i.d. Rayleigh fading, which can readily be used to determine the optimum transmit structure. Results show that TOSM improves the BER performance of the original SM significantly, and outperforms V-BLAST and STBC greatly in terms of the overall BS energy consumption. A further study shows that TOSM is more energy efficient when combined with the DTX mode than the continuous mode. Furthermore, the issue with respect to the maximum transmission rate in the SM systems has been addressed, which is caused by the limited output power of a single RF chain. It was shown that TOSM uplifts the maximum transmission rate of the original SM greatly, and diminishes the gap between SM and STBC significantly. All these merits make TOSM a highly energy-efficient, low-complexity scheme to satisfy the requirement of high data rate transmission, and an ideal candidate for massive MIMO [28]. Further research will extend the optimum transmit structure to generalized SM [29], where several antennas are activated simultaneously.

Acknowledgement

We gratefully acknowledge support from the European Union's Seventh Framework Programme (FP7) under grant agreement No. 264759 (GREENET Project). Professor H. Haas greatly acknowledges support from the Engineering and Physical Sciences Research Council (EPSRC) under Established Career Fellowship grant EP/K008757/1.

References

[1] X. Wu, S. Sinanovic, M. Di Renzo, and H. Haas, "Structure optimisation of spatial modulation over correlated fading channels," in *2012 IEEE Global Commun. Conf. (GLOBECOM)*, Dec. 2012, pp. 4049–4053.

[2] ——, "Base station energy consumption for transmission optimised spatial modulation (TOSM) in correlated channels," in *17th IEEE Computer-Aided Modeling Analysis and Design of Communication Links and Networks (CAMAD)*, Sept. 2012, pp. 261–265.

[3] A. Fehske, G. Fettweis, J. Malmodin, and G. Biczok, "The global footprint of mobile communications: The ecological and economic perspective," *IEEE Commun. Mag.*, vol. 49, no. 8, pp. 55–62, Aug. 2011.

[4] H. Haas and S. McLaughlin, Eds., *Next Generation Mobile Access Technologies: Implementing TDD*. Cambridge University Press, ISBN: 13:9780521826228, Jan. 2008.

[5] M. Gruber, O. Blume, D. Ferling, D. Zeller, M. Imran, and E. Strinati, "EARTH - Energy Aware Radio and Network Technologies," in *20th IEEE International Symposium on Personal, Indoor and Mobile Radio Commun. (PIMRC)*, Sept. 2009, pp. 1–5.

[6] G. Auer, V. Giannini, M. Olsson, M. Gonzalez, and C. Desset, "Framework for energy efficiency analysis of wireless networks," in *2nd International Conference on Wireless Commun., Veh. Technol., Inf. Theory and Aerospace Electronic Systems Technol. (Wireless VITAE)*, Feb. 2011, pp. 1–5.

[7] P. Frenger, P. Moberg, J. Malmodin, Y. Jading, and I. Godor, "Reducing energy consumption in LTE with cell DTX," in *73rd IEEE Veh. Technol. Conf. (VTC Spring)*, May 2011, pp. 1–5.

[8] A. Chatzipapas, S. Alouf, and V. Mancuso, "On the minimization of power consumption in base stations using on/off power amplifiers," in *2011 IEEE Online Conference on Green Commun. (GreenCom)*, Sept. 2011, pp. 18–23.

[9] Z. Xu, C. Yang, G. Li, S. Zhang, Y. Chen, and S. Xu, "Energy-efficient MIMO-OFDMA systems based on switching off RF chains," in *74th IEEE Veh. Technol. Conf. (VTC Fall)*, Sept. 2011, pp. 1–5.

[10] M. Di Renzo, H. Haas, and P. M. Grant, "Spatial modulation for multiple-antenna wireless systems: A survey," *IEEE Commun. Mag.*, vol. 49, no. 12, pp. 182–191, Dec. 2011.

[11] R. Mesleh, H. Haas, S. Sinanovic, C. W. Ahn, and S. Yun, "Spatial modulation," *IEEE Trans. Veh. Technol.*, vol. 57, no. 4, pp. 2228–2241, July 2008.

[12] J. Jeganathan, A. Ghrayeb, and L. Szczecinski, "Spatial modulation: Optimal detection and performance analysis," *IEEE Commun. Lett.*, vol. 12, no. 8, pp. 545–547, Aug. 2008.

[13] M. Di Renzo and H. Haas, "A general framework for performance analysis of space shift keying (SSK) modulation for MISO correlated Nakagami-m fading channels," *IEEE Trans. Commun.*, vol. 58, no. 9, pp. 2590–2603, Sept. 2010.

[14] P. Yang, Y. Xiao, Y. Yu, and S. Li, "Adaptive spatial modulation for wireless MIMO transmission systems," *IEEE Commun. Lett.*, vol. 15, no. 6, pp. 602–604, June 2011.

[15] H. Holtkamp, G. Auer, and H. Haas, "On minimizing base station power consumption," in *74th IEEE Veh. Technol. Conf. (VTC Fall)*, Sept. 2011, pp. 1–5.

[16] S. Loyka, "Channel capacity of MIMO architecture using the exponential correlation matrix," *IEEE Commun. Lett.*, vol. 5, no. 9, pp. 369–371, Sept. 2001.

This article has been accepted for publication in a future issue of this journal, but has not been fully edited. Content may change prior to final publication. Citation information: DOI 10.1109/TWC.2015.2409067, IEEE Transactions on Wireless Communications

[17] G. Auer, V. Giannini, I. Godor, P. Skillermark, M. Olsson, M. Imran, D. Sabella, M. Gonzalez, C. Desset, and O. Blume, "Cellular energy efficiency evaluation framework," in *73rd IEEE Veh. Technol. Conf. (VTC Spring)*, May 2011, pp. 1–6.

[18] M. Di Renzo and H. Haas, "Bit error probability of SM-MIMO over generalized fading channels," *IEEE Trans. Veh. Technol.*, vol. 61, no. 3, pp. 1124–1144, March 2012.

[19] Z. Hasan, H. Boostanimehr, and V. Bhargava, "Green cellular networks: A survey, some research issues and challenges," *IEEE Commun. Surveys Tutorials*, vol. 13, no. 4, pp. 524–540, Fourth 2011.

[20] M. Di Renzo and H. Haas, "Bit error probability of space modulation over Nakagami-m fading: Asymptotic analysis," *IEEE Commun. Lett.*, vol. 15, no. 10, pp. 1026–1028, Oct. 2011.

[21] M. K. Simon and M. S. Alouini, *Digital Communication over Fading Channels*, 2nd ed. Wiley-IEEE Press, 2005.

[22] M. S. Bazaraa, H. D. Sherali, and C. Shetty, *Nonlinear programming: Theory and algorithms*, 3rd ed. Hoboken, N.J. : Wiley-Interscience, 2006.

[23] N. Serafimovski, M. Di Renzo, S. Sinanović, R. Y. Mesleh, and H. Haas, "Fractional Bit Encoded Spatial Modulation (FBE–SM)," *IEEE Commun. Lett.*, vol. 14, no. 5, pp. 429–431, May 2010.

[24] K. Stphenson, *Introduction to Circle Packing: The Theory of Discrete Analytic Function*. Cambridge University Press, 2005.

[25] G. Matz, "Recursive MMSE estimation of wireless channels based on training data and structured correlation learning," in *13th IEEE Workshop on Statistical Signal Processing*, July 2005, pp. 1342–1347.

[26] P. Wolniansky, G. Foschini, G. Golden, and R. Valenzuela, "V-BLAST: An architecture for realizing very high data rates over the rich-scattering wireless channel," in *1998 International Symposium on Signals, Systems, and Electronics (ISSSE)*, Sept. 1998, pp. 295–300.

[27] V. Tarokh, H. Jafarkhani, and A. Calderbank, "Space-time block codes from orthogonal designs," *IEEE Trans. Inf. Theory*, vol. 45, no. 5, pp. 1456–1467, 1999.

[28] T. Marzetta, "Noncooperative cellular wireless with unlimited numbers of base station antennas," *IEEE Trans. Wireless Commun.*, vol. 9, no. 11, pp. 3590–3600, Nov. 2010.

[29] A. Younis, N. Serafimovski, R. Mesleh, and H. Haas, "Generalised spatial modulation," in *44th Asilomar Conference on Signals, Systems and Computers*, Nov. 2010, pp. 1498–1502.

Marco Di Renzo (S'05-AM'07-M'09-SM'14) received the Laurea (cum laude) and the Ph.D. degrees in Electrical and Information Engineering from the Department of Electrical and Information Engineering, University of L'Aquila, Italy, in April 2003 and in January 2007. In October 2013, he received the Habilitation à Diriger des Recherches (HDR) from the University of Paris-Sud XI, Paris, France. Since January 2010, he has been a Tenured Academic Researcher ("Chargé de Recherche Titulaire") with the French National Center for Scientific Research (CNRS), as well as a faculty member of the Laboratory of Signals and Systems (L2S), a joint research laboratory of the CNRS, the École Supérieure d'Électricité (SUPÉLEC) and the University of Paris-Sud XI, Paris, France. His main research interests are in the area of wireless communications theory.

Dr. Di Renzo is a recipient of several awards, which include a special mention for the outstanding five-year (1997-2003) academic career, University of L'Aquila, Italy; the THALES Communications fellowship (2003-2006), University of L'Aquila, Italy; the 2004 Best Spin-Off Company Award, Abruzzo Region, Italy; the 2006 DEWS Travel Grant Award, University of L'Aquila, Italy; the 2008 Torres Quevedo Award, Ministry of Science and Innovation, Spain; the "Dérogation pour l'Encadrement de Thèse" (2010), University of Paris-Sud XI, France; the 2012 IEEE CAMAD Best Paper Award; the 2012 IEEE WIRELESS COMMUNICATIONS LETTERS Exemplary Reviewer Award; the 2013 IEEE VTC-Fall Best Student Paper Award; the 2013 Network of Excellence NEWCOM# Best Paper Award; the 2013 IEEE TRANSACTIONS ON VEHICULAR TECHNOLOGY Top Reviewer Award; the 2013 IEEE-COMSOC Best Young Researcher Award for Europe, Middle East and Africa (EMEA Region); and the 2014 IEEE ICNC Single Best Paper Award Nomination (Wireless Communications Symposium). Currently, he serves as an Editor of the IEEE COMMUNICATIONS LETTERS and of the IEEE TRANSACTIONS ON COMMUNICATIONS (Heterogeneous Networks Modeling and Analysis).

Xiping Wu received the B.Sc. degree from Southeast University, Nanjing, China in 2008 and the M.Sc. degree with distinction from the University of Edinburgh, Scotland, United Kingdom in 2011. From September 2011 to August 2014, he was Marie-Curie Early-Stage Researcher (ESR) as well as Ph.D. candidate at the University of Edinburgh, funded by the European Union's Seventh Framework Programme (FP7) project GREENET. From December 2013 to April 2014, he was on secondment to the Department of Electrical and Information Engineering, University of L'Aquila, Italy. Since September 2014, he has been Research Associate with the Institute for Digital Communications (IDCOM), the University of Edinburgh, funded by British Engineering and Physical Sciences Research Council (EPSRC). His main research interests are in the areas of wireless communication theory, optical wireless communications, and wireless networking. In 2010, he was granted the Scotland Saltire Scholarship by the Scottish Government.

Harald Haas received the PhD degree from the University of Edinburgh in 2001. He currently holds the Chair of Mobile Communications at the University of Edinburgh. His main research interests are in optical wireless communications, hybrid optical wireless and RF communications, spatial modulation, and interference coordination in wireless networks. He first introduced and coined "spatial modulation" and "Li-Fi". Li-Fi was listed among the 50 best inventions in TIME Magazine 2011.

Prof Haas was an invited speaker at TED Global 2011, and his talk has been watched online more than 1.5 million times. He is co-founder and chief scientific officer (CSO) of pureLiFi Ltd. Professor Haas holds 31 patents and has more than 30 pending patent applications. He has published 300 conference and journal papers including a paper in Science. He was co-recipient of a best paper award at the IEEE Vehicular Technology Conference in Las Vegas in 2013. In 2012, he was the only recipient of the prestigious Established Career Fellowship from the EPSRC (Engineering and Physical Sciences Research Council) within Information and Communications Technology in the UK. Haas is recipient of the Tam Dalyell Prize 2013 awarded by the University of Edinburgh for excellence in engaging the public with science. In 2014, he was selected by EPSRC as one of ten RISE (Recognising Inspirational Scientists and Engineers) Leaders.

4362 IEEE TRANSACTIONS ON COMMUNICATIONS, VOL. 62, NO. 12, DECEMBER 2014

Channel Estimation for Spatial Modulation

Xiping Wu, *Student Member, IEEE*, Holger Claussen, *Member, IEEE*,
Marco Di Renzo, *Senior Member, IEEE*, and Harald Haas, *Member, IEEE*

***Abstract*—In this paper, a novel channel estimation (CE) method is proposed for spatial modulation (SM), a unique single-stream multiple-input–multiple-output transmission technique. In SM, there is only one transmit antenna being active at any time instance. While this property completely avoids inter-channel interference, it results in a challenge to estimate the channel information. In conventional CE (CCE) methods for SM, all transmit antennas have to be sequentially activated for sending pilots. Therefore, the time consumed in CE is proportional to the number of transmit antennas, which significantly compromises the throughput. By exploiting channel correlation, the proposed method, named transmission cross CE (TCCE), has the following characteristics: i) the entire channel is estimated by sending pilots through one transmit antenna; ii) it requires no overhead or feedback; and iii) it achieves a low computational complexity at the receiver. In addition, we propose an analytical framework to compute the distribution of the CE errors over time-varying fading channels. The corresponding average bit error probability (ABEP) bound of SM is also derived for the proposed method. Results show that the proposed ABEP bound matches with the simulations very well. When compared with CCE, the new method obtains a signal-to-noise ratio gain of up to 7.5 dB for medium and high correlations between the transmit antennas. Moreover, an adaptive CE technique can be readily implemented for SM via switching between CCE and TCCE.**

***Index Terms*—Spatial modulation, MIMO, channel estimation, channel correlation, time-varying channel.**

I. Introduction

SPATIAL MODULATION (SM) is a unique single-stream transmission technique for multiple-input–multiple-output (MIMO) wireless communication systems [2]–[4]. In SM, the locations of the transmit antennas are used to carry information as well as the traditional signal modulation. Therefore, compared with single antenna systems, SM achieves an increase of the spectral efficiency by the factor of the base-two logarithm of the transmit antenna number. More importantly, only one transmit antenna is active at any given time in SM, which completely avoids inter-channel interference encountered in traditional MIMO systems. Furthermore, SM only requires a single radio-frequency (RF) chain, regardless of the number of transmit antennas used. This key property makes SM a truly energy-efficient technique for large scale MIMO systems. Recent research on SM has focused on studying its bit error ratio (BER) performance over fading channels with the assumption of perfect channel state information (CSI) [5]–[7]. Results show that SM offers a better performance than many state-of-the-art (SOTA) MIMO techniques while allowing a low-complexity implementation.

However, perfect channel knowledge is always impractical and channel estimation (CE) is of vital importance that can not be neglected. In order to obtain the CSI at the receiver, pilot-based CE [8] is commonly used where pilots, i.e. deterministic symbols, are conveyed followed by the symbols carrying information. The pilot ratio is defined as the ratio of the number of pilots to the number of total symbols. Unlike multi-stream MIMO schemes such as vertical Bell Labs layered space-time (VBLAST) [9] and space-time block coding (STBC) [10], SM can send the pilots through only one antenna at a time. This challenges the channel estimation process for SM which has to sequentially activate the transmit antennas for sending pilots. We refer to this method as the conventional channel estimation (CCE), of which the pilot ratio is proportional to the number of transmit antennas. Unfortunately, this fact has so far been neglected in the SOTA literature. In [11] and [12], the BER performance of SM with imperfect CSI is respectively studied for uncorrelated and correlated fading channels. A similar work on space shift keying (SSK) is proposed in [13], where different lengths of the pilot sequence are considered. Although the above papers fill some gaps in the knowledge, they have the following limitations: i) the CE errors are arbitrary without considering practical CE methods; ii) the relation between the pilot ratio and the number of transmit antennas is not addressed. Until now, only a few studies have been conducted in studying CE techniques for SM. In [14], recursive least square (RLS) is investigated for MIMO systems based on a single RF chain. Another CE method for SM is proposed in [15], in which joint channel estimation with data detection is applied. However, these methods are developed based on existing CE techniques, and the issue of costly CE time is unsolved. It appears that no CE method specially tailored for SM has so far been proposed.

Because of the limited separation between antennas, MIMO channels are normally correlated to some degree in practical systems. This causes a degradation in the BER performance

Manuscript received May 25, 2014; revised September 20, 2014; accepted October 22, 2014. Date of publication November 3, 2014; date of current version December 15, 2014. This work was supported by the European Union's Seventh Framework Programme (FP7) under Grant 264759 (GREENET Project). The work of H. Haas was supported by the Engineering and Physical Sciences Research Council under the Established Career Fellowship Grant EP/K008757/1. This paper was presented in part at the IEEE PIMRC 2013 [1]. The associate editor coordinating the review of this paper and approving it for publication was H. Dai.

X. Wu and H. Haas are with the Institute for Digital Communications, Joint Research Institute for Signal and Image Processing School of Engineering, The University of Edinburgh, Edinburgh, EH9 3JL, U.K. (e-mail: xiping.wu@ed.ac.uk; h.haas@ed.ac.uk).

H. Claussen is with the Autonomous Networks and Systems Research Department, Bell Labs, Alcatel-Lucent, Blanchardstown Business and Technology Park, Dublin 15, Ireland (e-mail: holger.claussen@alcatel-lucent.com).

M. Di Renzo is with the French National Centre for Scientific Research, Laboratory for Signals and Systems, École Supérieure d'Électricité (SUPELEC), 75016 Paris, France (e-mail: marco.direnzo@lss.supelec.fr).

Color versions of one or more of the figures in this paper are available online at http://ieeexplore.ieee.org.

Digital Object Identifier 10.1109/TCOMM.2014.2366750

for all MIMO schemes including SM. Therefore, CE in this situation is required to be more accurate than that of uncorrelated channels. To date, most research in this area has focused on the optimal design of training signals [16]–[18]. Few estimators are specially designed for correlated MIMO channels, and those few are based on specific channel correlation models [19], [20]. Due to the complexity and uncertainty of channel models in practical systems, the viability of those methods is limited. In addition to spatial correlation, time-varying is another challenge in channel estimation. With the aim of coping with time-varying MIMO channels, sequential channel estimation is proposed in [21], which is based on random-set theory. However, to the best of the authors' knowledge, no channel estimation method has so far been proposed to exploit the temporal and spatial channel correlation together.

In this paper, we aim to improve the CE performance for SM by exploiting the channel correlation information in both space and time. A novel CE approach, named transmission cross channel estimation (TCCE), is proposed. Unlike CCE, the new method estimates the whole MIMO channel by sending pilots through only one transmit antenna. As a result, the CE time is significantly reduced. More importantly, the proposed method requires no overhead or feedback, while achieving a low computational complexity at the receiver. Further, we propose an analytical framework to compute the distribution of the CE errors for time-varying channels. The corresponding Average Bit Error Probability (ABEP) bound is also derived for SM. Simulation results show that when the channel correlation between transmit antennas is larger than 0.35, TCCE offers a better performance than CCE with an Signal-to-Noise Ratio (SNR) gain of up to 7.5 dB. Moreover, an adaptive CE approach is available for SM by switching between CCE and TCCE.

The remainder of this paper is organized as follows. Section II describes the system model, including the SM transmitter, the channel model, and the receiver. The novel CE approach for SM is proposed in Section III. Section IV proposes a framework to compute the distribution of the CE errors for time-varying channels. In Section V, we derive the ABEP bound for SM associated with the proposed CE method. Simulation results are presented in Section VI, and the paper is concluded in Section VII.

II. System Model

A. Spatial Modulation

An $N_t \times N_r$ SM-MIMO system is considered, where N_t and N_r are the number of transmit antennas and the number of receive antennas, respectively. The information to be conveyed is separately carried by the spatial constellation diagram and signal constellation diagram. The size of the spatial constellation diagram is exactly the number of transmit antennas, while the size of the signal constellation diagram is denoted by M. The bit stream is divided into blocks of η_s bits, where $\eta_s = \log_2(N_t M)$ is the number of bits per symbol. Each block is then split into two units of $\log_2(N_t)$ and $\log_2(M)$ bits and: i) the first segment activates one of the transmit antennas, and we denote the currently active antenna by t_{act}; ii) the remaining bits are used to determine a symbol in the signal constellation digram, and the active antenna conveys this symbol that is denoted by χ_l, $l = 1, 2, \ldots, M$. The transmitted signal is expressed by a vector $\mathbf{x}_{t_{\text{act}},l} = [x_1, x_2, \ldots, x_{N_t}]^T$, of which the t_{act}-th element carries χ_l and all other elements are zero.

B. Channel Model

In this paper, we consider a time-varying and spatially-correlated MIMO channel. The fading coefficient of the link between the t-th transmit antenna and the r-th receive antenna is denoted by $h_{r,t(n)}$, where n is the discrete time index. The corresponding $N_r \times N_t$ channel matrix, denoted by $\mathbf{H}_{(n)}$, is generated in two stages: i) create a channel matrix of spatial correlation for the initial time, i.e. $\mathbf{H}_{(0)}$; ii) yield a consecutive channel based on the temporal correlation, while maintaining the spatial correlation. It is worth noting that the proposed CE method is not restricted to a specific channel model. The channel model in this paper is for the purpose of theoretical analysis and performance validation for the proposed method. The study of different channel models is outside the scope of this paper.

1) Spatial Correlation: The Kronecker model is widely used to generate spatially-correlated channels [22]. According to this model, the channel matrix is initialized as:

$$\mathbf{H}_{(0)} = \mathbf{R}_{\text{r}}^{1/2} \mathbf{G} \left(\mathbf{R}_{\text{t}}^{1/2} \right)^H, \tag{1}$$

where $\mathbf{G}$ has the same dimension as $\mathbf{H}_{(0)}$, and its entries are independent and identically distributed (i.i.d.) complex Gaussian distribution $\mathcal{CN}(0,1)$; $\mathbf{R}_{\text{t}}$ and $\mathbf{R}_{\text{r}}$ denote the transmit correlation matrix and the receive correlation matrix, respectively. In this paper, the CE methods involved are individually implemented at each receive antenna. Therefore, the receive antennas are assumed to be independent without loss of generality, i.e. $\mathbf{R}_{\text{r}}$ is an $N_r \times N_r$ identity matrix. The correlation coefficient between the t_1-th and t_2-th transmit antennas is denoted by ρ_{t_1,t_2}, and the transmit correlation matrix is written as:

$$\mathbf{R}_{\text{t}} = \begin{bmatrix} 1 & \rho_{1,2} & \cdots & \rho_{1,N_t} \\ \rho_{2,1} & 1 & \cdots & \rho_{2,N_t} \\ \vdots & \vdots & \ddots & \vdots \\ \rho_{N_t,1} & \rho_{N_t,2} & \cdots & 1 \end{bmatrix}. \tag{2}$$

The exponential correlation model in [23] is considered, which is based on the fact that the spatial correlation decreases as the distance between antennas increases. We use d_{t_1,t_2} to represent the Euclidean distance between t_1 and t_2, and d is the reference distance. Then the correlation coefficient between two transmit antennas can be expressed as:

$$\rho_{t_1,t_2} = \rho^{\frac{d_{t_1,t_2}}{d}}, \tag{3}$$

where ρ is the correlation degree when two antennas are separated at the reference distance.

2) Temporal Correlation: The Gauss-innovations channel model in [24] is used to establish time-varying channels. The channel matrix at the n-th time index is formulated as follows:

$$\mathbf{H}_{(n)} = \sqrt{\alpha}\mathbf{H}_{(n-1)} + \sqrt{1-\alpha}\mathbf{H}'_{(n)}, \tag{4}$$

where α is a parameter related to the user speed, and it is given by [24, Eq. (10)]:

$$\alpha = J_0\left(\frac{2\pi v f_c T_s}{c}\right)^2, \tag{5}$$

where $J_0(\cdot)$ is the zeroth-order Bessel function of the first kind; T_s is the sampling period; f_c is the center carrier frequency; v and c denote the speed of mobile user and the speed of light, respectively. The term $\mathbf{H}'_{(n)}$ is also generated from (1), but it is independent of $\mathbf{H}_{(n-1)}$. In addition, $\mathbf{H}'_{(n)}$ is independent from time to time. Substituting (1) into (4), we have:

$$\mathbf{H}_{(1)} = \mathbf{R}_r^{1/2}\left(\sqrt{\alpha}\mathbf{G}_{(0)} + \sqrt{1-\alpha}\mathbf{G}'_{(1)}\right)\left(\mathbf{R}_t^{1/2}\right)^H. \tag{6}$$

It is straightforward to infer that $\mathbf{H}_{(n)}$ is a correlated Rayleigh fading channel of the same correlation matrices as $\mathbf{H}_{(0)}$. Note that the above model also suits spatially-uncorrelated and/or time-invariant channels, by setting the correlation coefficients and/or the speed of mobile user to be zero.

C. Maximum Likelihood Optimum Detector

We denote the noise at the input of the r-th receive antenna by w_r, which is assumed to be a complex Additive White Gaussian Noise (AWGN) process with distribution $\mathcal{CN}(0, N_0)$. Across the receive antennas, the noise components are statistically independent and denoted by $\mathbf{w} = [w_1, w_2, \ldots, w_{N_r}]^T$. The received signal is given by:

$$\mathbf{y} = \mathbf{h}_{t_{\text{act}}}\chi_l + \mathbf{w}, \tag{7}$$

where $\mathbf{y} = [y_1, y_2, \ldots, y_{N_r}]^T$ and $\mathbf{h}_{t_{\text{act}}}$ is the t_{act}-th column of $\mathbf{H}$. The signal-to-noise ratio (SNR) is defined as $\gamma = E_m/N_0$, where E_m is the average energy per transmission. The estimated CSI is denoted by $\hat{\mathbf{H}}$, and it is used to decode the transmitted signal. Based on the joint maximum likelihood detection in [5], the decoded information is obtained by:

$$\left[\hat{t}_{\text{act}}, \hat{l}\right] = \arg\min_{t,l} \parallel \hat{\mathbf{h}}_t\chi_l \parallel^2 - 2\Re\left\{\mathbf{y}^H\hat{\mathbf{h}}_t\chi_l\right\}, \tag{8}$$

where $\Re\{\cdot\}$ is an operator to extract the real part of a complex number.

III. Transmission Cross Channel Estimation

A. Conventional Methods

In the conventional channel estimation (CCE) methods for SM, the transmit antennas are sequentially activated for sending the pilots. At the receiver, the channel information pertaining to the currently active antenna is estimated by a specific estimator such as least square (LS), minimum mean square error (MMSE), and recursive least square (RLS) [25]. In this paper, we consider LS in both CCE and the proposed method to ensure a fair comparison. Fig. 1 shows the pilot structure for CCE. During each blue colored slot, a pilot symbol is sent through the corresponding transmit antenna. Those slots are referred to as pilot slots. The remaining time slots are used to convey information-carrying symbols. The pilot ratio, denoted by η, is

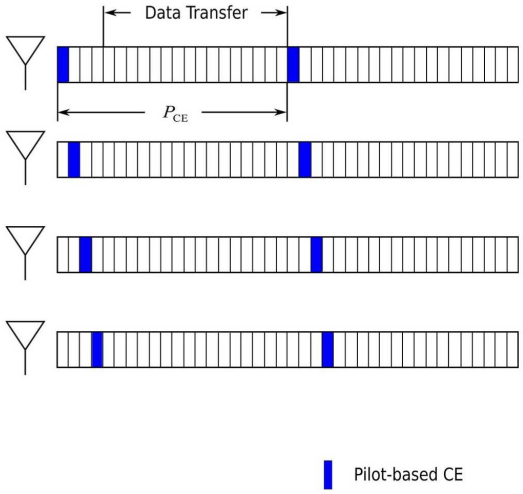

Fig. 1. Block diagram of CCE for SM with $N_t = 4$.

defined as the ratio of the number of pilots to the number of total symbols. The estimation period P_{CE} is defined as the interval between two adjacent CE processes of any transmit antenna. The estimation period for CCE is given by:

$$P_{\text{CE}} = \frac{N_t T}{\eta}, \tag{9}$$

where T denotes the symbol period. It can be found that the CE period for CCE is proportional to the number of transmit antennas. We use q_t to denote the pilot symbol sent from the t-th transmit antenna, and the signal obtained at the r-th receive antenna is written as:

$$y_{r(n)} = h_{r,t(n)}q_t + w_{r(n)}. \tag{10}$$

Since the channel estimation is individually implemented at each receive antenna, the index of receive antennas is omitted for the purpose of simplicity. The LS estimate for the t-th transmit antenna is then denoted by $\tilde{h}_{t(n)}$, and it is given by [25, p. 224, Eq. (8.9)]:

$$\tilde{h}_{t(n)} = \arg\min_h \left\|y_{(n)} - hq_t\right\|^2. \tag{11}$$

As both $y_{(n)}$ and q_t are scalar, we have:

$$\tilde{h}_{t(n)} = \frac{y_{(n)}}{q_t}. \tag{12}$$

After the channel information for all transmit antennas is obtained at the receiver, it is used to decode the data symbols until the next CE process comes. It is worth noting that, as the transmit antennas are activated sequentially, a gap exists between the pilot slot and the beginning of data transfer.

B. Proposed Method

The channel difference information (CDI), denoted by $\Delta J_{t_1,t_2} = h_{t_1} - h_{t_2}$, is defined as the difference between the channel fading coefficients of two transmit antennas t_1 and t_2. If CDI is known, then it is possible to obtain the full CSI of

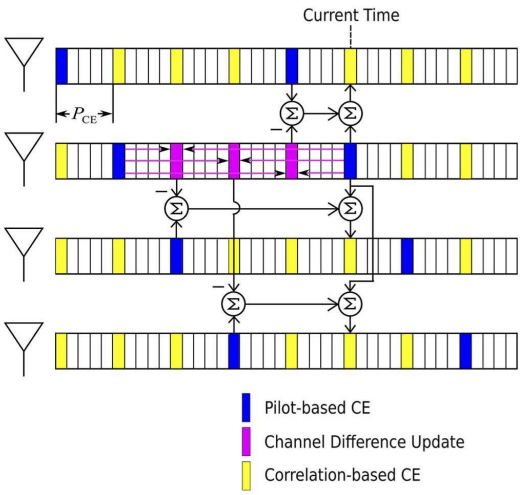

Fig. 2. Block diagram of TCCE for SM with $N_t = 4$.

MIMO channels by estimating the channel information of any single transmit antenna. In the other words, only one transmit antenna is required to send the pilot signal to estimate the entire MIMO channel. As a result, the CE time is significantly shortened in comparison with CCE.

A constant channel difference is however unrealistic. In order to make it available for time-varying channels, the channel difference information needs to keep updated. Taking four transmit antennas as an example, Fig. 2 depicts the block diagram of the proposed method. The pilot transmissions are represented by blue colored slots, similar as in Fig. 1. Note that, unlike CCE, the pilot slots pertaining to different transmit antennas are equally allocated along the time. At any pilot slot, the CSI of the currently active antenna is obtained in the same way as that of CCE. For those idle antennas, CSI is measured based on the estimated CSI of the active antenna and the CDI between the active antenna and the corresponding idle antenna. We refer to this type of CE as correlation-based CE, which is shown by yellow colored slots. The CDI for a certain idle antenna is calculated at the latest pilot slot of that antenna. The CSI of the currently active antenna at that slot, which is highlighted in pink color, is corrected by using interpolation based on the estimated CSIs at the current pilot slot and some previous pilot slots. At any pilot slot, the algorithm comprises four steps as follows.

1) Pilot-Based CE: At first, the pilot-based CE is implemented for the currently active antenna, i.e. t_{act}. The corresponding estimation result is denoted by $\tilde{h}_{t_{\mathrm{act}}(n)}$.

2) Channel Difference Update: For each transmit antenna, the pilot is conveyed once for every N_t pilot slots. At the previous $N_t - 1$ pilot slots, the CSI of t_{act} is estimated by the correlation-based CE described in step 3. In this step, these CSIs are corrected by a low-pass interpolation based on $\tilde{h}_{t_{\mathrm{act}}(n)}$ and $L-1$ previous estimates $\tilde{h}_{t_{\mathrm{act}}(n-lN_t/\eta)}$, $l=1,2,\ldots,L-1$. The number of totally used estimates, i.e. L, is defined as the interpolation sequence length. The corrected CSI is denoted by $\dot{h}_{t_{\mathrm{act}}(n-k/\eta)}$, $k = 1, 2, \ldots, N_t - 1$. For clarity, we choose the simplest case of $L = 2$, and it gives:

$$\dot{h}_{t_{\mathrm{act}}(n-k/\eta)} = \left(1 - \frac{k}{N_t}\right) \tilde{h}_{t_{\mathrm{act}}(n)} + \left(\frac{k}{N_t}\right) \tilde{h}_{t_{\mathrm{act}}(n-N_t/\eta)}, \quad k = 1, 2, \ldots, N_t - 1. \quad (13)$$

For $L > 2$, interested readers are referred to [26]. Regarding the t-th antenna, the last pilot-based CE happened at $k_{t,t_{\mathrm{act}}}/\eta$ slots before, where:

$$\begin{cases} t_{\mathrm{act}} - t & \text{if } t \le t_{\mathrm{act}} \\ t_{\mathrm{act}} - t + N_t & \text{if } t > t_{\mathrm{act}}. \end{cases} \quad (14)$$

The channel difference between t and t_{act} is updated as follows:

$$\Delta J_{t,t_{\mathrm{act}}\left(n-k_{t,t_{\mathrm{act}}}/\eta\right)} = \tilde{h}_{t\left(n-k_{t,t_{\mathrm{act}}}/\eta\right)} - \dot{h}_{t_{\mathrm{act}}\left(n-k_{t,t_{\mathrm{act}}}/\eta\right)}. \quad (15)$$

3) Correlation-Based CE: After collecting the CDI, it is possible to measure the CSI of the idle antennas. To be distinguished from pilot-based CE, the estimation result of correlation-based CE is denoted by $\acute{h}_{t(n)}$ and it is obtained by:

$$\acute{h}_{t(n)} = \tilde{h}_{t_{\mathrm{act}}(n)} + \Delta J_{t,t_{\mathrm{act}}\left(n-k_{t,t_{\mathrm{act}}}/\eta\right)}, \quad t \neq t_{\mathrm{act}}. \quad (16)$$

Substituting (13) and (15) into (16), we have:

$$\acute{h}_{t(n)} = \tilde{h}_{t\left(n-k_{t,t_{\mathrm{act}}}/\eta\right)} + \frac{k_{t,t_{\mathrm{act}}}}{N_t}\left(\tilde{h}_{t_{\mathrm{act}}(n)} - \tilde{h}_{t_{\mathrm{act}}(n-N_t/\eta)}\right), \quad t \neq t_{\mathrm{act}}. \quad (17)$$

Note that when $t = t_{\mathrm{act}}$ in (14), the value of $k_{t,t_{\mathrm{act}}}$ equals zero. Correspondingly, the right side of the above equation reduces to $\tilde{h}_{t_{\mathrm{act}}(n)}$. Therefore, the estimated CSI obtained by both pilot-based CE and correlation-based CE can be written as the same expression in (17). We denote the estimated CSI of all transmit antennas as $\hat{h}_{t(n)}$, and rewrite (17) as:

$$\hat{h}_{t(n)} = \tilde{h}_{t\left(n-k_{t,t_{\mathrm{act}}}/\eta\right)} + \frac{k_{t,t_{\mathrm{act}}}}{N_t}\left(\tilde{h}_{t_{\mathrm{act}}(n)} - \tilde{h}_{t_{\mathrm{act}}(n-N_t/\eta)}\right), \quad t = 1, \ldots, N_t. \quad (18)$$

4) Antenna Index Update: The index of the transmit antenna to convey the pilot next time is then updated to:

$$t_{\mathrm{act}} = \begin{cases} t_{\mathrm{act}} + 1 & \text{if } t_{\mathrm{act}} < N_t \\ 1 & \text{if } t_{\mathrm{act}} = N_t. \end{cases} \quad (19)$$

The flowchart of the proposed method is shown in Fig. 3, where the dash lines indicate the communications between the transmitter and the receiver. It is worth noting that there is no need for extra transmission or feedback in TCCE. Compared with CCE, the novel method only requires to store the previous estimation results at the receiver. The CE period for TCCE is computed by:

$$P_{\mathrm{CE}} = \frac{T}{\eta}, \quad (20)$$

which is regardless of the number of transmit antennas used.

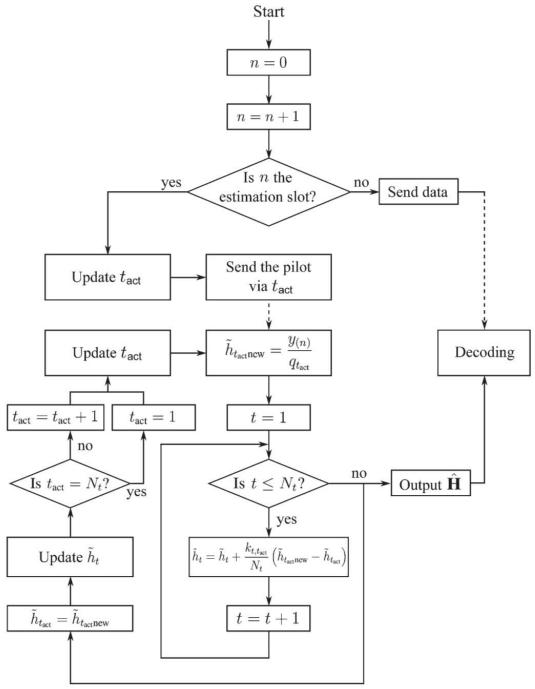

Fig. 3. Flowchart of the proposed CE method.

IV. Theoretical Analysis of Channel Estimation Errors

In this section, we focus on analyzing the CE error, which is defined as the difference between the true CSI and its estimate. At the receiver, the CE errors can be thought of as an additive noise in addition to AWGN. The noise power, i.e. the CE error variance, affects the SNR together with AWGN. In this section: i) a framework is proposed to evaluate the CE errors for time-varying channels; ii) for both CCE and TCCE, a closed-form expression is derived for the distribution of the CE error.

A. Channel Estimation Error Modelling for Time-Varying Channels

For a certain CE period, the CE error is denoted by $\epsilon_{t(n)} = \hat{h}_t - h_{t(n)}$, where $\hat{h}_t$ is the constant channel estimation for that period, and $h_{t(n)}$ is the actual CSI. For time-varying channels, a CE error consists of two parts: i) the error that occurs at the estimation point, which we refer to as the estimator error; ii) the error caused by the channel variation and this is referred to as the variation error. As the CE process is periodic, we focus on a single period and set the beginning of the estimation process to be the time origin. Then the estimator error is expressed by $\epsilon_{t(0)} = \hat{h}_t - h_{t(0)}$. It is presented in [27] that $\epsilon_{t(0)}$ is a random variable (r.v.) with a distribution of $\mathcal{CN}(0, \sigma_t^2)$, where σ_t^2 is the variance. We use $\epsilon_{h(n)} = h_{t(0)} - h_{t(n)}$ to denote the variation error, and the CE error is therefore formulated as follows:

$$\epsilon_{t(n)} = \epsilon_{t(0)} + \epsilon_{h(n)}. \tag{21}$$

The variation error can be rewritten as:

$$\epsilon_{h(n)} = \sum_{i=1}^{n} \left(h_{t(i-1)} - h_{t(i)}\right). \tag{22}$$

According to (4), we have:

$$h_{t(i)} = \sqrt{\alpha} h_{t(i-1)} + \sqrt{1-\alpha} h'_{t(i)}. \tag{23}$$

Assuming the user speed in (5) does not exceed 50 m/s, this results in an $\alpha \geq 0.989$. Therefore, we can approximate $\sqrt{\alpha} \approx 1$. Substituting (23) into (22), it gives:

$$\epsilon_{h(n)} = -\sqrt{1-\alpha} \sum_{i=1}^{n} h'_{t(i)}. \tag{24}$$

The variance of $\epsilon_{h(n)}$ is denoted by $\sigma^2_{h(n)}$, and it is calculated by:

$$\sigma^2_{h(n)} = n(1-\alpha). \tag{25}$$

Note that both $\epsilon_{h(n)}$ and $\epsilon_{t(0)}$ comply with the complex Gaussian distribution and they are independent of each other. Therefore, the CE error $\epsilon_{t(n)}$ in (21) is distributed according to $\mathcal{CN}(0, \sigma_t^2 + \sigma^2_{h(n)})$. The parameter σ_t^2 for both CCE and the proposed method is studied in the following sections.

B. Conventional Channel Estimation

Based on (10) and (12), we obtain the estimator error of an LS estimator is $\epsilon_{\text{LS}} = \frac{w}{q_t}$. The variance of ϵ_{LS} is the reciprocal of the SNR value, and we denote it by $\sigma^2_{\text{LS}} = \frac{1}{\gamma}$. It is worth noting that for the t-th transmit antenna, the gap between the pilot slot and the beginning of data transfer is $N_t - t$ slots. As a result, the parameter σ_t^2 for CCE is calculated by:

$$\sigma_t^2 = \frac{1}{\gamma} + (N_t - t)(1-\alpha). \tag{26}$$

After completing the CE process, information-carried symbols are conveyed for the next $N_t(N_d - 1)$ slots where N_d is the reciprocal of the pilot ratio. Combining (25) and (26), the variance of the CE error for CCE is obtained as follows:

$$\sigma^2_{\epsilon_t(n)} = \frac{1}{\gamma} + (N_t - t + n)(1-\alpha), \quad n = 1, 2, \ldots, N_t(N_d - 1). \tag{27}$$

C. Transmission Cross Channel Estimation

We denote the latest pilot slot in TCCE by n'. Since there is no gap between the pilot slot and the beginning of data transfer in TCCE, we have:

$$\epsilon_{t(0)} = \hat{h}_{t(n')} - h_{t(n')}. \tag{28}$$

Substituting (18) and (24) into (28) results in (29), shown at the bottom of the next page.

Proposition IV.1: Terms A, B, and C are independent of each other.

Proof: Term C consists of all noise components, and hence it is straightforward to infer that term C is independent

of the other two terms. The terms A and B contain partial information of $\mathbf{H}'_{(i)}$ for different periods, i.e. different i. As stated, $\mathbf{H}'_{(i)}$ and $\mathbf{H}'_{(j)}$ are independent $\forall\, i \neq j$. Therefore, terms A and B are also independent. ■

Consequently, the variance of $\epsilon_{t(0)}$ is the sum of the variances of terms A, B, and C. Similar to (25), the variance of A is obtained as follows:

$$\mathrm{Var}(A) = \frac{N_t - k_{t,t_{\mathrm{act}}}}{\eta}\left(\frac{k_{t,t_{\mathrm{act}}}}{N_t}\right)^2(1-\alpha), \tag{30}$$

where $\mathrm{Var}(\cdot)$ is the variance of the variate in the bracelets. Regarding term B, we denote $\delta_{(i)} = k_{t,t_{\mathrm{act}}} h'_{t_{\mathrm{act}}(i)}/N_t - h'_{t(i)}$.

Proposition IV.2: The variance of $\delta_{(i)}$ is $(\frac{k_{t,t_{\mathrm{act}}}}{N_t})^2 + 1 - \frac{2\rho_{t_{\mathrm{act}},t} k_{t,t_{\mathrm{act}}}}{N_t}$.

Proof: See Appendix A. ■

The variance of term B is then calculated by:

$$\mathrm{Var}(B) = \frac{k_{t,t_{\mathrm{act}}}}{\eta}\left(\left(\frac{k_{t,t_{\mathrm{act}}}}{N_t}\right)^2 + 1 - \frac{2\rho_{t_{\mathrm{act}},t} k_{t,t_{\mathrm{act}}}}{N_t}\right)(1-\alpha). \tag{31}$$

Term C is the sum of noise components, and its variance is given by:

$$\mathrm{Var}(C) = \left(1 + 2\left(\frac{k_{t,t_{\mathrm{act}}}}{N_t}\right)^2\right)\frac{1}{\gamma}. \tag{32}$$

Adding (30), (31) and (32), the estimator error of TCCE for the t-th transmit antenna is formulated as follows:

$$\sigma_t^2 = \left(\frac{k_{t,t_{\mathrm{act}}}}{N_t}(1 - 2\rho_{t,t_{\mathrm{act}}}) + 1\right)\frac{k_{t,t_{\mathrm{act}}}}{\eta}(1-\alpha) + \left(1 + 2\left(\frac{k_{t,t_{\mathrm{act}}}}{N_t}\right)^2\right)\frac{1}{\gamma}. \tag{33}$$

Note that TCCE-based SM conveys $(N_d - 1)$ symbols after each estimation. The variance of the CE error for TCCE is calculated by (34), shown at the bottom of the page.

V. ABEP Bound for SM With Practical Channel Estimates

Some research has been conducted on the BER performance analysis for SM in the presence of CE errors, e.g., [12]. In the SOTA literature, however, the distribution of CE errors for all transmit antennas are assumed to be identical. In fact, in both CCE and TCCE, the distribution of CE errors is related to the index of transmit antennas. Based on an existing ABEP bound for SM with perfect CSI, we derive a closed-form ABEP bound in the case of practical channel estimations, where the CE errors for different transmit antennas are considered to have different variances.

A. ABEP Bound for SM With Perfect CSI

With the assumption of perfect CSI, a closed-form ABEP bound for SM is proposed in [28]. When the signal $\mathbf{x}_{t_{\mathrm{act}},l}$ is transmitted, the conditional average pair-wise probability (APEP) of deciding on $\mathbf{x}_{t,l'}$ is given by [28, Eq. (22)] as in (35), shown at the bottom of the page. . The parameter γ_l denotes the SNR for the symbol χ_l, and:

$$\Lambda = \mathbf{R}_{\mathrm{r}} \otimes \left(\Psi\Psi^H \mathbf{R}_{\mathrm{t}}\right), \tag{36}$$

where $\Psi = (\mathbf{x}_{t_{\mathrm{act}},l} - \mathbf{x}_{t,l'})$, and $\otimes$ is the Kronecker product. The parameters $\bar{\mathbf{H}}$ and $\mathbf{L}$ are the mean and the covariance matrix of $\mathbf{H}$, respectively. In the case of Rayleigh fading, we have $\bar{\mathbf{H}} = \mathbf{0}_{N_r \times N_t}$ which is an $N_r \times N_t$ all zeros matrix, and $\mathbf{L} = \mathbf{I}_{N_r N_t}$ where $\mathbf{I}_n$ is an $n \times n$ identity matrix. The vectorization operator $\mathrm{vec}(\cdot)$ stacks the columns of the matrix in a column vector.

$$\epsilon_{t(0)} = \underbrace{\sqrt{1-\alpha}\left(\frac{k_{t,t_{\mathrm{act}}}}{N_t}\sum_{i=n'-N_t/\eta+1}^{n'-k_{t,t_{\mathrm{act}}}/\eta} h'_{t_{\mathrm{act}}(i)}\right)}_{A} + \underbrace{\sqrt{1-\alpha}\sum_{j=n'-k_{t,t_{\mathrm{act}}}/\eta+1}^{n'}\left(\frac{k_{t,t_{\mathrm{act}}}}{N_t}h'_{t_{\mathrm{act}}(j)} - h'_{t(j)}\right)}_{B} + \underbrace{\frac{w_{(n'-k_{t,t_{\mathrm{act}}})}}{q_t} + \frac{k_{t,t_{\mathrm{act}}}}{N_t}\left(\frac{w_{(n')}}{q_{t_{\mathrm{act}}}} + \frac{w_{(n'-N_t/\eta)}}{q_{t_{\mathrm{act}}}}\right)}_{C} \tag{29}$$

$$\sigma^2_{\epsilon_t(n)} = \left\{\left(\frac{k_{t,t_{\mathrm{act}}}}{N_t}(1 - 2\rho_{t,t_{\mathrm{act}}}) + 1\right)\frac{k_{t,t_{\mathrm{act}}}}{\eta} + n\right\}(1-\alpha) + \left(1 + 2\left(\frac{k_{t,t_{\mathrm{act}}}}{N_t}\right)^2\right)\frac{1}{\gamma}, \quad n = 0, 1, \ldots, N_d - 1 \tag{34}$$

$$\mathrm{APEP}(\mathbf{x}_{t_{\mathrm{act}},l} \to \mathbf{x}_{t,l'}) = \frac{1}{2\pi}\frac{\exp\left(-\frac{\gamma_l}{4}\mathrm{vec}(\bar{\mathbf{H}}^H)^H \Lambda \left(\mathbf{I} + \frac{\gamma_l}{4}\mathbf{L}\Lambda\right)^{-1}(\bar{\mathbf{H}}^H)^H\right)}{\left|\mathbf{I} + \frac{\gamma_l}{4}\mathbf{L}\Lambda\right|} \tag{35}$$

Consequently, the ABEP for SM can be approximated by using the union bound [29], and this gives:

$$\text{ABEP} \leq \frac{1}{2\eta_s} \sum_{t_{\text{act}},l} \sum_{t,l'} \frac{N(\mathbf{x}_{t_{\text{act}},l} \to \mathbf{x}_{t,l'})}{\eta_s} \text{APEP}(\mathbf{x}_{t_{\text{act}},l} \to \mathbf{x}_{t,l'}), \tag{37}$$

where $N(\mathbf{x}_{t_{\text{act}},l} \to \mathbf{x}_{t,l'})$ is the number of bits in error between $\mathbf{x}_{t_{\text{act}},l}$ and $\mathbf{x}_{t,l'}$.

B. ABEP Bound for SM With Practical Channel Estimates

There are two aspects of the effect of CE errors on decoding: i) the CE error of the currently active antenna, and ii) the CE error of the idle antenna that is incorrectly decoded. The effective SNR γ_{eff} is defined as the SNR that considers both the CE error and AWGN as the noise, and it is formulated as follows:

$$\gamma_{\text{eff}}\left(\mathbf{x}_{t_{\text{act}},l} \to \mathbf{x}_{t,l'}\right) = \frac{\gamma_l}{1 + \sigma^2_{\epsilon_t} + \gamma_l \sigma^2_{\epsilon_{t_{\text{act}}}}}, \tag{38}$$

where $\sigma^2_{\epsilon_t}$ is the average of the variances of the CE error for the t-th transmit antenna. It is worth noting that $\sigma^2_{\epsilon_{t_{\text{act}}}}$ and $\sigma^2_{\epsilon_t}$ affect the effective SNR in different ways. Since the signal is sent through t_{act}, the noise caused by its CE error is the product of the transmit power and $\sigma^2_{\epsilon_{t_{\text{act}}}}$. The ABEP bound for SM associated with a practical CE method can be obtained by replacing γ_l in (35) with γ_{eff}.

VI. Simulation Results

In this section, Monte Carlo simulation results are presented to validate the performance of the proposed CE approach. The framework for the CE errors and the proposed ABEP bound are verified. Further, the BER performance of SM using TCCE is compared with CCE. Different numbers of transmit antennas are considered. To ensure a fair comparison, the antennas are located in a matrix with a normalized diagonal distance. The correlation coefficient between the two ends of the diagonal is thought of as the reference correlation [30], which is denoted by ρ_{tx}. Based on this, the effect of channel correlations on both CCE and TCCE is also studied. Furthermore, we analyze the BER performance of SM under different user speeds. A pilot ratio of 5% is assumed in all simulations [31]. The user speed is fixed to be 5 m/s, except when studying its effect.

A. The Distribution of Channel Estimation Errors

At first, we study the CE error in terms of probability density function (PDF). The main purpose is to validate the analytical framework proposed in Section IV. The derivation in (34) shows that the CE performance of the proposed method only depends on N_t, SNR and channel correlation, regardless of N_r and η_s. Taking $N_t = 8$, $\gamma = 20$ dB and $\rho_{\text{tx}} = 0.5$ as an example, the PDFs of the CE errors for CCE and TCCE are shown in Fig. 4 and Fig. 5, respectively. As mentioned previously, the CE error is a complex variate like AWGN. Therefore, in each figure, the results for the real part and the imaginary part of errors are depicted separately. As shown, the CE errors present a zero-mean complex Gaussian distribution, and the theoretical

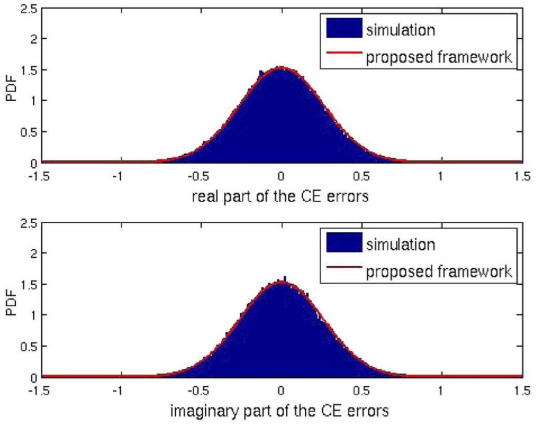

Fig. 4. PDF of the CE errors for CCE.

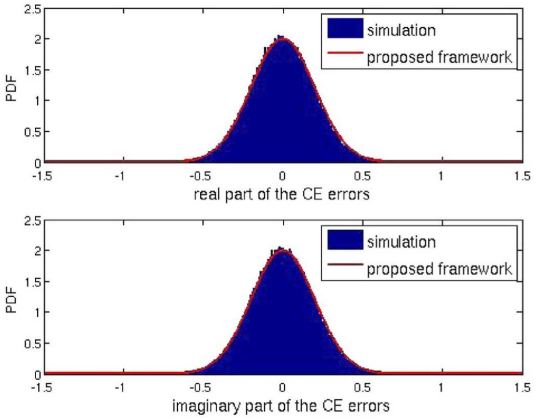

Fig. 5. PDF of the CE errors for TCCE.

PDF matches the simulation results very well. Another finding is that the CE errors of TCCE are closer to their expectation than that of CCE. In other words, the variance of CE errors in TCCE is smaller than that in CCE. This signifies that, in this case, TCCE offers a more accurate CE for SM than CCE.

B. ABEP Bound for SM Based on TCCE

Secondly, we focus on validating the proposed ABEP bound for SM with practical channel estimates in Section V. Assuming $N_t = 4$, Fig. 6 and Fig. 7 show the BER performance of SM based on TCCE for uncorrelated channels and correlated channels, respectively. Two values of η_s, 3 bits per channel per user (bpcu) and 4 bpcu, are considered. It can be observed that in both cases, the analytical bound is tightly close to the simulations. Additionally, the BER performance tends toward stability with an increase of SNR. When SNR is larger than 25 dB, the BER curve becomes almost flat and a limit is put on the achievable BER. The reason for this trend is that the CE error becomes the dominant factor instead of noise.

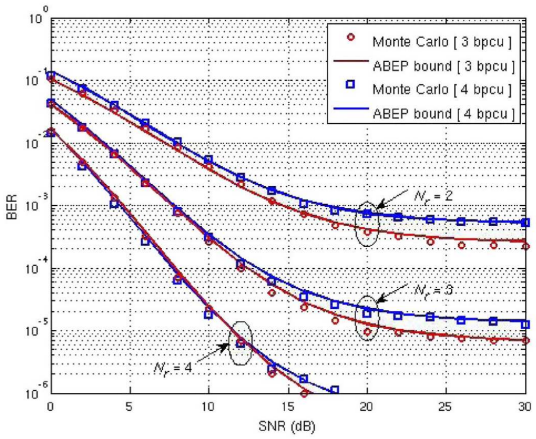

Fig. 6. BER of SM using TCCE over uncorrelated Rayleigh fading channels. (Line) Analytical bound, (Dot) Simulation.

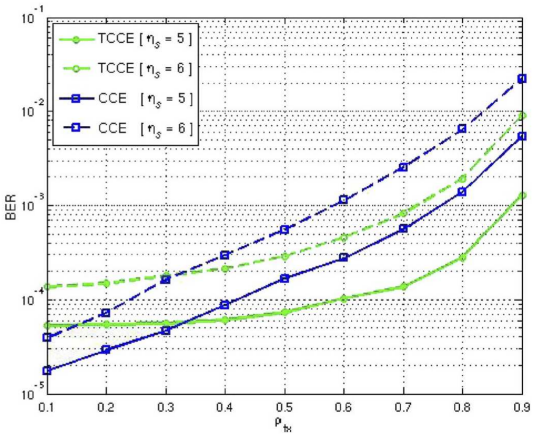

Fig. 8. BER performance of SM in terms of ρ_{tx}. The SNR is assumed to be 20 dB.

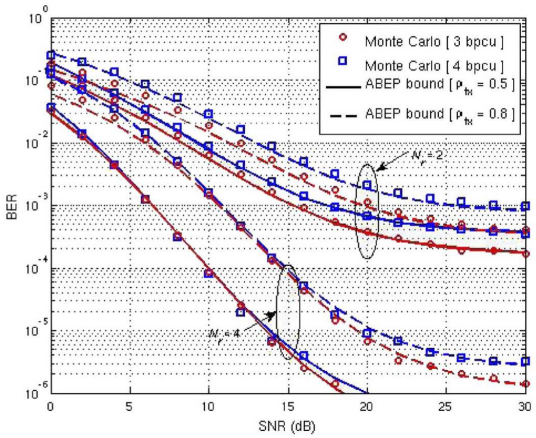

Fig. 7. BER of SM using TCCE over correlated Rayleigh fading channels. (Line) Analytical bound, (Dot) Simulation.

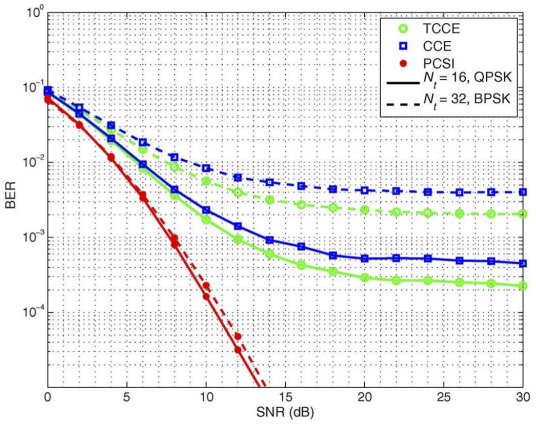

Fig. 9. BER performance of SM in terms of SNR. A medium channel correlation of $\rho_{\text{tx}} = 0.5$ is considered.

C. BER Comparison With CCE

Thirdly, the BER performance of TCCE is compared with CCE in three aspects: the channel correlation, the number of transmit antennas, and the user speed. In order to focus on studying the effect of the above factors, the number of receive antennas is assumed to be four in all comparisons.

1) Effect of Channel Correlation: Fig. 8 shows the BER performance of TCCE and CCE as a function of the channel correlation. Sixteen transmit antennas and an SNR of 20 dB are assumed. As shown in Fig. 8, the proposed approach falls behind CCE when the correlation coefficient ρ_{tx} is smaller than 0.3. The reason is that the performance of TCCE relies on the channel correlation. For a low channel correlation, it is difficult to track the channel difference information between transmit antennas. However, when the parameter ρ_{tx} is larger than 0.4, TCCE offers a much better BER performance than CCE. Similar, but less pronounced trends are noticed at lower SNRs. Based on the above analysis, an adaptive CE technique is available for SM by switching between CCE and TCCE.

2) Effect of the Number of Transmit Antennas: Assuming different numbers of transmit antennas, the BER performance of SM for $\rho_{\text{tx}} = 0.5$ and $\rho_{\text{tx}} = 0.8$ is shown in Fig. 9 and Fig. 10, respectively. The parameter η_s is fixed to be six to ensure a fair comparison. Additionally, the case of perfect CSI (PCSI) is considered as a benchmark.

The following outcomes are observed: i) compared with CCE, the BER performance of TCCE is much closer to that of PCSI; ii) when N_t increases, the BER performance for both CE methods degrades more rapidly than PCSI. However, the reasons for CCE and TCCE are different. The CE period of CCE is proportional to N_t, and therefore, the CE results become less accurate when more transmit antennas are used. Unlike in CCE, the CE period of TCCE is irrelevant to N_t. However, with an increase of N_t, the interval between two adjacent pilot slots for a certain transmit antenna is increased.

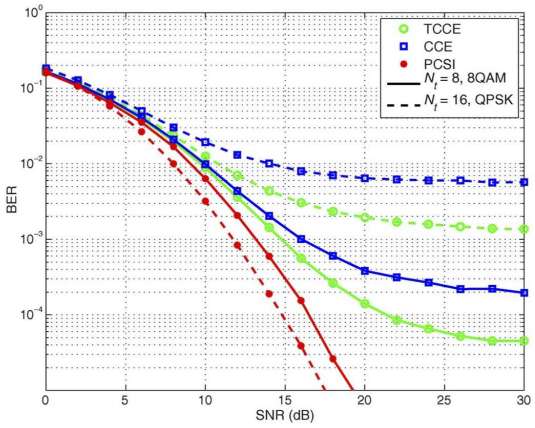

Fig. 10. BER performance of SM in terms of SNR. A high channel correlation of $\rho_{\text{tx}} = 0.8$ is considered.

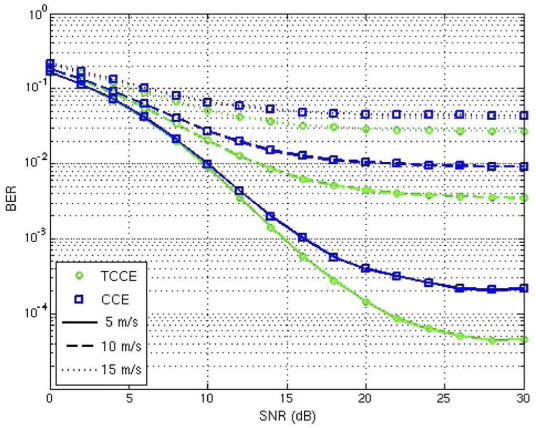

Fig. 11. BER performance of SM in terms of SNR for various user speeds. The parameter ρ_{tx} is assumed to be 0.8.

This results in a less accurate channel difference information, which causes a performance degradation in the correlation-based CE. Furthermore, in a comparison to CCE, the energy gain achieved by TCCE becomes greater as N_t increases. Given $\rho_{\text{tx}} = 0.8$ and $N_t = 8$, for example, an SNR gain of 2.8 dB is obtained by TCCE to achieve the same BER value of CCE at $\gamma = 20$ dB. While $N_t = 16$, this gain is increased to 7.5 dB.

3) Effect of User Speed: The user speed directly affects the coherence time in time-varying channels, and therefore, it is essential to study its effect on the CE performance. Assuming $\rho_{\text{tx}} = 0.8$ and $N_t = 8$, Fig. 11 shows the BER performance of SM for different user speeds. The following outcomes are observed: i) for both CCE and TCCE, the BER performance degrades as the user speed increases; ii) with an increase of the user speed, the difference between the performance of TCCE and CCE diminishes. The reason for this trend is that when the channel varies very rapidly, all CE techniques would fail to perform properly for a fixed pilot ratio. Nevertheless, TCCE still outperforms CCE in a significant way for a high user speed. In the case of 15 m/s, for example, CCE reaches its achievable BER of 5% at $\gamma = 15$ dB. Meanwhile, TCCE requires only 10 dB to achieve the same BER value, which provides an SNR gain of 5 dB when compared with CCE.

VII. Conclusion

In this paper, we propose a novel CE method that aims to improve the performance for SM over correlated fading channels. The basic concept of this new approach is to track the channel difference information between transmit antennas, and estimate the entire channel by sending the pilot signal through only one antenna. Therefore, the CE period of the proposed method depends on the pilot ratio only, regardless of the number of transmit antennas used. Further, we propose an analytical framework for the distribution of CE errors in time-varying channels, and the corresponding ABEP bound for SM based on the a practical CE method. Simulation results show that for medium and high channel correlations, TCCE achieves an SNR gain of up to 7.5 dB in comparison with CCE. When the channel correlation is very low, TCCE performs worse than CCE because the channel difference information is difficult to track in this situation. By switching between CCE and TCCE, an adaptive CE technique is available for SM that is a promising MIMO scheme for future communication systems.

Appendix A

For two complex variates X and Y, the variance of their sum is given by:

$$\text{Var}(X+Y) = \text{Var}(X) + \text{Var}(Y) + 2\text{Cov}(XY), \quad (39)$$

where $\text{Cov}(X,Y) = \mathbf{E}[(X-\mu_X)(Y-\mu_Y)^*]$ is the covariance of X and Y; $\mathbf{E}[\cdot]$ is the mathematical expectation; μ_X and μ_Y are the means of X and Y, respectively; $(\cdot)^*$ is the conjugate operator. Therefore, the variance of $\delta_{(i)}$ is formulated as follows:

$$\text{Var}(\delta_{(i)}) = \left(\frac{k_{t,t_{\text{act}}}}{N_t}\right)^2 \text{Var}\left(h'_{t_{\text{act}}(i)}\right) + \text{Var}\left(-h'_{t(i)}\right) + 2\text{Cov}\left(\frac{k_{t,t_{\text{act}}}}{N_t} h'_{t_{\text{act}}(i)}, \left(-h'_{t(i)}\right)\right). \quad (40)$$

Since $h'_{t_{\text{act}}(i)}$ and $h'_{t(i)}$ are both zero-mean complex Gaussian random variables with variance of one, so we have $\text{Var}(h'_{t_{\text{act}}(i)}) = 1$ and $\text{Var}(-h'_{t(i)}) = 1$. Using the definition of covariance, the covariance part in (40) is computed by:

$$\text{Cov}\left(\frac{k_{t,t_{\text{act}}}}{N_t} h'_{t_{\text{act}}(i)}, \left(-h'_{t(i)}\right)\right) = -\frac{k_{t,t_{\text{act}}}}{N_t} \mathbf{E}\left[h'_{t_{\text{act}}(i)} \left(h'_{t(i)}\right)^*\right]. \quad (41)$$

Note that, because the means of $h'_{t_{\text{act}}(i)}$ and $h'_{t(i)}$ are zeros, $\mathbf{E}[h'_{t_{\text{act}}(i)}(h'_{t(i)})^*]$ is exactly the covariance of $h'_{t_{\text{act}}(i)}$ and $h'_{t(i)}$. According to the definition of correlation, we have:

$$\rho_{t,t_{\text{act}}} = \frac{\text{Cov}\left(h'_{t_{\text{act}}(i)}, h'_{t(i)}\right)}{\sqrt{\text{Var}\left(h'_{t_{\text{act}}(i)}\right) \text{Var}\left(h'_{t(i)}\right)}}. \quad (42)$$

Therefore, the covariance part in (40) is obtained by:

$$\mathrm{Cov}\left(\frac{k_{t,t_{\mathrm{act}}}}{N_t}h'_{t_{\mathrm{act}}(i)},\left(-h'_{t(i)}\right)\right)=-\frac{k_{t,t_{\mathrm{act}}}}{N_t}\rho_{t,t_{\mathrm{act}}}. \quad (43)$$

The variance of $\delta_{(i)}$ is then computed by:

$$\mathrm{Var}\left(\delta_{(i)}\right)=\left(\frac{k_{t,t_{\mathrm{act}}}}{N_t}\right)^2+1-\frac{2\rho_{t,t_{\mathrm{act}}}k_{t,t_{\mathrm{act}}}}{N_t}. \quad (44)$$

REFERENCES

[1] X. Wu, M. Di Renzo, and H. Haas, "Channel estimation for spatial modulation," in *Proc. 24th IEEE Int. Symp. PIMRC*, Sep. 2013, pp. 306–310.

[2] R. Mesleh, H. Haas, S. Sinanovic, C. W. Ahn, and S. Yun, "Spatial modulation," *IEEE Trans. Veh. Technol.*, vol. 57, no. 4, pp. 2228–2241, Jul. 2008.

[3] R. Mesleh, H. Haas, C. W. Ahn, and S. Yun, "Spatial modulation—A new low complexity spectral efficiency enhancing technique," in *Proc. 1st Int. Conf. ChinaCom*, Oct. 2006, pp. 1–5.

[4] M. Di Renzo, H. Haas, and P. M. Grant, "Spatial modulation for multiple-antenna wireless systems: A survey," *IEEE Commun. Mag.*, vol. 49, no. 12, pp. 182–191, Dec. 2011.

[5] J. Jeganathan, A. Ghrayeb, and L. Szczecinski, "Spatial modulation: Optimal detection and performance analysis," *IEEE Commun. Lett.*, vol. 12, no. 8, pp. 545–547, Aug. 2008.

[6] M. Di Renzo and H. Haas, "Performance analysis of spatial modulation," in *Proc. 5th Int. Conf. CHINACOM*, Aug. 2010, pp. 1–7.

[7] M. D. Renzo and H. Haas, "Bit error probability of SM-MIMO over generalized fading channels," *IEEE Trans. Veh. Technol.*, vol. 61, no. 3, pp. 1124–1144, Mar. 2012.

[8] M. Biguesh and A. B. Gershman, "Training-based MIMO channel estimation: A study of estimator tradeoffs and optimal training signals," *IEEE Trans. Signal Process.*, vol. 54, no. 3, pp. 884–893, Mar. 2006.

[9] P. Wolniansky, G. Foschini, G. Golden, and R. Valenzuela, "V-BLAST: An architecture for realizing very high data rates over the rich-scattering wireless channel," in *Proc. ISSSE*, Sep. 1998, pp. 295–300.

[10] V. Tarokh, H. Jafarkhani, and A. Calderbank, "Space-time block codes from orthogonal designs," *IEEE Trans. Inf. Theory*, vol. 45, no. 5, pp. 1456–1467, Jul. 1999.

[11] M. Koca and H. Sari, "Performance of spatial modulation over correlated fading channels with channel estimation errors," in *Proc. IEEE WCNC*, Apr. 2013, pp. 3937–3942.

[12] E. Basar, U. Aygolu, E. Panayirci, and H. Poor, "Performance of spatial modulation in the presence of channel estimation errors," *IEEE Commun. Lett.*, vol. 16, no. 2, pp. 176–179, Feb. 2012.

[13] M. Di Renzo, D. De Leonardis, F. Graziosi, and H. Haas, "Space shift keying (SSK-) MIMO with practical channel estimates," *IEEE Trans. Commun.*, vol. 60, no. 4, pp. 998–1012, Apr. 2012.

[14] M. Faiz, S. Al-Ghadhban, and A. Zerguine, "Recursive least-squares adaptive channel estimation for spatial modulation systems," in *Proc. 9th IEEE MICC*, Dec. 2009, pp. 785–788.

[15] S. Sugiura and L. Hanzo, "Effects of channel estimation on spatial modulation," *IEEE Signal Process. Lett.*, vol. 19, no. 12, pp. 805–808, Dec. 2012.

[16] J. H. Kotecha and A. Sayeed, "Transmit signal design for optimal estimation of correlated MIMO channels," *IEEE Trans. Signal Process.*, vol. 52, no. 2, pp. 546–557, Feb. 2004.

[17] N. Shariati, J. Wang, and M. Bengtsson, "Robust training sequence design for correlated MIMO channel estimation," *IEEE Trans. Signal Process.*, vol. 62, no. 1, pp. 107–120, Jan. 2014.

[18] C.-T. Chiang and C. Fung, "Robust training sequence design for spatially correlated MIMO channel estimation," *IEEE Trans. Veh. Technol.*, vol. 60, no. 7, pp. 2882–2894, Sep. 2011.

[19] Y. H. Kho and D. Taylor, "MIMO channel estimation and tracking based on polynomial prediction with application to equalization," *IEEE Trans. Veh. Technol.*, vol. 57, no. 3, pp. 1585–1595, May 2008.

[20] Y.-C. Chen and Y.-T. Su, "MIMO channel estimation in correlated fading environments," *IEEE Trans. Wireless Commun.*, vol. 9, no. 3, pp. 1108–1119, Mar. 2010.

[21] D. Angelosante, E. Biglieri, and M. Lops, "Sequential estimation of multipath MIMO-OFDM channels," *IEEE Trans. Signal Process.*, vol. 57, no. 8, pp. 3167–3181, Aug. 2009.

[22] C. Oestges, "Validity of the Kronecker model for MIMO correlated channels," in *Proc. 63rd IEEE VTC Spring*, May 2006, vol. 6, pp. 2818–2822.

[23] S. Loyka, "Channel capacity of MIMO architecture using the exponential correlation matrix," *IEEE Commun. Lett.*, vol. 5, no. 9, pp. 369–371, Sep. 2001.

[24] C. Peel and A. Swindlehurst, "Performance of space-time modulation for a generalized time-varying Rician channel model," *IEEE Trans. Wireless Commun.*, vol. 3, no. 3, pp. 1003–1012, May 2004.

[25] S. M. Kay, *Fundamentals of Statistical Signal Processing: Estimation Theory*, 1st ed. Englewood Cliffs, NJ, USA: Prentice-Hall, 1993.

[26] M. Hazewinkel, *Linear Interpolation*, 1st ed. New York, NY, USA: Springer-Verlag, 2001.

[27] J. Wu and C. Xiao, "Optimal diversity combining based on linear estimation of Rician fading channels," *IEEE Trans. Commun.*, vol. 56, no. 10, pp. 1612–1615, Oct. 2008.

[28] A. Younis, D. A. Basnayaka, and H. Haas, "Performance analysis for generalised spatial modulation," in *20th European Wireless Conference*, May 2014, pp. 1–6.

[29] P. J. G. , *Digital Communications*, 4th ed. New York, NY, USA: McGraw-Hill, 2000.

[30] H. Kim *et al.*, "Efficient transmit antenna selection for correlated MIMO channels," in *Proc. IEEE WCNC*, Apr. 2009, pp. 1–5.

[31] J. Berkmann, C. Carbonelli, F. Dietrich, C. Drewes, and W. Xu, "On 3G LTE terminal implementation-standard, algorithms, complexities and challenges," in *Proc. IWCMC*, Aug. 2008, pp. 970–975.

Xiping Wu received the B.Sc. degree from Southeast University, Nanjing, China, in 2008 and the M.Sc. degree with distinction from the University of Edinburgh, Scotland, U.K., in 2011. He is a Ph.D. candidate at the University of Edinburgh, funded by the European Union's Seventh Framework Programme (FP7) project GREENET. From September 2011 to August 2014, he was a Marie-Curie Early-Stage Researcher (ESR). From December 2013 to April 2014, he was on secondment to the Department of Electrical and Information Engineering, University of L'Aquila, L'Aquila, Italy. Since September 2014, he has been a Research Associate with the Institute for Digital Communications (IDCOM), University of Edinburgh, funded by British Engineering and Physical Sciences Research Council (EPSRC). His main research interests are in the areas of wireless communication theory, visible light communications, and wireless network management. Dr. Wu was the recipient of the Scotland Saltire Scholarship by the Scottish Government in 2010.

Holger Claussen received the Ph.D. degree in signal processing for digital communications from the University of Edinburgh, Scotland, U.K., in 2004.

In 2004, he joined Bell Labs and began his research in the areas of auto-configuration and dynamic optimization of networks, flat cellular network architectures, user mobility, resource management, end-to-end network modeling, and improving the energy efficiency of networks. He was the Head of the Autonomous Networks and Systems Research Department at Bell Labs Ireland, where he directed research in the area of self-managing networks to enable the first large scale femtocell deployments from 2009 onward. During this time, he also built a cloud computing research team, focusing on predicable performance and reducing latency to enable running telecommunication applications on a cloud infrastructure. He is currently the Leader of Small Cells Research at Bell Labs, Alcatel-Lucent. In this role, he and his team are innovating in all areas related to future evolution, deployment, and operation of small cell networks to address the exponential growth in mobile data traffic. His research in this domain has been commercialized in Alcatel-Lucent's Small Cell product portfolio and continues to have significant impact. He is the author of more than 70 publications and 100 filed patent applications. Dr. Claussen is a member of the IET.

Marco Di Renzo (S'05–AM'07–M'09–SM'14) received the Laurea *(cum laude)* and Ph.D. degrees in electrical and information engineering from the Department of Electrical and Information Engineering, University of L'Aquila, L'Aquila, Italy, in April 2003 and January 2007. He received the Habilitation à Diriger des Recherches (HDR) from the University of Paris-Sud XI, Paris, France, in October 2013. Since January 2010, he has been a Tenured Academic Researcher ("Chargé de Recherche Titulaire") with the French National Center for Scientific Research (CNRS), as well as a Faculty Member of the Laboratory of Signals and Systems (L2S), which is a joint research laboratory of the CNRS; the École Supérieure d'Électricité (SUPÉLEC); and the University of Paris-Sud XI, Paris, France. His main research interests are in the area of wireless communications theory.

Dr. Di Renzo is a recipient of several awards, which include a special mention for the outstanding five-year (1997–2003) academic career, University of L'Aquila, Italy; the THALES Communications fellowship (2003–2006), University of L'Aquila, Italy; the 2004 Best Spin-Off Company Award, Abruzzo Region, Italy; the 2006 DEWS Travel Grant Award, University of L'Aquila, Italy; the 2008 Torres Quevedo Award, Ministry of Science and Innovation, Spain; the "Dérogation pour l'Encadrement de Thèse" (2010), University of Paris-Sud XI, France; the 2012 IEEE CAMAD Best Paper Award; the 2012 IEEE WIRELESS COMMUNICATIONS LETTERS Exemplary Reviewer Award; the 2013 IEEE VTC-Fall Best Student Paper Award; the 2013 Network of Excellence NEWCOM# Best Paper Award; the 2013 IEEE TRANSACTIONS ON VEHICULAR TECHNOLOGY Top Reviewer Award; the 2013 IEEE-COMSOC Best Young Researcher Award for Europe, Middle East and Africa (EMEA Region); and the 2014 IEEE ICNC Single Best Paper Award Nomination (Wireless Communications Symposium). Currently, he serves as an Editor of the IEEE COMMUNICATIONS LETTERS and of the IEEE TRANASACTIONS ON COMMUNICATIONS (Heterogeneous Networks Modeling and Analysis).

Harald Haas received the Ph.D. degree from the University of Edinburgh, Scotland, United Kingdom, in 2001. He was an Invited Speaker at the TED Global 2011, and his talk has been watched online more than 1.5 million times. He is the Cofounder and Chief Scientific Officer (CSO) of pureLiFi Ltd. He holds 31 patents and has more than 30 pending patent applications. He has published 300 conference and journal papers, including a paper in Science. He currently holds the Chair of Mobile Communications with the University of Edinburgh. His main research interests are in optical wireless communications, hybrid optical wireless and RF communications, spatial modulation, and interference coordination in wireless networks. He first introduced and coined "spatial modulation" and "Li-Fi." Li-Fi was listed among the 50 best inventions in TIME Magazine 2011.

Prof. Haas was the only recipient of the prestigious Established Career Fellowship from the EPSRC (Engineering and Physical Sciences Research Council) within Information and Communications Technology in the U.K. in 2012. He was the corecipient of a Best Paper Award at the IEEE Vehicular Technology Conference in Las Vegas in 2013. He is the recipient of the Tam Dalyell Prize 2013 awarded by the University of Edinburgh for excellence in engaging the public with science. In 2014, he was selected by EPSRC as one of ten RISE (Recognising Inspirational Scientists and Engineers) Leaders.

Globecom 2012 - Wireless Communications Symposium

Structure Optimisation of Spatial Modulation over Correlated Fading Channels

Xiping Wu*, Sinan Sinanović*, and Marco Di Renzo† and Harald Haas*

*Institute for Digital Communications
Joint Research Institute for Signal and Image Processing
School of Engineering
The University of Edinburgh
EH9 3JL, Edinburgh, UK
{xiping.wu, s.sinanovic, h.haas}@ed.ac.uk

†French National Centre for Scientific Research (CNRS)
Laboratory for Signals and Systems (LSS)
École Supérieure d'Électricité (SUPELEC)
3 rue Joliot-Curie, 91192 Gif-sur-Yvette (Paris), France
marco.direnzo@lss.supelec.fr

***Abstract*—A unique characteristic of spatial modulation (SM) is the three dimensional constellation diagram. This enables to trade-off traditional signal constellation diagrams with spatial constellation diagrams where the latter is defined by the physical antenna array. In this paper we investigate the optimum pairs of signal and spatial constellation sizes with respect to average bit error probability (ABEP) and energy efficiency. The analysis is performed for varying antenna correlations and channel conditions. Both numerical and closed-form results are presented which show that a significant performance gain can be obtained when the optimal constellation pairs are used.**

I. Introduction

Spatial modulation (SM) is a recently proposed modulation concept for Multiple-Input-Multiple-Output (MIMO) wireless systems [1], which combines traditional signal modulation and space shift keying (SSK). Unlike conventional spatial multiplexing schemes, it achieves the diversity gain by exploiting the location-specific property. Recently, it has been shown that SM can outperform many state-of-the-art MIMO schemes while achieving a low-complexity implementation [1], [2], [3].

In order to improve the performance of SM, an optimal power allocation across the transmitters is considered to minimise the bit error probability [4], [5]. On one hand, these results are based on specific values of two key SM parameters: signal modulation order and the number of transmit antennas. On the other hand, the SM performance depends on the channel correlation which plays a significant role in MIMO technology. As a result, optimising two key SM spatial modulation parameters should result in a better SM performance. The average bit error probability (ABEP) of SM over correlated fading channels has been extensively studied recently [3], [6]. In [6], an ABEP union bound of SSK is proposed which indicates the performance of SSK worsens as the correlation degree increases. It is well known that the conventional signal modulation (*i.e.,* phase shift keying (PSK) or quadrature amplitude modulation (QAM)) bit error performance deteriorates as the constellation size increases. Since the bit stream is split in SM and transmitted either via signal modulation or antenna number, there exists a trade-off between the sizes of signal and spatial constellation over correlated fading channels. An optimal deployment can be obtained through minimising the closed-form ABEP proposed in [3]. Of course, the price to be paid for this adaptive deployment is the need of *a priori* correlation degree information between each pair of channels, which can be realised by the correlation estimator in [7]. To keep a moderate level of analytical complexity, we restrict the number of receive antennas to one and use PSK modulation. All the derivations are done under the high SNR assumption in order to obtain a closed-form solution. With the above assumptions, the contributions of this paper are as follows: i) the ABEP optimisation problem across deployments is solved in closed-form; ii) analysis of the properties of optimal solution in different fading environments; iii) the energy saving of optimal deployment with respect to other structures is analysed. Finally, numerical results are given to support the solution in some example scenarios.

II. System Model

A $N_{\mathrm{t}} \times 1$ SM system is considered in this paper, where N_{t} is the number of transmitting antennas and there is only one receiving antenna. The total symbol alphabet size and signal constellation size are defined as R and M, respectively. SM processing splits the $\log_2(R)$ bits into two parts with $\log_2(M)$ and $\log_2(N_t)$ bits, which implies that $R = M \times N_t$. The first part of the bits is modulated by a signal constellation scheme, *i.e.,* PSK or QAM, and emitted through one of the N_t transmitters determined by the bits in the second part. In this paper, identical distributed fading channels and PSK are selected to give an analytical solution.

A. Notation

The notation adopted in this paper is as follows: i) If a channel is Nakagami-m fading, define $h \sim$Nakagami(m, Ω). When $m = 1$, it is Rayleigh fading; ii) E_m is the average energy per transmission; iii) N_0 presents the power spectral density of the additive white Gaussian noise (AWGN) at the receiver; iv) $\gamma = E_m/N_0$; v) $0 \leq \rho_{t_1,t_2} \leq 1$ is the correlation degree between two propagation fading paths from transmitters t_1 and t_2 to the receiver. An identical correlation degree is considered and denoted as ρ; vi) $N_H(\cdot)$ denotes the Hamming distance.

978-1-4673-0921-9/12/$31.00 ©2012 IEEE

B. Channel Model

A flat slow fading channel model is considered. The impulse response of the t-th transmitter to the receiver is $h_t(\zeta) = \alpha_t \delta(\zeta - \tau_t)$, where $\alpha_t = \beta \exp(j\varphi_t)$ is the complex channel gain and τ_t is the time delay which can be ignored under the assumption of perfect time-synchronisation.

C. Average Bit Error Probability of SM

The ABEP of SM can be computed by an improved upper bound as follows [3, Eq. (6)]:

$$\text{ABEP} \leq \text{ABEP}_{\text{signal}} + \text{ABEP}_{\text{spatial}} + \text{ABEP}_{\text{joint}} \tag{1}$$

where:

$$\text{ABEP}_{\text{signal}} = \tfrac{\log_2(M)}{\log_2(R)} \tfrac{1}{N_t} \sum_{t=1}^{N_t} \text{ABEP}_{\text{MOD}}(t) \tag{2}$$

$$\text{ABEP}_{\text{spatial}} = \tfrac{\log_2(N_t)}{\log_2(R)} \tfrac{1}{M} \sum_{l=1}^{M} \text{ABEP}_{\text{SSK}}(l) \tag{3}$$

$$\text{ABEP}_{\text{joint}} = \tfrac{1}{\log_2(R)} \tfrac{1}{MN_t} \sum_{t=1}^{N_t} \sum_{l=1}^{M} \sum_{\tilde{t} \neq t=1}^{N_t} \sum_{\tilde{l} \neq l=1}^{M} \text{ABEP}_{\text{MIX}} \tag{4}$$

with the terms in summations defined as follows

$$\text{ABEP}_{\text{MOD}}(t) = \tfrac{1}{\log_2(M)} \tfrac{1}{M} \sum_{l=1}^{M} P_{s,l}(e) \tag{5}$$

where $P_{s,l}(e)$ is the average symbol error of the l-th symbol,

$$\text{ABEP}_{\text{SSK}}(l) = \tfrac{1}{\log_2(N_t)} \tfrac{1}{N_t} \sum_{t=1}^{N_t} \sum_{\tilde{t}=1}^{N_t} N_H(\tilde{t} \to t) \text{APEP}(\tilde{t} \to t) \tag{6}$$

$$\text{ABEP}_{\text{MIX}} = N_H((\tilde{t}, \chi_{\tilde{l}}) \to (t, \chi_l)) \text{APEP}((\tilde{t}, \chi_{\tilde{l}}) \to (t, \chi_l)) \tag{7}$$

where APEP denotes average pair-wise error probability and χ represents signal symbol. Average pair-wise error probability (APEP) is the average error probability of pair-wise error events. The APEP can be calculated as [3, Eq. (5)]:

$$\text{APEP}((\tilde{t}, \chi_{\tilde{l}}) \to (t, \chi_l)) = E_\alpha\{Q(\sqrt{\gamma |\alpha_{\tilde{t}} \chi_{\tilde{l}} - \alpha_t \chi_l|^2 / 4})\} \tag{8}$$

III. Optimisation of SM ABEP

A. Objective function over Nakagami-m Fading

1) ABEP of SSK Part: Firstly, we focus on $\text{ABEP}_{\text{spatial}}$ in the union bound. Under the assumption of high SNR, a closed-form APEP of SSK over correlated Nakagami-m fading channels is proposed in [8, Eq. (15)]. The APEP formula can be rewritten as:

$$\text{APEP}(\tilde{t} \to t) = \frac{\Gamma(1.5)}{\sqrt{\pi}\Gamma(2)} \frac{4}{\gamma} \sum_{k=0}^{+\infty} \frac{c_{\tilde{t},t}^{m+2k-1} b_{\tilde{t},t}}{2^{m-1} 4^k (k!) \Gamma(k+m)} \tag{9}$$

where

$$c_{\tilde{t},t} = \frac{(m_{\tilde{t}} + m_t)\sqrt{\rho_{\tilde{t},t}}}{\sqrt{\Omega_{\tilde{t}} \Omega_t}(1 - \rho_{\tilde{t},t})} \tag{10}$$

$$b_{\tilde{t},t} = \frac{m_t^{m_t+1} \Gamma(m_t + m_{\tilde{t}} + 2k - 1)}{\Omega_t \Omega_{\tilde{t}} (1 - \rho_{t,\tilde{t}}) (\sqrt{\Omega_t \Omega_{\tilde{t}} \rho_{t,\tilde{t}}})^{m_t - 1} \Gamma(m_t)} \left(\frac{m_t}{\Omega_t (1 - \rho_{t,\tilde{t}})} + \frac{m_{\tilde{t}}}{\Omega_{\tilde{t}} (1 - \rho_{t,\tilde{t}})} \right)^{1 - m_t - m_{\tilde{t}} - 2k} \tag{11}$$

In the case of identically distributed fading channels and identical correlation coefficients, *i.e.*, $m_{t_1} = m_{t_2} = m$, $\Omega_{t_1} = \Omega_{t_2} = \Omega$ and $\rho_{t_1,t_2} = \rho$, based on (10) and (11), we can obtain c and b as:

$$\begin{cases} c = \frac{2m}{\Omega} \frac{\sqrt{\rho}}{1 - \rho} \\ b = \frac{m^{m+1} \Gamma(2m + 2k - 1)}{\Omega^{2-m-2k} (1-\rho) \rho^{\frac{m-1}{2}} \Gamma(m)} \left(\frac{2m}{1-\rho} \right)^{1 - 2m - 2k} \end{cases} \tag{12}$$

Substituting (12) into (9) provides:

$$\text{APEP}(\tilde{t} \to t) = \frac{1}{\gamma} \left(\frac{1 - \rho}{4} \right)^{m-1} \frac{m}{\Omega \Gamma(m)} \sum_{k=0}^{+\infty} \left(\frac{\rho}{4} \right)^k \frac{\Gamma(2m + 2k - 1)}{(k!) \Gamma(k + m)} \tag{13}$$

We set $C = \frac{1}{2} \left(\frac{1-\rho}{4} \right)^{m-1} \frac{m}{\Omega \Gamma(m)} \sum_{k=0}^{+\infty} \left(\frac{\rho}{4} \right)^k \frac{\Gamma(2m+2k-1)}{(k!)\Gamma(k+m)}$ which is a constant for a certain scenario (specific m, Ω, ρ). By considering encoding the $\log_2(N_t)$ bits provided to spatial constellation by Gray codes, there are $\log_2(N_t)/2$ errors. The total Hamming distance of any one symbol to all the other symbols can be computed as follows:

$$\sum_{\tilde{t}=1}^{N_t} N_H(\tilde{t} \to t) = \frac{N_t}{2} \log_2(N_t) \tag{14}$$

Substituting (13) and (14) into (3) gives:

$$\text{ABEP}_{\text{spatial}} = \frac{C}{\gamma \log_2(R)} N_t \log_2(N_t) \tag{15}$$

2) ABEP of Signal Modulation Part: The average symbol error of PSK over Nakagami-m fading channel for a single receiver can be computed as follows [9, p. 271, Eq. (9.16)]:

$$P_s(e) = \frac{1}{\pi} \int_0^{\frac{M-1}{M}\pi} \left(1 + \frac{\gamma \sin^2(\frac{\pi}{M})}{m \sin^2 \theta} \right)^{-m} d\theta. \tag{16}$$

Considering the assumption of high SNR, which means $\frac{\gamma \sin^2(\frac{\pi}{M})}{m \sin^2 \theta} \gg 1$, (16) can be approximated as

$$P_s(e) = \frac{1}{\pi} \left(\frac{m}{\gamma \sin^2(\frac{\pi}{M})} \right)^m \int_0^{\frac{M-1}{M}\pi} \sin^{2m}(\theta) d\theta. \tag{17}$$

For enough large M, $\int_0^{\frac{M-1}{M}\pi} \sin^{2m}(\theta) d\theta = \int_0^{\pi} \sin^{2m}(\theta) d\theta$ which is independent of M and $\sin(\frac{\pi}{M}) \approx \frac{\pi}{M}$. A simplified closed-form $\text{ABEP}_{\text{signal}}$ can be obtained by substituting (17) into (2):

$$\text{ABEP}_{\text{signal}} = \frac{1}{\log_2(R)\pi} \left(\frac{m}{\gamma \pi^2} \right)^m M^{2m} \int_0^{\pi} \sin^{2m}(\theta) d\theta \tag{18}$$

We denote $B = \frac{m^m}{\pi^{2m+1}} \int_0^{\pi} \sin^{2m}(\theta) d\theta$, which is a constant for a specific fading scenario. Thus, the above equation can be rewritten as:

$$\text{ABEP}_{\text{signal}} = \frac{B}{\gamma^m \log_2(R)} M^{2m} \quad (19)$$

3) ABEP of Joint Part: Since PSK modulation is used, the symbol of signal constellation is $\chi_l = k_l \exp(j\varphi_l)$, where $k_1 = k_2 = \ldots = k = 1$. We can then rewrite (8) as follows:

$$\text{APEP}((\tilde{t}, \chi_{\tilde{l}}) \to (t, \chi_l)) = E_\alpha\{Q(\sqrt{\gamma|\beta_{\tilde{t}} \exp(j(\varphi_{\tilde{t}} + \varphi_{\tilde{l}})) - \beta_t \exp(j(\varphi_t + \varphi_l))|^2/4})\} \quad (20)$$

φ_t is a random variable (RV) with uniform distribution over $[0, 2\pi]$, while φ_l is a constant. The new RV, $\varphi_t + \varphi_l$, also has a uniform distribution over $[0, 2\pi]$, and, as a result, $\text{APEP}((\tilde{t}, \chi_{\tilde{l}}) \to (t, \chi_l)) = \text{APEP}(\tilde{t} \to t) = 2C/\gamma$. Denoting $D = \frac{1}{R} \sum_{t=1}^{N_t} \sum_{l=1}^{M} \sum_{\tilde{t} \neq t=1}^{N_t} \sum_{\tilde{l} \neq l=1}^{M} N_H((\tilde{t}, \chi_{\tilde{l}}) \to (t, \chi_l))$, $\text{ABEP}_{\text{joint}}$ can be formulated from (4) and (7) by:

$$\text{ABEP}_{\text{joint}} = \frac{D}{\log_2(R)} \frac{2C}{\gamma} \quad (21)$$

where D can be calculated similar to (14) as:

$$D = \frac{N_t(M-1)}{2} \log_2(N_t) + \frac{(N_t - 1)M}{2} \log_2(M) \quad (22)$$

Substituting (22) into (21):

$$\text{ABEP}_{\text{joint}} = \frac{C}{\gamma \log_2(R)} \{R \log_2(R) - M \log_2(M) - N_t \log_2(N_t)\} \quad (23)$$

Combining (15), (19) and (23), the objective function to be minimised can be obtained as:

$$\text{Obj}(M) = \frac{C}{\gamma \log_2(R)} \{R \log_2(R) - M \log_2(M)\} + \frac{B}{\gamma^m \log_2(R)} M^{2m}, M \in [1, R] \quad (24)$$

B. Minimisation of Objective Function

In order to reduce the variable to a moderate scale, we choose $x = \log_2(M)$ rather than the signal constellation size M. Denoting $K = \log_2(R)$, the objective function is rewritten as

$$\text{Obj}(x) = \frac{C}{K\gamma}(2^K K - 2^x x) + \frac{B}{K\gamma^m}(2^x)^{2m}, x \in [0, K] \quad (25)$$

The minimum of the objective function can only exist at the zero-derivative point(s) or the borders. After differentiating the right side of (25) with respect to x and setting it equal it to zero:

$$\frac{2mB \log(2)}{K\gamma^m}(2^x)^{2m} - \frac{C}{K\gamma}\{1 + x \log(2)\}2^x = 0 \quad (26)$$

However, applying this method as is infeasible due to recursive searching. Instead, we propose a segmental optimisation solution with low complexity which maintains the performance. Since it is difficult to expand 2^x by Taylor expansion on a large scale, we break up the whole interval to decrease the expansion order. Three term expansion and range $[a-1, a+1)$ are selected, where $a = 1, 3, \ldots$. $2^x - 1$ can be expanded as:

$$2^x|_{x \in [a-1, a+1)} = 2^a\{1 + (x-a)\log(2) + \frac{1}{2}(x-a)^2(\log(2))^2\} \quad (27)$$

Now we can obtain a posynomial objective function by substituting (27) into (25) and work out a closed-form solution in each segment. A specific form for the Rayleigh fading scenario will be given in the next subsection.

C. Special Case of Rayleigh Fading

Considering Rayleigh fading scenario, we substitute $m = 1$ into (26) to get:

$$\frac{2B \log(2)}{K\gamma}(2^x)^2 - \frac{C}{K\gamma}\{1 + x \log(2)\}2^x = 0 \quad (28)$$

K and γ are non-zero and can therefore be removed from the above equation to get:

$$2B \log(2) 4^x - C\{1 + x \log(2)\}2^x = 0 \quad (29)$$

As mentioned before, B and C are determined by the Nakagami fading parameters (m, Ω) and the correlation coefficient ρ between transmitters. Therefore, without considering the influence of the segment ends $[0, K]$, the minimum point does not depend on the total bits number K or signal to noise ratio γ but it only depends on the correlation coefficient ρ. A specific form objective function under the Rayleigh fading can be obtained from (27) and (25) as:

$$\text{Obj}(x)|_{x \in [a-1, a+1)} = A_4 x^4 + A_3 x^3 + A_2 x^2 + A_1 x^1 + A_0 \quad (30)$$

where

$$\begin{cases} A_4 = \frac{4^a B}{24}(\log 4)^4 \\ A_3 = 4^a B\{-\frac{1}{3}(\log 4)^3 \tilde{a} + \frac{1}{6}(\log 4)^3\} - \frac{C}{2} 2^a (\log 2)^2 \\ A_2 = 4^a B\{(\log 4)^2 \tilde{a}^2 - (\log 4)^2 \tilde{a} + \frac{1}{2}(\log 4)^2\} \\ \qquad -2^a C\{-\log(2)\tilde{a} + \log(2)\} \\ A_1 = 4^a B\{-\frac{4\log(4)}{3}\tilde{a}^3 + 2\log(4)\tilde{a}^2 - 2\log(4)\tilde{a} + \log(4)\} \\ \qquad -2^a C(\frac{1}{2}\tilde{a}^2 - \tilde{a} + 1) \\ A_0 = 4^a B(\frac{2}{3}\tilde{a}^4 - \frac{4}{3}\tilde{a}^3 + 2\tilde{a}^2 - 2\tilde{a} + 1) + 2^K KC \end{cases} \quad (31)$$

and $\tilde{a} = a \log(2)$. By substituting $a = 1, 3, \ldots$, the minimum point of each segment can be directly obtained and denoted as m_i. Including the borders value, the minimisation of the global range $[0, K]$ can then be calculated as

$$\min_{m_i} \quad \{\text{Obj}(m_i)|_{i=1,2,\ldots}\}. \quad (32)$$

IV. Results

A. Optimisation Results Over Different Scenarios

In this Section, we investigate how optimum signal constellation size, M, is affected by correlation, parameter m in Nakagami-m fading, SNR and total symbol size R. In Fig.1(a) and Fig.1(b), we show numerically obtained results for optimal M, as indicated by circles, on curves for a

range of possible values. For a fixed SNR, the optimal M increases as the channels are more correlated, as can be seen from Fig.1(a). Meanwhile, as the Nakagami parameter m is increased, the optimal M increases, as seen in Fig.1(b). In the case of identically distributed Rayleigh fading channels with a fixed correlation degree ($\rho = 0.5$) and SNR equal to 40 dB, optimisation results for different R are displayed in Fig.2(a). Although (29) does not depend on R, due to the fact that the segment limit *does* depend on R, one can see in Fig.2(a) that, for relatively small R, optimum M is smaller than for larger R. However, in the case of identically distributed Rayleigh fading channels with a fixed correlation degree ($\rho = 0.5$) and $R = 64$, optimisation results show in Fig.2(b), as expected from (29), that the optimum M does not vary for different SNRs. Therefore, we can summarise the trends as: in the case of Rayleigh fading, optimal M increases as correlation increases, it has no dependence on SNR and the influence of total symbol size R is only noticed for small R. When the Nakagami parameter m increases, optimal M increases.

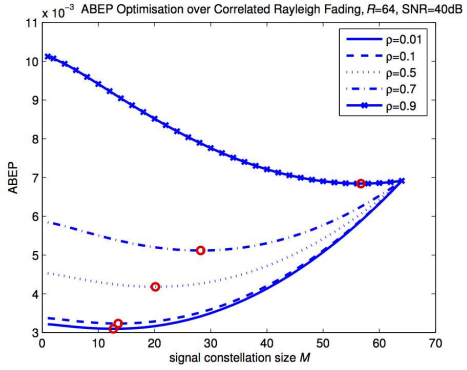

(a) Rayleigh fading with different correlations

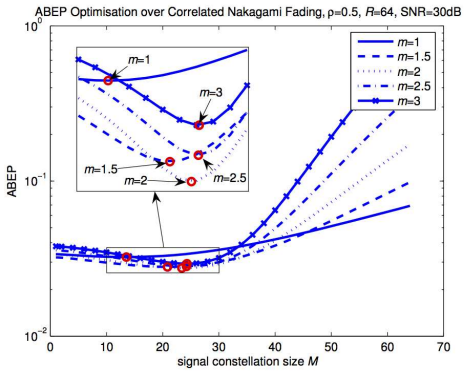

(b) Nakagami-m fading for different m values and ρ = 0.5

Fig. 1. ABEP optimisation over correlated fading channels

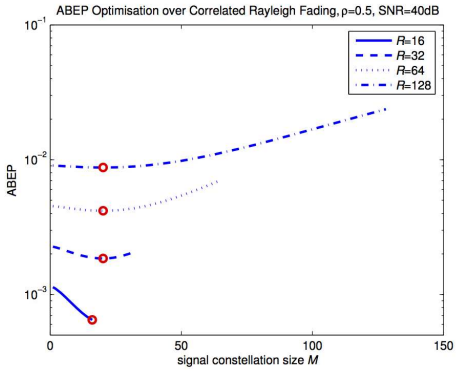

(a) Rayleigh fading under different R

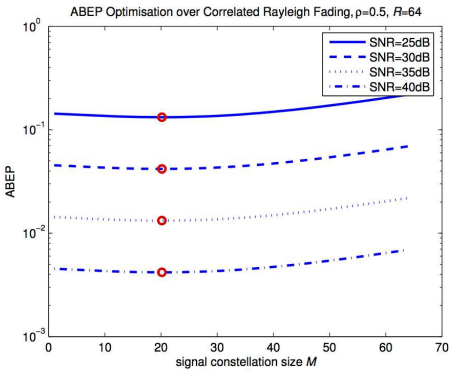

(b) Rayleigh fading under different SNR

Fig. 2. ABEP optimisation over Rayleigh fading with certain correlation

TABLE I
PRACTICAL OPTIMISED SM DEPLOYMENT (M, N_t)

ρ/R	R=16	R=32	R=64	R=128	R=256
ρ=0.01	(16,1)	(16,2)	(16,4)	(16,8)	(16,16)
ρ=0.1	(16,1)	(16,2)	(16,4)	(16,8)	(16,16)
ρ=0.5	(16,1)	(16,2)	(16,4)	(16,8)	(16,16)
ρ=0.7	(16,1)	(32,1)	(32,2)	(32,4)	(32,8)
ρ=0.9	(16,1)	(32,1)	(64,1)	(64,2)	(64,4)

B. Practical Optimised SM Deployment

In practical SM deployment, both the transmitter number N_t and PSK symbol alphabet size M must be an integer power of 2. Table I lists best combinations of M and N_t over correlated, identically distributed Rayleigh fading channels. As can be seen, the optimal choice depends on the correlation degree ρ and R in an intricate way: for smallest value of R, it is best to have $N_t = 1$, but as R increases, best choice of M and N_t depends strongly on the correlation degree.

C. Comparison of Required SNR for a Fixed BER

Optimised deployment of SM also provides a decrease in the required SNR while maintaining a certain bit error probability. Fig.3 shows the SNR needed over different deployments in correlated Rayleigh fading with $\rho = 0.5, R = 64$, which is one of the examples listed in Table I. As can be seen, in this scenario, to maintain a BER=$1 \cdot 10^{-3}$, the optimised deployment can save up to 2.16 dB when compared to the worst case.

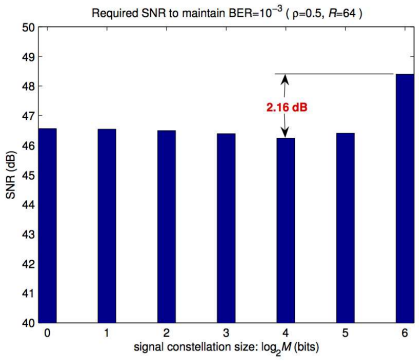

Fig. 3. Comparison of required SNR for varying M

V. Summary and Conclusions

In this paper, a closed-form ABEP optimisation has been proposed. Under channels with time-variant correlation degree, the adaptive optimal deployment for spatial modulation can significantly improve the performance while maintaining the total symbol size. In the scenario of Rayleigh fading, the optimal choice of (M, N_t) only depends on the correlation degree for large total symbol size R and it does not depend on the SNR. An SNR required to maintain the same BER can be decreased if the optimal signal symbol size M has been used for SM deployment. We also note that the optimum M increases as the m parameter of Nakagami fading increases. We note that the optimal power allocation in [4],[5] can be embedded in this scheme to further improve the performance. In future research, other modulation schemes, such as QAM, and the case of multiple receivers will be studied.

Acknowledgment

We gratefully acknowledge support from the European Union (PITNGA2010264759, GREENET project) for this work. Professor Harald Haas acknowledges the Scottish Funding Council support of his position within the Edinburgh Research Partnership in Engineering and Mathematics between the University of Edinburgh and Heriot Watt University.

References

[1] R. Mesleh, H. Haas, S. Sinanović, C. W. Ahn, and S. Yun, "Spatial Modulation," *IEEE Trans. Veh. Technol.*, vol. 57, no. 4, pp. 2228 – 2241, July 2008.

[2] M. D. Renzo and H. Haas, "Performance analysis of spatial modulation," in *Communications and Networking in China (CHINACOM), 2010 5th International ICST Conference on*, aug. 2010, pp. 1 –7.

[3] ——, "Bit error probability of sm-mimo over generalized fading channels," *Vehicular Technology, IEEE Transactions on*, vol. 61, no. 3, pp. 1124 –1144, march 2012.

[4] T. Handte, A. Muller, and J. Speidel, "BER Analysis and Optimization of Generalized Spatial Modulation in Correlated Fading Channels," in *Vehicular Technology Conference Fall (VTC Fall-2009)*, Sep. 2009, pp. 1 –5.

[5] M. Di Renzo and H. Haas, "Improving the performance of space shift keying (SSK) modulation via opportunistic power allocation," *Communications Letters, IEEE*, vol. 14, no. 6, pp. 500 –502, 2010.

[6] ——, "A General Framework for Performance Analysis of Space Shift Keying (SSK) Modulation for MISO Correlated Nakagami-m Fading Channels," *IEEE Transactions on Communications*, vol. 58, no. 9, pp. 2590 –2603, Sep. 2010.

[7] N. Czink, G. Matz, D. Seethaler, and F. Hlawatsch, "Improved mmse estimation of correlated mimo channels using a structured correlation estimator," in *Signal Processing Advances in Wireless Communications, 2005 IEEE 6th Workshop on*, june 2005, pp. 595 – 599.

[8] M. Di Renzo and H. Haas, "Bit error probability of space modulation over nakagami-m fading: Asymptotic analysis," *IEEE Communications Letters*, vol. 15, no. 10, pp. 1026 –1028, Oct. 2011.

[9] M. K. Simon and M.-S. Alouini, *Digital Communication over Fading Channels*, 2nd ed. Wiley-IEEE Press, 2005.

2012 IEEE 17th International Workshop on Computer Aided Modeling and Design of Communication Links and Networks (CAMAD)

Base Station Energy Consumption for Transmission Optimised Spatial Modulation (TOSM) in Correlated Channels

Xiping Wu*, Sinan Sinanović*, Marco Di Renzo† and Harald Haas*

*Institute for Digital Communications
Joint Research Institute for Signal and Image Processing
School of Engineering
The University of Edinburgh
EH9 3JL, Edinburgh, UK
{xiping.wu, s.sinanovic, h.haas}@ed.ac.uk

†French National Centre for Scientific Research (CNRS)
Laboratory for Signals and Systems (LSS)
École Supérieure d'Électricité (SUPELEC)
3 rue Joliot-Curie, 91192 Gif-sur-Yvette (Paris), France
marco.direnzo@lss.supelec.fr

***Abstract*—Radio frequency (RF) chains are responsible for a large percentage of the total BS energy consumption and each RF chain can only support one activated transmit antenna at a time. This fact greatly benefits spatial modulation (SM) since at any given time instance only one antenna in an array is active. The proposed transmission optimised spatial modulation (TOSM) is an adaptive SM scheme which trades off the spatial constellation size with the signal constellation size to minimise the average bit error probability (ABEP) for a given channel correlation. It outperforms fixed-SM scheme for different channel correlation degrees. In this paper, we construct a single RF chain BS based on TOSM which has low complexity and high energy-efficiency. Simulation results show that for a given spectral efficiency of 6 bits/s/Hz and two receive antennas, the proposed scheme outperforms 2x2 V-BLAST by at least 3.8 dB in energy consumption.**

***Index Terms*—Base station, energy consumption, MIMO, spatial modulation (SM), transmission optimised spatial modulation (TOSM), single RF chain BS, correlated fading.**

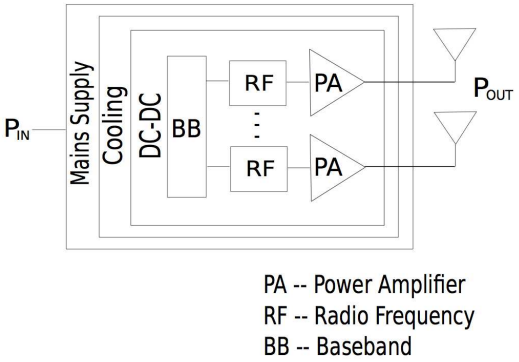

Fig. 1. SotA base station structure [2]

I. Introduction

With the aim to reduce operating cost and the carbon footprint of wireless networks, an overall energy reduction is required in the region of two to three orders of magnitude [1]. At the same time, a significant increase of the network spectral efficiency from currently around 1.5 bits/s/Hz to at least 10 bits/s/Hz is needed to cope with the exponentially increasing traffic loads. Fig. 1 shows the structure of a State-of-the-Art (SotA) BS which consists of such components as RF chains, baseband processors, DC-DC converters, cooling fans, etc [2], [3]. Each RF chain requires a power amplifier (PA) and PAs consume about 60% of the entire energy of an RF chain [2].

Minimising the RF transmit power is not sufficient because of the large amount of quiescent power in the power amplifier. Cell discontinuous transmission (DTX) enables to put a BS into a sleep mode where energy consumption is reduced to a lower value than the active mode [4]. Based on that, an optimisation of the BS power consumption is proposed by using on/off PAs [5]. A similar research is done in MIMO orthogonal frequency division multiple access (OFDMA) systems [6]. However, the above paper focus on the optimisation within one RF chain. While MIMO systems offer high spectral efficiency, unfortunately, they require multiple RF chains, i.e., multiple power amplifiers which heavily compromise energy efficiency. Meanwhile, spatial modulation (SM) is a recently proposed modulation concept which combines traditional signal modulation and space shift keying (SSK) [7]–[9]. It is an unique three dimensional modulation scheme and uses only one activated transmitter. This offers a significant opportunity to save energy given that only one RF chain, and, hence, only one PA is required. However, like all spatial multiplexing MIMO systems, SM suffers from correlated fading channels [10], [11]. With the aim to improve the performance of SM in correlated channels, TOSM is proposed in [12]. It trades off signal constellation size with spatial constellation size to minimize the average bit error probability (ABEP) for a given channel correlation degree. By combining the TOSM scheme and the single RF chain structrue, a low complexity

978-1-4673-3125-8/12/$31.00 ©2012 IEEE

and energy-efficient BS system is proposed in this paper.

The remainder of this paper is structured as follows. Section II introduces the SotA 2010 power model. Section III proposes a novel scheme based on TOSM to reduce BS energy consumption. Simulation results are presented in Section IV. The paper is concluded in Section V.

II. System Model

A $N_t \times N_r$ SM system is considered in this paper, where N_t and N_r are the numbers of transmit antennas and receive antennas, respectively. The spectral efficiency and the signal constellation size are defined as η and M. SM processing divides up the bit stream into blocks and each block has K bits. A block is split into two parts with $\log_2(M)$ and $\log_2(N_t)$ bits. The first part is modulated by the signal constellation diagram and emitted through one of the N_t transmitters determined by the second part. Perfect channel state information (CSI) is assumed known at the receiver and the specific channel signatures are exploited to extract the spatial constellation points. Hence no explicit signalling for the spatial constellation is required. The transmitted symbol is detected by the joint maximum likelihood (ML) detection [13].

A. Channel Model

The channel distribution h is Nakagami-m fading with parameters (m, Ω), where m is the shape parameter (when $m = 1$, the channel is Rayleigh fading) and Ω is the spread controlling parameter. $0 \leq \rho_{t_1,t_2} \leq 1$ is the correlation degree between two propagation fading paths from transmitters t_1 and t_2 to any one of the receive antennas. N_0 presents the power spectral density of the additive white Gaussian noise (AWGN) at the receiver.

B. BS Power Model

1) BS with a single RF chain: A relationship between RF output power and the total required power of a BS is established in [3]. It divides the BS supply power into two parts: constant and load-dependent (related to the RF output power). Additionally, a sleep mode is provided to switch off unneeded components when no data is transmitted. Under the above consideration, several power models are proposed in [14] to represent a single transmit antenna, one-sector BS. In this paper, we adopt the SotA 2010 BS power model as shown in Table I. l denotes the slope of the trajectory that quantifies the load dependence. $P_{\max}$ is the maximum transmit power, P_0 and P_s represent constant consumption for the active mode and sleep mode, respectively. The instantaneous power consumption is given by [14, Eq. (1)] as a function of the RF output power P_m:

$$P_{\text{supply}} = \begin{cases} P_0 + lP_m & \text{if} \quad 0 < P_m \leqslant P_{\max} \\ P_s & \text{if} \quad P_m = 0 \end{cases} \tag{1}$$

By defining the normalized duration of transmission as μ, the average overall power consumption is formulated as:

$$P_{\text{BS}} = \mu(P_0 + lP_m) + (1 - \mu)P_s \tag{2}$$

TABLE I
Power Model Parameters

Power Model	P_0 /W	l	P_s /W	$P_{\max}$ /W
SotA 2010	119	2.4	63	40

In this paper, the antenna is assumed to be active all the time, i.e., $\mu = 1$. Thus, the overall power consumption for one transmit system is simplified to:

$$P_{\text{BS}} = P_0 + lP_m \tag{3}$$

2) BS with multiple RF chains: For multiple RF chains with N_{act} *activated* transmitters, the transmission power of each antenna is $1/N_{\text{act}}$ of the total RF output power P_m. Thus, the power consumption of a BS with multiple RF chains can be formulated as:

$$P_{\text{BS}} = N_{\text{act}} \left(P_0 + l \frac{P_m}{N_{\text{act}}} \right) \tag{4}$$

When $N_{\text{act}} = 1$, the above formula is the same as Eq. (3) in the single RF chain scenario.

C. Fixed-SM and TOSM

Fixed-SM denotes the SM scheme which uses a fixed combination of the spatial constellation size N_t and the signal constellation size M. Without considering special encoding methods, i.e., fractional bit encoding [15], both N_t and M must be a power of 2 to provide a full usage in the constellation diagram. Thus, for a given spectral efficiency η, there are several feasible combinations of $[N_t, M]$. Fig. 2 gives an example of the available Fixed-SM structures for given spectral efficiency. In [12], we show that for given correlation degree and η, there exists a best choice of $[N_t, M]$. For a given η, TOSM adopts the corresponding optimal $[N_t, M]$ for various correlation degrees. Hence, it is an adaptive SM scheme to channel correlation.

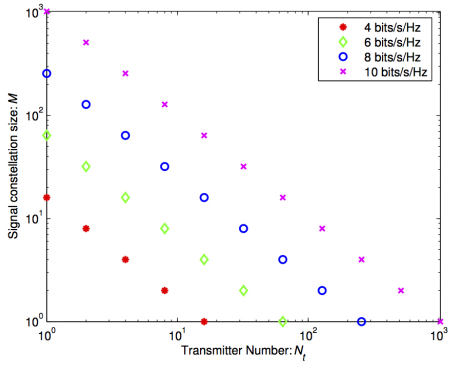

Fig. 2. Available Fixed-SM structures for given spectral efficiency

III. Base Station Energy Consumption

A. TOSM

The key of TOSM is to obtain the optimal choice of $[M, N_t]$ by minimising the ABEP over correlated fading channels. We denote $\gamma = E_m G/N_0$, where E_m is the average energy per transmission and G is the free space loss without shadowing. An improved ABEP union bound of SM-MIMO is proposed in [10]. Based on that, [12, Eq. (22)] provides the ABEP objective function for a single receiver system where M is the only variable. We extend that result to the multiple-receiver scenario:

$$\text{ABEP} = \frac{C}{\eta}[2^\eta\eta - M\log_2(M)]\gamma^{-N_r} + \frac{B}{\eta}M^{2mN_r}\gamma^{-mN_r} \quad (5)$$

with

$$\begin{cases} C = \frac{2^{3N_r-2}\Gamma(N_r+0.5)}{\sqrt{\pi}\Gamma(N_r+1)} f_{(m,\Omega,\rho)}^{N_r} \\ B = (2m/\Omega)^{mN_r}\pi^{-2mN_r-1}\int_0^\pi(\sin\theta)^{2mN_r}d\theta \end{cases} \quad (6)$$

where:

$$f_{(m,\Omega,\rho)} = \frac{m(1-\rho)^{m-1}}{2^{2m-1}\Omega\Gamma(m)}\sum_{k=0}^{+\infty}(\frac{\rho}{4})^k\frac{\Gamma(2m+2k-1)}{(k!)\Gamma(m+k)} \quad (7)$$

It can be observed that parameters C and B are constant for given fading distribution and correlation coefficient (m, Ω, ρ). With the assumption of identically distributed Rayleigh fading ($m = 1$, $\Omega = 1$), Eq. (5) can be simplified to:

$$\text{ABEP} = \frac{\gamma^{-N_r}}{\eta}\{C[2^\eta\eta - M\log_2(M)] + BM^{2N_r}\} \quad (8)$$

The term $\frac{\gamma^{-N_r}}{\eta}$ does not depend on M thus can be removed from the objective function. The optimisation problem is formulated as:

$$\begin{aligned} &\min_M \quad \text{Obj} = C[2^\eta\eta - M\log_2(M)] + BM^{2N_r} \\ &\text{subject to:} \quad M = 2^x, \quad \text{where} \quad x = 0, 1, ..., \eta \end{aligned} \quad (9)$$

As can be seen, over identically distributed Rayleigh fading channels, the optimisation remains independent of SNR for multiple receivers. The best selection of $[M, N_t]$ only depends on the spectral efficiency η, receiver number N_r and correlation coefficient ρ. After obtaining the optimal combination $[M_{\text{opt}}, N_{t_{\text{opt}}}]$, the required E_m to maintain a given ABEP R_e can be calculated as:

$$E_m = \frac{N_0}{G}\left(\frac{\text{Obj}(M_{\text{opt}})}{\eta R_e}\right)^{-N_r} \quad (10)$$

By defining the transmission rate as R_b bits/s, the RF output power of TOSM is given by:

TABLE II
Simulation Configurations. Transmissions of 6 bits/s/Hz, Using TOSM, Fixed-SM, and V-BLAST

Transmitted bits	TOSM	Fixed SM	V-BLAST
6 bits/s/Hz	Variable	2x2 32PSK 4x2 16PSK	2x2 8PSK 3x3 4PSK

$$P_m = E_m\frac{R_b}{\eta} \quad (11)$$

Substituting Eq. (10) into Eq. (11):

$$P_m = \frac{N_0 R_b}{\eta G}\left(\frac{\text{Obj}(M_{\text{opt}})}{\eta R_e}\right)^{-N_r} \quad (12)$$

B. BS energy consumption based on a single RF chain

Without considering the switching time, the overall BS power consumed by SM can be formulated by directly applying Eq. (3):

$$P_{\text{SM}} = P_0 + lP_m \quad (13)$$

The energy consumption per bit E_{SM} is given by:

$$E_{\text{SM}} = \frac{P_{\text{SM}}}{R_b} \quad \text{[Joule/bit]} \quad (14)$$

By substituting Eq. (12) and Eq. (13) into Eq. (14), the energy consumption per bit of a BS based on TOSM is obtained as:

$$E_{\text{TOSM}} = \frac{P_0}{R_b} + \frac{lN_0}{\eta G}\left(\frac{\text{Obj}(M_{\text{opt}})}{\eta R_e}\right)^{-N_r} \quad \text{[Joule/bit]} \quad (15)$$

IV. Results

For the numerical analysis, we evaluate the TOSM scheme in a Monte Carlo simulation and compare it with fixed-SM and V-BLAST. A constant spectral efficiency η = 6 bits/s/Hz and correlated, identically distributed Rayleigh fading channels are assumed. All compared systems are selected such that they achieve the same spectral efficiency, as shown in Table II. With the aim to provide a comparable receiver structure with V-BLAST, we consider two receive antennas in both TOSM and fixed-SM. Perfect time synchronization is assumed.

A. ABEP

As proved in Section III.A, for a certain spectral efficiency and receiver number, the best combination of $[M, N_t]$ in TOSM is only dependent on the correlation coefficient ρ. Table III lists optimal selection of transmitter number N_t. As can be seen, the best choice of N_t decreases as ρ increases.

Based on the optimal N_t selection, Fig. 3 shows the simulation results of ABEP at an E_b/N_0 of 25 dB. Fig. 3(a) demonstrates that the ABEP of TOSM, as a function of the correlation coefficient ρ, matches the simulation result well. Since the obtained relationship is an approximation of the upper bound [10], it is below the simulation result for high

TABLE III
TRANSMITTER NUMBER SELECTION OF TOSM (SPECTRAL EFFICIENCY=6 BITS/S/HZ, N_r=2)

Tx Correlation ρ	0.1	0.2	0.3	0.4	0.5
TOSM Transmitter Number	16	16	16	16	16
Tx Correlation ρ	0.6	0.7	0.8	0.9	1
TOSM Transmitter Number	8	8	8	8	2

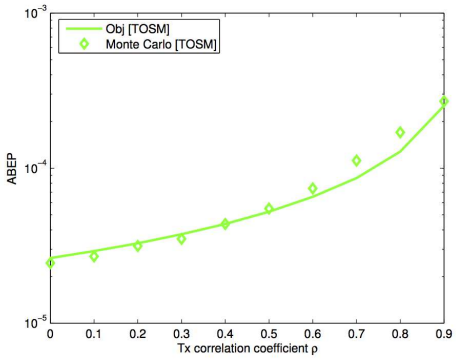

(a) Simulation for TOSM

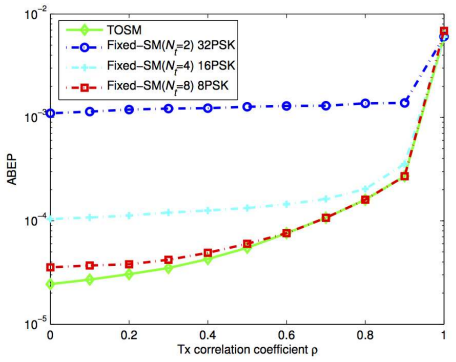

(b) TOSM v.s. Fixed-SM

Fig. 3. Monte Carlo simulation results for ABEP at Spectral Efficiency=6 bits/s/Hz, E_b/N_0=25 dB

correlation. In Fig. 3(b), it is shown that TOSM always outperforms fixed-SM schemes, except at a few overlapping points where they use the same transceiver structure. Specifically, TOSM is significantly better than two-transmitter fixed-SM all the times except when ρ is close to 1. Furthermore, four-transmitter fixed-SM has a performance close to the TOSM for large ρ. However, TOSM performs better than fixed-SM schemes when ρ is small. Similar, but less pronounced trends are noticed at lower SNRs.

TABLE IV
SIMULATION PARAMETERS

Parameter	Value
Carrier frequency	2 GHz
Bandwidth W	10 MHz
Pathloss	120 dB, without shadowing
Operating temperature T	290 K
Transmission Rate	10 Mbits/s
Target ABEP	10^{-3}
Iterations	10000

B. Energy Consumption

In Fig. 4 and 5, we compare the energy consumption of TOSM with other schemes in two forms: transmit energy consumption and BS overall energy consumption, respectively. The simulation is implemented under the parameters shown in Table IV. To maintain a certain ABEP at low correlation degrees, fixed-SM with a small N_t requires a large SNR. This is because SSK offers a large amplitude distinction when channels are sufficiently diverse. As shown in Fig. 4, TOSM reduces the required transmit energy per bit by up to 2.9 dB. A similar situation, but with smaller margin, occurs in BS energy consumption comparison, as shown in Fig. 5(a). The reason is that transmission power 2.1 W∼5.4 W (calculated from Fig. 4) results into a load-dependent power from 5 W to 13 W through being multiplied by the slope coefficient. Compared to that, the constant equipment-consumed power (119 W) has a stronger influence in SotA 2010 power model. Fig. 5(b) shows that TOSM outperforms 2x2 V-BLAST and 3x3 V-BLAST by at least 3.8 dB and 4.8 dB, respectively, due to the advantage of a single RF chain and optimisation of SM.

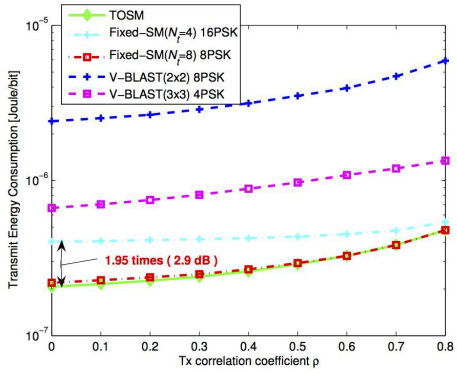

Fig. 4. Transmit Energy Consumption for target ABEP=10^{-3}, transmission rate=10 Mbits/s

V. SUMMARY AND CONCLUSION

In this paper, we have presented a comparison of TOSM, fixed-SM and V-BLAST on the energy consumption metric of the BS. Results show that fixed-SM with a small number

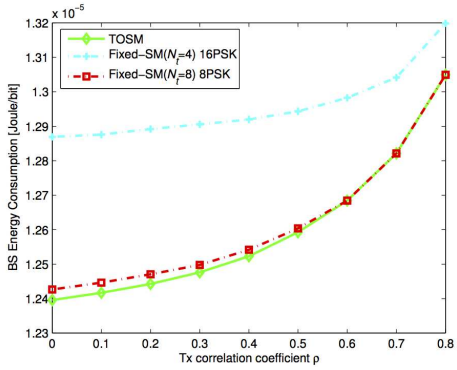

(a) TOSM v.s. Fixed-SM

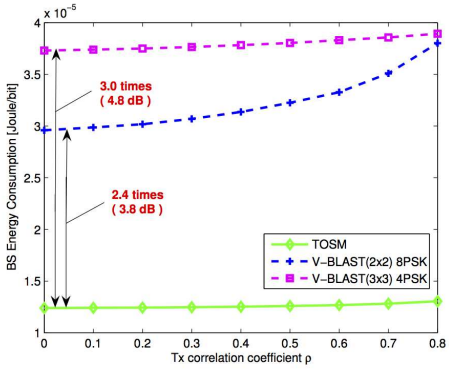

(b) TOSM v.s. V-BLAST

Fig. 5. BS Energy Consumption for target ABEP=10^{-3}, transmission rate=10 Mbits/s

of transmit-antennas requires large transmit power to maintain a given ABEP at low correlation. By optimising the number of transmitters, TOSM improves the performance for various correlation degrees. Furthermore, TOSM requires only one RF chain. This advantage enables it to outperform traditional spatial multiplexing schemes on the metric of BS overall energy consumption. Results show that for a given spectral efficiency of 6 bits/s/Hz and two receive antennas, the proposed scheme outperforms V-BLAST by at least 3.8 dB in terms of BS energy consumption per bit. All these merits make TOSM a promising scheme for low complexity, highly energy-efficient transceivers and an ideal candidate for massive MIMO. Future research directions will combine the proposed scheme with other power optimisation methods such as DTX [4].

ACKNOWLEDGMENT

We gratefully acknowledge support from the European Union (PITNGA2010264759, GREENET project) for this work. Professor Harald Haas acknowledges the Scottish Funding Council support of his position within the Edinburgh Research Partnership in Engineering and Mathematics between the University of Edinburgh and Heriot Watt University.

REFERENCES

[1] A. Fehske, G. Fettweis, J. Malmodin, and G. Biczok, "The global footprint of mobile communications: The ecological and economic perspective," *IEEE Communications Magazine*, vol. 49, no. 8, pp. 55 –62, August 2011.

[2] G. Auer, V. Giannini, I. Godor, P. Skillermark, M. Olsson, M. Imran, D. Sabella, M. Gonzalez, C. Desset, and O. Blume, "Cellular Energy Efficiency Evaluation Framework," in *Vehicular Technology Conference (VTC Spring), 2011 IEEE 73rd*, May 2011, pp. 1 –6.

[3] L. Correia, D. Zeller, O. Blume, D. Ferling, Y. Jading, I. Godor, G. Auer, and L. Van Der Perre, "Challenges and enabling technologies for energy aware mobile radio networks," *IEEE Communications Magazine*, vol. 48, no. 11, pp. 66 –72, November 2010.

[4] P. Frenger, P. Moberg, J. Malmodin, Y. Jading, and I. Godor, "Reducing Energy Consumption in LTE with Cell DTX," in *Vehicular Technology Conference (VTC Spring), 2011 IEEE 73rd*, May 2011, pp. 1 –5.

[5] A. Chatzipapas, S. Alouf, and V. Mancuso, "On the minimization of power consumption in base stations using on/off power amplifiers," in *Online Conference on Green Communications (GreenCom), 2011 IEEE*, Sept. 2011, pp. 18 –23.

[6] Z. Xu, C. Yang, G. Li, S. Zhang, Y. Chen, and S. Xu, "Energy-Efficient MIMO-OFDMA Systems Based on Switching off RF Chains," in *Vehicular Technology Conference (VTC Fall), 2011 IEEE*, Sept. 2011, pp. 1 –5.

[7] R. Mesleh, H. Haas, C. W. Ahn, and S. Yun, "Spatial Modulation – A New Low Complexity Spectral Efficiency Enhancing Technique," in *IEEE International Conference on Communication and Networking in China (CHINACOM)*, Beijing, China, Oct. 25–27, 2006, pp. 1–5.

[8] R. Mesleh, H. Haas, S. Sinanović, C. W. Ahn, and S. Yun, "Spatial Modulation," *IEEE Trans. Veh. Technol.*, vol. 57, no. 4, pp. 2228 – 2241, July 2008.

[9] M. Di Renzo, H. Haas, and P. M. Grant, "Spatial Modulation for Multiple-Antenna Wireless Systems: A Survey," *IEEE Commun. Mag.*, vol. 49, no. 11, pp. 182–191, Nov. 2011.

[10] M. D. Renzo and H. Haas, "Bit error probability of sm-mimo over generalized fading channels," *Vehicular Technology, IEEE Transactions on*, vol. 61, no. 3, pp. 1124 –1144, march 2012.

[11] M. Di Renzo and H. Haas, "A General Framework for Performance Analysis of Space Shift Keying (SSK) Modulation for MISO Correlated Nakagami-m Fading Channels," *IEEE Transactions on Communications*, vol. 58, no. 9, pp. 2590 –2603, Sep. 2010.

[12] X. Wu, S. Sinanovic, M. Di Renzo, and H. Haas, "Structure Optimisation of Spatial Modulation over Correlated Fading Channels," in *(accepted) Proc. of the MMCOM'12 Workshop at the Global Communications Conference (GLOBECOM), IEEE*, 2012.

[13] J. Jeganathan, A. Ghrayeb, and L. Szczecinski, "Spatial Modulation: Optimal Detection and Performance Analysis," *IEEE Commun. Lett.*, vol. 12, no. 8, pp. 545–547, 2008.

[14] H. Holtkamp, G. Auer, and H. Haas, "On Minimizing Base Station Power Consumption," in *Proc. of the Vehicular Technology Conference (VTC)*, IEEE. San Francisco, CA, USA: IEEE, Sep. 5–8, 2011, pp. 1–5.

[15] N. Serafimovski, M. Di Renzo, S. Sinanović, R. Y. Mesleh, and H. Haas, "Fractional Bit Encoded Spatial Modulation (FBE–SM)," *IEEE Commun. Lett.*, vol. 14, no. 5, pp. 429–431, May 2010.

Direct Transmit Antenna Selection for Transmit Optimized Spatial Modulation

Xiping Wu*, Marco Di Renzo†, and Harald Haas*

*Institute for Digital Communications
Joint Research Institute for Signal and Image Processing
School of Engineering
The University of Edinburgh
EH9 3JL, Edinburgh, UK
{xiping.wu, h.haas}@ed.ac.uk

†French National Centre for Scientific Research (CNRS)
Laboratory for Signals and Systems (LSS)
École Supérieure d'Électricité (SUPELEC)
3 rue Joliot-Curie, 91192 Gif-sur-Yvette (Paris), France
marco.direnzo@lss.supelec.fr

***Abstract*—To improve the performance of spatial modulation (SM) over correlated MIMO channels, transmit optimized spatial modulation (TOSM) has been proposed recently. It trades off traditional signal constellation diagrams with spatial constellation diagrams to minimize the average bit error probability (ABEP). After the optimum number of transmit antennas is determined, the specific antennas need to be carefully chosen from the entire array to provide a minimum ABEP. Like in conventional transmit antenna selection (TAS) schemes, the problem can be solved by an exhaustive search. However, this results in an unaffordable complexity especially when the spectral efficiency is high. In this paper, we propose a creative TAS approach for TOSM. Given a required number of antennas, the novel technique determines the selection solution based on circle packing. Simulation results show that for various channel correlations and spectral efficiencies, the proposed method achieves performance results close to exhaustive search with a gap of less than 0.3 dB. The complexity is reduced to an extremely low level.**

***Index Terms*—Realistic circle packing (RCP), transmit antenna selection (TAS), transmit optimized spatial modulation (TOSM), correlated MIMO, average bit error probability (ABEP)**

I. Introduction

Spatial modulation (SM) [1]–[3], combining traditional signal modulation and space shift keying (SSK), is a relatively new transmission technique for multiple-input-multiple-output (MIMO) wireless systems. Unlike conventional MIMO schemes, SM achieves multiplexing gains by considering antenna locations as spatial constellation points. The result of which is that SM only requires a single radio frequency (RF) chain independent of the number of antenna elements. This key property makes SM a truly energy-efficient large MIMO technique. In [3]–[5], it has been demonstrated that SM offers better performance than many state-of-the-art MIMO schemes while achieving a low-complexity implementation.

Some recent works have considered using transmit antenna selection (TAS) techniques to further enhance the performance of SM. The basic idea revolves around selecting the optimum antennas for the spatial constellation points [6]. In [7], a TAS method is proposed by maximizing the minimum Euclidean distance between received symbols. Additionally, a capacity optimized TAS technique is conceived for SM in [8]. However, both approaches have the following critical limitations: i) they assume independent and identically distributed (i.i.d.) channels; ii) they need instant channel state information (CSI), which results in the fitness for slow fading only; iii) although a simplified criterion has been proposed to lower the complexity, an exhaustive search is still required to obtain the optimum antenna selection. This leads to an unaffordable amount of computation for higher spectrum efficiencies. Meanwhile, based on the unique characteristic of the three-dimensional modulation in SM, transmit optimized spatial modulation (TOSM) is proposed [9], [10]. For different channel correlations, TOSM trades off signal constellation size with spatial constellation size to obtain the optimal number of transmit antennas. This provides the minimum average bit error probability (ABEP). One of the most notable advantages is that, since the optimization is carried out by involving statistic CSI rather than instant CSI, TOSM is also suitable for fast fading channels. In our previous research [9], a constant channel correlation model was assumed. As a result, each antenna has an equal status and the required subset can be picked arbitrarily. However, for a more practical scenario, such as the exponential correlation model [11], there is a challenge now to identify the optimum subset of antennas for SM.

Unlike conventional TAS problems, the issue here is to arrange the required number of antennas in a position-fixed array. In this paper, a novel TAS method based on circle packing is proposed for TOSM. This heuristic scheme can directly solve the previously mentioned selection problem without invoking exhaustive search. Apart from the benefit of low complexity, the optimum number of transmit antennas is the only needed information at the transmitter, whereas those methods based on exhaustive search require the index of each selected antenna. The reason is that in the proposed method, the selecting procedure is carried out at the transmitter instead of the receiver. Thus, the feedback cost can be extremely downsized as well. Simulation results demonstrate that the proposed approach can achieve almost the same bit error ratio (BER) performance as the exhaustive search.

The rest of this paper is organized as follows. Section II describes the system model, including channel distribution and correlation model. In Section III, the circle packing based

978-1-4673-6187-3/13/$31.00 ©2013 IEEE

TAS method for TOSM is proposed. Simulation results are presented in Section IV. We conclude the paper in Section V.

II. System Model

A $N_t \times N_r$ MIMO system is considered, where N_t and N_r are the numbers of transmit antennas and receive antennas, respectively. It is worth noting that the transmit antennas actually used for SM are a subset of N_t. We define $N_t = 2^{\eta_s}$, where η_s represents the target spectrum efficiency. The symbol alphabet sizes of the spatial and signal constellation diagrams are respectively denoted as N and M, and it is assumed that: $N \times M = N_t$. The bit stream is divided into blocks with the length of η_s bits and then each block is split into two units of $\log_2(N)$ and $\log_2(M)$ bits: i) the first part activates a single antenna out of N transmit antennas, which are chosen from the entire size-N_t array; ii) the second part is modulated by a traditional signal modulation scheme, such as phase shift keying (PSK) or quadrature amplitude modulation (QAM). The selected symbol in the signal domain is transmitted by the activated antenna.

The noise at the input of each receive antenna is assumed to be complex Additive White Gaussian Noise (AWGN) with power spectral density N_0 per dimension. Across the receive antennas, the noise is statistically independent. The signal-to-noise ratio (SNR) is defined by $\gamma = \eta_s E_b / N_0$, where E_b denotes the transmit energy per bit. At the receiver, perfect CSI is assumed. The transmitted symbol is detected by the joint maximum likelihood (ML) detection proposed in [12].

A. Channel Model

A frequency-flat fading channel model is assumed. The impulse response of the channel from the t-th transmit antenna to the r-th receive antenna is denoted as $h_{t,r}$. Correlated and identically distributed (c.i.d.) Rayleigh fading channels are considered, *i.e.,* $h_{t,r} \sim$ Rayleigh(σ), where σ is the standard deviation in each dimension.

B. Correlation Matrix Model

Since we focus on the transmit antenna selection, the receive antennas are assumed to be independent, *i.e.,* only the correlation between transmit antennas is taken into account. The correlation between two propagation links from the transmit antennas t_i and t_j to the receiver is denoted as ρ_{t_i,t_j}. In this paper, we adopt the exponential correlation matrix model stated in [11], which is based on the fact that the correlation degree decreases with increasing distance between antennas.

As shown in Fig. 1, the total N_t transmit antennas are located in a normalized square area, *i.e.,* the length between t_1 and t_A is unity and the corresponding correlation coefficient between them is denoted as ρ_s. Given η_s, the number of antennas in the first row of the antenna array results in:

$$A = \begin{cases} 2^{\frac{\eta_s}{2}} & \text{if } \eta_s \text{ is even} \\ 3 \times 2^{\frac{\eta_s - 3}{2}} & \text{if } \eta_s \text{ is odd} \end{cases} \tag{1}$$

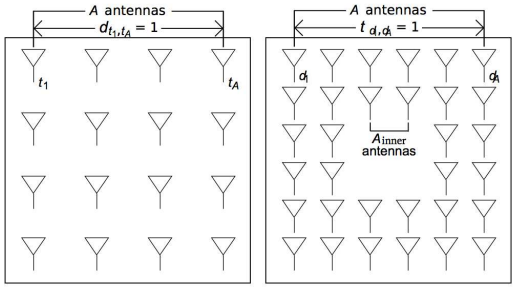

(a) η_s = 4 bits/s/Hz (b) η_s = 5 bits/s/Hz

Fig. 1. Transmit antenna array

When η_s is even, this results in a square antenna array of dimension $A \times A$. If η_s is odd, the antennas are arranged in the shape depicted in Fig. 1(b), where $A_{\text{inner}} = 2^{\frac{\eta_s - 3}{2}}$. According to [11, Eq. (10)], ρ_{t_i,t_j} is calculated by:

$$\rho_{t_i,t_j} = \rho_s^{d_{t_i,t_j}}, \qquad 0 \le \rho_s \le 1 \tag{2}$$

where d_{t_i,t_j} represents the absolute distance between transmit antennas t_i and t_j.

C. Fixed-SM and TOSM

Fixed-SM denotes the SM scheme using a constant combination of the signal constellation size M and the spatial constellation size N. Without considering special encoding methods, *e.g.,* fractional bit encoding [13], both M and N must be a power of two. Therefore, for a given spectrum efficiency, there are several feasible combinations of (N, M), *i.e.,* $N = 2^x$ and $M = 2^{\eta_s - x}$, $x = 0, 1, ..., \eta_s$.

In [9], we show that given a correlation degree, there exists a best choice of (N, M). Furthermore, for a certain η_s with different situations, such as different correlation degrees and N_r, the optimum number of transmit antennas for SM is variable. A general finding in [9] is that it is better to use a larger N for lower correlations and vice versa. By minimizing the ABEP, the TOSM scheme chooses the optimal transmit structure and, thus, improves the performance of SM over correlated channels.

III. Transmit Antenna Selection

After the optimal N is determined by TOSM, the specific antennas for the spatial constellation points need to be selected from the size-N_t array.

A. Exhaustive Search Criterion

A simplified expression of ABEP upper bound over Rayleigh fading is given by (3), originally derived in [10, Eq. (8)].

$$\text{ABEP} = \underbrace{\frac{\eta_s \times 2^{\eta_s} - M\log_2(M)}{\eta_s}\gamma^{-N_r}\overline{C}_N}_{\text{affected by correlation}} + \underbrace{\frac{M^{2N_r}}{\eta_s}\gamma^{-N_r}B}_{\text{signal modulation}} \quad (3)$$

where B and $\overline{C}_N$ are respectively specified in (4) and (5).

$$B = \left(\frac{1}{\sigma^2}\right)^{N_r} \pi^{-2N_r-1}\int_0^{\pi}(\sin\theta)^{2N_r}d\theta \quad (4)$$

Given N_r and a fading parameter σ, B is a constant and therefore, the signal modulation term in (3) does not affect the selection. The exhaustive search problem can be formulated as:

$$\begin{aligned} T_{\text{opt}} &= \underset{T}{\text{argmin}} \quad \overline{C}_N \\ \text{subject to:} \quad & T \in S \end{aligned} \quad (6)$$

where T is an N-element vector containing the selected transmit antennas, and S represents the set of all feasible combinations $\binom{N_t}{N}$. Assuming $N_t = 64$ and $N = 16$, for example, the full search space is nearly 5×10^{14} which is prohibitive for practical implementations.

B. Direct TAS based on Circle Packing

Since the correlation coefficient ρ_{t_i,t_j} is inversely proportional to the distance d_{t_i,t_j}, one rational selection rule is to maximize the minimum geometric distance between any pair of selected antennas. This can be transformed to a circle packing problem which can be solved numerically [14]. Fig. 2 shows circle packing in a square for various numbers of antennas which are located at the circle centers. In the original mathematical problem, each circle must fit inside the square boundary. Our problem is slightly different where only the center of each circle must be inside the boundary. It is not hard to infer that this scheme yields the same result as the exhaustive search for $N = 2$ and $N = 4$. It is worth noticing that this solution requires fully flexible positions. Therefore, we refer to it as ideal circle packing (ICP).

As the antenna positions are fixed in the array, the required antennas cannot be allocated perfectly by ICP. Instead, a realistic circle packing (RCP) is designed through selecting those antennas which are closest to the ideal positions. In Fig. 3, an RCP selection result is illustrated for the case of $\binom{N_t=32}{N=8}$. As can be seen, the pattern presents a similarity to the solution for $N = 8$ in ICP. With an increase of N_t, the entire array provides a larger flexibility in positions and, thus, the RCP pattern becomes closer to ICP. Furthermore, based on a similar sphere packing, this approach can be easily extended to three-dimensional antenna arrays without increasing the TAS complexity.

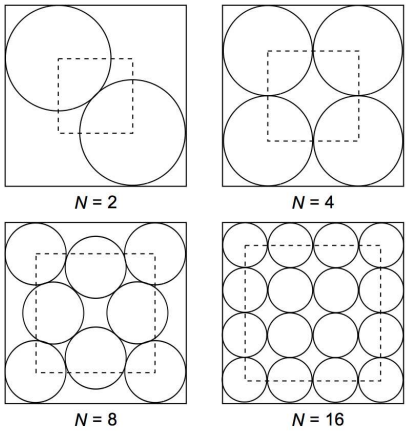

Fig. 2. Block diagram of circle packing in a square

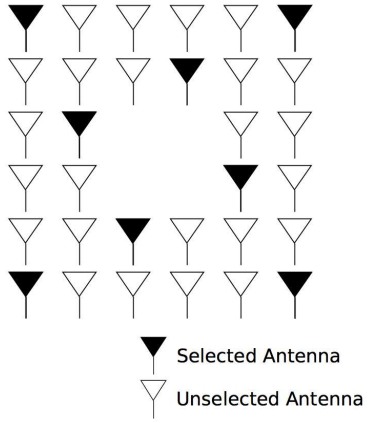

Fig. 3. Selection pattern based on circle packing (N_t = 32, N = 8)

IV. Simulation Results

A. BER Performance of RCP

In this section, the performance of the proposed RCP approach is evaluated using Monte Carlo simulation. Two baseline schemes are considered for comparison: i) the exhaustive search of the optimization problem in (6) which is denoted as "ES" in the following figures; ii) the worst selection scheme which chooses neighbouring antennas. This scheme is represented by "WS" in the sequel.

In Fig. 4, the BER performance is shown in terms of E_b/N_0 for $\eta_s = 4$ and 5 bits/s/Hz, respectively. Due to the intractable complexity of ES, the results when $\eta_s > 5$ bits/s/Hz are not presented. As can be seen, in both cases, the RCP scheme achieves almost the same performance as ES with a gap of less than 0.3 dB. Furthermore, the negligible difference between RCP and ES is barely affected by the correlation degrees,

$$\overline{C}_N = \frac{1}{N(N-1)} \sum_{i=1}^{N} \sum_{j \neq i=1}^{N} \left(\frac{2}{\sigma^2}\right)^{N_r} \frac{\Gamma(N_r+0.5)}{4\sqrt{\pi}\Gamma(N_r+1)} \times \left[\sum_{k=0}^{+\infty} \left(\frac{\rho_{t_i,t_j}}{4}\right)^k \frac{\Gamma(2k+1)}{(k!)\Gamma(k+1)}\right]^{N_r} \tag{5}$$

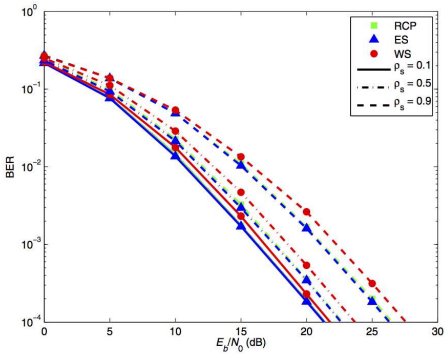

(a) η_s = 4 bits/s/Hz (N_t = 16), N = 8 (BPSK)

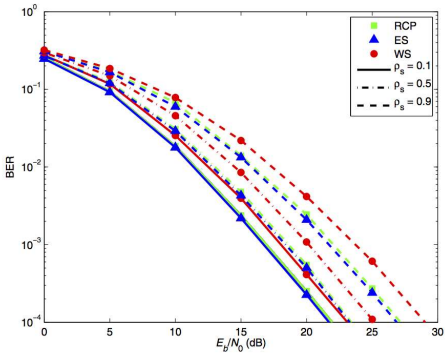

(b) η_s = 5 bits/s/Hz (N_t = 32), N = 8 (QPSK)

Fig. 4. BER performance of RCP against E_b/N_0 with N_r = 2 over c.i.d. Rayleigh fading

while the performance of WS compared to ES worsens as the correlation increases. To achieve a target BER of 1×10^{-4} in the case of $\binom{N_t=32}{N=8}$, when compared with WS, RCP exhibits SNR gains of 1.1 dB and 2.0 dB at $\rho_s = 0.1$ and 0.9, respectively.

B. Comparison between RCP and ICP

The comparison between RCP and ICP at an E_b/N_0 of 25 dB is demonstrated in Fig. 5. It can be observed that ICP provides an upper bound of BER, while the performance of RCP is very close to this bound. Furthermore, the gap between RCP and ICP decreases further when the correlation changes from the medium to two extremes. This is expected as both

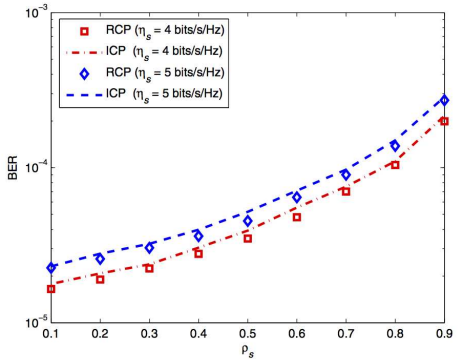

Fig. 5. RCP v.s. ICP for N = 8, N_r = 2 with E_b/N_0 = 25 dB

TABLE I
SIMULATION CONFIGURATIONS. TRANSMISSION OF 5 BITS/S/HZ WITH N_r = 2, USING TOSM AND FIXED-SM SCHEMES

ρ_s	TOSM	fixed-SM (N=2)	fixed-SM (N=32)
0.1	N = 8, QPSK	N = 2, 16PSK	SSK
0.5	N = 8, QPSK		
0.9	N = 4, 8PSK		

methods are identical for the extreme cases of $\rho_s = 0$ and 1. Similar, but less pronounced trends are observed at lower SNRs.

C. Energy Consumption

It is shown in [15] that SM exhibits significant energy savings compared to other MIMO techniques since it only requires a single transmitter chain including a single power amplifier, regardless of the number of antennas used. Motivated by this key property of SM, we compare the energy consumption of TOSM with conventional fixed-SM schemes. The sizes of spatial and signal constellations for each scheme are arranged in Table I. More specifically, TOSM is performed by combining with different TAS methods mentioned previously to illustrate the advantages of the proposed scheme. The optimal N for TOSM is determined by the approach proposed in [10]. To carry out a fair comparison, the fixed-SM scheme with two antennas uses the antennas at the two ends of the diagonal, which provide the largest separation. Simulations are implemented using the parameters listed in Table II. With the aim to evaluate the RF output energy consumption at the transmitter, we assume the free space path loss is 100 dB.

TABLE II
SIMULATION PARAMETERS

Parameter	Value
Carrier frequency	2 GHz
Path loss	100 dB, without shadowing
Operating temperature T	290 K
Target BER	1×10^{-4}

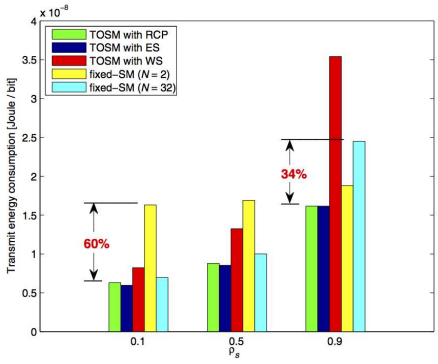

Fig. 6. Transmit energy consumption for η_s = 5 bits/s/Hz, N_r = 2 with a target BER = 1×10^{-4}

From Fig. 6, the following outcomes are observed. Firstly, RCP closely approaches the performance of ES with the difference of 5.7% and 2.8% for $\rho_s = 0.1$ and 0.5, respectively. When $\rho_s = 0.9$, the energy efficiency of RCP is equal to that of ES. This is because both schemes arrive at the same selection pattern for $N = 4$. The energy efficiency performance of WS is inferior to all other schemes, especially at high channel correlations where it causes TOSM to perform worse than the fixed-SM schemes. Secondly, the energy saving of TOSM is up to 34% compared to fixed-SM ($N = 32$) for various correlations. In other words, more transmit antennas may not provide a larger multiplexing gain for SM. The reasons for this are two fold: 1) high correlations result in compact points in the spatial constellation; 2) the signal constellation can balance the minimum Euclidean distance when the spatial constellation is becoming too dense. As can be seen, when the correlation increases, the increasing speed of energy consumption is proportional to N. Thus, when compared with fixed-SM ($N = 2$), TOSM obtains a greater energy saving (up to 60%) at lower correlations.

V. CONCLUSION

In this paper, a direct TAS approach called RCP, which is based on circle packing, has been proposed for TOSM. Results show that for various channel correlations and spectral efficiencies, the proposed scheme closely approaches the performance of the exhaustive search while achieving a negligible computational complexity. On the contrary, conventional TAS techniques which are based on an exhaustive search or partial search, have an exponentially increasing complexity. This benefit makes RCP more suitable for high spectral efficiencies. Moreover, the number of required transmit antennas is the only information that needs to be known at the transmitter for RCP. When compared to fixed-SM schemes, RCP-based TOSM reduces the transmit energy consumption by up to 60%. All these merits make RCP-based TOSM a promising scheme for low-complexity, highly energy-efficient transceivers and an ideal candidate for large MIMO systems. Futher researches will involve more advanced cases, such as imperfect exponential correlation model and arbitrary correlation matrices.

ACKNOWLEDGEMENT

We gratefully acknowledge support from the European Union (PITNGA2010264759, GREENET project) for this work.

REFERENCES

[1] M. Di Renzo, H. Haas, and P. M. Grant, "Spatial Modulation for Multiple-Antenna Wireless Systems: A Survey," *IEEE Commun. Mag.*, vol. 49, no. 11, pp. 182–191, Nov. 2011.

[2] R. Mesleh, H. Haas, C. W. Ahn, and S. Yun, "Spatial Modulation – A New Low Complexity Spectral Efficiency Enhancing Technique," in *IEEE International Conference on Communication and Networking in China (CHINACOM)*, Beijing, China, Oct. 25–27, 2006, pp. 1–5.

[3] R. Mesleh, H. Haas, S. Sinanović, C. W. Ahn, and S. Yun, "Spatial Modulation," *IEEE Trans. Veh. Technol.*, vol. 57, no. 4, pp. 2228 – 2241, July 2008.

[4] M. D. Renzo and H. Haas, "Performance analysis of spatial modulation," in *Communications and Networking in China (CHINACOM), 2010 5th International ICST Conference on*, aug. 2010, pp. 1 –7.

[5] M. Di Renzo and H. Haas, "Bit Error Probability of SM-MIMO Over Generalized Fading Channels," *IEEE Trans. Veh. Technol.*, vol. 61, no. 3, pp. 1124 –1144, March 2012.

[6] R. Mesleh, M. Di Renzo, H. Haas, and P. M. Grant, "Trellis Coded Spatial Modulation," *IEEE Trans. on Wireless Commun.*, vol. 9, no. 7, pp. 2349–2361, July 2010.

[7] P. Yang, Y. Xiao, L. Li, Q. Tang, Y. Yu, and S. Li, "Link Adaptation for Spatial Modulation With Limited Feedback," *IEEE Trans. Veh. Technol.*, vol. 61, no. 8, pp. 3808 –3813, Oct. 2012.

[8] R. Rajashekar, K. Hari, and L. Hanzo, "Antenna Selection in Spatial Modulation Systems," *IEEE Commun. Lett.*, vol. 17, no. 3, pp. 521 – 524, March 2013.

[9] X. Wu, S. Sinanovic, M. Di Renzo, and H. Haas, "Structure Optimisation of Spatial Modulation over Correlated Fading Channels," in *2012 IEEE Global Communications Conference (GLOBECOM)*, Dec. 2012, pp. 4049 –4053.

[10] ——, "Base Station Energy Consumption for Transmission Optimised Spatial Modulation (TOSM) in Correlated Channels," in *Computer Aided Modeling and Design of Communication Links and Networks (CAMAD), 2012 IEEE 17th International Workshop on*, Sept. 2012, pp. 261 –265.

[11] S. Loyka, "Channel Capacity of MIMO Architecture Using the Exponential Correlation Matrix," *IEEE Commun. Lett.*, vol. 5, no. 9, pp. 369 –371, Sept. 2001.

[12] J. Jeganathan, A. Ghrayeb, and L. Szczecinski, "Spatial Modulation: Optimal Detection and Performance Analysis," *IEEE Commun. Lett.*, vol. 12, no. 8, pp. 545–547, 2008.

[13] N. Serafimovski, M. Di Renzo, S. Sinanović, R. Y. Mesleh, and H. Haas, "Fractional Bit Encoded Spatial Modulation (FBE–SM)," *IEEE Commun. Lett.*, vol. 14, no. 5, pp. 429–431, May 2010.

[14] K. Stphenson, *Introduction to Circle Packing: The Theory of Discrete Analytic Function*. Cambridge University Press, 2005.

[15] A. Stavridis, S. Sinanovic, M. Di Renzo, H. Haas, and P. Grant, "An energy saving base station employing spatial modulation," in *Computer Aided Modeling and Design of Communication Links and Networks (CAMAD), 2012 IEEE 17th International Workshop on*, Sept. 2012, pp. 231 –235.

2013 IEEE 24th International Symposium on Personal, Indoor and Mobile Radio Communications: Fundamentals and PHY Track

Channel Estimation for Spatial Modulation

Xiping Wu*, Marco Di Renzo†, and Harald Haas*

*Institute for Digital Communications
Joint Research Institute for Signal and Image Processing
School of Engineering
The University of Edinburgh
EH9 3JL, Edinburgh, UK
{xiping.wu, h.haas}@ed.ac.uk

†French National Centre for Scientific Research (CNRS)
Laboratory for Signals and Systems (LSS)
École Supérieure d'Électricité (SUPELEC)
3 rue Joliot-Curie, 91192 Gif-sur-Yvette (Paris), France
marco.direnzo@lss.supelec.fr

***Abstract*—In single-stream multiple-input multiple-output (MIMO) schemes, such as spatial modulation (SM) and space shift keying (SSK), a single transmit antenna is activated at any given time. Therefore, unlike multi-stream MIMO transmitters, simultaneous pilot transmissions are prohibitive because of a single radio-frequency (RF) chain. In state-of-the-art literature, the channels of different transmit antennas are individually estimated. As a result, more time is required to transfer pilots and the effective data rate is compromised. In this paper, we propose a novel channel estimation (CE) technique for single-stream MIMO systems. Given a pilot ratio, the proposed scheme achieves the same estimation period as multi-stream MIMO systems without needing any additional information or feedback. Simulations are implemented under a practical base station environment. Results show that for various speeds of the mobile user, the proposed approach significantly improves the performance of SM in comparison to the conventional CE method.**

***Index Terms*—Channel estimation, multiple-input multiple-output (MIMO), single-stream, spatial modulation (SM)**

I. Introduction

WIRELESS systems continue to strive for exponentially increasing traffic loads. To mitigate the enormous resource consumption in bandwidth and energy, the space domain has been exploited to increase the channel capacity, *i.e.,* multiple-input multiple-output (MIMO) systems. With respect to the number of activated transmit antennas, MIMO techniques can be categorized into two types: multi-stream and single-stream. Multi-stream MIMO schemes, such as vertical Bell Labs layered space-time (V-BLAST) and space-time block coding (STBC), convey different information through multiple active transmit antennas. In contrast, spatial modulation (SM) is a relatively new single-stream MIMO transmission technique, which achieves a multiplexing gain by considering antenna locations as spatial constellation points [1], [2]. Unlike conventional multi-stream MIMO schemes, SM activates only one antenna at a given time and therefore, fully avoids inter-channel interference (ICI). In [1]–[3], assuming perfect channel state information (CSI), it has been presented that SM offers a better performance than many state-of-the-art MIMO schemes while achieving a low-complexity implementation.

However, perfect channel knowledge is always impractical and channel estimation (CE) is essential to all of the above schemes. A massive body of literature, *e.g.*, [4] and [5], exists on the topic of CE for multi-stream MIMO systems, in which all channels can be estimated simultaneously. Meanwhile, regardless of the number of antennas used, SM only employs a single radio-frequency (RF) chain including a single power amplifier and thus, exhibits significant energy savings [6]. However, at each time, the pilots can be sent out through only one transmit antenna as well. Consequently, using pilot-based channel estimation, only the channel knowledge of the active transmit antenna can be obtained at the receiver. This leads to a challenge in channel estimation for single-stream MIMO techniques, since more time is required to estimate the full MIMO channel. In other words, for a fixed pilot ratio, *i.e.*, the ratio between pilot and total transmission time, the estimation period is proportional to the number of transmit antennas. Therefore, single-stream MIMO schemes suffer more from CE errors, especially for a fast fading scenario. Until now, little research has been conducted in this field. To the best of the authors' knowledge, only in [7] and [8], CE techniques specifically tailored for SM are proposed. They use recursive least-square (RLS) and joint channel estimation with data detection, respectively. However, both methods were developed based on existing techniques and did not cope with the issue of more estimation time consumption.

Against this background, a novel channel estimation approach for single-stream MIMO schemes is proposed in this paper. By exploiting channel correlation, this new method greatly reduces the channel estimation time without increasing the pilot ratio. Moreover, there is no need for any extra information or feedback. An SM system is considered to study the proposed method and to evaluate its performance compared to a conventional CE technique used as a benchmark. A practical spatial channel model [9], which is consistent with a channel model developed within the 3rd Generation Partnership Project (3GPP), is used to validate our technique. Simulation results demonstrate that the proposed method significantly outperforms the benchmark channel estimation scheme.

The remainder of this paper is organized as follows. Section II describes the system model, including the SM structure, channel model and channel estimator. In Section III, the novel channel estimation approach for SM is proposed. Section IV presents the simulation results. The paper is summarized in Section V.

978-1-4577-1348-4/13/$31.00 ©2013 IEEE

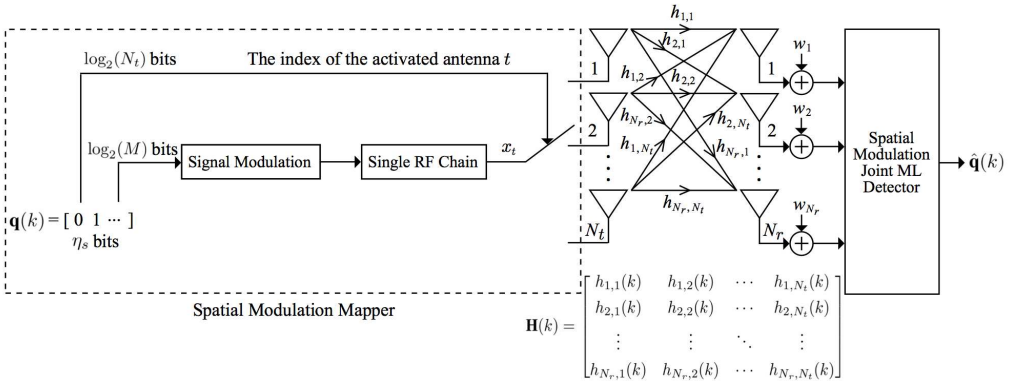

Fig. 1. $N_t \times N_r$ Spatial Modulation System Model

II. System Model

A. MIMO System

A $N_t \times N_r$ SM-MIMO system is considered where N_t and N_r are the numbers of transmit antennas and receive antennas, respectively. Fig. 1 illustrates the system structure which is comprised of an SM mapper, N_t transmit antennas, MIMO channels, N_r receive antennas, and a detector.

In the SM mapper, the bit stream is divided into blocks with the length of η_s bits, where η_s represents the spectrum efficiency. The block at the discrete time index k is denoted as $\mathbf{q}(k)$. Each block is then split into two units of $\log_2(N_t)$ bits and $\log_2(M)$ bits, where $M = 2^{\eta_s}/N_t$ is the size of signal constellation points. The first part activates a single antenna from the spatial constellation, and we denote the currently active transmit antenna as t. The second part determines the corresponding symbol from a specific signal constellation diagram, such as quadrature amplitude modulation (QAM) and phase shift keying (PSK), and sends it through the activated antenna. Thus, the transmitted signal can be represented by a vector $\mathbf{x} = [x_1, x_2, ..., x_{N_t}]^T$, where all elements are zero except x_t.

By denoting the channel gain between the i-th transmit antenna and the j-th receive antenna as $h_{j,i}$, the MIMO channel $\mathbf{H}$ can be written as:

$$\mathbf{H} = \begin{bmatrix} h_{1,1} & h_{1,2} & \cdots & h_{1,N_t} \\ h_{2,1} & h_{2,2} & \cdots & h_{2,N_t} \\ \vdots & \vdots & \ddots & \vdots \\ h_{N_r,1} & h_{N_r,2} & \cdots & h_{N_r,N_t} \end{bmatrix} \quad (1)$$

and the received signal at the k-th time index is given by:

$$\mathbf{y}(k) = \mathbf{H}(k)\mathbf{x}(k) + \mathbf{w}(k) \quad (2)$$

where $\mathbf{w} = [w_1, w_2, ..., w_{N_r}]^T$ is the noise vector. At the input of each receive antenna, the noise is assumed to be a complex Additive White Gaussian Noise (AWGN) process with distribution $\mathcal{CN}(0, N_0)$. Across the receive antennas, the noise components are statistically independent. We define the signal-to-noise ratio (SNR) as $\gamma = E_m/N_0$, where E_m is the average energy per symbol transmission. At the receiver, estimated CSI is used to decode the transmitted symbol by the joint maximum likelihood (ML) detection.

TABLE I
Parameters Setting of Spatial Channel Model

Parameter	Value
Number of BS Elements	N_t
Number of MS Elements	N_r
Height of BS	32 m
Height of MS	1.5 m
BS Antenna Separation	1 wavelength
MS Velocity	1 / 5 / 10 m/s
Scenario	'urban micro'
Number of Paths	6
Carrier Center Frequency	2 GHz

B. Channel Model

With the aim to evaluate the proposed approach in a practical environment, the spatial channel model (SCM) proposed in [9] is implemented. Complying with 3GPP TR 25.996, this particular model provides time-variant channels for MIMO simulations. In order to offer a reasonable separation between transmit antennas, simulations are carried out assuming the downlinks. Three scenarios are supported in SCM: urban macro, urban micro and suburban macro. In this paper the urban micro scenario with a single user is assumed, and path loss and lognormal shadowing are not considered. Furthermore for each channel realization, the mobile user is uniformly distributed in a circular cell with the inner and outer radius of 35 and 500 meters, respectively. Some important parameters are specified in Table I. Due to the space limitation, we refer

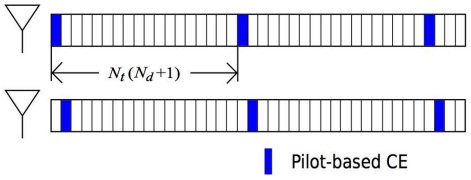

Fig. 2. Block diagram of conventional channel estimation for SM

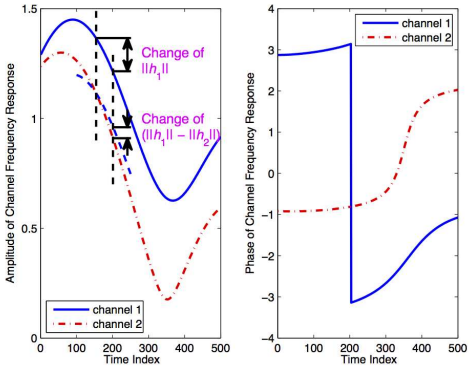

Fig. 3. Channel realization based on SCM

the interested reader to [9] for more detailed information about the channel model.

C. Least Square Estimator

In this paper, least square (LS) technique is applied for pilot-based channel estimation in both the conventional and proposed methods. As only the t-th element in $\mathbf{x}(k)$ is nonzero, the signal obtained at the j-th receive antenna in (2) can be simplified to:

$$y_j(k) = h_{j,t}(k)x_t(k) + w_j(k) \tag{3}$$

According to [10, p. 224, Eq. (8.9)], the LS estimator of the above equation is given by:

$$\hat{h}_{j,t}(k) = \arg\min_{h} \|y_j(k) - hx_t(k)\|^2 \tag{4}$$

Since $x_t(k)$ and $y_j(k)$ are both scalar, the channels of the t-th transmit antenna are estimated by:

$$\hat{h}_{j,t}(k) = \frac{y_j(k)}{x_t(k)}, \qquad j = 1, 2, ..., N_r \tag{5}$$

III. Channel Estimation

A. Conventional Channel Estimation

For single-stream MIMO schemes, conventional methods estimate the channels of different transmit antennas sequentially [7]. In Fig. 2, an illustration of the sequential CE procedure is shown for a two-stream system. As can be seen, the CE

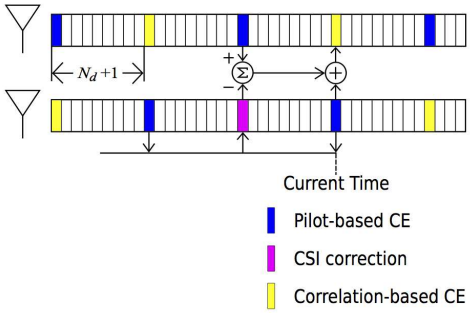

Fig. 4. Block diagram of the proposed channel estimation method

process takes up two time slots. The time interval between two successive CE samples for the same transmit antenna is defined by the estimation period T_{CE}. By denoting the symbol time as T_s, the estimation period of the conventional CE method is calculated by:

$$T_{\text{CE}} = N_t(N_d + 1)T_s \tag{6}$$

where N_d is the ratio between data and pilot slots for one full channel estimation period, *i.e.*, the number of data symbols per pilot.

B. Proposed Method

In practice, MIMO channels are correlated to some degree because of the limited separation between antennas and the given propagation environment. Based on SCM, Fig. 3 presents a realization for the channels from different transmit antennas to the same receive antenna. The margin between two such channels is defined by channel difference. It can be observed that, the change of the channel difference is relatively slow in contrast with the change of the actual channels which is due to the channel correlation. This effect can be exploited to improve the CE performance of single chain MIMO systems. Fig. 4 demonstrates the concept of the proposed method. Unlike the conventional scheme, the pilots for different antennas are equally distributed along the time axis. For a concise expression, we denote the index of the estimation points as n as the index of data is not involved in the estimation procedure. At any estimation point, the algorithm encompasses four steps:

i) Pilot-based CE: In this step, the pilot is sent through the t-th transmit antenna like in the conventional method. At each receive antenna, the channel from the currently activated antenna is estimated by a specific estimator (LS in this paper) and denoted as $\hat{h}_t(n)$.

ii) CSI correction: For each transmit antenna, the pilot is conveyed once for every N_t estimation points. The previous $N_t - 1$ estimated CSIs of the t-th antenna are obtained via the correlation-based CE described in step iii. Those points can be corrected by a low-pass interpolation based on the current channel estimation $\hat{h}_t(n)$ and $L-1$ previous estimates

$\hat{h}_t(n - lN_t), l = 1, 2, \ldots, L-1$. The number of used estimates for the currently active antenna, *i.e.*, L, is defined by the interpolation sequence length. After being obtained from the interpolation, the corrected CSI of the t-th transmit antenna is denoted as $\dot{h}_t(n - n')$, where $n' = 1, 2, \ldots, N_t - 1$.

Regarding the i-th transmit antenna, the latest pilot-based CE happened at $n'_{i,t}$ time slots before where:

$$n'_{i,t} = \begin{cases} t - i & \text{if} \quad i < t \\ t - i + N_t & \text{if} \quad i > t \end{cases} \tag{7}$$

Thus at the time index $n - n'_{i,t}$, the difference between the channels of the i-th and the t-th antennas can be expressed as:

$$\Delta J_{i,t}(n - n'_{i,t}) = \hat{h}_i(n - n'_{i,t}) - \dot{h}_t(n - n'_{i,t}) \tag{8}$$

iii) Correlation-based CE: In contrast to the individual channel variations, the difference between channels can be assumed changing less rapidly. Then, the estimated CSI for those inactive antennas, denoted as $\tilde{h}_i(n)$, can be computed based on $\hat{h}_t(n)$ and the previous channel difference:

$$\tilde{h}_i(n) = \hat{h}_t(n) + \Delta J_{i,t}(n - n'_{i,t}), \quad i \neq t \tag{9}$$

During the following data transmissions, $\hat{h}_t(n)$ and $\tilde{h}_i(n)$ are used for decoding.

iv) Antenna index update: At last, the index of the antenna to convey the pilot next time is updated to:

$$t = \begin{cases} t + 1 & \text{if} \quad t < N_t \\ 1 & \text{if} \quad t = N_t \end{cases} \tag{10}$$

It is worth noting that all computations are processed at the receiver and no additional feedback is required. Apart from this, the computational complexity is linear to N_t. By applying the proposed method, the estimation period is reduced to:

$$T_{\text{CE}} = (N_d + 1)T_s \tag{11}$$

IV. Simulation Results

In this section, the performance of SM based on the novel channel estimation method is evaluated under the practical environment depicted in Sec. II. Two benchmarks are considered for comparison: i) the conventional method, which is denoted as "CCE" in the sequel; ii) SM with perfect CSI. According to the long term evolution (LTE) standards [11], the symbol time $T_s = 0.07$ ms and the pilot ratio is given by $\frac{1}{21}$, *i.e.*, $N_d = 20$. Additionally, in order to balance the accuracy against the complexity, the interpolation sequence length in the proposed method is chosen to be $L = 9$.

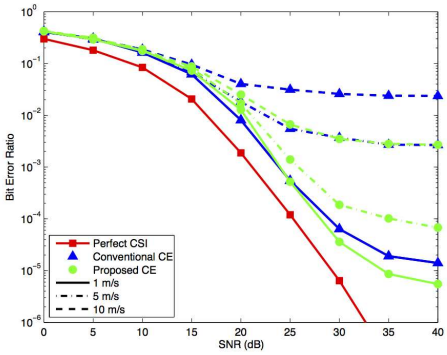

(a) QPSK, 2×2 SM-MIMO

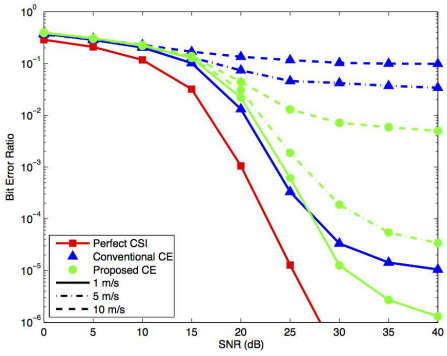

(b) BPSK, 4×2 SM-MIMO

Fig. 5. BER performance of SM over realistic channels at 3 bits/s/Hz

A. BER Performance

Fig. 5 presents the bit error ratio (BER) performance of SM as a function of the SNR, which is the same for pilots and data, for different number of transmit antennas, *i.e.*, the power for data symbols and pilots is assumed to be the same. In Fig. 5(a), a 2×2 SM system with quadrature PSK (QPSK) is considered for various speeds of the mobile user. It is worth noting that the case of perfect CSI is independent of the user velocity. Unfortunately, the performance in the presence of estimation error decreases while the speed increases. In addition, the BER performance tends towards stability with increasing SNR. This is because the CE error becomes the dominant factor instead of noise. When compared to CCE, in general terms, the performance of the novel approach is closer to the performance of perfect CSI. At 1 m/s, the proposed method outperforms CCE when SNR is larger than 25 dB. However, for a larger user velocity, the proposed scheme is always better than CCE. The reasons are twofold: i) at a low velocity, the channel fading is relatively slow and thus, the

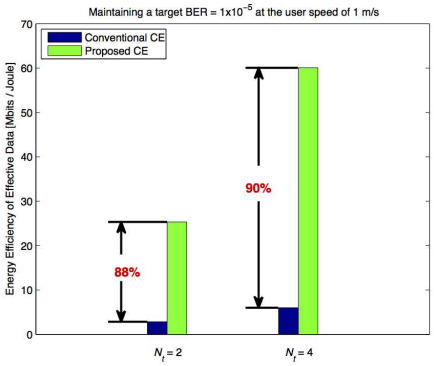

Fig. 6. Transmit energy consumption

benefit of the proposed method do not fully come into play; ii) when transferring pilots with a smaller SNR, the impact of the CE error is strong which causes the correlation-based CE to suffer from error propagation.

The same evaluation for a 4×2 SM is studied in Fig. 5(b). Assuming perfect CSI, SM with four transmit antennas, which exploits more spatial information, is better than two-transmitter SM in BER performance. However, SM based on CCE performs much worse when compared to the $N_t = 2$ scenario. Given an example of 5 m/s, the achievable BER of CCE-based SM drops from 2.7×10^{-3} to 3.4×10^{-2}. The reason for this is that CCE has a longer estimation period with increasing N_t and the estimation error is correspondingly much larger. In contrast, SM based on the proposed method can still benefit from the larger N_t because its CE period is regardless of N_t. In the same situation, the achievable BER is improved from 6.8×10^{-5} to 3.3×10^{-5} by applying the proposed approach.

B. Energy Efficiency

In this section, the transmitted data (not including the pilots) per unit energy is compared between the conventional and proposed CE methods in different N_t. With the aim to calculate the RF output energy consumption at the transmitter, we assume the free-space path loss is 100 dB, which corresponds to an average receiver-transmitter separation of 1200 m assuming the channel model used in this paper [9]. From Fig. 6, the following outcomes can be observed. Firstly, comparing the proposed method with CCE, the data amount per unit energy is increased by 8.3 and 10.0 times for $N_t = 2$ and $N_t = 4$, respectively. In other words, the novel approach saves 88% and 90% RF output energy to convey the same amount of data. Secondly, when the number of transmit antennas is increased from two to four, the increase of data per unit energy in SM based on the proposed method is much larger than CCE.

V. Conclusion

A novel channel estimation scheme has been proposed for single-stream MIMO systems. Unlike conventional methods, where the channels from different antennas are individually estimated, the proposed approach exploits the correlation information between transmit antennas. Without the need for feedback, the proposed technique achieves the same estimation period as multi-stream MIMO schemes, and consequently, the channel estimation time is independent of the number of transmit antennas. In contrast, the channel estimation period of the conventional method for single RF chain MIMO systems is proportional to the number of transmit antennas. Simulation results assuming a 3GPP channel model show that the proposed method significantly outperforms the conventional channel estimation scheme, especially for a fast fading scenario. By applying the proposed method, the SM-MIMO systems can save up to 90% RF output energy. Furthermore, the proposed channel estimation approach allows SM to be used in deployment scenarios where it unfolds its main advantages which is in large antenna systems. This significant improvement makes SM a promising candidate for practical future large MIMO systems.

Acknowledgement

We gratefully acknowledge support from the European Union (GREENET project) for this work.

References

[1] R. Mesleh, H. Haas, C. W. Ahn, and S. Yun, "Spatial Modulation - A New Low Complexity Spectral Efficiency Enhancing Technique," in *Communications and Networking in China, 2006. ChinaCom '06. First International Conference on*, Oct. 2006, pp. 1 –5.

[2] R. Mesleh, H. Haas, S. Sinanović, C. W. Ahn, and S. Yun, "Spatial Modulation," *IEEE Trans. Veh. Technol.*, vol. 57, no. 4, pp. 2228 – 2241, July 2008.

[3] M. D.Renzo and H. Haas, "Bit Error Probability of SM-MIMO over Generalized Fading Channels," in *IEEE Trans. Veh. Technol.*, vol. 61, no. 3, march 2012, pp. 1124 –1144.

[4] S.-J. Lee, "On the training of MIMO-OFDM channels with least square channel estimation and linear interpolation," *IEEE Commun. Lett.*, vol. 12, no. 2, pp. 100–102, 2008.

[5] Z. Luo and F. Yang, "Joint maximum-likelihood channel estimation and data detection for v-blast systems," in *IEEE Global Telecommun. Conference (GLOBECOM)*, 2008, pp. 1–5.

[6] A. Stavridis, S. Sinanovic, M. Di Renzo, H. Haas, and P. Grant, "An energy saving base station employing spatial modulation," in *Computer Aided Modeling and Design of Communication Links and Networks (CAMAD), 2012 IEEE 17th International Workshop on*, sept. 2012, pp. 231 –235.

[7] M. Faiz, S. Al-Ghadhban, and A. Zerguine, "Recursive least-squares adaptive channel estimation for spatial modulation systems," in *Communications (MICC), 2009 IEEE 9th Malaysia International Conference on*, 2009, pp. 785–788.

[8] S. Sugiura and L. Hanzo, "Effects of channel estimation on spatial modulation," *IEEE Signal Processing Lett.*, vol. 19, no. 12, pp. 805–808, 2012.

[9] J. Salo, G. Del Galdo, J. Salmi, P. Kyösti, M. Milojevic, D. Laselva, and C. Schneider, "MATLAB implementation of the 3GPP Spatial Channel Model (3GPP TR 25.996)," On-line, Jan. 2005.

[10] S. M. Kay, *Fundamentals of Statistical Signal Processing: Estimation Theory*, 1st ed. Prentice Hall PTR, 1993.

[11] J. Berkmann, C. Carbonelli, F. Dietrich, C. Drewes, and W. Xu, "On 3G LTE Terminal Implementation - Standard, Algorithms, Complexities and Challenges," in *Wireless Communications and Mobile Computing Conference, 2008. IWCMC '08. International*, Aug. 2008, pp. 970 –975.

2013 IEEE 18th International Workshop on Computer Aided Modeling and Design of Communication Links and Networks (CAMAD)

Effect of Pilot Ratio on Channel Estimation for Spatial Modulation

Xiping Wu*, Marco Di Renzo†, and Harald Haas*

*Institute for Digital Communications
Joint Research Institute for Signal and Image Processing
School of Engineering
The University of Edinburgh
EH9 3JL, Edinburgh, UK
{xiping.wu, h.haas}@ed.ac.uk

†French National Centre for Scientific Research (CNRS)
Laboratory for Signals and Systems (LSS)
École Supérieure d'Électricité (SUPELEC)
3 rue Joliot-Curie, 91192 Gif-sur-Yvette (Paris), France
marco.direnzo@lss.supelec.fr

***Abstract*—Spatial modulation (SM) is a single-stream multiple-input multiple-output (MIMO) technique which only activates one transmit antenna at a time. Apart from the complete avoidance of inter-channel interference, SM also exhibits a great energy saving in the radio-frequency (RF) chain. However, in contrast to multi-stream MIMO systems, channel estimation (CE) for SM becomes a challenge since the MIMO channel cannot be estimated in one transmission step due to the single RF chain. Motivated by this fact, a novel CE scheme has been recently proposed which exploits the channel correlation and jointly estimates the channels for different transmit antennas. Without needing feedback, this new method achieves the same estimation period as multi-stream MIMO schemes. In this paper, a varying pilot ratio has been investigated in SM for both the conventional and the novel CE methods. Balancing the accuracy and the amount of data, an optimal pilot ratio can be achieved for the peak throughput. Simulation results present that the novel CE approach significantly outperforms the conventional method with a much lower optimal pilot ratio.**

***Index Terms*—Channel estimation, pilot ratio, spatial modulation (SM), single-stream, MIMO**

I. Introduction

During the past decade, multiple-input multiple-output (MIMO) techniques have been studied as a means to exploit the space domain to increase the channel capacity. With respect to the number of active transmit antennas, MIMO systems can be classified to multi-stream and single-stream. Two typical multi-stream MIMO schemes are vertical Bell Labs layered space-time (V-BLAST) [1] and space-time block coding (STBC) [2], in which different data streams are transferred through multiple antennas simultaneously. In contrast, considering antenna locations as spatial constellation points, spatial modulation (SM) is a relatively new single-stream MIMO system [3]. Unlike multi-stream MIMO schemes, SM activates a single antenna at any given time and, thus, entirely avoids inter-channel interference. Furthermore, SM exhibits a significant saving in quiescent power at the power amplifier stage since it requires only one radio-frequency (RF) chain, regardless of the number of antennas used.

In both schemes, channel state information (CSI) is required at the receiver for decoding. As a result, channel estimation (CE) is of vital importance, but it is often neglected and ideal CSI is assumed. While the usage of a single RF chain brings the previously mentioned advantages to SM, it leads to a challenge in CE. Unlike multi-stream MIMO schemes, SM requires more time to transmit pilots. In [4], a channel estimation scheme for SM using the recursive least-square (RLS) is proposed. Based on joint channel estimation with data detection, another CE method is introduced in [5]. However, in both methods, channels for different transmit antennas are individually estimated which is referred to conventional CE (CCE) in this paper. Given a proportion between the pilot and total symbols, *i.e.*, pilot ratio, the estimation period of CCE is proportional to the number of transmit antennas. In other words, the throughput of SM is compromised to maintain a certain estimation period. To overcome this issue, we proposed a novel CE approach for single-stream MIMO in [6]. On the basis of channel correlation, this new method requires the same channel estimation time as multi-stream MIMO schemes without needing extra transmission or feedback. It has been shown that, under a practical base station environment, the proposed scheme can greatly improve the bit error ratio (BER) performance of SM when compared to CCE.

In this paper, the effect of pilot ratio is investigated in both the conventional and novel CE methods for SM. Pilot ratios are essential for channel estimation in two aspects. On the one hand, a larger pilot ratio can increase the estimation accuracy and, thus, reduce the need for retransmissions. On the other hand, the data rate is compromised since more time is required to send the pilots. Therefore, by trading off between these two factors, an appropriate pilot ratio can be determined to achieve the peak throughput. Simulations are conducted for a single mobile user under a practical spatial channel model [7], which complies with 3rd Generation Partnership Project (3GPP) TR 25.996. Results show that the proposed approach achieves a much larger throughput than CCE.

The rest of this paper is organized as follows. Section II describes the system model. In Section III, the conventional and the novel CE methods for SM are respectively introduced. Section IV states the criterion to evaluate the performance on different pilot ratios. The simulation results are presented in Section V. The paper is summarized in Section VI.

978-1-4673-4919-2/13/$31.00 ©2013 IEEE

2013 IEEE 18th International Workshop on Computer Aided Modeling and Design of Communication Links and Networks (CAMAD)

II. System Model

A. MIMO system

A $N_t \times N_r$ SM system is considered in this paper, where N_t and N_r represent the numbers of transmit and receive antennas, respectively. In the SM encoding procedure, the bit stream is divided into blocks with the length of η_s bits, where η_s denotes the number of bits per symbol. Each block is then split into two units, corresponding to the spatial constellation diagram and the signal constellation diagram. The first part of $\log_2(N_t)$ bits activates a single transmit antenna from the antenna array. We use t to represent the currently active antenna. The second part of the rest bits is used to select a symbol from a specific signal constellation, such as quadrature amplitude modulation (QAM) or phase shift keying (PSK). Then the chosen symbol is sent out through antenna t.

The signal to be transmitted can be represented by a vector $\mathbf{x} = [x_1, \ldots, x_t, \ldots, x_{N_t}]^T$, where the t-th element is the chosen symbol while others are zero. Denoting the channel gain between the i-th transmit antenna and the j-th receive antenna as $h_{j,i}$, the MIMO channel $\mathbf{H}$ is written as:

$$\mathbf{H} = \begin{bmatrix} h_{1,1} & h_{1,2} & \cdots & h_{1,N_t} \\ h_{2,1} & h_{2,2} & \cdots & h_{2,N_t} \\ \vdots & \vdots & \ddots & \vdots \\ h_{N_r,1} & h_{N_r,2} & \cdots & h_{N_r,N_t} \end{bmatrix} \tag{1}$$

The received signal is also a vector which can be expressed as:

$$\mathbf{y} = \mathbf{H}\mathbf{x} + \mathbf{w} \tag{2}$$

where $\mathbf{w} = [w_1, \ldots, w_j, \ldots, w_{N_r}]^T$ is the noise vector with each element representing the noise at the input of each receive antenna. Complex Additive White Gaussian Noise (AWGN) is assumed, , *i.e.*, $w_j \sim \mathcal{CN}(0, N_0)$. Across the receive antennas, the noise is statistically independent. The signal-to-noise ratio (SNR) is defined by E_m/N_0, where E_m represents the average energy per symbol transmission. Joint maximum likelihood (ML) detection [8] is used to decode the transmitted symbol utilizing the estimated CSI.

B. Channel Model

The spatial channel model (SCM) [7], complying with 3GPP TR 25.996, is considered in this paper to generate time-variant channels for MIMO simulations. In order to provide a reasonable separation between transmit antennas, simulations are implemented in downlink. In SCM, three scenarios are supported: urban macro, urban micro and suburban macro. In this paper, the urban micro scenario is assumed for a single user. Moreover, for each channel realization, the user is uniformly distributed in a circular cell with the inner and outer radius of 35 m and 500 m. Table I specifies the parameters used the simulations. Due to the space limitation, we refer the interested reader to [7] for more detailed information about the channel model.

TABLE I
Parameters Setting in Spatial Channel Model

Parameter	Value
Number of BS Elements	N_t
Number of MS Elements	N_r
Height of BS	32 m
Height of MS	1.5 m
BS Antenna Separation	1 wavelength
MS Velocity	1 / 5 / 10 m/s
Scenario	'urban micro'
Number of Paths	6
Carrier Center Frequency	2 GHz

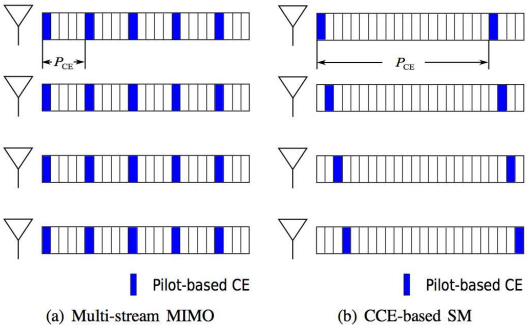

(a) Multi-stream MIMO (b) CCE-based SM

Fig. 1. Transfer procedure of pilots

III. Channel Estimation Methods

A. Conventional Channel Estimation (CCE) for SM

Conventional channel estimation for SM estimates the channels of different transmit antennas individually. The corresponding pilot structure is illustrated in Fig. 1, alongside a comparison with multi-stream MIMO. The time interval between two successive CE samples for the same transmit antenna is defined by the estimation period. For each estimation period, the transmit antennas are activated one by one to convey the pilots in CCE. It can be observed that, to achieve the same pilot ratio, CCE-based SM requires a much longer estimation period than multi-stream MIMO shemes. The pilot ratio is denoted as η, and the estimation period for CCE is given by:

$$T_{\text{CCE}} = \frac{N_t T_s}{\eta} \tag{3}$$

where T_s represents the symbol period.

At each channel estimation slot assuming CCE, a specific estimator, such as least square (LS), minimum mean square error (MMSE) or recursive least square (RLS) [9], is applied to estimate the CSI of the currently activated antenna. For a fair comparison, LS is assumed in both CCE and the novel approach described in the following paragraph.

2013 IEEE 18th International Workshop on Computer Aided Modeling and Design of Communication Links and Networks (CAMAD)

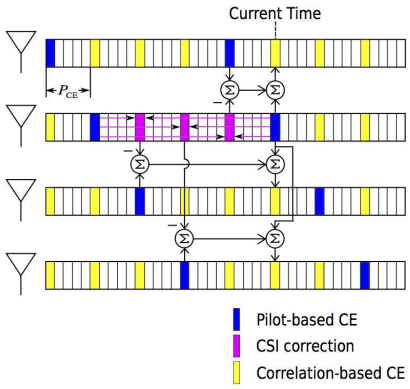

Fig. 2. Transmit cross channel estimation

B. Transmit Cross Channel Estimation (TCCE)

A novel CE method exploring the channel correlation is proposed in [6]. Fig. 2 demonstrates the concept of this approach which jointly estimates the channels for different transmit antennas. Unlike in CCE, the pilots allocated to different antennas are equally distributed along the time axis. The entire algorithm is independently implemented at each receive antenna. Therefore, in the rest of this paper, we use h_i to denote the channels from the i-th transmit antenna to the receiver for the sake of simplicity. At any pilot slot, the algorithm is executed in four steps:

i) Pilot-based CE: In the first step, the t-th antenna is activated to transfer the pilot. The estimated CSI for the currently active antenna is denoted as $\hat{h}_t(n)$, where n represents the index of pilot slots.

ii) CSI correction: For each transmit antenna, the pilot is transmitted once for every N_t pilot slots. In the other N_t-1 slots, the t-th antenna is inactive and the corresponding estimates are obtained by the correlation-based CE described in step iii. In this step, these estimates are corrected by a low-pass interpolation based on the current estimate $\hat{h}_t(n)$ and $L-1$ previous estimates $\hat{h}_t(n-lN_t)$, $l=1,2,\ldots,L-1$. The number of used estimates for the currently active antenna, *i.e.*, L, is defined by the interpolation sequence length. After being obtained from the interpolation, the corrected CSI of the t-th transmit antenna is denoted as $\dot{h}_t(n-n')$, where $n'=1,2,\ldots,N_t-1$.

For the i-th transmit antenna, the most recent pilot-based CE happened $n'_{i,t}$ time slots before where:

$$n'_{i,t}=\begin{cases} t-i & \text{if} \quad i<t \\ t-i+N_t & \text{if} \quad i>t \end{cases} \tag{4}$$

Taken $N_t=4$ and $t=2$ as an example, the values of $n'_{i,t}$ for $i=1,3,4$ are 1, 3, and 2, respectively. At the time index $n-n'_{i,t}$, the difference between the channels of the i-th and the t-th transmit antennas is given by:

$$\Delta J_{i,t}(n-n'_{i,t})=\hat{h}_i(n-n'_{i,t})-\dot{h}_t(n-n'_{i,t}) \tag{5}$$

iii) Correlation-based CE: The idle antennas are estimated based on the current estimates of the t-th antenna and the corresponding channel difference obtained in the previous step. We denote the CSI obtained in this way as $\tilde{h}_i(n)$ which is computed by:

$$\tilde{h}_i(n)=\hat{h}_t(n)+\Delta J_{i,t}(n-n'_{i,t}), \quad i\neq t \tag{6}$$

$\hat{h}_t(n)$ and $\tilde{h}_i(n)$ comprise the channel estimates for all transmit antennas that are used for decoding in the subsequent data transmission.

iv) Antenna index update: The last step is to set the next active antenna, which is an increment by one to the antenna index:

$$t=\begin{cases} t+1 & \text{if} \quad t<N_t \\ 1 & \text{if} \quad t=N_t \end{cases} \tag{7}$$

IV. Evaluation Criteria

In practical communications, data is always transferred in packets. At the receiver, incorrectly decoded packets require a retransmission. The successfully received data rate is defined as effective data. The effective data rate, *i.e.*, throughput, is used to evaluate the CE performance for different pilot ratios.

A. Effective Data Rate

Forward error correction (FEC) is usually applied to correct errors in the physical layer. In this paper, two modes are considered: with and without FEC. The total raw data rate including the pilots is given by:

$$R_{\text{tot}}=\frac{\eta_s}{T_s} \tag{8}$$

Denoting the retransmission rate as e_{packet}, the throughput, represented by T, is calculated by:

$$T=R_{\text{tot}}(1-\eta)(1-e_{\text{packet}})\eta_c \tag{9}$$

where η_c represents the coding rate. In the case that no FEC is assumed, $\eta_c=1$.

B. Energy Consumption

Furthermore, the proposed CE technique requires less pilot transmissions which has an impact on energy consumption. Therefore, we have analyzed the attainable energy efficiency gains. This is analyzed in terms of the amount of effective data per unit energy, which can be expressed as:

$$\eta_E=\frac{T\times T_s}{E_m} \qquad \text{[bits / Joule]} \tag{10}$$

2013 IEEE 18th International Workshop on Computer Aided Modeling and Design of Communication Links and Networks (CAMAD)

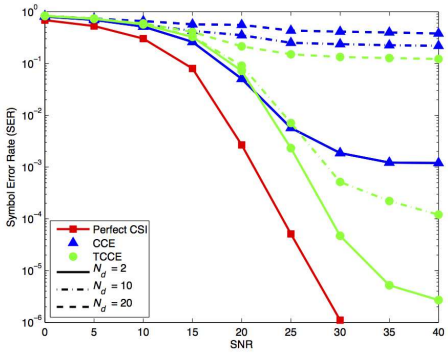

Fig. 3. SER performance of SM with $N_t = 8$ and BPSK in terms of SNR at a speed of 10 m/s

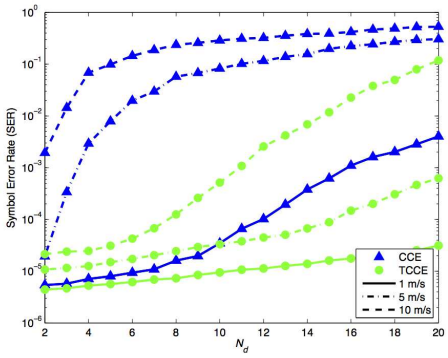

Fig. 4. SER performance of SM with $N_t = 8$ with BPSK in terms of pilot ratio at an SNR of 30 dB

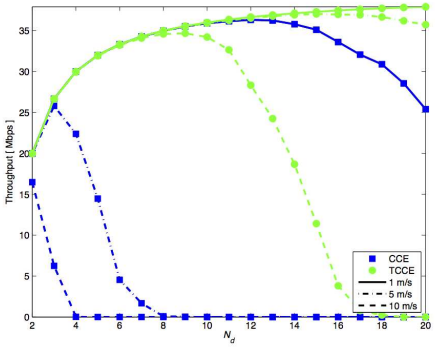

(a) Without FEC

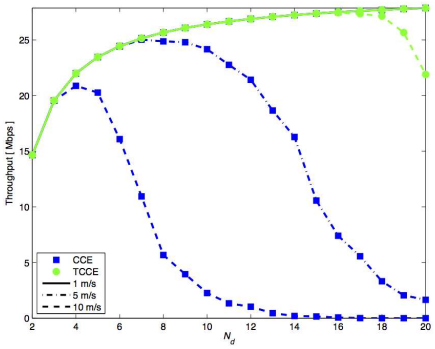

(b) With FEC

Fig. 5. Throughput at an SNR of 30 dB

V. Simulation Results

In this section, the performance of SM taking into account estimated CSI is evaluated under the realistic channel model introduced in Sec. II. The number of raw data symbols per pilot is denoted as N_d, *i.e.*, $N_d \times \eta = 1$. Since N_d must be an integer, for the sake of simplicity, we use N_d instead of η in the following analysis. A varying N_d from 2 to 20, *i.e.*, the pilot ratio from 50% to 5%, is applied for both CCE and TCCE. In all simulations, it is assumed that $N_r = 2$.

A. Symbol Error Rate

In Fig. 3, given a user speed of 10 m/s, the symbol error rate (SER) of SM with $N_t = 8$ and BPSK is presented against different pilot ratios. In contrast to CCE, TCCE performs significantly closer to the scenario of perfect CSI for $N_d = 2$ and 10. At $N_d = 20$, the difference between these two schemes becomes much smaller, but still TCCE gains a noticeable reduction of about 50% in the attainable SER. The reason for this trend is that while the estimation period largely exceeds the channel coherence time, both methods can not provide a sufficiently accurate CSI and, thus, they trend to a ceiling effect. However, with a CE period proportional to N_t, CCE approaches the ceiling much faster than TCCE when decreasing the pilot ratio. This is clearly demonstrated in Fig. 4, where the SER is presented as a function of N_d. Furthermore, as the speed increases, the performance of CCE drops dramatically whereas TCCE maintains reasonably good performance. At 10 m/s, for example, CCE approaches the SER ceiling of 5×10^{-1} when N_d increases to 6. Meanwhile, TCCE achieves an SER of 4×10^{-5}.

B. Throughput

Fig. 5 shows the change of throughput along with the pilot ratio for various velocities. The packet length is assumed to be 50 bytes and a 3/4 block coding is used for FEC. As can be seen in Fig. 5(a), when reducing the pilot ratio, the throughput increases at first then falls down. For each case, a corresponding optimum pilot ratio can be determined to

2013 IEEE 18th International Workshop on Computer Aided Modeling and Design of Communication Links and Networks (CAMAD)

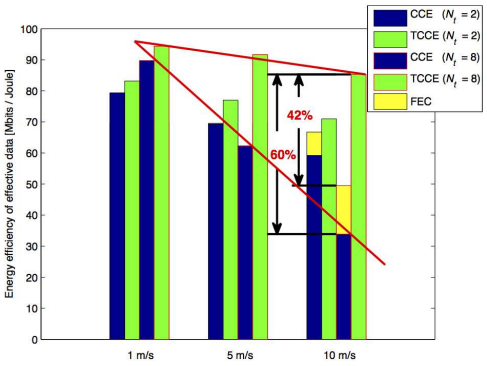

Fig. 6. Transmit energy consumption

achieve the peak throughput. This is the result of trading off between the amount of data and retransmission rates. At the speed of 5 m/s, for example, TCCE attains 37.1 Mbps at $N_d = 15$ while CCE can achieve only 25.2 Mbps at $N_d = 3$. Compared with CCE, TCCE obtains 47% more throughput with a much lower optimal pilot ratio. Moreover, the benefit becomes more striking as the velocity grows. When the user speed is increased to 10 m/s, TCCE achieves 140% more throughput than CCE.

The results involving FEC is shown in Fig. 5(b). Only in the case of CCE at 10 m/s, the peak throughput is improved from 14 to 19.6 Mbps compared with the scenario when no FEC is used. This is because that the cost for using FEC is adding the redundancy. Therefore, when the retransmission rate is fairly low, FEC can not improve the throughput but causes a degradation instead. However, the aim here focuses on the influence of FEC on the optimum pilot rate. Generally, compared to Fig. 5(a), the peak throughput moves towards a lager N_d. The reason for this trend is that FEC reduces the retransmission rate which has the same effect as increasing the pilot ratio. The second outcome is that, TCCE still outperforms CCE for various speeds. Taken 5 m/s as an example, compared to CCE, TCCE gains 11% more throughput.

C. Energy Efficiency

In this section, an energy efficiency comparison is made of CCE and TCCE at their optimum pilot ratios for different N_t, while the spectral efficiency is maintained at 4 bits/s/Hz. In order to compute the RF output energy consumption at the transmitter, the path loss is assumed to be 100 dB without shadowing [7].

In Fig. 6, comparisons are carried out in terms of mobile speeds, where the following three outcomes can be observed. Firstly, consuming the same amount of energy, TCCE enables higher throughput than CCE. Taken 10 m/s and $N_t = 8$ as an instance, compared to CCE, TCCE reduces the energy by 60% when no FEC is applied for both methods. In the case of using FEC, although the performance of CCE is improved, TCCE still achieves an energy saving of 42%. Secondly, with an increase of speed, the energy efficiency of CCE rapidly decreases. Meanwhile, the energy efficiency of TCCE degrades much more slowly for the same conditions. Furthermore, based on TCCE, the performance of SM is boosted along with an increase of N_t. This trend matches the results in the case of perfect CSI [3], where the benefit of multiple antennas is exploited. However, the energy efficiency of CCE drops because more time is required to send pilots.

VI. Conclusion

In this paper, the effect of pilot ratio on channel estimation has been investigated for SM. Trading off the amount of data with the retransmission rate, an optimal pilot ratio can be determined to achieve the peak throughput. When compared to CCE, TCCE significantly increases the throughput of SM with a much lower optimal pilot ratio. This improvement is more remarkable for a faster user speed. Furthermore, the energy efficiency of CCE degrades when the number of transmit antennas increases. In contrast, TCCE can still benefit from a larger size of antennas. Simulation results validate that TCCE is a robust channel estimation technique for SM.

Acknowledgement

We gratefully acknowledge support from the European Union (PITNGA2010264759, GREENET project) for this work. We would also like to thank Dr. Holger Claussen for the very fruitful discussions.

References

[1] P. Wolniansky, G. Foschini, G. Golden, and R. Valenzuela, "V-blast: an architecture for realizing very high data rates over the rich-scattering wireless channel," in *Signals, Systems, and Electronics, 1998. ISSSE 98. 1998 URSI International Symposium on*, 1998, pp. 295–300.

[2] V. Tarokh, H. Jafarkhani, and A. Calderbank, "Space-time block codes from orthogonal designs," *IEEE Trans. Information Theory*, vol. 45, no. 5, pp. 1456–1467, 1999.

[3] R. Mesleh, H. Haas, S. Sinanović, C. W. Ahn, and S. Yun, "Spatial Modulation," *IEEE Trans. Veh. Technol.*, vol. 57, no. 4, pp. 2228 – 2241, July 2008.

[4] M. Faiz, S. Al-Ghadhban, and A. Zerguine, "Recursive least-squares adaptive channel estimation for spatial modulation systems," in *Communications (MICC), 2009 IEEE 9th Malaysia International Conference on*, 2009, pp. 785–788.

[5] S. Sugiura and L. Hanzo, "Effects of channel estimation on spatial modulation," *IEEE Signal Proc. Lett.*, vol. 19, no. 12, pp. 805–808, 2012.

[6] X. Wu, M. Di Renzo, and H. Haas, "Channel Estimation for Single-stream MIMO Techniques," in *22nd IEEE International Symposium on Personal, Indoor and Mobile Radio Communications (PIMRC): Fundamentals and PHY Track*, 2013.

[7] J. Salo, G. Del Galdo, J. Salmi, P. Kyösti, M. Milojevic, D. Laselva, and C. Schneider, "MATLAB implementation of the 3GPP Spatial Channel Model (3GPP TR 25.996)," Jan. 2005. [Online]. Available: http://www.tkk.fi/Units/Radio/scm/

[8] J. Jeganathan, A. Ghrayeb, and L. Szczecinski, "Spatial Modulation: Optimal Detection and Performance Analysis," *IEEE Commun. Lett.*, vol. 12, no. 8, pp. 545–547, 2008.

[9] S. M. Kay, *Fundamentals of Statistical Signal Processing: Estimation Theory*, 1st ed. Prentice Hall PTR, 1993.

Spatially-Averaging Channel Estimation for Spatial Modulation

Xiping Wu*, Marco Di Renzo†, and Harald Haas*

*Institute for Digital Communications
School of Engineering
The University of Edinburgh
EH9 3JL, Edinburgh, UK
{xiping.wu, h.haas}@ed.ac.uk

†French National Centre for Scientific Research (CNRS)
Laboratory for Signals and Systems (LSS)
École Supérieure d'Électricité (SUPELEC)
3 rue Joliot-Curie, 91192 Gif-sur-Yvette (Paris), France
marco.direnzo@lss.supelec.fr

***Abstract*—Spatial modulation (SM) is a unique single-stream, multiple-input multiple-output (MIMO) transmission technique. Unlike multi-steam MIMO schemes, a single transmit antenna is activated in SM at any given time. Therefore, inter-channel interference is completely avoided. In addition, SM requires only one radio-frequency (RF) chain, regardless of the number of transmit antennas used. This key property results in a significant saving in quiescent power of power amplifiers. However, a challenge occurs when channel estimation (CE) is implemented for SM: the transmit antennas have to send pilots sequentially. Thus, in order not to compromise the throughput, the pilot number of each transmit antenna is restricted. This means we focus on improving the CE performance without increasing the number of pilots. In this paper, we propose a novel CE method for SM, in which the channel is jointly estimated across receive antennas. Simulation results show that the proposed approach outperforms the conventional method for various channel correlations between the receive antennas.**

***Index Terms*—Spatial Modulation, MIMO, channel estimation, channel correlation**

I. Introduction

MULTIPLE-input multiple-output (MIMO) transmission techniques offer a significant increase in spectrum efficiency without additional bandwidth or increased transmit power. According to the number of active antennas, MIMO schemes are classified into two categories: multi-stream and single-stream. Unlike the conventional multi-stream MIMO, spatial modulation (SM) activates a single transmit antenna at any time [1]–[3]. As a result, inter-channel interference is completely avoided. Also, SM exhibits a significant saving in quiescent power at the power amplifier stage, because it requires only one radio-frequency (RF) chain regardless of the number of antennas used. Assuming perfect channel state information (CSI) at the receiver, it is shown in [4] that SM offers a better performance than many state-of-the-art MIMO schemes, while achieving a low-complexity implementation.

However, perfect CSI is not realistic, and channel estimation (CE) is of vital importance that can not be neglected. In order to obtain the CSI at the receiver, training-based CE methods are commonly used in which deterministic symbols, *i.e.* pilots, are conveyed followed by information-carrying symbols. The pilot ratio is defined as the ratio of the number of pilots to the number of total symbols. When compared with multi-stream MIMO schemes, CE becomes challenging for SM since the transmit antennas have to be sequentially activated for sending the pilots. Consequently, the time consumed in the CE process for SM is proportional to the number of transmit antennas. To date there has only been a few studies on CE for SM. In [5], a CE method using recursive least-square (RLS) is proposed for SM. Another approach is introduced in [6], which is based on joint channel estimation with data detection. Both methods are developed using existing techniques, where the channel is individually estimated at different receive antennas. We refer to this type of CE methods as conventional channel estimation (CCE). To improve the CE accuracy, CCE requires either a longer pilot sequence length or a larger transmission power for pilots. However, in order not to compromise the throughput, the pilot sequence length for each transmit antenna is constrained in SM, especially when a large number of transmit antennas are used. In addition, the transmission power is usually restricted due to the maximum output of power amplifiers. This raises the question, how to improve the CE performance for SM with a fixed number of pilots. To the best of the authors' knowledge, this issue has not been addressed before.

With the aim of improving the CE performance without increasing the pilot sequence length, we propose a novel CE method for SM in this paper. Unlike the conventional methods, the proposed approach jointly estimates the channel of different antennas at the receiver. The basic idea is to think of the estimation results at different receive antennas as individual samples. By exploring the channel correlation between antennas, these samples can be jointly used to achieve a more accurate CE for each receive antenna. Simulation results show that when compared with CCE, the proposed method obtains a signal-to-noise ratio (SNR) gain of up to 2 dB.

The remainder of this paper is organized as follows. Section II describes the system model, including the SM structure, the channel model and the channel estimator. In Section III, a novel CE method is proposed for SM in which the channel is jointly estimated at the receiver. Section IV presents the simulation results. The paper is concluded in Section V.

978-1-4799-4449-1/14/$31.00 ©2014 IEEE

II. System Model

A. SM-MIMO

An $N_t \times N_r$ SM-MIMO system is considered, where N_t and N_r denote the number of transmit antennas and the number of receive antennas, respectively. The size of the spatial constellation points is equal to the number of transmit antennas, and the size of signal constellation points is denoted by M. The bit stream is divided into blocks of η_s bits, where $\eta_s = \log_2(MN_t)$ is the number of bits per symbol. Each block is then split into two units of $\log_2(N_t)$ bits and $\log_2(M)$ bits. The first part activates one of the transmit antennas, and the currently active antenna is denoted by l. The second part determines one symbol from the signal constellation diagram, and the active antenna conveys this symbol which is denoted by s. The transmitted signal is expressed by a vector $\mathbf{x}_{l,s} = [x_1, \ldots, x_l, \ldots, x_{N_t}]^T$, where the l-th element carries the symbol s, and all other elements are zero.

B. Channel Model

A time-varying Rayleigh fading channel is assumed. The fading coefficient of the channel between the t-th transmit antenna and the r-th receive antenna is denoted by $h_{t,r(n)}$, where n is the discrete time index. The corresponding MIMO channel matrix is represented by $\mathbf{H}_{(n)}$, and it is established in two stages.

1) Spatial correlation: Based on the Kronecker model [7], the initial channel matrix is given by:

$$\mathbf{H}_{(0)} = \mathbf{R}_r^{1/2}\mathbf{G}\left(\mathbf{R}_t^{1/2}\right)^H, \tag{1}$$

where $\mathbf{G}$ has the same dimension as $\mathbf{H}_{(0)}$, and its entries are independent and identically distributed (i.i.d.) complex Gaussian distribution $\mathcal{CN}(0,1)$; $\mathbf{R}_t$ and $\mathbf{R}_r$ respectively denote the transmit correlation matrix and the receive correlation matrix; $(\cdot)^H$ is the operator of hermitian transpose. Since we focus on studying the channel correlation at the receiver, the transmit antennas are assumed to be independent without a loss of generality. Thus, $\mathbf{R}_t$ reduces to an identity matrix. The correlation coefficient between the r_1-th and r_2-th receive antennas is denoted by ρ_{r_1,r_2}, and the receive correlation matrix is written as:

$$\mathbf{R}_r = \begin{bmatrix} 1 & \rho_{1,2} & \cdots & \rho_{1,N_r} \\ \rho_{2,1} & 1 & \cdots & \rho_{2,N_r} \\ \vdots & \vdots & \ddots & \vdots \\ \rho_{N_r,1} & \rho_{N_r,2} & \cdots & 1 \end{bmatrix} \tag{2}$$

2) Variation in time: Using the Gauss-innovations channel model [8], the channel matrix at the n-th time index is formulated as follows:

$$\mathbf{H}_{(n)} = \sqrt{\alpha}\mathbf{H}_{(n-1)} + \sqrt{1-\alpha}\mathbf{H}'_{(n)}, \tag{3}$$

where α is a parameter related to the user speed, and it is given by [8, Eq. (10)]:

$$\alpha = J_0\left(\frac{2\pi v f_c T_s}{c}\right)^2, \tag{4}$$

where $J_0(\cdot)$ is the zeroth-order Bessel function of the first kind; f_c is the center carrier frequency; T_s is the sampling period; v and c denote the speeds of the mobile user and the light, respectively. The term $\mathbf{H}'_{(n)}$ is also produced by (1), but it is independent of $\mathbf{H}_{(n-1)}$. In addition, $\mathbf{H}'$ is independent from time to time, *i.e.* $\mathbf{H}'_{(n)}$ is irrelevant to $\mathbf{H}'_{(m)}$ for all $m \neq n$. Substituting (1) into (3), we have:

$$\mathbf{H}_{(1)} = \mathbf{R}_r^{1/2}\left(\sqrt{\alpha}\mathbf{G}_{(0)} + \sqrt{1-\alpha}\mathbf{G}_{(1)}\right)\left(\mathbf{R}_t^{1/2}\right)^H \tag{5}$$

Note that $\mathbf{H}_{(1)}$ is a Rayleigh fading channel of the same correlation matrices as $\mathbf{H}_{(0)}$. Similarly, $\mathbf{H}_{(n)}$ can be expressed by:

$$\mathbf{H}_{(n)} = \mathbf{R}_r^{1/2}\bar{\mathbf{G}}_{(n)}\left(\mathbf{R}_t^{1/2}\right)^H, \tag{6}$$

and

$$\bar{\mathbf{G}}_{(n)} = \sum_{m=0}^{n}\left(\sqrt{1-\alpha}\right)^{\mathrm{sgn}(m)}\left(\sqrt{\alpha}\right)^{n-m}\mathbf{G}_{(m)} \tag{7}$$

where $\mathrm{sgn}(\cdot)$ is the sign function.

C. Maximum Likelihood (ML) Optimum Detector

The signal received at the r-th receive antenna is expressed as follows:

$$y_{r(n)} = h_{l,r(n)}s_{(n)} + w_{r(n)}, \tag{8}$$

where $w_{r(n)}$ is a sample of the additive white Gaussian noise (AWGN) at the r-th receive antenna. Across the receive antennas, the noise components are statistically independent. We define $\gamma = E_m/N_0$ as the signal-to-noise ratio (SNR), where E_m is the average energy per symbol and N_0 denotes the power spectrum density of AWGN. The estimated CSI, denoted by $\hat{\mathbf{H}}$, is used to decode the conveyed signal. Based on the joint maximum likelihood (ML) detection [9], the decoded information is computed by:

$$\left[\hat{l}_{(n)}, \hat{s}_{(n)}\right] = \arg\min_{l,s}\sum_{r=1}^{N_r} \parallel \hat{h}_{l,r}s \parallel^2 - 2\Re\{y^*_{r(n)}\hat{h}_{l,r}s\}, \tag{9}$$

where $\Re\{\cdot\}$ is an operator to extract the real part of a complex number.

III. Channel Estimation for Spatial Modulation

One of the key properties of SM is that a single transmit antenna is activated at any given time. Therefore, all transmit antennas have to send the pilot signal sequentially. Fig. 1 shows the pilot structure for SM with four transmit antennas. The CE period is defined as the interval between two adjacent CE processes for any transmit antenna. The pilot ratio, denoted

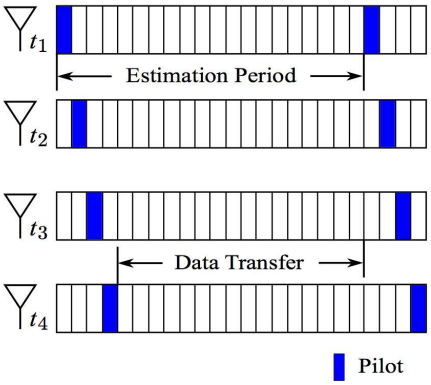

Fig. 1. Pilot structure for SM with $N_t = 4$

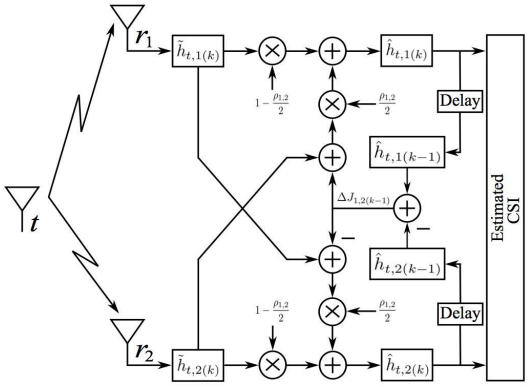

Fig. 2. Block diagram of the proposed channel estimation method

by η, is defined as the ratio of the number of pilots to the number of total symbols during a single CE period. The pilot sequence length is assumed at one, *i.e.* during any CE period, only one pilot is sent from each transmit antenna.

A. Conventional Channel Estimation (CCE)

In the conventional methods, the channel estimation is implemented individually at each receive antenna. The index of CE periods is denoted by k. The pilot sent from the t-th transmit antenna in the k-th CE period is denoted by $p_{t(k)}$. The corresponding signal received at the r-th receive antenna is written as:

$$y_{r(k)} = h_{t,r(k)} p_{t(k)} + w_{r(k)} \tag{10}$$

A specific estimator such as least square (LS), minimum mean square error (MMSE), and recursive least square (RLS) [10], is used to estimate the CSI of the currently active antenna. In order for a fair comparison, LS is considered for both CCE and the proposed method in this paper. The estimation result for CCE is denoted by $\tilde{h}_{t,r(k)}$, and it is computed by:

$$\tilde{h}_{t,r(k)} = \arg\min_{h} \parallel y_{r(k)} - h p_{t(k)} \parallel^2 \tag{11}$$

After the CSI for all transmit antennas is obtained at the receiver, it is used to decode the subsequently transmitted symbols which carry information bits.

B. Spatially-Averaging Channel Estimation (SACE)

The basic concept of SACE is to jointly estimate the MIMO channel across the receive antennas. Taking $N_r = 2$ as an example, Fig. 2 depicts the block diagram of the proposed method. For a generalized number of receive antennas, the algorithm comprises two steps as follows.

1) Update channel difference information: The proposed method exploits the difference between the fading channel coefficients of different receive antennas, which is referred to as channel difference information (CDI). To be distinguished from CCE, we use $\hat{h}_{t,r}$ to denote the estimated CSI for the proposed method. The CDI between the r-th and j-th receive antennas, denoted by $\Delta J_{r,j}$, is obtained from the previous estimated CSI:

$$\Delta J_{r,j(k-1)} = \hat{h}_{t,r(k-1)} - \hat{h}_{t,j(k-1)} \tag{12}$$

2) Weighted average: Based on the CDI, it is possible to obtain the CSI for one receive antenna by the CCE result of another receive antenna. In order to achieve a more accurate CE, the estimation results are averaged across the receive antennas. The estimated CSI for the r-th receive antenna, *i.e.* $\hat{h}_{t,r(k)}$, is formulated as follows:

$$\hat{h}_{t,r(k)} = \left(1 - \frac{1}{N_r} \sum_{j=1 \neq r}^{N_r} \rho_{r,j}\right) \tilde{h}_{t,r(k)} + \frac{1}{N_r} \sum_{j=1 \neq r}^{N_r} \rho_{r,j} \left(\tilde{h}_{t,j(k)} + \Delta J_{r,j(k-1)}\right) \tag{13}$$

Note that the estimated CSI for SACE is a weighted average of the CCE results of all receive antennas. The weights depend on the channel correlation between the receive antennas. When the channel correlation increases, the weight for the estimated antenna decreases, while the weights for the remaining antennas increase. If the receive antennas are completely correlated, *i.e.* $\rho_{r,j} = 1$ for all j, (13) reduces to:

$$\hat{h}_{t,r(k)} = \frac{1}{N_r} \sum_{j=1}^{N_r} \tilde{h}_{t,j(k)} \tag{14}$$

As shown, in this case, the estimated CSI is an equal average of the CCE results of all receive antennas. If the receive

antennas are independent, the estimation results for SACE are equivalent to that of CCE.

IV. Simulation Results

In this section, Monte Carlo simulation results are shown to validate the performance of the proposed method. The pilots and information-carrying symbols are allocated the same transmission power, and the pilot ratio is assumed at 5% [11]. To ensure a fair comparison, the same pilot sequence length is considered for both SACE and CCE. In this paper, we only take into account the pilot sequence length of one. In all simulations, Quadrature Phase Shift Keying (QPSK) symbols are conveyed by an SM-MIMO system with four transmit antennas. In addition, the constant correlation model is considered [12], where the correlation coefficient between any pair of receive antennas is the same, and it is denoted by ρ_{rx}. Further, the bit error ratio (BER) performance of SACE is compared with CCE for different numbers of receive antennas. Furthermore, we study the effects of user speed on the BER performance for the proposed method.

A. BER Performance

Fig. 3 presents the BER performance of the proposed method in comparison with CCE. The user speed is assumed at 13.3 m/s (48 km/h), which is a typical suburban speed limit [13].

The simulation results for two receive antennas are shown in Fig. 3(a). Two outcomes are observed: i) SACE always offers a better performance than CCE; ii) when the channel correlation increases, SACE outperforms CCE more significantly. As an example, for $\rho_{\text{rx}} = 0.2$, SACE exhibits an SNR gain of 0.3 dB in comparison with CCE. When ρ_{rx} increases to 0.8, this gain increases to 2 dB. The reason for this trend is that the performance of the proposed approach is related to the channel correlations. As the channel correlation decreases, the CDI between receive antennas becomes larger and more random. In this case, SACE obtains a less accurate CDI and therefore, a smaller improvement is achieved in comparison with CCE. Despite this, SACE is still better than CCE for a low channel correlation.

When N_r is increased to four, the corresponding BER performance for SACE and CCE is presented in Fig. 3(b). As seen, for a certain ρ_{rx}, the SNR gap between SACE and CCE is basically the same as that in Fig. 3(a). Taking $\rho_{\text{rx}} = 0.8$ as an example, the SNR gap is 1.8 dB which is slightly less than 2 dB when $N_r = 2$. However, to achieve a certain BER, the required SNR in $N_r = 4$ is much smaller than that in $N_r = 2$. Considering this, SACE outperforms CCE more significantly for a larger number of receive antennas. The reason is that when more receive antennas are involved, SACE obtains a more accurate CSI for each antenna. Since the simulations are conducted without channel coding, we are more interested in the BER range between 1×10^{-3} and 1×10^{-2}. At $\rho_{\text{rx}} = 0.2$, CCE requires an SNR of 10.3 dB to achieve a BER of 1×10^{-2}. Meanwhile, by consuming the same amount of transmission energy, SACE reduces the BER to 7×10^{-3}. When the channel correlation decreases to 0.8, the BER for SM is reduced from 1×10^{-2} to 5×10^{-3} by using SACE instead of CCE.

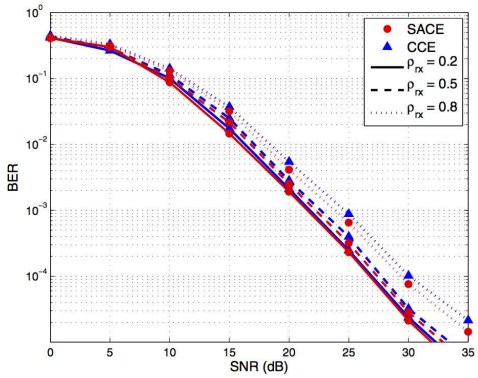

(a) $N_r = 2$

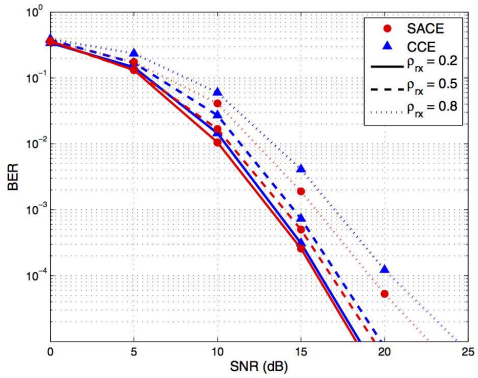

(b) $N_r = 4$

Fig. 3. BER performance of SACE for various channel correlations.

B. Effects of User Speed

Fig. 4 shows the BER performance of SM at different user speeds. The case of perfect CSI is considered as a benchmark, which is referred to as "P-CSI" in the sequel. A medium channel correlation of $\rho_{\text{rx}} = 0.5$ is assumed, and the number of receive antennas is set at four.

The following outcomes are observed: i) compared with CCE, the BER performance of SACE is much closer to that of P-CSI; ii) for various user speeds, SACE achieves a constant SNR gain of 1 dB on the basis of CCE; iii) for both SACE and CCE, the BER performance of SM degrades notably when the user speed increases from 20 m/s to 30 m/s. The reason is that if the channel varies very rapidly, all CE techniques would fail to function properly for a fixed pilot ratio.

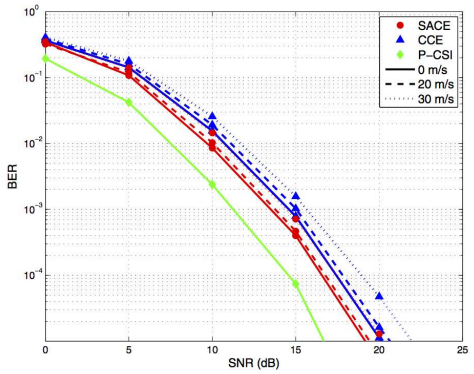

Fig. 4. BER performance of SM at different user speeds

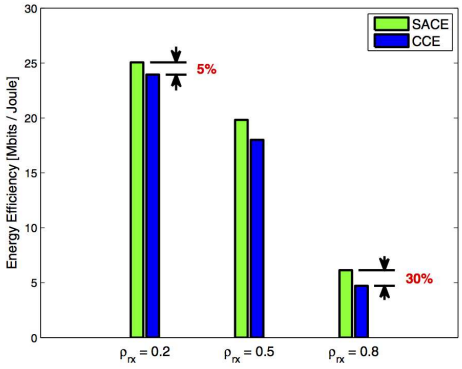

Fig. 5. Energy efficiency comparison between SACE and CCE

C. Energy Efficiency

In this section, the energy efficiency of the proposed method is evaluated. The successfully transmitted data is defined as throughput, and the energy efficiency is measured in terms of the amount of throughput per unit transmission energy. The path loss is assumed to be 100 dB without consideration of shadow fading [14].

In Fig. 5, the energy efficiencies of SACE and CCE are presented for different channel correlations. As seen, with the same energy consumption, SACE conveys more information bits than CCE. Taking $\rho_{\text{rx}} = 0.5$ for example, CCE transmits 17.9 Mbits per joule while SACE obtains an extra 1.8 Mbits. Furthermore, in contrast to CCE, SACE saves more energy when the channel correlation increases. For $\rho_{\text{rx}} = 0.2$, SACE requires 5% less energy than CCE. When the channel correlation increases to 0.8, SACE achieves a great energy saving of 30%.

V. Conclusion

In this paper, we propose a novel CE approach for SM, which is named SACE. Unlike the traditional CE methods, SACE estimates the channel jointly for all receive antennas. By constructively exploiting channel correlation, SACE improves the CE accuracy without increasing the pilot sequence length. Therefore, the proposed method enables SM to improve the BER performance, while not compromising the throughput. Results show that when compared with CCE, SACE obtains an SNR gain of up to 2 dB. Moreover, SACE outperforms CCE more significantly as the channel correlation increases. This means the proposed CE method makes SM robust against the degradation caused by channel correlations.

Acknowledgement

We gratefully acknowledge support from the European Union's Seventh Programme under grant agreement No 264759 (GREENET Project). Prof. Haas acknowledges partial support from the Engineering and Physical Sciences Research Council (EPSRC) under Established Career Fellowship grant EP/K008757/1.

References

[1] R. Mesleh, H. Haas, S. Sinanović, C. W. Ahn, and S. Yun, "Spatial Modulation," *IEEE Trans. Veh. Technol.*, vol. 57, no. 4, pp. 2228 – 2241, July 2008.

[2] M. Di Renzo, H. Haas, and P. M. Grant, "Spatial Modulation for Multiple-Antenna Wireless Systems: A Survey," *IEEE Commun. Mag.*, vol. 49, no. 11, pp. 182–191, Nov. 2011.

[3] L. Hanzo, H. Haas, S. Imre, D. O'brien, M. Rupp, and L. Gyongyosi, "Wireless Myths, Realities, and Futures: From 3G/4G to Optical and Quantum Wireless," *Proc. IEEE*, vol. 100, no. Special Centennial Issue, pp. 1853–1888, May 2012.

[4] M. Di Renzo and H. Haas, "Bit Error Probability of SM-MIMO Over Generalized Fading Channels," *IEEE Trans. Veh. Technol.*, vol. 61, no. 3, pp. 1124 –1144, march 2012.

[5] M. Faiz, S. Al-Ghadhban, and A. Zerguine, "Recursive least-squares adaptive channel estimation for spatial modulation systems," in *9th IEEE Malaysia International Conference on Commun. (MICC)*, 2009, pp. 785–788.

[6] S. Sugiura and L. Hanzo, "Effects of channel estimation on spatial modulation," *IEEE Signal Processing Lett.*, vol. 19, no. 12, pp. 805–808, 2012.

[7] C. Oestges, "Validity of the Kronecker Model for MIMO Correlated Channels," in *Proc. IEEE Veh. Technol. Conf.*, vol. 6, 2006, pp. 2818–2822.

[8] C. Peel and A. Swindlehurst, "Performance of space-time modulation for a generalized time-varying rician channel model," *IEEE Trans. Wireless Commun.*, vol. 3, no. 3, pp. 1003–1012, 2004.

[9] J. Jeganathan, A. Ghrayeb, and L. Szczecinski, "Spatial Modulation: Optimal Detection and Performance Analysis," *IEEE Commun. Lett.*, vol. 12, no. 8, pp. 545–547, 2008.

[10] S. M. Kay, *Fundamentals of Statistical Signal Processing: Estimation Theory*, 1st ed. Prentice Hall PTR, 1993.

[11] J. Berkmann, C. Carbonelli, F. Dietrich, C. Drewes, and W. Xu, "On 3G LTE Terminal Implementation - Standard, Algorithms, Complexities and Challenges," in *Wireless Communications and Mobile Computing Conference, 2008. IWCMC '08. International*, Aug. 2008, pp. 970 –975.

[12] G. Karagiannidis, D. Zogas, and S. Kotsopoulos, "An efficient approach to multivariate nakagami-m distribution using green's matrix approximation," *IEEE Trans. Wireless Commun.*, vol. 2, no. 5, pp. 883–889, Sept 2003.

[13] Speed limits for vehicle and boat safety. [Online]. Available: https://www.gov.uk/speed-limits

[14] J. Salo, G. Del Galdo, J. Salmi, P. Kyösti, M. Milojevic, D. Laselva, and C. Schneider, "MATLAB implementation of the 3GPP Spatial Channel Model (3GPP TR 25.996)," On-line, Jan. 2005.

IEEE ICC 2014 - Wireless Communications Symposium

Optimal Power Allocation for Channel Estimation in Spatial Modulation

Xiping Wu*, Marco Di Renzo†, and Harald Haas*

*Institute for Digital Communications
Joint Research Institute for Signal and Image Processing
School of Engineering
The University of Edinburgh
EH9 3JL, Edinburgh, UK
{xiping.wu, h.haas}@ed.ac.uk

†French National Centre for Scientific Research (CNRS)
Laboratory for Signals and Systems (LSS)
École Supérieure d'Électricité (SUPELEC)
3 rue Joliot-Curie, 91192 Gif-sur-Yvette (Paris), France
marco.direnzo@lss.supelec.fr

***Abstract*—This work investigates the impact of power allocation for channel estimation (CE) in spatial modulation (SM). SM is a unique single-stream multiple-input multiple-output (MIMO) transmission technique that achieves spatial multiplexing gains. While SM completely avoids inter-channel interference, a single active antenna leads to a challenge for CE, *i.e.*, all transmit antennas have to be activated sequentially to send the pilot signal. More time as well as energy is therefore consumed for CE. Driven by this motivation, we propose a closed-form optimal power allocation (OPA) for SM in this paper. Regardless of the SM transceiver structure, the optimal solution only depends on the pilot sequence length and the ratio between the number of pilots and the number of total symbols. Simulations results show that the bit error ratio performance of OPA-based SM tightly approaches the case of perfect channel state information with a gap of less than 0.8 dB.**

***Index Terms*—Spatial modulation (SM), MIMO, channel estimation, optimal power allocation**

I. Introduction

SPATIAL modulation is a promising multiple-input multiple-output (MIMO) transmission technique that considers antenna locations as spatial constellation points [1]. Unlike the conventional MIMO schemes, SM activates a single transmit antenna at a time, and thereby can completely avoid inter-channel interference. Moreover, SM exhibits a significant saving in quiescent power at the power amplifier stage because it requires only one radio-frequency (RF) chain, regardless of the number of antennas used. In [2], assuming perfect channel state information (P-CSI) at the receiver, it has been shown that SM offers a better performance than many state-of-the-art MIMO schemes while achieving a low-complexity implementation.

In practical applications, P-CSI is infeasible and channel estimation (CE) is of vital importance. Training-based estimation methods are most commonly used [3] whereby deterministic symbols, *i.e.*, pilots, are transmitted followed by data. The ratio between the number pilots and the number of total information carrying symbols is defined by the pilot ratio. In general, CE affects the bit error ratio (BER) performance of SM in two aspects: i) an extra additive noise is introduced to the transmitted signal. This is caused by the CE error of the activated antenna; ii) the channel state information (CSI) of the idle antennas is also inaccurate that affects the ability of correctly decoding the active antenna. In [4], the performance of space shift keying (SSK) with practical channel estimates is studied. Similar work on SM is conducted in [5]. However, both papers are based on the following assumptions: i) the power allocated to pilots was assumed to be either fixed or equal to the signal power of data symbols. The later method is referred to as equal power allocation (EPA); ii) the performance analysis is with respect to the power allocated to data symbols, but here we are interested in the performance with respect to the total average power. Unlike in multi-stream MIMO schemes, simultaneous pilot transmissions are infeasible for SM since only a single antenna is activated at a given time instance. In order to estimate the entire channel, all transmit antennas are required to send the pilot signal sequentially. This compromises the data rate, especially when a large number of transmit antennas is used. As the pilot ratio increases, EPA potentially impairs the BER performance. To the best of the authors' knowledge, the issue of optimum power allocation for pilots in SM has not been addressed before.

When considering practical channel estimates, the power allocation affects the BER performance in two aspects. On the one hand, the CE accuracy increases as more energy is consumed for the pilot signal. On the other hand, the signal-to-noise ratio (SNR) is reduced because less energy is available for data. In this paper, a closed-form optimal power allocation (OPA) is proposed for SM by balancing the power consumption of pilot and data symbols. Simulation results validate the optimization accuracy and show that OPA can significantly improve the BER performance of SM when compared to EPA.

The remainder of this paper is organized as follows. Section II describes the system model, including the SM structure, the channel model and the channel estimator. In Section III, the optimization problem is formulated with respect to a constraint on the average power, and a closed-form solution is obtained. Section IV presents the simulation results. The paper is summarized in Section V.

978-1-4799-2003-7/14/$31.00 ©2014 IEEE

II. System Model

A. SM-MIMO

We consider a MIMO system operating with N_t transmit and N_r receive antennas. The number of bits per symbol is denoted as η_s and the sizes of spatial constellation and signal constellation points are N_t and $M = 2^{\eta_s}/N_t$, respectively. At the transmitter, the bit-stream is divided into blocks of η_s bits. Afterwards, each block is split into two units of $\log_2(N_t)$ and $\log_2(M)$ bits. The first part activates one of the transmit antennas, and we denote the currently active antenna as l. The second part chooses one symbol from the signal constellation diagram and the active antenna conveys this symbol that is denoted by s.

The transmitted signal can be expressed by a vector $\mathbf{x}_{l,s} = [x_1, \ldots, x_l, \ldots, x_{N_t}]^T$, where the l-th element $x_l = s$ and all other elements are zero. The fading coefficient of the channel between the t-th transmit antenna and the r-th receive antenna is denoted by $h_{t,r}$. The channel is assumed to be identical and independently distributed Rayleigh fading, *i.e.*, $h_{t,r} \sim \mathcal{CN}(0,1)$. The received signal at the r-th receive antenna is given by:

$$y_r = h_{l,r}s + w_r, \tag{1}$$

where w_r is a sample of complex additive white Gaussian noise and the power spectrum density is denoted as N_0. Across the receive antennas, the noise components are statistically independent. We define the SNR of data by $\gamma_s = E_s/N_0$, where E_s is the average energy per data symbol. The estimated CSI is denoted as $\hat{h}_{t,r}$, and is used to decode the transmitted symbol by joint maximum likelihood detection [6]:

$$(\hat{l}, \hat{s}) = \arg\min_{l,s} \sum_{r=1}^{N_r} \parallel \hat{h}_{l,r}s \parallel^2 - 2\Re\{y_r^* \hat{h}_{l,r} s\}, \tag{2}$$

where $\Re\{\cdot\}$ is an operator to extract the real part of a complex number.

B. Channel Estimation

Fig. 1 illustrates the pilot structure of SM with four transmit antennas. As can be seen, the antennas are activated sequentially to send the pilot signal. The time interval between two adjacent pilot signals for one antenna is defined by the CE period. During a single estimation period, the number of pilot symbols allocated to each antenna is defined by the pilot sequence length N_p. Correspondingly, $N_t \times N_p$ symbol periods are required to fully estimate the channel. Additionally, the pilot ratio is expressed by η and it is defined as the ratio between $N_t \times N_p$ and the total number of symbols transmitted during one CE period. The least square (LS) estimator is considered, and the estimate of $h_{t,r}$ is therefore given by:

$$\begin{aligned} \hat{h}_{t,r} &= \arg\min_{h} \sum_{n=1}^{N_p} \parallel y_r(n) - h p_t(n) \parallel^2 \\ &= \frac{1}{N_p} \sum_{n=1}^{N_p} \frac{y_r(n)}{p_t(n)}, \end{aligned} \tag{3}$$

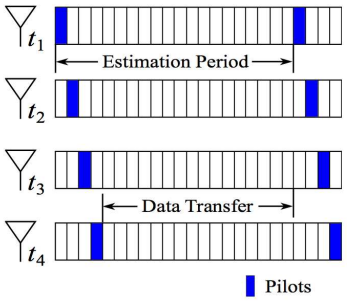

Fig. 1. Pilot structure for SM with $N_t = 4$

where $p_t(n)$ denotes the n-th pilot symbol sent from the t-th transmit antenna. The SNR of pilots is defined by $\gamma_p = E_p/N_0$, where E_p represents the energy per pilot symbol. The estimation error is denoted as $\epsilon_{t,r}$ and is computed as follows:

$$\begin{aligned} \epsilon_{t,r} &= h_{t,r} - \hat{h}_{t,r} \\ &= -\frac{1}{N_p} \sum_{n=1}^{N_p} \frac{w_r(n)}{p_t(n)} \end{aligned} \tag{4}$$

Since the pilot signal is deterministic, $\epsilon_{t,r}$ actually is a weighted average of noise samples $w_r(n)$, $n = 1, \ldots, N_p$. As a result, $\epsilon_{t,r}$ is also a complex Gaussian distributed random variable (r.v.), *i.e.*, $\epsilon_{t,r} \sim \mathcal{CN}(0, \sigma_\epsilon^2)$, where $\sigma_\epsilon^2 = 1/(\gamma_p N_p)$ is the variance. This can readily be extended to other CE methods by replacing the variance by $1/(\gamma_p N_p N)$, where N depends on the chosen estimation approach [7].

III. Optimal Power Allocation

A. Optimization Problem

In [5], an upper bound of the average bit error probability (ABEP) is derived for SM with practical channel estimates. By trading off E_p with E_s, our aim is to minimize the ABEP for a given power budget at the transmitter. We denote the total average energy consumption per symbol period as E_a, and the average SNR is defined by $\gamma_a = E_a/N_0$. Thus, the optimization problem can be formulated by:

$$\begin{aligned} (E_p^\dagger, E_s^\dagger) = \arg\min_{(E_p,E_s)} \quad & \text{ABEP}(E_p, E_s), \\ \text{subject to:} \quad & \eta E_p + (1-\eta)E_s = E_a \end{aligned} \tag{5}$$

where $(E_p^\dagger, E_s^\dagger)$ denote the optimum points for (E_p, E_s) that solve the constrained minimization problem in (5). However, the expression for ABEP in [5] is not closed-form, and hence is not applicable for obtaining a closed-form solution. Alternatively, we focus on the pair-wise error probability (PEP) of SM that is given by [5, Eq. (12)]:

$$\text{PEP}_{\hat{\mathbf{H}}}(\mathbf{x}_{l,s} \to \mathbf{x}_{t,s'}) = \frac{1}{\pi}\int_0^{\pi/2}\left(1+\frac{\mathrm{g}_{\text{SM}}}{4\sin^2\theta}\times\frac{E_s}{N_0(1+\sigma_\epsilon^2)+E_s\sigma_\epsilon^2}\right)^{-N_r} d\theta, \quad (6)$$

where $\mathbf{x}_{l,s}$ and $\mathbf{x}_{t,s'}$ respectively denote the transmitted and detected signal, and:

$$\mathrm{g}_{\text{SM}} = \begin{cases} 2, & \text{if} \quad t \neq l \\ |s-s'|^2, & \text{if} \quad t = l \end{cases} \quad (7)$$

The PEP of SM assuming P-CSI is calculated by [2]:

$$\text{PEP}_{\mathbf{H}}(\mathbf{x}_{l,s} \to \mathbf{x}_{t,s'}) = \frac{1}{\pi}\int_0^{\pi/2}\left(1+\frac{\mathrm{g}_{\text{SM}}\gamma_s}{4\sin^2\theta}\right)^{-N_r} d\theta \quad (8)$$

Comparing (6) with (8), it is straightforward to infer that the only difference between these two cases is that γ_s is replaced by γ_e where:

$$\gamma_e = \frac{E_s}{N_0(1+\sigma_\epsilon^2)+E_s\sigma_\epsilon^2} \quad (9)$$

Note that γ_e is a function with respect to both E_s and E_p. The objective is thus simplified to the maximization of γ_e and this can be formulated as follows:

$$\begin{aligned} (E_p^\dagger, E_s^\dagger) = \arg\max_{(E_p,E_s)} \quad & \gamma_e(E_p,E_s) \\ \text{subject to:} \quad & \eta E_p + (1-\eta)E_s = E_a \end{aligned} \quad (10)$$

B. Closed-form OPA Solution

Since the above problem is subject to equality constraints, the Lagrange multiplier maximization method [8] can be used. The corresponding Lagrangian function is written as:

$$\Lambda(E_p, E_s, \lambda) = \gamma_e(E_p,E_s) + \lambda(\eta E_p + (1-\eta)E_s - E_a), \quad (11)$$

where λ is the Lagrange multiplier. In order to achieve the maximum of the Lagrangian function, stationary points can be obtained by solving the following system of equations:

$$\begin{cases} \partial\Lambda(E_p^s, E_s^s, \lambda^s)/\partial E_p^s &= 0 \\ \partial\Lambda(E_p^s, E_s^s, \lambda^s)/\partial E_s^s &= 0 \\ \partial\Lambda(E_p^s, E_s^s, \lambda^s)/\partial \lambda^s &= 0 \end{cases} \quad (12)$$

where λ^s is the Lagrange multiplier associated to the stationary point (E_p^s, E_s^s). After solving (12), the stationary points of E_p are given by:

$$E_p^{s_1,s_2} = E_a\frac{-f(\gamma_a) \pm \sqrt{f^2(\gamma_a)+\frac{g}{\eta}f(\gamma_a)}}{g}, \quad (13)$$

where

$$\begin{cases} f(\gamma_a) = 1+\dfrac{1-\eta}{\gamma_a} & (14a) \\ g = (1-\eta)N_p - \eta & (14b) \end{cases}$$

Note that $f(\gamma_a)$ is always positive, and $g \geq 1-2\eta$ because $N_p \geq 1$. In practice, the pilot ratio is usually less than 10% [9]. Therefore, the parameter g is also positive. Consequently, $E_p^{s_1}$ is positive whereas $E_p^{s_2}$ is negative. However, energy is non-negative and, thus, $E_p^{s_1}$ is the only possible stationary point. The second derivative of Λ with respect to E_p is calculated by:

$$\frac{\partial\Lambda(E_p)}{\partial^2 E_p} = -\frac{2N_pE_a^2}{N_0}\times\frac{\eta f^2(\gamma_a)+gf(\gamma_a)}{(gE_p+f(\gamma_a)E_a)^3} \quad (15)$$

Substituting (13) into (15) gives:

$$\left.\frac{\partial\Lambda(E_p)}{\partial^2 E_p}\right|_{E_p=E_p^{s_1}} = -\frac{2\eta N_p}{E_aN_0}\left(f^2(\gamma_a)+\frac{g}{\eta}f(\gamma_a)\right)^{-\frac{1}{2}} \quad (16)$$

It is worth noting that the right side of the above equation is negative. Based on the second derivative, it can be shown that $(E_p^{s_1}, \frac{E_a-\eta E_p^{s_1}}{1-\eta})$ is the only maximum point of the constrained optimization problem in (10). The optimal choice for E_p is hence given by:

$$E_p^\dagger = E_a\frac{\sqrt{f^2(\gamma_a)+\left(\frac{1-\eta}{\eta}N_p-1\right)f(\gamma_a)}-f(\gamma_a)}{(1-\eta)N_p-\eta} \quad (17)$$

C. Simplified Solution assuming a high SNR

With the assumption of a high average SNR, *i.e.*, $\gamma_a \gg 1$, (14a) can be approximated to:

$$f(\gamma_a) \cong 1 \quad (18)$$

Substituting (18) into (17), we have:

$$E_p^\dagger = \frac{\sqrt{\frac{1-\eta}{\eta}N_p}-1}{(1-\eta)N_p-\eta}E_a \quad (19)$$

It can be observed that in this case the ratio between $E_p^\dagger$ and E_a only depends on the pilot sequence length N_p and the pilot ratio η. Fig. 2 plots the OPA against N_p and η and compares the result with EPA. As can be seen, when ηN_p is larger than one, the optimum power for pilots is slightly below the average power. However, more power is required for pilots while $\eta N_p < 1$. Furthermore, the equivalent SNR of SM using OPA can be computed by substituting (19) into (9):

$$\gamma_e = \gamma_a\left(\frac{\sqrt{N_p}}{\sqrt{(1-\eta)N_p}+\sqrt{\eta}}\right)^2 \quad (20)$$

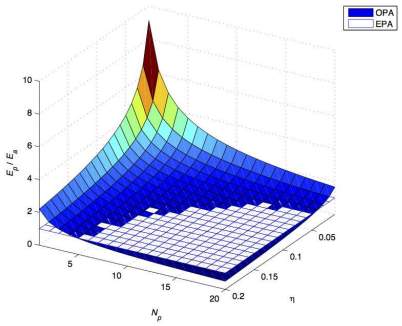

Fig. 2. Power allocation in terms of N_p and η

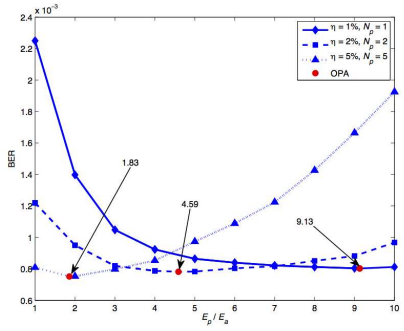

Fig. 3. BER performance of SM ($N_t = 4$, QPSK) at $\gamma_a = 20$ dB

IV. Simulation Results

In this section, the proposed OPA method is evaluated by Monte Carlo simulations. The simulation is implemented for two purposes: i) to validate the accuracy of the optimization solutions; ii) to compare the BER performance of OPA with the cases of EPA and P-CSI. Furthermore, the energy efficiency of OPA is presented and it is compared with EPA. In all simulations, the number of receive antennas is assumed to be two, while the number of transmit antennas is varied.

A. Optimization Accuracy

Assume $N_t = 4$ as an example, Fig. 3 shows the BER performance of SM as a function of E_p/E_a. A number of pilot ratios are considered, and N_p is also varied to validate for a broad range of scenarios. In case for the (η, N_p)s, the respective OPA solution is marked by red dots.

As can be seen from Fig. 3, the optimization approach achieves the minimum value for each BER curve. Furthermore, the optimal E_p/E_a varies along with the pilot ratio. In general and as expected, it can be found that it is better to allocate more power to the pilot signal when the pilot ratio is decreased. For $\eta = 5\%$, the optimum E_p/E_a approaches one. This is equivalent to the EPA method. However, this value is increased to 4.59 when the pilot ratio reduces to 2%. As η is further decreased to 1%, the best E_p/E_a results in 9.13. The reason for this trend is that a low pilot ratio results in a poor CE accuracy and this impairs the BER performance more significantly than reducing the power for the data symbols. In this situation, it is beneficial to increase the pilot power so that the CE accuracy can be improved. In contrast, more power should be allocated to data symbols when the channel estimation produces more accurate results.

B. BER Performance

In this section, the BER performance of OPA is presented against the average SNR for $N_t = 2$ and $N_t = 4$, respectively. The CE period is fixed in order to offer a fair comparison. Therefore, when the number of transmit antennas increases from two to four, the pilot sequence length is shortened to be a half. Additionally, the cases of P-CSI as well as EPA are taken into account as benchmarks.

Fig. 4(a) shows the BER performance of SM with two transmit antennas. The following outcomes are observed. Firstly, compared to EPA, the performance of OPA is much closer to the case of P-CSI with a gap of less than 0.8 dB. Secondly, the BER performance of EPA degrades rapidly when the pilot ratio is decreased. In contrast, OPA provides a fairly stable performance. For example, the BER performance of OPA for $\eta = 1\%$ is only 0.3 dB less than for $\eta = 5\%$. In contrast, EPA results in a loss of more than 1 dB. This is because OPA decreases the impact of the pilot ratio by trading off the power allocated to pilots and data symbols. Therefore, OPA significantly outperforms EPA for a low pilot ratio.

When the number of transmit antennas is increased to four, the BER performance of SM is shown in Fig. 4(b). Compared to the case of $N_t = 2$, the gap between EPA and P-CSI becomes even larger. Assume $\eta = 1\%$ for example, EPA requires 3.2 dB more SNR than P-CSI. However this loss is only 1.6 dB when two transmit antennas are applied. The reason for this is that the pilot sequence length is reduced, resulting in a less accurate CE. However, by adjusting the power of the pilot signal, the BER performance of OPA can still be tightly close to the case of P-CSI. To achieve the same BER target at $\eta = 1\%$, the gap between OPA and P-CSI is only about 0.7 dB. This is basically the same as in the case of $N_t = 2$.

C. Energy Efficiency

Throughput is another important measurement that defines the successfully transmitted data. Motivated by this, we evaluate the energy efficiency of the throughput for the proposed method. The path loss is assumed to be 100 dB without consideration of shadow fading [10].

Fig. 5 shows the throughput per unit energy for various pilot ratios. As can be seen, when increasing the pilot ratio,

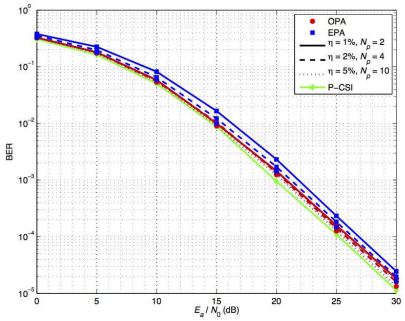

(a) $N_t = 2$, 8PSK

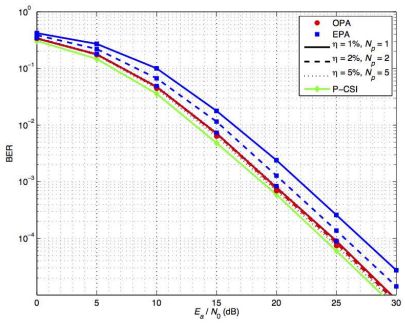

(b) $N_t = 4$, QPSK

Fig. 4. BER performance of SM against the average SNR for different number of transmit antennas

the energy efficiency is high for $\eta = 5\%$, but subsequently decays when η further increases. This trend signifies the trade-off between the CE accuracy and the SNR for data symbols. Furthermore, compared to EPA, OPA obtains an energy saving of up to 72% when $N_t = 4$ and $\eta = 1\%$. Moreover, at a low pilot ratio, the energy efficiency of EPA decreases with an increasing N_t. As can be seen, when using $N_t = 4$ at $\eta = 1\%$, the throughput of EPA-based SM is 6% less than for $N_t = 2$. The pilot sequence length is a product of η and $17N_t$, and therefore is quite small for a low η and a large N_t. As a result, the CE performance becomes very poor if the power for pilots is constant. In contrast to EPA, OPA achieves a higher energy efficiency when using a larger number of transmit antennas.

V. Conclusion

In this paper, we propose a closed-form optimal power allocation for pilots in SM. The optimization result is only related to the pilot ratio and the pilot sequence length, regardless of the number of transmit antennas used. Simulation results validate the accuracy of the optimization approach.

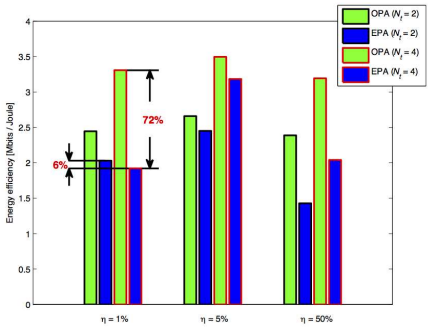

Fig. 5. Energy consumption at the transmitter

Furthermore, the BER performance of OPA is close to the case of P-CSI for various pilot ratios with a gap of less than 0.8 dB. When compared to EPA, OPA achieves a higher energy efficiency when the number of transmit antennas increases. The demonstrated performance shows that OPA-based SM is a more robust scheme especially when a large number of transmit antennas are used.

Acknowledgement

We gratefully acknowledge support from the European Union (PITNGA2010264759, GREENET project) for this work.

References

[1] M. Di Renzo, H. Haas, and P. M. Grant, "Spatial Modulation for Multiple-Antenna Wireless Systems: A Survey," *IEEE Commun. Mag.*, vol. 49, no. 11, pp. 182–191, Nov. 2011.

[2] M. Di Renzo and H. Haas, "Bit Error Probability of SM-MIMO Over Generalized Fading Channels," *IEEE Trans. Veh. Technol.*, vol. 61, no. 3, pp. 1124 –1144, march 2012.

[3] M. Biguesh and A. B. Gershman, "Training-based mimo channel estimation: a study of estimator tradeoffs and optimal training signals," *IEEE Trans. Signal Proc.*, vol. 54, no. 3, pp. 884–893, 2006.

[4] M. Di Renzo and H. Haas, "Training-based MIMO channel estimation: a study of estimator tradeoffs and optimal training signals," *IEEE Trans. Veh. Technol.*, march 2012.

[5] E. Basar, U. Aygolu, E. Panayirci, and H. Poor, "Performance of Spatial Modulation in the Presence of Channel Estimation Errors," *IEEE Commun. Lett.*, vol. 16, no. 2, pp. 176–179, 2012.

[6] J. Jeganathan, A. Ghrayeb, and L. Szczecinski, "Spatial Modulation: Optimal Detection and Performance Analysis," *IEEE Commun. Lett.*, vol. 12, no. 8, pp. 545–547, 2008.

[7] W. Gifford, M. Win, and M. Chiani, "Diversity with practical channel estimation," *IEEE Trans. Wireless Commun.*, vol. 4, no. 4, pp. 1935–1947, 2005.

[8] D. P. Bertsekas, *Constrained Optimization and Lagrange Multiplier Methods*, 1st ed. Athena Scientific, Jan. 1996.

[9] J. Berkmann, C. Carbonelli, F. Dietrich, C. Drewes, and W. Xu, "On 3G LTE Terminal Implementation - Standard, Algorithms, Complexities and Challenges," in *'08. International Conference on Wireless Communications and Mobile Computing (IWCMC)*, Aug. 2008, pp. 970 –975.

[10] J. Salo, G. Del Galdo, J. Salmi, P. Kyösti, M. Milojevic, D. Laselva, and C. Schneider, "MATLAB implementation of the 3GPP Spatial Channel Model (3GPP TR 25.996)," On-line, Jan. 2005.

A Novel Multiple Access Scheme based on Spatial Modulation MIMO

Xiping Wu*, Marco Di Renzo†, and Harald Haas*

*Institute for Digital Communications
School of Engineering
The University of Edinburgh
EH9 3JL, Edinburgh, UK
{xiping.wu, h.haas}@ed.ac.uk

†French National Centre for Scientific Research (CNRS)
Laboratory for Signals and Systems (LSS)
École Supérieure d'Électricité (SUPELEC)
3 rue Joliot-Curie, 91192 Gif-sur-Yvette (Paris), France
marco.direnzo@lss.supelec.fr

***Abstract*—Spatial modulation (SM) is a unique single-stream Multiple-Input Multiple-Output (MIMO) transmission technique. Unlike conventional MIMO schemes, SM activates a single transmit antenna at any time instance, and therefore completely avoids inter-channel interference in single user scenarios. When considering multiple users, precoding techniques can be applied to realise multi-user SM (MU-SM) and coordinate multi-user interference. The transmit antennas in MU-SM are divided into groups, and each group is dedicated to one user. This means that the management and selection of antennas are crucial with respect to capacity in MU-SM. Therefore, we propose a novel multiple access method in this paper, named spatial modulation multiple access (SMMA). Unlike in MU-SM where a fixed antenna arrangement is used, the concept of SMMA is to adaptively allocate the transmit antennas to multiple users. Results show that SMMA obtains a signal-to-noise ratio (SNR) gain of up to 6 dB over MU-SM. More importantly, the performance of SMMA degrades insignificantly as the number of users increases.**

***Index Terms*—MIMO, spatial modulation (SM), space-division multiple access**

I. Introduction

SPATIAL modulation (SM) is a relatively new Multiple-Input Multiple-Output (MIMO) transmission technique [1]–[3], in which antenna positions are exploited to carry information bits. In contrast with traditional MIMO systems, SM activates a single transmit antenna at any time instance. As a result, inter-channel interference is completely avoided in SM for single user scenarios. Also, SM exhibits a significant saving in quiescent power at the power amplifier stage, because it requires only one radio-frequency (RF) chain regardless of the number of antennas used. With the assumption of a single user, recent studies show that SM offers a better performance than many state-of-the-art MIMO schemes, while achieving a low-complexity implementation [4], [5].

However, multiple access is essential and significant in practical communication systems. In order to realise multiple access for MIMO schemes, space-division multiple access (SDMA) techniques are developed, where users are multiplexed in the same time-frequency slot [6]–[8]. In [6], dirty paper coding (DPC) and precoding techniques are summarised with the purpose of eliminating or minimising multi-user interference (MUI). Despite of DPC can achieve the full sum capacity, it is difficult to implement in practice due to the high computational complexity. Unlike DPC, precoding methods, such as block diagonalisation, are simple and straightforward for MUI cancellation [7]. In addition, the opportunistic SDMA (OSDMA) was proposed in [8], which enables each user to report the best beam and its signal-to-interference-plus-noise ratio (SINR) to the base station. Based on the received SINR, the base station then schedules transmissions to multiple users.

So far, the study of SDMA has focused on multi-stream MIMO, and only a few investigations have been conducted with respect to multi-user SM (MU-SM). In [9], a precoding method is proposed to coordinate MUI when multiple users are involved in SM systems. However, [9] has two limitations: i) the antenna allocation to different users is fixed, and ii) only one receive antenna is allowed at each user end. To the best of the authors' knowledge, an adaptive management and selection of antennas for MU-SM has not been studied before.

In this paper, we propose a novel multiple access scheme, named spatial modulation multiple access (SMMA). The concept of SMMA is to adaptively allocate transmit antennas to different users. By exploiting the antenna diversity, SMMA realises the improvement of capacity in MU-SM. Another important advantage of SMMA is the availability of multiple receive antennas. Results show that SMMA offers a significant signal-to-noise ratio (SNR) gain against MU-SM. In addition, SMMA outperforms MU-SM greatly for a larger number of users. Moreover, the performance of SMMA increases as the number of receive antennas increases, while the performance of MU-SM is confined by a single receive antenna.

The remainder of this paper is organised as follows. The working principles of both SM and MU-SM are described in Section II. The proposed SMMA is introduced in Section III. Section IV presents the simulation results. The paper is summarized in Section V.

II. System Model

In this study, we consider the downlink in single-cell scenarios. The base station (BS) simultaneously serves N_u users assuming equal bandwidth per user. The total number of transmit antennas at the BS is denoted by N_{tot}, while the number of receive antennas for each mobile user is N_r. The transmit antennas are divided into N_u groups, and each group

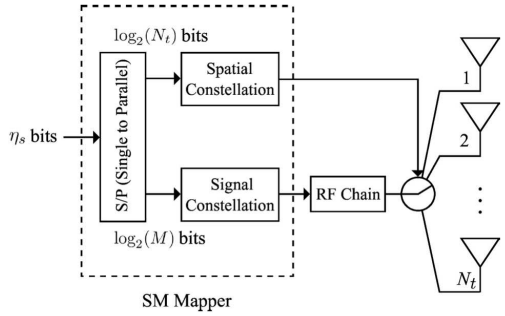

Fig. 1. Block diagram of Spatial Modulation for a single user

contains $N_t = N_{\text{tot}}/N_u$ antennas. For each user, a $N_t \times N_r$ MIMO system is applied.

A. SM for a Single User

In SM, as shown in Fig. 1, information bits are carried by two constellation diagrams. The size of the spatial constellation diagram is N_t, and the size of the signal constellation diagram is denoted by M. The bit-stream is divided into blocks of η_s bits, where $\eta_s = \log_2(N_t M)$ is the number of bits per symbol. Each block is then split into two units of $\log_2(N_t)$ and $\log_2(M)$ bits. The first part activates one of the transmit antennas, and the currently active antenna is denoted by l. The second part determines one symbol from the signal constellation diagram, and the active antenna conveys this symbol, which is denoted by s.

The fading coefficient of the channel between the t-th transmit antenna and the r-th receive antenna is denoted by $h_{t,r}$. In this paper, a quasistatic Rayleigh fading channel is assumed, without the consideration of path loss or shadow fading, *i.e.*, $h_{t,r} \sim \mathcal{CN}(0,1)$. The received signal at the r-th receive antenna is given by:

$$y_r = h_{l,r} s + w_r, \tag{1}$$

where w_r is a sample of complex Additive White Gaussian Noise (AWGN). Across the receive antennas, the noise components are statistically independent. The transmitted symbol is decoded by joint maximum likelihood (ML) detection [10] as follows:

$$(\hat{l}, \hat{s}) = \arg\min_{l,s} \sum_{r=1}^{N_r} \| y_r - h_{l,r} s \|^2, \tag{2}$$

where $\hat{l}$ and $\hat{s}$ denote the decoding results of l and s, respectively.

B. Multi-user SM

In order to eliminate the interference between the co-channel users, the precoding method in [9] is applied, where perfect channel state information is assumed at both the transmitter and the receiver. The precoding mask is defined as a vector for shaping the signal before it is sent out. We denote the precoding mask by $\mathbf{P} = [p_1, p_2, \ldots, p_{N_u}]^T$, where p_k is the element for user k. The transmitted signal for each user is the product of the chosen symbol and the corresponding element in the precoding mask, which is denoted by $\dot{s}_k = s_k p_k$. In addition, h_{l_k,r_j} represents the channel from the active antenna of user k to the receive antenna of user j. The received signal for user k is then written as:

$$y_{r_k} = \underbrace{h_{t_k,r_k}\dot{s}_k}_{A} + \sum_{j=1\neq k}^{N_u} h_{t_j,r_k}\dot{s}_j + w_{r_k} \tag{3}$$

Substituting $\dot{s}_k = s_k p_k$ into (3), we have:

$$y_{r_k} = \underbrace{[h_{t_1,r_k}s_1, h_{t_2,r_k}s_2, \cdots, h_{t_{N_u},r_k}s_{N_u}]\mathbf{P}}_{B} + w_{r_k} \tag{4}$$

In order to eliminate multi-user interference, term B must equal term A for all users. The effective channel-modulation matrix is defined as:

$$\mathbf{H}_{\text{eff}} = \begin{bmatrix} h_{t_1,r_1}s_1 & h_{t_2,r_1}s_2 & \cdots & h_{t_{N_u},r_1}s_{N_u} \\ h_{t_1,r_2}s_1 & h_{t_2,r_2}s_2 & \cdots & h_{t_{N_u},r_2}s_{N_u} \\ \vdots & \vdots & \ddots & \vdots \\ h_{t_1,r_{N_u}}s_1 & h_{t_2,r_{N_u}}s_2 & \cdots & h_{t_{N_u},r_{N_u}}s_{N_u} \end{bmatrix} \tag{5}$$

and the required signals of all users form a vector as follows:

$$\mathbf{H}_{\text{req}} = \begin{bmatrix} h_{t_1,r_1}s_1 \\ h_{t_2,r_2}s_2 \\ \vdots \\ h_{t_{N_u},r_{N_u}}s_{N_u} \end{bmatrix} \tag{6}$$

Equalizing A and B for all users is equivalent to:

$$\mathbf{H}_{\text{eff}}\mathbf{P} = \mathbf{H}_{\text{req}} \tag{7}$$

Note that $\mathbf{H}_{\text{req}}$ is the diagonal of the matrix $\mathbf{H}_{\text{eff}}$. Therefore, the precoding mask is obtained by:

$$\mathbf{P} = (\mathbf{H}_{\text{eff}})^{-1}\text{diag}(\mathbf{H}_{\text{eff}}), \tag{8}$$

where diag$(\cdot)$ extracts the diagonal of a matrix.

At the receiver of each user, the decoding process is the same as that in SM for a single user. Note that due to a single active antenna of SM, the above precoding method is available for a single receive antenna only.

III. Spatial Modulation Multiple Access

In MU-SM, the transmit antennas are allocated to multiple users in a fixed way, and therefore it does not take full advantage of antenna diversity. In order to improve the capacity in MU-SM, we propose an adaptive method to allocate the antennas. Fig. 2 shows the block diagram of SMMA for an example of two users. At the transmitter, the antennas are divided into N_u groups, and each group belongs to a

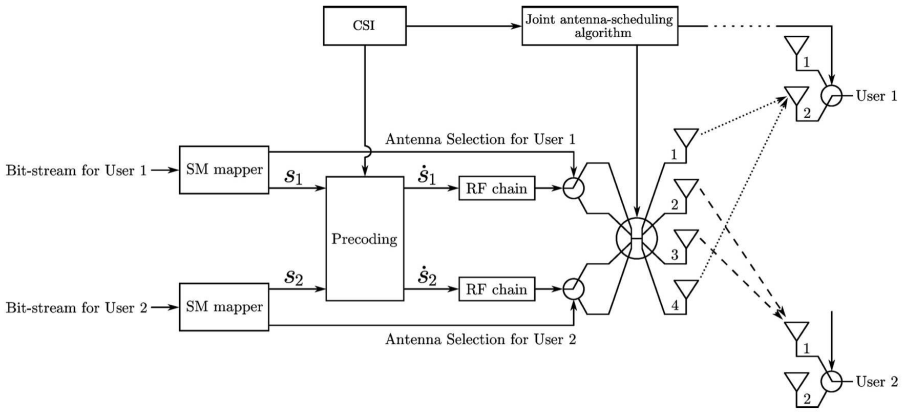

Fig. 2. SMMA ($N_{\text{tot}} = 4$, $N_u = 2$). Dotted lines: transmit antennas allocated to user 1; Dashed lines: transmit antennas allocated to user 2.

single user. Meanwhile, one of the receive antennas is chosen at each user end. In SMMA, the selection of the transmit antennas and the receive antennas are jointly implemented in order to maximise the capacity. After allocating the antennas, precoding is applied in the same way as that in MU-SM.

The ratio of the power of received signal to the noise power is defined as received SNR. For the channel from the t-th transmit antenna to the r-th receive antenna of user k, the received SNR is denoted by Γ^k_{t,r_k}. Firstly, the scenario of a single receive antenna is considered at each user end. In order to maximise the channel capacity, the transmit antennas resulting in the largest SNR values would be chosen for each of the users. However, one transmit antenna could be the best candidate for several users at the same time. In order to avoid a certain user from being allocated all strong antenna candidates, the antenna selection is implemented sequentially among the users, and each user selects one antenna at a time. This round-robin antenna selection heuristic does not guarantee optimality, but introduces a level of fairness.

When there are N_r receive antennas at each user, there are $(N_r)^{N_u}$ possible combinations of choosing one antenna from each user. The above algorithm is implemented for each combination. Then the average received SNR, denoted by $\bar{\Gamma}$, is calculated over all users, and the combination that maximises $\bar{\Gamma}$ is selected. The index of the combination is denoted by n, and the set of all combinations is denoted by $\mathcal{I}$. The set of Γ^k_{t,r_k} for all t and k in the n-th combination is denoted by $\mathcal{G}_n$. The detailed antenna allocation algorithm is as follows:

1) select the n-th combination of $[r_1, \ldots, r_k, \ldots, r_{N_u}]$ from $\mathcal{I}$, where n is initialized to be one;
2) the index of the antenna-selection round is denoted by $\mathcal{F}$, which is initialized to be one. Set a vector $f = \bar{0}$, where $f = [f_1, \ldots, f_k, \ldots, f_{N_u}]$ and f_k indicates whether user k has been allocated one transmit antenna in the current round;
3) select the strongest Γ_{t,r_k} in $\mathcal{G}_n$, and the corresponding antenna and user are denoted by $\tilde{t}$ and $\tilde{k}$;
4) if $f_{\tilde{k}} = 0$, then allocate $\tilde{t}$ to user $\tilde{k}$, and set $f_{\tilde{k}} = 1$. Otherwise, ignore the chosen result and repeat 3);
5) remove all Γ_{t,r_k} related to $\tilde{t}$ from $\mathcal{G}_n$. If $f_k = 0$ for any k, repeat 3);
6) if $\mathcal{F} < \dfrac{N_{\text{tot}}}{N_u}$, let $\mathcal{F} = \mathcal{F} + 1$ and repeat 2);
7) compute $\bar{\Gamma}_n$ for the n-th combination;
8) let $n = n + 1$ and repeat 1). After going through all combinations, select the one of the largest $\bar{\Gamma}_n$.

IV. Simulation Results

In this section, Monte Carlo simulations are conducted to validate the proposed scheme. The performance of SMMA is compared with MU-SM of a random antenna allocation. The comparison is conducted using two metrics: the outage probability and the bit error ratio (BER). In addition, we investigate the effects of the number of users and the number of antennas on the BER performance of SMMA. Furthermore, the energy efficiency in terms of the energy consumption per bit is evaluated for the proposed method. In all simulations, η_s is assumed to be 4 bits/s/Hz for each user, and Quadrature Amplitude Modulation (QAM) is used for the signal constellation diagram.

A. Outage Probability

Firstly, we study the outage probability for both SMMA and MU-SM, which is defined as the probability that the received SNR is below a certain target. The total number of transmit antennas is assumed to be 16, and different user numbers of 4 and 8 are considered. The Cumulative Distribution Function (CDF) of the received SNR is shown in Fig. 3, where the SNR at the transmitter is fixed to be 20 dB [11]. As shown, SMMA achieves a much lower outage probability than MU-SM. To achieve a received SNR of 10 dB, the outage probabilities of MU-SM are 9% and 24% for 4 and 8 users, respectively. In contrast, the outage probabilities of SMMA are 2.1% and

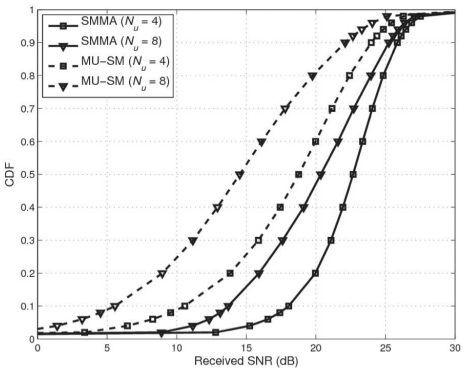

Fig. 3. CDF of received SNR for SMMA in comparison with MU-SM. The transmitted SNR is fixed at 20 dB.

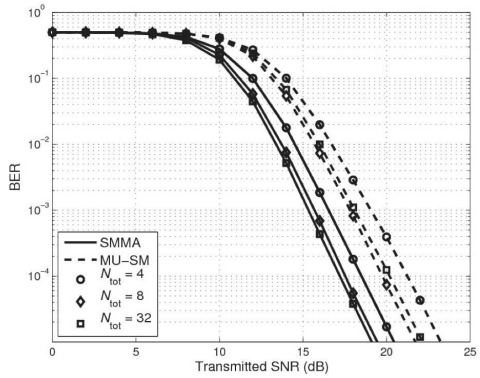

Fig. 4. BER performance of SMMA with different numbers of total transmit antennas ($N_u = 2$). A single receive antenna is considered.

3.3%. When the SNR target increases to 15 dB, the outage probability of MU-SM increases to 26% in the case of four users. Meanwhile, the outage probability of SMMA remains below 4%.

B. Bit Error Ratio

Secondly, the BER performance is compared between SMMA and MU-SM for different N_{tot}, N_u and N_r. As noted, MU-SM is available for a single receive antenna only. To ensure a fair comparison, the number of receive antennas is considered to be one for SMMA, except when studying its effect. In addition, convolutional coding with a code rate of 3/4 is applied.

1) Effect of the Number of Total Transmit Antennas: Fig. 4 shows the BER performance of SMMA with different numbers of the total transmit antennas, where the user number is fixed to be two. As shown, for various N_{tot}, SMMA always offers a better performance than MU-SM. Taking $N_{\text{tot}} = 4$ as an example, SMMA obtains an SNR gain of 2.7 dB against MU-SM to achieve a BER of 1×10^{-3}. When N_{tot} increases, the performance of MU-SM increases at first and then decreases, which fits the trend of SM for a single user [12]. In contrast, the BER performance of SMMA keeps increasing with an increase of N_{tot}. The reason is that the number of candidate antennas for each user increases when more transmit antennas are involved. Therefore, the users are more likely to be allocated a set of antennas that result in a high SNR.

2) Effect of the Number of Users: Fig. 5 presents the BER performance of SMMA for different user numbers, where the total number of transmit antennas is assumed to be 16. The following outcomes are observed: i) SMMA outperforms MU-SM for various user numbers; ii) for a larger number of users, the BER performance degrades for both SMMA and MU-SM. However, the performance of MU-SM reduces more dramatically than SMMA, especially when the number of users increases from 4 to 8. The reason for this trend is that when

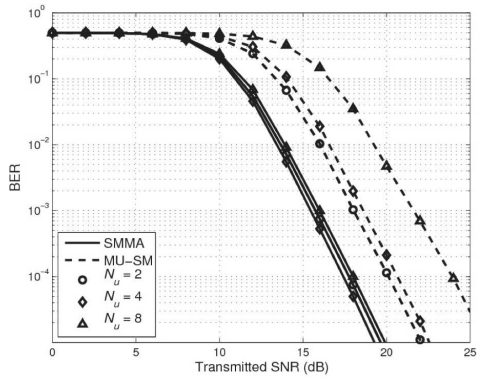

Fig. 5. BER performance of SMMA for different numbers of users ($N_{\text{tot}} = 16$). A single receive antenna is considered.

more users are involved, each user has more opportunities to obtain a strong antenna. As a result, SMMA outperforms MU-SM more significantly for a larger N_u. Taking $N_u = 4$ and $N_u = 8$ for example, compared with MU-SM, SMMA obtains SNR gains of 3.2 dB and 6 dB, respectively.

3) Effect of the Number of Receive Antennas: When SMMA employs multiple receive antennas, the corresponding BER performance is shown in Fig. 6, where the total number of transmit antennas is 16 and the number of users is fixed to be 8. As can be seen, the performance of SMMA increases as the number of receive antennas increases, while the performance of MU-SM is confined by a single receive antenna. For two receive antennas, SMMA obtains an SNR gain of 7.2 dB in comparison with MU-SM. When four receive antennas are used, the SNR gap between SMMA and MU-SM is further increased to 8 dB. Therefore, compared with MU-SM, SMMA

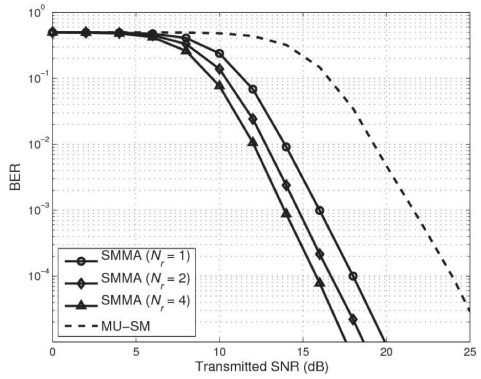

Fig. 6. BER performance of SMMA with different numbers of receive antennas ($N_{\text{tot}} = 16$, $N_u = 8$).

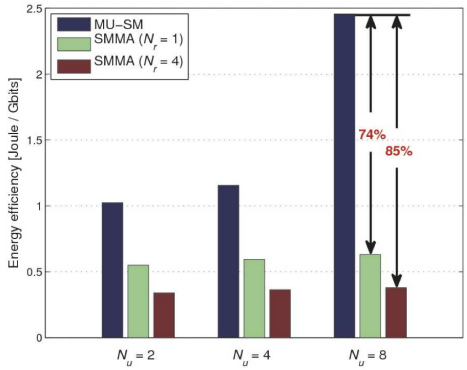

Fig. 7. Transmit Energy Efficiency

is more robust when multiple receive antennas are used.

C. Energy Efficiency

Thirdly, the energy efficiency of the proposed scheme is evaluated in terms of Joule per Gbits, as shown in Fig. 7. Assuming the same number of transmitted bits per unit time, SMMA with one receive antenna requires 74% less energy than MU-SM. The energy efficiency is further increased to 85% when four receive antennas are used in SMMA. Moreover, the energy consumption of MU-SM exponentially increases as the number of users increases. In contrast, the energy efficiency of SMMA is only very slightly affected by the increase of the number of users.

V. Conclusion

In this paper, we proposed a novel multiple access scheme for SM, named SMMA. In SMMA, the transmit antennas and the receive antennas are jointly scheduled for multiple users. Then precoding techniques are used to eliminate the interference between users. SMMA is available for multiple receive antennas at each user end, whereas MU-SM is only suitable for a single receive antenna. Simulation results show that SMMA significantly improves the BER performance of MU-SM systems. In comparison with MU-SM, SMMA achieves an SNR gain of up to 8 dB. When the number of users increases, the performance degradation of SMMA is much smaller than that of MU-SM. Furthermore, the BER performance of SMMA is improved when more receive antennas are used. All these merits make SMMA a promising multiple access method for multi-user MIMO systems. Future research will consider allocating a different number of transmit antennas to different users in SMMA.

Acknowledgement

We gratefully acknowledge support from the European Union's Seventh Framework Programme (FP7) under grant agreement No. 264759 (GREENET Project). Professor Haas acknowledges support from the Engineering and Physical Sciences Research Council (EPSRC) under Established Career Fellowship grant EP/K008757/1.

References

[1] R. Mesleh, H. Haas, S. Sinanovic, C. W. Ahn, and S. Yun, "Spatial modulation," *IEEE Trans. Veh. Technol.*, vol. 57, no. 4, pp. 2228–2241, July 2008.

[2] M. Di Renzo, H. Haas, and P. M. Grant, "Spatial Modulation for Multiple-Antenna Wireless Systems: A Survey," *IEEE Commun. Mag.*, vol. 49, no. 11, pp. 182–191, Nov. 2011.

[3] L. Hanzo, H. Haas, S. Imre, D. O'brien, M. Rupp, and L. Gyongyosi, "Wireless Myths, Realities, and Futures: From 3G/4G to Optical and Quantum Wireless," *Proc. IEEE*, vol. 100, no. Special Centennial Issue, pp. 1853–1888, May 2012.

[4] M. Di Renzo and H. Haas, "Performance analysis of spatial modulation," in *5th International Conference on Communications and Networking in China (CHINACOM)*, Aug. 2010, pp. 1–7.

[5] E. Basar, U. Aygolu, E. Panayirci, and H. Poor, "Performance of spatial modulation in the presence of channel estimation errors," *IEEE Commun. Lett.*, vol. 16, no. 2, pp. 176–179, Feb. 2012.

[6] Q. Spencer, C. Peel, A. Swindlehurst, and M. Haardt, "An introduction to the multi-user MIMO downlink," *IEEE Commun. Mag.*, vol. 42, no. 10, pp. 60–67, Oct. 2004.

[7] D. Gesbert, M. Kountouris, R. Heath, C.-B. Chae, and T. Salzer, "Shifting the MIMO paradigm," *IEEE Signal Process. Mag.*, vol. 24, no. 5, pp. 36–46, Sept. 2007.

[8] M. Sharif and B. Hassibi, "On the capacity of mimo broadcast channel with partial side information," in *Signals, Systems and Computers, 2004. Conference Record of the Thirty-Seventh Asilomar Conference on*, vol. 1, Nov. 2003, pp. 958–962 Vol.1.

[9] S. Narayanan, M. Chaudhry, A. Stavridis, M. Di Renzo, F. Graziosi, and H. Haas, "Multi-user spatial modulation MIMO," in *2014 IEEE Wireless Communications and Networking Conference (WCNC)*, April 2014.

[10] J. Jeganathan, A. Ghrayeb, and L. Szczecinski, "Spatial modulation: Optimal detection and performance analysis," *IEEE Commun. Lett.*, vol. 12, no. 8, pp. 545–547, Aug. 2008.

[11] 3GPP TR 36.814 v9.0.0., "Evolved universal terrestrial radio access (E-UTRA); further advancements for E-UTRA physical layer aspects (Release 9)," Mar 2010.

[12] M. Di Renzo and H. Haas, "Bit error probability of SM-MIMO over generalized fading channels," *IEEE Trans. Veh. Technol.*, vol. 61, no. 3, pp. 1124 –1144, March 2012.

References

[1] A. Fehske, G. Fettweis, J. Malmodin, and G. Biczok, "The global footprint of mobile communications: The ecological and economic perspective," *IEEE Communications Magazine*, vol. 49, pp. 55 –62, August 2011.

[2] M. Rumney, *LTE and the Evolution to 4G Wireless: Design and Measurement Challenges*. Keysight Technologies Publication, 2nd ed., 2013.

[3] R. Mesleh, H. Haas, C. W. Ahn, and S. Yun, "Spatial modulation - a new low complexity spectral efficiency enhancing technique," in *First International Conference on Communications and Networking in China (ChinaCom)*, pp. 1–5, Oct. 2006.

[4] R. Mesleh, H. Haas, S. Sinanovic, C. W. Ahn, and S. Yun, "Spatial modulation," *IEEE Trans. Veh. Technol.*, vol. 57, pp. 2228–2241, July 2008.

[5] M. Di Renzo, H. Haas, and P. M. Grant, "Spatial modulation for multiple-antenna wireless systems: a survey," *IEEE Commun. Mag.*, vol. 49, pp. 182–191, Dec. 2011.

[6] G. Auer, V. Giannini, I. Godor, P. Skillermark, M. Olsson, M. Imran, D. Sabella, M. Gonzalez, C. Desset, and O. Blume, "Cellular energy efficiency evaluation framework," in *73rd IEEE Veh. Technol. Conf. (VTC Spring)*, pp. 1–6, May 2011.

[7] Y. Chau and S.-H. Yu, "Space modulation on wireless fading channels," in *54th IEEE Veh. Technol. Conf. (VTC Fall)*, vol. 3, pp. 1668–1671 vol.3, 2001.

[8] H. Haas, E. Costa, and E. Schulz, "Increasing spectral efficiency by data multiplexing using antenna arrays," in *13th IEEE International Symposium on Personal, Indoor and Mobile Radio Communications (PIMRC)*, vol. 2, pp. 610–613 vol.2, Sept. 2002.

[9] J. Jeganathan, A. Ghrayeb, and L. Szczecinski, "Spatial modulation: Optimal detection and performance analysis," *IEEE Commun. Lett.*, vol. 12, pp. 545–547, Aug. 2008.

[10] E. Basar, U. Aygolu, E. Panayirci, and H. Poor, "Space-time block coded spatial modulation," *IEEE Trans. Commun.*, vol. 59, pp. 823–832, March 2011.

[11] S. Ganesan, R. Mesleh, H. Haas, C. W. Ahn, and S. Yun, "On the performance of spatial modulation ofdm," in *40th Asilomar Conference on Signals, Systems and Computers (ACSSC)*, pp. 1825–1829, Oct. 2006.

[12] M. Di Renzo and H. Haas, "Bit error probability of SM-MIMO over generalized fading channels," *IEEE Trans. Veh. Technol.*, vol. 61, pp. 1124–1144, March 2012.

[13] M. Koca and H. Sari, "Performance analysis of spatial modulation over correlated fading channels," in *IEEE 76th Vehicular Technology Conference (VTC Fall)*, pp. 1–5, Sept. 2012.

[14] A. Younis, D. A. Basnayaka, and H. Haas, "Performance analysis for generalised spatial modulation," in *Proceedings of 20th European Wireless Conference*, pp. 1–6, May 2014.

[15] J. Jeganathan, A. Ghrayeb, L. Szczecinski, and A. Ceron, "Space shift keying modulation for mimo channels," *IEEE Trans. on Wireless Commun.*, vol. 8, pp. 3692–3703, July 2009.

[16] A. Younis, N. Serafimovski, R. Mesleh, and H. Haas, "Generalised spatial modulation," in *44th Asilomar Conference on Signals, Systems and Computers (ASILOMAR)*, pp. 1498–1502, Nov. 2010.

[17] L.-L. Yang, "Transmitter preprocessing aided spatial modulation for multiple-input multiple-output systems," in *73rd IEEE Veh. Technol. Conf. (VTC Spring)*, pp. 1–5, May 2011.

[18] M. Di Renzo and H. Haas, "A general framework for performance analysis of space shift keying (SSK) modulation for MISO correlated Nakagami-m fading channels," *IEEE Trans. Commun.*, vol. 58, pp. 2590–2603, Sept. 2010.

[19] R. Heath, S. Sandhu, and A. Paulraj, "Antenna selection for spatial multiplexing systems with linear receivers," *IEEE Commun. Lett.*, vol. 5, pp. 142–144, April 2001.

[20] J. Wang, A. Perez-Neira, Q. Zhang, M. Gao, and X. Bian, "Closed-loop spatial modulation with antenna selection," in *11th IEEE International Conference on Signal Processing (ICSP)*, vol. 2, pp. 1291–1294, Oct 2012.

[21] R. Rajashekar, K. Hari, and L. Hanzo, "Antenna selection in spatial modulation systems," *IEEE Commun. Lett.*, vol. 17, pp. 521–524, March 2013.

[22] K. Ntontin, M. Di Renzo, A. Perez-Neira, and C. Verikoukis, "Antenna subset selection for spatial modulation: A novel and energy efficient single rf technique," in *2013 IEEE International Conference on Communications (ICC)*, pp. 2454–2458, June 2013.

[23] P. Yang, Y. Xiao, Y. Yu, and S. Li, "Adaptive spatial modulation for wireless mimo transmission systems," *IEEE Commun. Lett.*, vol. 15, pp. 602–604, June 2011.

[24] S. Sanayei and A. Nosratinia, "Antenna selection in mimo systems," *IEEE Commun. Mag.*, vol. 42, pp. 68–73, Oct. 2004.

[25] A. Ghrayeb, "A survey on antenna selection for mimo communication systems," in *2006 Information and Communication Technologies (ICTTA)*, vol. 2, pp. 2104–2109, 2006.

[26] A. Molisch, M. Win, Y. seok Choi, and J. Winters, "Capacity of mimo systems with antenna selection," *IEEE Trans. Wireless Commun.*, vol. 4, pp. 1759–1772, July 2005.

[27] A. Gorokhov, D. GORE, and A. Paulraj, "Receive antenna selection for mimo spatial multiplexing: theory and algorithms," *IEEE Trans. Signal Processing*, vol. 51, pp. 2796–2807, Nov. 2003.

[28] C. Jiang and L. Cimini, "Antenna selection for energy-efficient mimo transmission," *IEEE Wireless Commun. Lett.*, vol. 1, pp. 577–580, December 2012.

[29] D. Love and R. Heath, "Limited feedback unitary precoding for spatial multiplexing systems," *IEEE Trans. Information Theory*, vol. 51, pp. 2967–2976, Aug. 2005.

[30] A. Scaglione, P. Stoica, S. Barbarossa, G. Giannakis, and H. Sampath, "Optimal designs for space-time linear precoders and decoders," *IEEE Trans. Signal Processing*, vol. 50, pp. 1051–1064, May 2002.

[31] M. Joham, W. Utschick, and J. Nossek, "Linear transmit processing in mimo communications systems," *IEEE Trans. Signal Processing*, vol. 53, pp. 2700–2712, Aug. 2005.

[32] F. Perez-Cruz, M. Rodrigues, and S. Verdu, "Mimo gaussian channels with arbitrary inputs: Optimal precoding and power allocation," *IEEE Trans. Information Theory*, vol. 56, pp. 1070–1084, March 2010.

[33] C. Komninakis, C. Fragouli, A. Sayed, and R. Wesel, "Multi-input multi-output fading channel tracking and equalization using kalman estimation," *IEEE Trans. Signal Processing*, vol. 50, pp. 1065–1076, May 2002.

[34] A. Swindlehurst and G. Leus, "Blind and semi-blind equalization for generalized space-time block codes," *IEEE Trans, Signal Processing*, vol. 50, pp. 2489–2498, Oct. 2002.

[35] T. Abe and T. Matsumoto, "Space-time turbo equalization in frequency-selective mimo channels," *IEEE Trans. Veh. Technol.*, vol. 52, pp. 469–475, May 2003.

[36] J. Tao, J. Wu, Y. Zheng, and C. Xiao, "Enhanced mimo lmmse turbo equalization: Algorithm, simulations, and undersea experimental results," *IEEE Trans. Signal Processing*, vol. 59, pp. 3813–3823, Aug. 2011.

[37] D. Gesbert, M. Shafi, D. shan Shiu, P. Smith, and A. Naguib, "From theory to practice: an overview of mimo space-time coded wireless systems," *IEEE Journal on Selected Areas in Commun.*, vol. 21, pp. 281–302, Apr. 2003.

[38] H. El Gamal and M. Damen, "Universal space-time coding," *IEEE Trans. Information Theory*, vol. 49, pp. 1097–1119, May 2003.

[39] M. Fozunbal, S. McLaughlin, R. Schafer, and J. Landsberg, "On space-time coding in the presence of spatio-temporal correlation," *IEEE Trans. Information Theory*, vol. 50, pp. 1910–1926, Sept 2004.

[40] D. GORE and A. Paulraj, "Mimo antenna subset selection with space-time coding," *IEEE Trans. Signal Processing*, vol. 50, pp. 2580–2588, Oct. 2002.

[41] S. ten Brink, G. Kramer, and A. Ashikhmin, "Design of low-density parity-check codes for modulation and detection," *IEEE Trans. Commun.*, vol. 52, pp. 670–678, April 2004.

[42] B. Lu, G. Yue, and X. Wang, "Performance analysis and design optimization of ldpc-coded mimo ofdm systems," *IEEE Trans. Signal Processing*, vol. 52, pp. 348–361, Feb. 2004.

[43] J. Zheng and B. Rao, "Ldpc-coded mimo systems with unknown block fading channels: soft mimo detector design, channel estimation, and code optimization," *IEEE Trans. Signal Processing*, vol. 54, pp. 1504–1518, April 2006.

[44] S. J. Lee, "On the training of MIMO-OFDM channels with least square channel estimation and linear interpolation," *IEEE Commun. Lett.*, vol. 12, pp. 100–102, Feb. 2008.

[45] Z. Luo and F. Yang, "Joint maximum-likelihood channel estimation and data detection for V-BLAST Systems," in *IEEE Global Telecommun. Conference (GLOBECOM)*, pp. 1–5, Nov. 2008.

[46] M. Koca and H. Sari, "Performance of spatial modulation over correlated fading channels with channel estimation errors," in *2013 IEEE Wireless Communications and Networking Conference (WCNC)*, pp. 3937–3942, April 2013.

[47] E. Basar, U. Aygolu, E. Panayirci, and H. Poor, "Performance of Spatial Modulation in the Presence of Channel Estimation Errors," *IEEE Commun. Lett.*, vol. 16, pp. 176–179, February 2012.

[48] M. Di Renzo, D. De Leonardis, F. Graziosi, and H. Haas, "Space shift keying (ssk-) mimo with practical channel estimates," *IEEE Trans. Commun.*, vol. 60, pp. 998–1012, April 2012.

[49] M. Faiz, S. Al-Ghadhban, and A. Zerguine, "Recursive least-squares adaptive channel estimation for spatial modulation systems," in *9th IEEE Malaysia International Conference on Commun. (MICC)*, pp. 785–788, Dec. 2009.

[50] S. Sugiura and L. Hanzo, "Effects of channel estimation on spatial modulation," *IEEE Signal Processing Lett.*, vol. 19, pp. 805–808, Dec. 2012.

[51] N. Serafimovski, S. Sinanovic, A. Younis, M. Di Renzo, and H. Haas, "2-user multiple access spatial modulation," in *2011 IEEE GLOBECOM Workshops*, pp. 343–347, Dec. 2011.

[52] S. Wang, Y. Li, and J. Wang, "Multiuser detection in massive spatial modulation mimo with low-resolution adcs," *IEEE Trans. Wireless Commun.*, vol. PP, no. 99, pp. 1–1, 2014.

[53] X. Li, Y. Zhang, L. Xiao, X. Xu, and J. Wang, "A novel precoding scheme for downlink multi-user spatial modulation system," in *IEEE 24th International Symposium on Personal Indoor and Mobile Radio Communications (PIMRC)*, pp. 1361–1365, Sept 2013.

[54] S. Narayanan, M. Chaudhry, A. Stavridis, M. Di Renzo, F. Graziosi, and H. Haas, "Multi-user spatial modulation mimo," in *2014 IEEE Wireless Communications and Networking Conference (WCNC)*, pp. 671–676, April 2014.

[55] R. Mesleh and S. S. Ikki, "Analysis of cooperative communication spatial modulation with imperfect channel estimation," in *24th IEEE International Symposium on Personal Indoor and Mobile Radio Communications (PIMRC)*, pp. 2027–2023, Sept. 2013.

[56] S. Narayanan, M. Di Renzo, F. Graziosi, and H. Haas, "Distributed spatial modulation for relay networks," in *78th IEEE Vehicular Technology Conference (VTC Fall)*, pp. 1–6, Sept. 2013.

[57] X. Wu, H. Claussen, M. Di Renzo, and H. Haas, "Channel estimation for spatial modulation," *IEEE Trans. Commun.*, vol. 62, pp. 4362–4372, Dec. 2014.

[58] X. Wu, M. Di Renzo, and H. Haas, "Adaptive selection of antennas for optimum transmission in spatial modulation," *IEEE Trans. Wireless Commun.*, 2015.

[59] X. Wu, S. Sinanovic, M. Di Renzo, and H. Haas, "Structure optimisation of spatial modulation over correlated fading channels," in *2012 IEEE Global Communications Conference (GLOBECOM)*, pp. 4049–4053, Dec. 2012.

[60] X. Wu, S. Sinanovic, M. Di Renzo, and H. Haas, "Base station energy consumption for transmission optimised spatial modulation (tosm) in correlated channels," in *17th IEEE International Workshop on Computer Aided Modeling and Design of Communication Links and Networks (CAMAD)*, pp. 261–265, Sept. 2012.

[61] X. Wu, M. Di Renzo, and H. Haas, "Direct transmit antenna selection for transmit optimized spatial modulation," in *78th IEEE Vehicular Technology Conference (VTC Fall)*, pp. 1–5, Sept. 2013.

[62] X. Wu, M. Di Renzo, and H. Haas, "Channel estimation for spatial modulation," in *24th IEEE International Symposium on Personal Indoor and Mobile Radio Communications (PIMRC)*, pp. 306–310, Sept. 2013.

[63] X. Wu, M. Di Renzo, and H. Haas, "Spatially-averaging channel estimation for spatial modulation," in *80th IEEE Vehicular Technology Conference (VTC Fall)*, pp. 1–5, Sept. 2014.

[64] X. Wu, M. Di Renzo, and H. Haas, "Optimal power allocation for channel estimation in spatial modulation," in *2014 IEEE International Conf. on Commun. (ICC)*, pp. 5481–5485, June 2014.

[65] X. Wu, M. Di Renzo, and H. Haas, "Effect of pilot ratio on channel estimation for spatial modulation," in *18th IEEE International Workshop on Computer Aided Modeling and Design of Communication Links and Networks (CAMAD)*, pp. 144–148, Sept. 2013.

[66] X. Wu, M. Di Renzoy, and H. Haas, "A novel multiple access scheme based on spatial modulation MIMO," in *19th IEEE International Workshop on Computer Aided Modeling and Design of Communication Links and Networks (CAMAD)*, pp. 285–289, Dec. 2014.

[67] G. Raleigh and J. Cioffi, "Spatio-temporal coding for wireless communications," in *1996 Global Telecommunications Conference (GLOBECOM)*, vol. 3, pp. 1809–1814 vol.3, Nov. 1996.

[68] G. J. Foschini, "Layered space-time architecture for wireless communication in a fading environment when using multi-element antennas," *Bell Labs Technical Journal*, vol. 1, pp. 41–59, Autumn 1996.

[69] P. Wolniansky, G. Foschini, G. Golden, and R. Valenzuela, "V-BLAST: An architecture for realizing very high data rates over the rich-scattering wireless channel," in *1998 International Symposium on Signals, Systems, and Electronics (ISSSE)*, pp. 295–300, Sept. 1998.

[70] S. Alamouti, "A simple transmit diversity technique for wireless communications," *IEEE Journal on Selected Areas in Commun.*, vol. 16, pp. 1451–1458, Oct. 1998.

[71] V. Tarokh, H. Jafarkhani, and A. Calderbank, "Space-time block codes from orthogonal designs," *IEEE Trans. Inf. Theory*, vol. 45, no. 5, pp. 1456–1467, 1999.

[72] G. Stuber, J. Barry, S. McLaughlin, Y. Li, M.-A. Ingram, and T. Pratt, "Broadband mimo-ofdm wireless communications," *IEEE Proceedings*, vol. 92, pp. 271–294, Feb. 2004.

[73] A. Paulraj, D. GORE, R. Nabar, and H. Bolcskei, "An overview of mimo communications - a key to gigabit wireless," *IEEE Proceedings*, vol. 92, pp. 198–218, Feb. 2004.

[74] L. Ordonez, D. Palomar, and J. Fonollosa, "On the diversity, multiplexing, and array gain tradeoff in mimo channels," in *2010 IEEE International Symposium on Information Theory Proceedings (ISIT)*, pp. 2183–2187, June 2010.

[75] T. Lo, "Maximum ratio transmission," *IEEE Trans. Commun.*, vol. 47, pp. 1458–1461, Oct. 1999.

[76] Q. Spencer, C. Peel, A. Swindlehurst, and M. Haardt, "An introduction to the multi-user mimo downlink," *Communications Magazine, IEEE*, vol. 42, pp. 60–67, Oct 2004.

[77] M. Jiang, J. Akhtman, and L. Hanzo, "Iterative joint channel estimation and multi-user detection for multiple-antenna aided ofdm systems," *IEEE Trans. Wireless Commun.*, vol. 6, pp. 2904–2914, Aug. 2007.

[78] V. Stankovic and M. Haardt, "Generalized design of multi-user mimo precoding matrices," *IEEE Trans. Wireless Commun.*, vol. 7, pp. 953–961, March 2008.

[79] T. Marzetta, "Noncooperative cellular wireless with unlimited numbers of base station antennas," *IEEE Trans. Wireless Commun.*, vol. 9, pp. 3590–3600, Nov. 2010.

[80] A. Nosratinia, T. Hunter, and A. Hedayat, "Cooperative communication in wireless networks," *IEEE Commun. Mag.*, vol. 42, pp. 74–80, Oct. 2004.

[81] A. Younis, R. Mesleh, H. Haas, and P. M. Grant, "Reduced complexity sphere decoder for spatial modulation detection receivers," in *2010 IEEE Global Telecommunications Conference (GLOBECOM)*, pp. 1–5, Dec. 2010.

[82] A. Younis, M. Di Renzo, R. Mesleh, and H. Haas, "Sphere decoding for spatial modulation," in *2011 IEEE International Conference on Communications (ICC)*, pp. 1–6, June 2011.

[83] S. Loyka, "Channel capacity of mimo architecture using the exponential correlation matrix," *IEEE Commun. Lett.*, vol. 5, pp. 369–371, Sept. 2001.

[84] H. Holtkamp, G. Auer, and H. Haas, "On minimizing base station power consumption," in *74th IEEE Veh. Technol. Conf. (VTC Fall)*, pp. 1–5, Sept. 2011.

[85] P. Frenger, P. Moberg, J. Malmodin, Y. Jading, and I. Godor, "Reducing energy consumption in LTE with cell DTX," in *73rd IEEE Veh. Technol. Conf. (VTC Spring)*, pp. 1–5, May 2011.

[86] O. Kallenberg, *Foundations of Modern Probability*. Springer Series in Statistics, 2nd ed., 2002.

[87] Z. Hasan, H. Boostanimehr, and V. Bhargava, "Green cellular networks: A survey, some research issues and challenges," *IEEE Commun. Surveys Tutorials*, vol. 13, pp. 524–540, Fourth 2011.

[88] M. Di Renzo and H. Haas, "Bit error probability of space modulation over Nakagami-m fading: Asymptotic analysis," *IEEE Commun. Lett.*, vol. 15, pp. 1026–1028, Oct. 2011.

[89] M. K. Simon and M. S. Alouini, *Digital Communication over Fading Channels*. Wiley-IEEE Press, 2nd ed., 2005.

[90] M. S. Bazaraa, H. D. Sherali, and C. Shetty, *Nonlinear programming: Theory and algorithms*. Hoboken, N.J. : Wiley-Interscience, 3rd ed., 2006.

[91] N. Serafimovski, M. Di Renzo, S. Sinanovic, R. Mesleh, and H. Haas, "Fractional bit encoded spatial modulation (FBE-SM)," *IEEE Commun. Lett.*, vol. 14, pp. 429–431, May 2010.

[92] K. Stphenson, *Introduction to Circle Packing: The Theory of Discrete Analytic Function*. Cambridge University Press, 2005.

[93] G. Matz, "Recursive MMSE estimation of wireless channels based on training data and structured correlation learning," in *13th IEEE Workshop on Statistical Signal Processing*, pp. 1342–1347, July 2005.

[94] J. Salo, G. Del Galdo, J. Salmi, P. Kyösti, M. Milojevic, D. Laselva, and C. Schneider, "MATLAB implementation of the 3GPP Spatial Channel Model (3GPP TR 25.996)," Jan. 2005.

[95] C. Oestges, "Validity of the Kronecker model for MIMO correlated channels," in *63rd IEEE Veh. Technol. Conf. (VTC Spring)*, vol. 6, pp. 2818–2822, May 2006.

[96] C. Peel and A. Swindlehurst, "Performance of space-time modulation for a generalized time-varying Rician channel model," *IEEE Trans. Wireless Commun.*, vol. 3, pp. 1003–1012, May 2004.

[97] J. H. Kotecha and A. Sayeed, "Transmit signal design for optimal estimation of correlated MIMO channels," *IEEE Trans. Signal Processing*, vol. 52, pp. 546–557, Feb. 2004.

[98] N. Shariati, J. Wang, and M. Bengtsson, "Robust training sequence design for correlated MIMO channel estimation," *IEEE Trans. Signal Processing*, vol. 62, pp. 107–120, Jan. 2014.

[99] C.-T. Chiang and C. Fung, "Robust training sequence design for spatially correlated MIMO channel estimation," *IEEE Trans. Veh. Technol.*, vol. 60, pp. 2882–2894, Sept. 2011.

[100] S. M. Kay, *Fundamentals of Statistical Signal Processing: Estimation Theory*. Prentice Hall PTR, 1st ed., 1993.

[101] M. Hazewinkel, *Linear Interpolation*. Springer, 1 ed., 2001.

[102] J. Berkmann, C. Carbonelli, F. Dietrich, C. Drewes, and W. Xu, "On 3G LTE Terminal Implementation - Standard, Algorithms, Complexities and Challenges," in *Wireless Communications and Mobile Computing Conference, 2008. IWCMC '08. International*, pp. 970 –975, Aug. 2008.

[103] M. Di Renzo and H. Haas, "Bit Error Probability of SM-MIMO Over Generalized Fading Channels," *IEEE Trans. Veh. Technol.*, vol. 61, pp. 1124 –1144, march 2012.

[104] W. Gifford, M. Win, and M. Chiani, "Diversity with practical channel estimation," *IEEE Trans. Wireless Commun.*, vol. 4, no. 4, pp. 1935–1947, 2005.

[105] D. P. Bertsekas, *Constrained Optimization and Lagrange Multiplier Methods*. Athena Scientific, 1st ed., Jan. 1996.

[106] B. Furht and S. A. Ahson, *Long Term Evolution: 3GPP LTE radio and cellular technology*. Auerbach Publications, 1st ed., 2009.

[107] L.-C. Wang and C.-J. Yeh, "3-Cell Network MIMO Architectures with Sectorization and Fractional Frequency Reuse," *IEEE Journal on Selected Areas in Commun.*, vol. 29, pp. 1185–1199, June 2011.

[108] FFR, *Interference mitigation considerations and results on frequency reuse*. 3GPP, TSG-RAN R1-050738, Siemens, Sept. 2005.

[109] SFR, *Soft frequency reuse scheme for UTRAN LTE*. 3GPP, Huawei R1-050507, May 2005.

[110] S. Faruque, "High capacity cell planning based on fractional frequency reuse with optimum trunking efficiency," in *48th IEEE Vehicular Technology Conference (VTC)*, vol. 2, pp. 1458–1460 vol.2, May 1998.

[111] 3GPP TR 36.814 v9.0.0., "Evolved universal terrestrial radio access (E-UTRA); further advancements for E-UTRA physical layer aspects (Release 9)," Mar 2010.

[112] J. Seybold, *Introduction to RF Propagation*. Wiley, 2005.

[113] H. Holm and M.-S. Alouini, "Sum and difference of two squared correlated Nakagami variates in connection with the McKay distribution," *IEEE Trans. Commun.*, vol. 52, pp. 1367–1376, Aug 2004.